Extracellular Vesicles in Hepatobiliary Cancer Management

Dissertation

zur Erlangung des Doktorgrades (PhD)

der Medizinischen Fakultät

der Rheinischen Friedrich-Wilhelms-Universität

Bonn

Sabine Katharina Urban

aus Ludwigshafen am Rhein

2023

Angefertigt mit der Genehmigung

der Medizinischen Fakultät der Universität Bonn

1. Gutachterin: Prof. Dr. rer. nat. Dr. med. Veronika Lukacs-Kornek

2. Gutachter: Prof. Dr. rer. nat. Bernd Giebel

Tag der Mündlichen Prüfung: 31. März 2023

Aus der Medizinischen Klinik und Poliklinik I für Gastroenterologie, Hepatologie, Infektiologie, Nephrologie und Endokrinologie

Direktor: Prof. Dr. med. Christian Strassburg

FÜR UNS.
WEIL WIR ES UNS VERDIENT HABEN.

FÜR JOHANNES.

“IT IS OUR CHOICES THAT SHOW WHAT WE TRULY ARE,
FAR MORE THAN OUR ABILITIES.”

ALBUS DUMBLEDORE

Table of Contents

List of abbreviations

#	number
%	percent
× *g*	units of gravity
°C	degrees Celsius
AFP	alpha-fetoprotein
ALT	alanine transaminase
AnnV	AnnexinV
ANOVA	analysis of variance
ASR	age-standardized rate
AUC	area under ROC curve
BCA	bicinchoninic acid
biliary CA	biliary carcinoma
BMI	body mass index
BSA	bovine serum albumin
CA19-9	carbohydrate antigen 19-9
CCA	cholangiocarcinoma
ccfDNA	circulating cell-free DNA
CD133	cluster of differentiation 133, prominin-1
CD44	cluster of differentiation 44
CD44v6	cluster of differentiation 44 variant 6
CEA	carcinoembryonic antigen
CEUS	contrast-enhanced ultrasonography
CIC	cancer initiating cell
CO_2	carbon dioxide
CRC	colorectal carcinoma
CT	computed tomography
ctDNA	Circulating tumor DNA
dCCA	distal cholangiocarcinoma
DMSO	dimethyl sulfoxide
DNA	desoxyribonucleic acid

eCCA	extrahepatic cholangiocarcinoma
EDTA	ethylenediaminetetraacetic acid
EpCAM	epithelial cell adhesion molecule, CD326
ERCP	endoscopic retrograde cholangiopancreatography
EUS	endoscopic ultrasound
EVs	extracellular vesicles
FACS	fluorescence-activated cell sorting
FBS	fetal bovine serum
FL	fluorescent
FNA	fine needle aspiration
g/mg/µg/ng	gram/milligram/microgram/nanogram
GbCA	gallbladder carcinoma
gp38	podoplanin
HBSS	Hank's buffered saline solution
HCC	hepatocellular carcinoma
HDI	human development index
iCCA	intrahepatic cholangiocarcinoma
IM	interferometric
INMFTG	I've no more fucks to give (song by Thomas Wild)
L/dL/mL/µL	liter/decilitre/millilitre/microliter
lEVs	large EVs
m/mm/µm/nm	meter/millimeter/micrometer/nanometer
miRNAs	microRNAs
MISEV	minimal information for studies of EVs
MRCP	magnetic resonance cholangiopancreatography
MRI	magnetic resonance imaging
mRNA	messenger RNA
n	sample size
n.a.	not available
NCD	noncommunicable disease
non-biliary CA	non-bilary carcinoma
NPV	negative predictive value

ns	not significant
NSCLC	non-small cell lung carcinoma
p	*p* value
P/S	penicillin-streptomycin
PBS	phosphate buffered saline
pCCA	perihilar cholangiocarcinoma
PET	positron emission tomography
PI	propidium iodide
PPV	positive predictive value
PS	phosphatidylserine
PSC	primary sclerosing cholangitis
R^2	coefficient of determination
RNA	ribonucleic acid
ROC	receiver-operating characteristic
RPMI	Roswell Park Memorial Institute
RT	room temperature
SD	standard deviation
SE	standard error
SEM	standard error of the mean
sens	sensitivity
sEVs	small EVs
SOC	single operator cholangioscopy
spec	specificity
TNM	tumor, nodules, metastases
U	unit
US	ultrasonography
v/v	volume per volume
w/v	weight per volume

1. Introduction

1.1. Cancer as a global contemporary disease

Noncommunicable diseases (NCDs) are chronic conditions that are not primarily caused by transmittable infections and often result in long-term health consequences and treatment (Pan American Health Organization 2021). During the last years, NCDs have become the leading cause of death worldwide, accounting for 72% of all deaths globally in 2016, with upward tendency (Wild *et al.* 2020). Out of these, 40.8% can be attributed to cardiovascular diseases, 29.8% to cancers, 7.0% to chronic respiratory diseases and 4.5% to diabetes, rendering cancer as the second leading cause of death worldwide. Furthermore, among almost all countries with high or very high human development index (HDI), cancer even represents the leading cause of death (Wild *et al.* 2020).

In terms of incidences, the worldwide most common cancer site in both sexes and all ages combined in 2020 was breast (11.7%, 2.3 million), followed by lung (11.4%, 2.2 million), colorectum (10%, 1.9 million), prostate (7.3%, 1.4 million), stomach (5.6%, 1.1 million) and liver (4.7%, 0.9 million) (Fig. 1A). However, the most common cancer sites with the highest mortality rates were lung (18%, 1.8 million), colorectum (9.4%, 9.4 thousand), liver (8.3%, 8.3 thousand), stomach (7.7%, 7.7 thousand), breast (6.9%, 6.9 thousand) and oesophagus (5.5%, 5.5 thousand) (Fig. 1B). When comparing annual mortality rates to incidence rates, the fatality of some cancers with poor survival becomes apparent. In 2020, pancreas cancer showed the highest mortality rates as compared to incidence rates (both sexes: ratio of 0.93), followed by liver (women: 0.92, men: 0.91), oesophagus (both 0.89), mesothelioma (women: 0.82, men: 0.85), brain and central nervous system (women: 0.80, men: 0.82), lung (women: 0.77, men: 0.82) and gallbladder cancer (women: 0.71, men: 0.73)(Fig. 1C) (GLOBOCAN 2020).

While in 2012 14.1 million new cancer cases were registered worldwide, new cases were predicted to exceed 20 million by the year 2025 (Stewart and Wild 2014). With more than 19 million new cancer diagnoses in 2020 the prediction was surpassed by almost 5 years (GLOBOCAN 2020). This trend concurs with the observation of demographic and epidemiological transitions of the global population that are based on a shift to an overall older, more susceptible population to ageing-related NCDs and on a decline of mortality from infectious diseases (Omran 1971, Caldwell 1976). Although in most countries with high HDI cancer mortality rates are declining due to effective preventions, early detection

and treatments, mortality rates in countries in transition with low HDI are still increasing for many cancer types, including liver cancer (Center *et al.* 2012, Siegel *et al.* 2014, DeSantis *et al.* 2015, Benson *et al.* 2021). Taking these global trends into account, providing new detection and treatment options, especially for poverty-related cancer types, remains in urgent need.

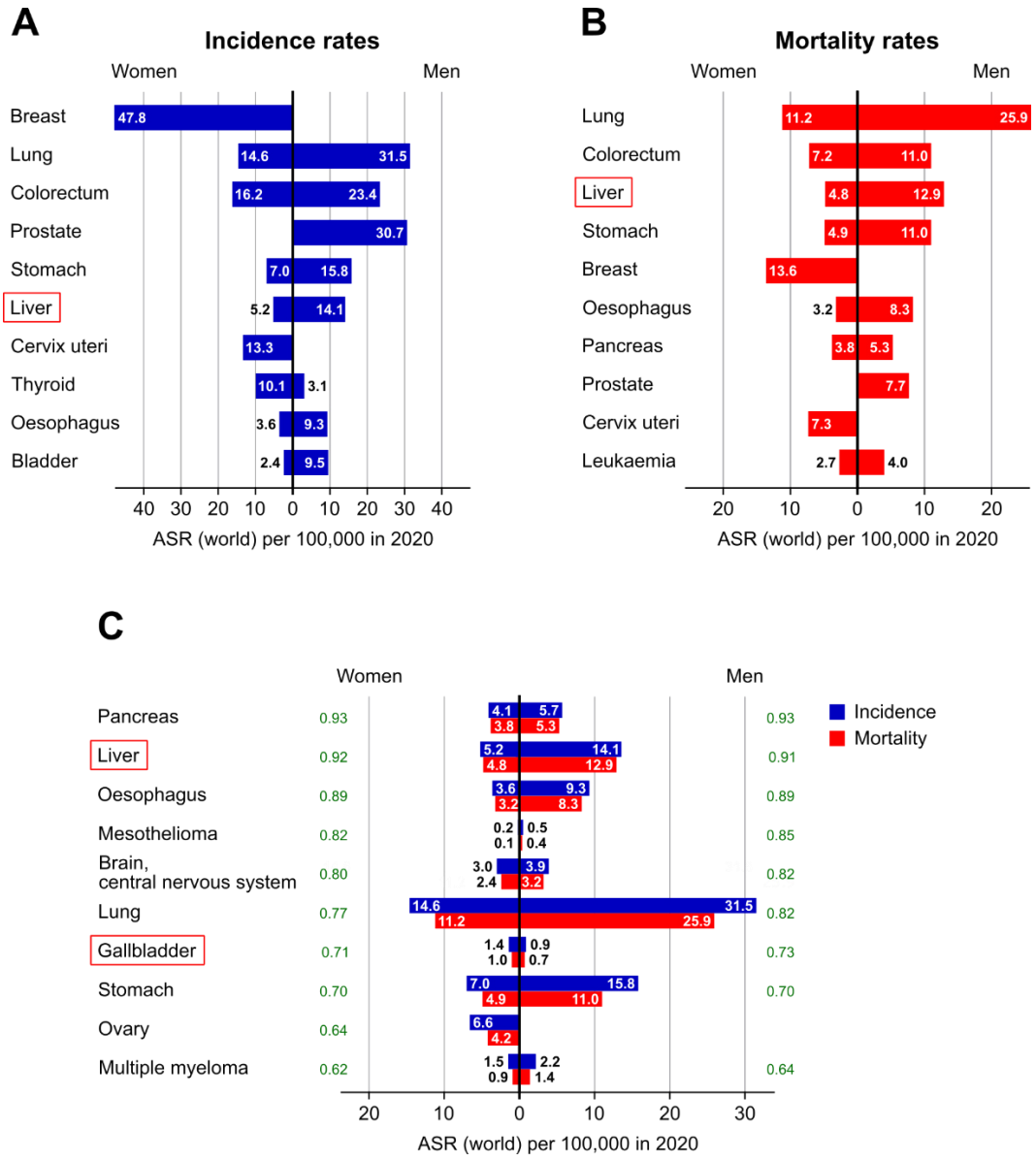

Fig. 1: The most common global cancer sites. Depicted are estimated age-standardized rates (ASR) worldwide for all ages per 100,000 persons in 2020 for both sexes separately. The 10 most common cancer sites sorted by either incidence rates (**A**) or mortality rates (**B**) are shown. In **C** cancer sites are sorted according to high mortality rates as compared to incidence rates. The respective ratio is indicated in green. Indicated in red are the hepatobiliary cancers. Data was obtained from the GLOBOCAN 2020 database (https://gco.iarc.fr/today) and was modified to create the graphs.

1.1.1. Hepatobiliary cancers

Hepatobiliary cancers are a heterogeneous group of diverse primary malignancies that develop either in the liver (hepatocellular carcinoma, HCC) or in the biliary tract system (Fig. 2). Biliary cancers can be divided into gallbladder carcinomas (GbCAs) that arise inside the gallbladder and cholangiocarcinomas (CCAs) that encompass all tumors originating in the biliary tree. According to their anatomical site of origin, CCAs can further be classified into three subtypes: (i) intrahepatic CCAs (iCCAs) that emerge in bile ducts inside the liver parenchyma, (ii) perihilar CCAs (pCCAs) that originate at or close to the junction of the left and right hepatic duct, and (iii) distal CCAs (dCCAs) that occur in distant bile ducts outside of the liver. pCCAs, often referred to as Klatskin tumors, and dCCAs can collectively be summarized as extrahepatic CCAs (eCCAs) (Benson *et al.* 2009, Duffy and Greten 2017, Banales *et al.* 2020). Since every hepatobiliary cancer subtype has its own distinct characteristics and requires specific individual workup, it is important to diagnostically distinguish between these types to ensure the best possible treatment outcome (Valle *et al.* 2016).

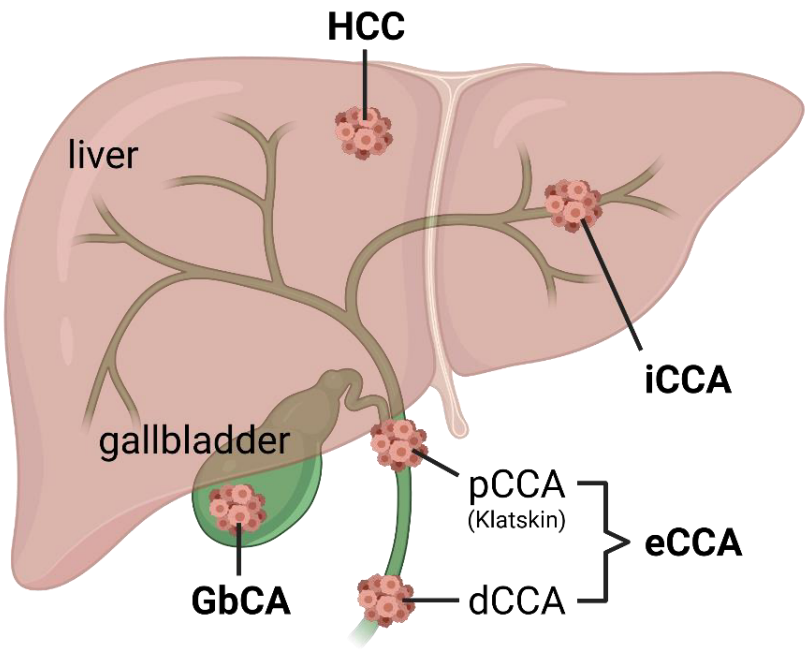

Fig. 2: Localisation of hepatobiliary cancers. Depicted are the respective locations and classifications of hepatobiliary cancers within the liver and the biliary tract system. HCC: hepatocellular carcinoma, GbCA: gallbladder carcinoma, CCA: cholangiocarcinoma, iCCA: intrahepatic CCA, pCCA: perihilar CCA, dCCA: distal CCA, eCCA: extrahepatic CCA. Figure was created with BioRender.com.

Hepatobiliary cancers, especially biliary cancers, are rare and are associated with poor survival rates that are often due to diagnoses in late stages. Although rare, incidences and mortalities have been increasing worldwide during the last decades, featuring a growing global health problem that urgently needs to be addressed in order to improve treatment outcomes and thus patient survival (Bertuccio *et al.* 2019, Van Dyke *et al.* 2019).

1.1.1.1. Hepatocellular carcinoma

Primary liver cancer is the sixth most commonly detected cancer site worldwide and the third leading cause of cancer-related mortality in 2020. Generally, it is more common in men than in women (GLOBOCAN 2020, Dasgupta *et al.* 2020). On a global scale, HCC constitutes the largest group of primary liver cancer with around 75%, followed by intrahepatic CCAs with 12-15% (Petrick and McGlynn 2019, Dasgupta *et al.* 2020, Florio *et al.* 2020). The highest age-standardized incidence and mortality rates for HCC are observed in eastern Asia and Sub-Saharan Africa, where it exceeds 15 per 100,000 people (Marrero *et al.* 2018, Llovet *et al.* 2021). Mongolia displays the highest incidence rate with 93.4 per 100,000 people. HCC is a highly fatal tumor with mortality-to-incidence-ratios approaching 1, thus, mortality rates in the aforementioned geographical regions are the highest worldwide as well (Singal *et al.* 2020). However, incidence and mortality of HCC are increasing rapidly in parts of Europe and the USA, rendering HCC a global health challenge (McGlynn *et al.* 2015).

More than 90% of all HCCs occur on the background of a chronic liver disease, whereby pre-existing cirrhosis from any etiology can be found in more than 80% of all HCC cases and can thus be considered as the strongest risk factor for HCC development (Galle *et al.* 2018, Marrero *et al.* 2018). Approximately 1-6% of cirrhosis patients develop HCC annually, while HCC constitutes the leading cause of death for these patients (Trinchet *et al.* 2015). Hence, any etiological factor leading to cirrhosis can be considered as a risk factor for HCC. Hepatitis B virus (HBV)-induced cirrhosis is the most prevalent risk factor for HCC development and accounts for ~50% of all HCC cases (Akinyemiju *et al.* 2017). Other important risk factors include chronic alcohol consumption, obesity- or diabetes-related non-alcoholic steatohepatitis (NASH), hepatitis C virus (HCV) infection and primary biliary cholangitis (Galle *et al.* 2018, Marrero *et al.* 2018, Llovet *et al.* 2021). Of note, especially in the West, NASH as a disease associated with metabolic syndrome and

diabetes, is becoming the fastest growing etiology of HCC in recent years (Estes *et al.* 2018).

Prognosis of HCC patients generally varies according to stage at diagnosis and treatment resulting in an overall 5-year survival rate of less than 20% (Brar *et al.* 2020). Thus, patients at risk for HCC development, particularly patients with underlying cirrhosis and/or HBV infection, should be screened regularly (Galle *et al.* 2018). International guidelines across scientific societies agree on semi-annual surveillance in a 6-month interval by ultrasonography (US) with or without assessment of serum α-fetoprotein (AFP) levels as the best surveillance strategy (Galle *et al.* 2018, Marrero *et al.* 2018, Benson *et al.* 2021). Since most HCC cases occur in patients with cirrhosis or HBV infection, many HCC patients are diagnosed during surveillance of these pre-existing diseases (Singal *et al.* 2020). Nevertheless, especially in developing countries, where access to screening resources is often limited, incidental diagnoses of liver masses identified during cross-sectional imaging performed for other indications account for approximately 50% of HCC cases (Llovet *et al.* 2021). Of note, in some parts of Asia and Africa, where HBV infection is endemic and the main risk factor for HCC development, vaccination against the virus as a preventive measure has led to a marked decrease in HCC incidence (Chang *et al.* 2016). If HCC is suspected, either incidentally or during surveillance, multiphasic contrast-enhanced CT or MRI should be carried out to assess the arterial enhancement and delayed washout of the potential tumor. This radiological characteristic is regarded sufficient for definitive diagnosis without the necessity of histological confirmation (Galle *et al.* 2018, Marrero *et al.* 2018, van der Pol *et al.* 2019). Thus, HCC is mostly detected based on non-invasive hallmarks. However, these radiological criteria are only applicable to cirrhotic patients with nodules ≥1 cm, while the diagnosis of all other patients still requires confirmation by pathology. Serological tumor markers such as AFP are not recommended to establish a diagnosis but might be beneficial for prognostic purposes (Galle *et al.* 2018).

Treatment strategies for HCC vary greatly according to tumor stage and overall patient health and should be revised carefully before any treatment decisions. Tumor staging by the BCLC staging system should be carried out and pre-existing comorbidities such as advanced cirrhosis, that compromises patient health and thus limits treatment possibilities, should be taken into account (Llovet *et al.* 2021). Surgical interventions that include tumor

resections as well as liver transplantations are the most commonly applied potentially curative treatments for HCC with 5-year survival rates exceeding 70% (Galle *et al.* 2018, Marrero *et al.* 2018). Additional neoadjuvant or adjuvant therapies are not recommended by international guidelines, since their benefit for overall patient survival has not been proven (Galle *et al.* 2018). According to the BCLC staging system, only patients in very early and early tumor stages are eligible for surgical treatments, while intermediate- and advanced-stage cases are typically subjected to ablation, chemoembolization or systemic chemotherapy. A combination therapy with the two drugs atezolizumab and bevacizumab is usually the method of choice for first-line chemotherapy, with sorafenib or lenvatinib as alternative monotherapies or subsequent second-line drugs (Galle *et al.* 2018, Marrero *et al.* 2018, Llovet *et al.* 2021). Of note, advanced-stage systemic therapies are associated with considerably worse prognosis than early-stage surgical interventions and often result in median survival of only 1-1.5 years (Villanueva 2019). If HCC is diagnosed in a terminal stage, only palliative treatments with best supportive care are possible.

1.1.1.2. Cholangiocarcinoma

With approximately 12-15% of all primary hepatic malignancies, iCCAs are the second most common type of primary liver cancer after HCCs (Petrick and McGlynn 2019). Among CCAs, iCCA accounts for approximately 10-20%, surpassed by dCCA (20-30%) and pCCA (50-60%) (Banales *et al.* 2020). Incidences of CCA vary greatly depending on geographic regions, with eastern Asian countries ranking among the highest incidences worldwide (85 per 100,000 in northeastern Thailand vs. 0.4 per 100,000 in Canada) (Strijker *et al.* 2019). Accordingly, mortality rates in Asian countries are higher than in the West, with the highest rate reported in Japanese men (2.81 per 100,000). Generally, CCA is more common in men than in women (Bertuccio *et al.* 2019). On a global scale, incidences as well as mortality from iCCA markedly increased during the last decades, while eCCA incidences and mortality decreased in most countries (Bertuccio *et al.* 2019, Khan *et al.* 2019).

Risk factors for CCA development are diverse and vary substantially depending on CCA subtype, geographic region and genetic background (Khan *et al.* 2019, Florio *et al.* 2020). Mostly, however, CCA develops in ducts that are affected by chronic inflammation such as chronic viral hepatitis, primary sclerosing cholangitis (PSC), Caroli's disease,

hepatolithiasis and liver fluke infections (Komuta *et al.* 2008, 2012, Zhou *et al.* 2008, Carpino *et al.* 2019). Furthermore, excessive alcohol and tobacco consumption as well as metabolic conditions (obesity, diabetes or non-alcoholic fatty liver disease) have been linked to a higher risk of CCA development (Donato *et al.* 2001, Shaib *et al.* 2005, Tyson and El-Serag 2011). The diversity of risk factors may contribute to the fact that approximately 50% of all diagnosed CCA cases occur sporadically without the presence of any identifiable risk factor (Khan *et al.* 2019).

Since CCAs are usually asymptomatic in early stages, they are mostly diagnosed during advanced disease progression, leading to greatly compromised therapeutic options and thus to generally poor 5-year survival rates of 7-20% (Lindnér *et al.* 2015, Kamsa-Ard *et al.* 2019, Strijker *et al.* 2019). Screening procedures such as ultrasonography (US), computed tomography (CT), magnetic resonance imaging (MRI) or assessment of carbohydrate antigen 19-9 (CA19-9) levels to identify malignant changes as early as possible are recommended for PSC patients, but have so far not proven reliable for a differential diagnosis of PSC and CCA (Beuers *et al.* 2009, Khan *et al.* 2012). Apart from PSC and cirrhosis, for which patients are already undergoing screening for HCC surveillance, no screening procedures have been established for other defined at-risk groups (Valle *et al.* 2016). Consequently, iCCA is mostly discovered incidentally (20-25% of all cases) as a result of surveillance scans performed for other indications (Alvaro *et al.* 2011). Serological tumor markers such as CA19-9 are not recommended to establish a diagnosis but might be beneficial for prognostic purposes (Bridgewater *et al.* 2014). Furthermore, distinguishing iCCA from HCC, mixed HCC-CCA and metastatic adenocarcinomas remains a difficult challenge (Khan *et al.* 2012, Banales *et al.* 2020). Consequently, up to date, a biopsy followed by histopathological evaluation is required for a definitive diagnosis (Bridgewater *et al.* 2014). Due to a lack of distinct imaging criteria, a location that is often difficult to access for biopsies, and insensitive minimal-invasive serological tumor biomarkers, CCAs can be extremely challenging to accurately diagnose (Banales *et al.* 2016, Rizvi *et al.* 2018). However, each CCA type requires differential risk assessment and specific staging according to the TNM 2010 system. These steps are crucial for following treatment decisions and need to be carried out with great care for each patient individually, taking underlying comorbidities and general patient health into account (Valle *et al.* 2016).

The only potentially curative option for CCA is a complete resection of the malignant tissue and adjacent parts. The extent of the resection varies greatly depending on CCA subtype and stage. Typically, hemi-hepatectomy with lymphadenectomy is carried out for iCCA resection, whereas pCCA requires an additional removal of the caudate lobe and extrahepatic bile duct. For dCCA, a partial duodeno-pancreatectomy with extended bile duct resection is usually necessary (Valle *et al.* 2016, Banales *et al.* 2020). After curative resection, adjuvant capecitabine treatment with subsequent surveillance of recurrences is recommended by international guidelines (Shroff *et al.* 2019). Most patients (~70%), however, are diagnosed at late stages of the disease and present with advanced and thus unresectable tumors. In these cases only palliative treatment with subsequent best supportive care is possible (Valle *et al.* 2016, Forner *et al.* 2019), with systemic chemotherapy (gemcitabine monotherapy or in combination with cisplatin) being the treatment of choice for inoperable tumors (Valle *et al.* 2016). Of note, liver transplantation as a potentially curative option for iCCA is currently under investigation and might be of benefit for patients with tumors smaller than 2 cm (Sapisochin *et al.* 2016).

1.1.1.3. Gallbladder carcinoma

Although rare on a global scale, gallbladder carcinomas (GbCAs) represent almost 50% of all biliary tract cancers (Siegel *et al.* 2017). Incidence rates of GbCAs vary depending on geographic region with the highest age-standardized rate for both sexes in 2020 being reached in Bolivia (8.5 per 100,000 people), followed by Chile (5.6), Bangladesh (4.9), Nepal (4.1) and both South (2.9) and North Korea (2.7) (GLOBOCAN 2020). The highest incidence, however, was found in women from northern India with 21.5 per 100,000 (Bailey and Shah 2019). Accordingly, mortality rates in the aforementioned countries are high as well with Bolivia displaying the highest value of 5.8 per 100,000 people. Among the tumors that can affect both genders, alongside thyroid cancer, GbCA is the only type of cancer that is more common in women than in men (GLOBOCAN 2020). While GbCA mortality has decreased in most countries over the last decades before the 2000s, in many countries this decrease has stopped or even reversed since then (Torre *et al.* 2018).

The development of GbCA is predominantly associated with the presence of chronic inflammation of the gallbladder. Thus, cholelithiasis that describes the accumulation of gallstones in the gallbladder is the most common risk factor for GbCA. Other risk factors

include gallbladder polyps, congenital biliary cysts, porcelain gallbladder, primary sclerosing cholangitis, chronic infection and obesity (Benson *et al.* 2009, Valle *et al.* 2016, Bailey and Shah 2019).

GbCAs are highly aggressive tumors that can spread rapidly and are consequently often diagnosed at advanced stages of the disease (Benson *et al.* 2009). Accordingly, the one-year mortality (85%) and 5-year survival rate (5%) are poor. Of note, 5-year survival can go up to 75%, if the malignancy is discovered at an early stage (Goodman and Yamamoto 2007, Goetze 2015, Siegel *et al.* 2017, Bailey and Shah 2019). Surveillance screening by ultrasonography is recommended for patients diagnosed with premalignant gallbladder polyps measuring 6-9 mm. Since lesions greater than 20 mm are potentially GbCA, enlarged polyps (10-20 mm) should be evaluated for resection (Andrén-Sandberg 2012). Besides that, no screening procedure for other at-risk groups has been established. Typically, GbCA is either diagnosed incidentally after histopathological evaluation of cholecystectomies (70% of all GbCA diagnoses) or during imaging of symptomatic patients as a late-stage tumor of the right upper quadrant (Goetze 2015, Valle *et al.* 2016). In both cases appropriate staging by imaging procedures (MRI or CT) and extensive histopathological analysis is required to decide about the necessity of further resections. As for CCAs, serological tumor markers such as CA19-9 are not recommended to establish an accurate diagnosis but might be beneficial for prognostic purposes (Valle *et al.* 2016).

Up until now, complete surgical resection is the only curative option for GbCA, however, only one third of patients are eligible for resection at the time of diagnosis (Bailey and Shah 2019). Depending on the anatomical site of the cancer, an additional major hepatectomy, a resection of the bile duct, the duodenal bulb or the pancreatic head might be necessary besides the removal of the gallbladder (Valle *et al.* 2016). The implementation of adjuvant treatment is associated with a survival benefit and should be considered after surgery (Horgan *et al.* 2012). As for CCAs, in case of an unresectable, advanced tumor, only palliative treatment with subsequent best supportive care is possible, with systemic chemotherapy (gemcitabine monotherapy or in combination with cisplatin) being the treatment of choice (Valle *et al.* 2016).

1.2. Liquid biopsies in hepatobiliary cancer diagnosis

Liquid biopsy describes the molecular analysis of tumor components that are released into biological fluids, such as blood, bile, urine or saliva, by solid tumors. Typical elements for investigation comprise circulating tumor cells (CTCs), circulating cell-free nucleic acids (DNA or RNA) and extracellular vesicles (EVs) (Labgaa *et al.* 2021). They can serve a variety of purposes, including early cancer diagnosis, customizing individual treatments based on tumor genotyping, decision-making for systemic therapies or monitoring cancer relapse and resistance to therapies (Parikh *et al.* 2019, Kwo and Aronson 2021, Labgaa *et al.* 2021). Currently, standard tissue biopsies are performed frequently, in order to accurately diagnose and distinguish hepatobiliary cancers. However, they are invasive procedures that subject the patient to risk of complications such as bleeding, infections and tumor seeding along the needle tract. Additionally, the quality of the biopsy greatly relies on the accessibility of the tumor and the level of skill of the operator (Silva *et al.* 2008, Rompianesi *et al.* 2021). In contrast to that, liquid biopsies are minimal-invasive procedures, that are easily accessible, repeatable and that reflect the tumor heterogeneity. Thus, they can provide a dynamic picture of the course of the disease and the molecular background of the patient (Labgaa *et al.* 2021). Furthermore, especially since hepatobiliary cancers are associated with markedly improved prognoses if detected and treated early, liquid biopsies as part of surveillance screenings play an important role in disease prevention and enhanced patient survival (Tanos and Thierry 2018).

Single cells that are disseminated into the bloodstream by solid tumors are generally referred to as circulating tumor cells and are responsible for distant tumor metastases (Akpe *et al.* 2020). In hepatobiliary cancers, the diagnostic capacity of overall CTC count as compared to controls has been explored for HCC (AUC 0.77, (Cheng *et al.* 2019)) and GbCA (sensitivity: 92.6%, specificity: 91.7%, (Awasthi *et al.* 2017)) detection, whereas diagnostic studies of CTCs in CCA are rare. Nevertheless, the prognostic value of CTCs has been investigated in CCA, showing that a higher number of CTCs was positively associated with tumor extent and aggressiveness (Yang *et al.* 2016).

Similarly, the diagnostic benefit of circulating cell-free tumor DNA (ctDNA) has been explored in hepatobiliary cancers. CtDNA are DNA fragments from solid tumors that are released into the bloodstream and that reflect the genomic and epigenetic information of the tumor (Labgaa *et al.* 2021). TERT promoter mutations in ctDNA have been found to

be a potential biomarker for early HCC detection (Jiao *et al.* 2018). In CCA patients, a panel of mutations in KRAS, NRAS, BRAF and PIK3CA was identified in ctDNA that perfectly concurred with mutations found in the original tumor, indicating their potential as a diagnostic biomarker (Andersen and Jakobsen 2016). Additionally, GbCA patients could successfully be distinguished from healthy subjects and cholecystitis patients by increased overall ctDNA levels (Kumari *et al.* 2017).

There are different forms of circulating cell-free RNAs (cfRNAs) that are released by solid tumors into the bloodstream. However, due to their molecular stability, microRNAs (miRNAs) are the most commonly investigated kind of cfRNA as a biomarker in liquid biopsies (Labgaa *et al.* 2021). Lin *et al.* found a panel of seven miRNAs that reliably identified early-stage HCC (AUC: 0.82), while iCCA could be distinguished from healthy controls by high miR-21 levels (AUC: 0.94) (Lin *et al.* 2015, Correa-Gallego *et al.* 2016). Similarly, a study on biliary tract cancers, including GbCA, iCCA and others, confirmed that miR-21 had a strong discriminatory potential for these malignant diseases as compared to healthy controls (AUC: 0.93) (Kishimoto *et al.* 2013). In addition to being freely available in serum and plasma, miRNAs can also be found protein-bound or inside of extracellular vesicles (EVs), contributing to the importance of EVs as liquid biopsies (Letelier *et al.* 2016).

1.2.1. Extracellular vesicles

The generic term ‘extracellular vesicles’ describes the entirety of all lipid bilayer-enclosed structures that can be found in the extracellular environment. All types of cells are capable of secreting such vesicles and the process seems to be conserved throughout all domains of life ranging from archaea to bacteria, yeast, plants and humans (Deatherage and Cookson 2012, Gill *et al.* 2019). Initially, the secretion of EVs was believed to be a mechanism for eliminating undesirable contents from cells (Johnstone *et al.* 1987). This opinion, however, has changed rapidly during the last decades. Nowadays, EVs are well characterized as a means of intercellular communication, providing another layer of complexity in addition to the already established mechanisms of communication via direct cell-to-cell contacts or soluble factors such as cytokines or hormones (Yáñez-Mó *et al.* 2015, Giebel 2017). EVs are majorly involved in the regulation of a wide variety of physiological processes such as tissue repair (Gatti *et al.* 2011), coagulation (Del Conde

et al. 2005) and stem cell maintenance (Ratajczak *et al.* 2006). Additionally, EVs have been identified as key drivers of a number of diseases such as viral infections (Mack *et al.* 2000), neurodegenerative disease (Bellingham *et al.* 2012) and cancer (Kalluri 2016). In cancer, EVs have been found to promote carcinogenesis by stimulating a variety of underlying key processes such as angiogenesis, immune modulation and pre-metastatic niche formation (Chalmin *et al.* 2010, Kucharzewska *et al.* 2013, Costa-Silva *et al.* 2015). EVs are enclosed by a phospholipid bilayer and can contain biomolecules from all categories, comprising proteins, lipids, nucleic acids and sugars. Thus, EVs provide both protection of their cargo from the extracellular environment and the possibility of transferring specific combinations of multiple signaling molecules even to remote recipient cells in order to induce behavioral changes (Yáñez-Mó *et al.* 2015). In this regard, rather than viewing EVs as mere transport vehicles, it was even proposed to view them as extended extracellular cell organelles of the donor cell (Ludwig and Giebel 2012). The specific cargo composition of EVs reflects their cellular origin and varies according to environmental parameters and physiological or pathophysiological state of the parental cell. Thus, different cell types and states thereof lead to the release of different EV variants with specific molecular signatures resulting in tremendous heterogeneity among EV populations (Van Niel *et al.* 2018, Willms *et al.* 2018).

In addition to the varying cargo compositions of EVs, cells can release a variety of different extracellular vesicle types. The most prominent among them are exosomes, microvesicles and apoptotic bodies. They differ mostly according to their subcellular origin, mode of biogenesis and size (Fig. 3). Exosomes form during endocytotic endosome maturation by inward budding of the endosomal membrane, resulting in intraluminal vesicles (ILVs). Late endosomes containing ILVs are also referred to as multivesicular endosomes (MVEs) or multivesicular bodies. MVEs can either fuse with lysosomes for degradation of their contents or with the plasma membrane in order to release their ILVs, now called exosomes, into the extracellular environment. ILV and thus exosome diameter typically ranges from 40 to 100 nm (Raposo and Stoorvogel 2013, Van Niel *et al.* 2018, Mathieu *et al.* 2019). In contrast to exosomes, microvesicles are formed by an outward budding process of the plasma membrane and they typically range from 100 to 1000 nm in size (Raposo and Stoorvogel 2013). Of note, both endosome ILVs (initially derived from endocytotic inward budding of the plasma membrane to form endosomes) and

microvesicles bud away from the cytosol, so that their membrane orientation and topology of proteins is identical to that of the plasma membrane (Mathieu *et al.* 2019). Apoptotic bodies are formed during fragmentation of apoptotic cells, are enclosed by the plasma membrane and are considerably larger than the aforementioned EV subtypes, ranging from 500 nm up to several µm (Raposo and Stoorvogel 2013).

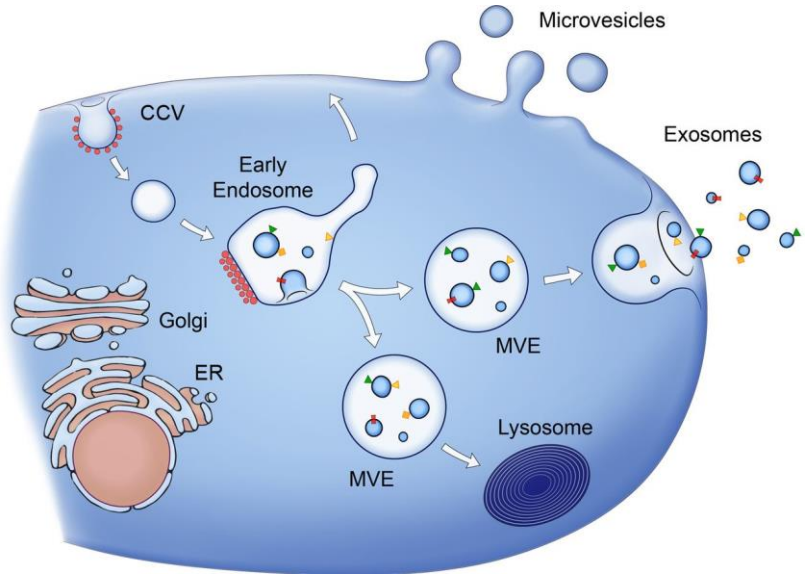

Fig. 3: Biogenesis of extracellular vesicles. Early endosomes are formed during an endocytotic trafficking pathway by clathrin-coated vesicles (CCV). During inward budding of the endosomal membrane intraluminal vesicles (ILVs) are formed. ILV-containing multivesicular endosomes (MVEs) can either fuse with the lysosome for degradation or with the plasma membrane to release their ILVs, now called exosomes or small EVs, into the extracellular environment. Microvesicles (large EVs) are formed by an outward budding process of the plasma membrane. ER: endoplasmatic reticulum (Raposo and Stoorvogel 2013).

Due to the great heterogeneity of secreted EVs and the fact that neither distinct markers nor accurate purification technologies have been established yet, the clear distinction of EV subtypes in experimental preparations remains a difficult challenge. Especially assigning a particular biogenesis pathway to isolated EVs, which is implied by the usage of the terms ‘microvesicles’ and ‘exosomes’, is nearly impossible to verify. Therefore, the International Society of Extracellular Vesicles endorses the use of a nomenclature according to either physical characteristics (e.g. size or density), biochemical composition (e.g. $CD63^+$ or $AnnV^+$) or descriptions of conditions or cellular origin of EVs (e.g. hypoxic or tumor-associated EVs) in their statement paper on ‘Minimal information for studies of

EVs' (MISEV) (Théry *et al.* 2018). Hence, the terms 'small EVs' (sEVs) for vesicles with diameters below 100 nm and 'large EVs' (lEVs) for vesicles larger than 100 nm will be used to describe EVs throughout this thesis from now on.

1.2.1.1. Extracellular vesicles in hepatobiliary cancer diagnosis

EVs can be found in almost all kinds of body fluids, including blood, saliva, urine and bile, rendering them ideal candidates for liquid biopsies (Raposo and Stoorvogel 2013). In addition to miRNAs or DNA, the intravesicular and surface protein composition as well as the total amount of circulating EVs can act as diagnostic indicators. In this regard, there are some promising reports on EVs as biomarkers for hepatobiliary cancers.

In HCC, total EV levels were found to be discriminatory of patients with early (AUC 0.83) and relatively early HCC (AUC 0.94) from cirrhosis patients (Wang *et al.* 2013). Moreover, HepPar1-positive EVs were observed to be significantly increased in HCC as compared to cirrhosis patients and healthy individuals (Abbate *et al.* 2017). A comprehensive proteomic study by Arbelaiz *et al.* revealed that the proteins LG3BP, PIGR and A2MG were more abundant in EVs from HCC than from healthy individuals (AUC 0.90, 0.84 and 0.80, respectively), highlighting them as potential diagnostic targets (Arbelaiz *et al.* 2017). Furthermore, in a previous study of our group combined analysis of several surface proteins on EVs comprising EpCAM, CD133 and ASGPR1 led to a diagnostic separation of HCC from cirrhosis patients (AUC 0.73) and healthy individuals (AUC 0.74) (Julich-Haertel *et al.* 2017b).

In the same study, CCA could be differentiated from healthy individuals (AUC 0.81) and cirrhosis patients (AUC 0.62) with the same experimental parameters. For CCA, the proteomic analysis of EVs by Arbelaiz *et al.* showed that the protein FIBG had discriminatory potential for both iCCA versus HCC patients (AUC 0.89) and CCA versus PSC patients (AUC 0.80), whereas the protein AMPN performed best for distinguishing CCA and healthy individuals (AUC 0.88) (Arbelaiz *et al.* 2017). In contrast to the aforementioned studies that were all conducted on EVs from serum or plasma, EVs isolated from bile can be an important source for CCA diagnosis. This way, total EVs in bile were found to be elevated in malignant common bile duct stenoses (pancreatic cancer and cholangiocarcinoma) versus non-malignant stenoses and they could be discriminated with 100% accuracy (Severino *et al.* 2017). Similarly, Claudin-3 was identified as a

biomarker in bile for distinguishing CCA from patients with benign bile duct stones (AUC 0.95) (Ikeda *et al.* 2021).

While there are some reports on differential EV-enclosed miRNAs or total EV count for GbCA diagnosis, to the best of the author's knowledge, EV-derived proteins as a biomarker for GbCA have not been investigated so far. Nevertheless, some proteomic analyses of GbCA versus surrounding normal tissue suggest ANXA4 (Huang 2014) or S100A10 and haptoglobin (Tan *et al.* 2011) as potential biomarkers for differential diagnosis, whose feasibility for GbCA diagnosis (with and without EVs) remains to be elucidated.

1.3. Objectives

Hepatobiliary cancers belong to the most severe cancers worldwide and are associated with high fatality and bad prognoses, often due to late-stage discoveries. To date, no reliable serum biomarker exists for accurate, early detection and differentiation of these cancers. Especially the distinction of HCC and iCCA remains an extremely difficult challenge that requires an invasive tissue biopsy for definitive diagnosis. However, considering that management, chemotherapy options and prognoses are very different between the two cancers, the distinction is crucial for following treatment decisions and thus patient survival. Hence, the aim of this thesis was to establish extracellular vesicles as minimal-invasive serum biomarkers for detection and differentiation of hepatobiliary cancers, focusing on the capability for HCC and iCCA distinction. In contrast to most biomarker studies on EVs that either concentrate on one type of EVs or on the entirety of all EVs without specifying their molecular characteristics, this study aims to comprehensively evaluate both large and small EVs separately in terms of their differential diagnostic capacity for hepatobiliary cancers. As a liquid biopsy, EVs not only offer the possibility of uncomplicated and easily applicable diagnosis but could also promote hepatobiliary cancer detection and differentiation at earlier stages, thus hopefully leading to immensely improved treatment outcomes and resulting patient survival in the future.

2. Material and Methods

2.1. Tissue culture methods

All tissue culture maintenance work was performed under sterile conditions in a laminar flow hood. All cells were grown under standard humidified conditions at 37 °C and 5% CO_2 in a CO_2 incubator.

2.1.1. Reagents

Roswell Park Memorial Institute (RPMI) 1640 medium: Gibco by Life Technologies, Paisley, UK
Fetal bovine serum (FBS): Gibco by Life Technologies, Paisley, UK
Penicillin-Streptomycin (P/S): 10,000 U/mL, Gibco by Life Technologies, Paisley, UK
Phosphate buffered saline (PBS): Sigma Aldrich, Steinheim, Germany
Ethylenediaminetetraacetic acid (EDTA): Invitrogen by life technologies, Paisley, UK
Trypsin: 0.5% with 4 mM EDTA, Thermo Fisher Scientific, Waltham, Massachusetts, USA
Dimethyl sulfoxide (DMSO): Sigma Aldrich, Steinheim, Germany
Trypan blue: 0.4%, Thermo Fisher Scientific, Waltham, Massachusetts, USA
Hank's buffered saline solution (HBSS): Gibco by Life Technologies, Paisley, UK
Sodium azide: 10%, Thermo Fisher Scientific, Waltham, Massachusetts, USA
Hu FcR binding inhibitor purified (Fc block): eBioScience Inc., San Diego, USA
Propidium iodide (PI): Miltenyi Biotec GmbH, Bergisch Gladbach, Germany
Growth medium: RPMI supplemented with 10% (v/v) FBS and 1% (v/v) P/S
Starvation medium: RPMI supplemented with 1% (v/v) P/S
Staining buffer: HBSS + 1% (v/v) FBS + 0.01% (v/v) sodium azide
Fc block mix: 47.5 µL staining buffer + 2.5 µL Fc block per staining

2.1.2. Human cancer cell lines

The human hepatocellular carcinoma cell lines HuH7 (CLS Cell Lines Service GmbH, Eppelheim, Germany, #300156), HepG2 (CLS Cell Lines Service GmbH, #300198) and Hep3B (DSMZ, Braunschweig, Germany, #ACC 93) were used as an *in vitro* hepatocellular carcinoma model. HuH7 was established from a 57-year-old Japanese male with differentiated hepatocellular carcinoma (Nakabayashi *et al.* 1982), HepG2

derived from liver tumor biopsies of a 14-year-old Caucasian male (Aden *et al.* 1979) and Hep3B was established from the liver tumor tissue of an 8-year-old Black male (Aden *et al.* 1979). Human bile duct carcinoma cell lines TFK-1 (DSMZ, Braunschweig, Germany, #ACC 344), EGI-1 (DSMZ, Braunschweig, Germany, #ACC 385) and CCC-5 (DSMZ, Braunschweig, Germany, #ACC 810) were used as an *in vitro* cholangiocarcinoma model. TFK-1 was established from a 63-year-old male with bile duct adenocarcinoma (Saijyo *et al.* 1995), EGI-1 derived from a 52-year-old male with advanced stage bile duct carcinoma (Scherdin *et al.* 1987) and CCC-5 was established from a 59-year-old Caucasian male with cholangiocarcinoma (Zach *et al.* 2017).

2.1.3. Thawing of cryopreserved cell lines

Frozen cell were thawed in a 37 °C water bath. After thawing, they were transferred to a 15 mL centrifugation tube containing 9 mL of growth medium. Subsequently, cells were centrifuged at 300 × *g* for 5 min at room temperature (RT). The supernatant was discarded and 3 mL of growth medium were added for resuspension of the cells. The suspension was transferred to a fresh T75 culture flask that was pre-filled with 10 mL of growth medium. Cells were incubated for 24 h under standard conditions, washed with 5 mL of PBS and the medium was exchanged to 10 mL of fresh growth medium. Cells were then incubated until further subcultivation.

2.1.4. Subcultivation of adherent cell lines

Cells were grown under standard conditions until confluency of 70-80% was achieved. For passaging, the medium was discarded and cells were gently washed with 5 mL of PBS. Subsequently, cells were incubated in 1 mL of 0.05% trypsin (stock was diluted 1:10 in PBS) for 5-20 minutes under standard conditions, depending on the respective cell line. After cells were detached, 4 mL of growth medium were added to stop the digestive reaction. Cells were centrifuged at 300 × *g* for 5 min at RT. The supernatant was discarded and growth medium was added for resuspension of the cells. Depending on the growth time of the respective cell line, a fraction of the cell suspension was transferred to a fresh T75 flask, prefilled with 10 mL growth medium and the cells were incubated under standard conditions. Cells were washed with 5 mL PBS and growth medium was

exchanged every 2-3 days until confluency of 70-80% was achieved. Cells were subcultivated at least once a week.

2.1.5. Cryopreservation of cell lines

When cells were grown to 70-80% confluency, growth medium was discarded and they were washed with 5 mL PBS. Subsequently, cells were incubated in 1 mL of 0.05% trypsin (stock was diluted 1:10 in PBS) for 5-20 minutes under standard conditions, depending on the respective cell line. After cells were detached, 4 mL of growth medium were added to stop the digestive reaction. Cells were centrifuged at 300 × *g* for 5 min at RT. The supernatant was discarded and 1 mL of growth medium was added for resuspension of the cells. 900 µL of the cell suspension were transferred to a sterile 2 mL cryopreservation tube and 100 µL of the cryoprotective agent DMSO were added. Cells were stored at -80 °C for 24 h immediately after handling and were afterwards transferred to liquid nitrogen for long term storage.

2.1.6. Cell counting

To determine the concentration of living cells, 10 µL of cell suspension were mixed with 10 µL of 0.4% trypan blue solution in a 1.5 mL reaction tube (1:2 dilution). Subsequently, 10 µL of the mixture were transferred to a hemocytometer (Neubauer improved chamber with 0.1 mm depth) and unstained cells were counted using a light microscope. After determining the mean cell count in the four corner squares of the chamber, the concentration of living cells was calculated as follows:

$$concentration/mL = mean\ cell\ count \times dilution\ factor \times 10{,}000$$

2.1.7. Surface staining of cell lines for flow cytometric analysis

When the cells reached 70% confluency, they were washed with 5 mL PBS and 10 mL starvation medium was added for 16-24 h. After incubation they were washed with 5 mL PBS again and 5 mL PBS + 4 mM EDTA were added to gently detach the cells. Cells were incubated at 37 °C for up to 20 min, depending on the respective cell line. If cells were still partly attached after incubation, a cell scraper was used to detach the remaining cells. The cell suspension was transferred to a fresh 15 mL centrifugation tube and was centrifuged at 300 × *g* for 5 min at RT. The supernatant was discarded and the pellet was

resuspended in 1-3 mL staining buffer depending on the pellet size. Cell suspension was filtered (0.02 µm) and was kept on ice from now on. After determining the cell count with a hemocytometer, 100,000 cells per staining were transferred to a fresh 1.5 mL reaction tube. Cells were centrifuged at 300 × *g* for 5 min at 4 °C. The supernatant was discarded and the cell pellet was resuspended in 50 µL Fc block mix per staining. Subsequently, the cells were incubated for 5 min on ice. After the incubation 50 µL of diluted antibodies in staining buffer were added to each staining (Tab. 1) and cells were incubated for 15 min on ice in the dark. All antibodies were titrated against their corresponding isotype prior use and isotype dilutions were concentration-matched to the respective antibody.

Tab. 1: Overview of antibodies for surface staining of human cancer cell lines. Listed are all used antibodies including information about antigen, conjugated fluorophor, host/isotype, vendor, catalog number, concentration and used dilution for the final staining mix of 100 µL. This table is part of the attached publication Urban *et al.* (2020) that resulted from this project. #: number, conc.: concentration, rec.: recombinant.

antibody (against human)	conjugate	host/isotype	vendor	catalog#	conc. [µg/µL]	dilution
gp38	PE-Vio770	rec. human IgG1 (REA)	Miltenyi	130-106-954	0.0055	1:100
CD133	APC	Mouse IgG2b	Miltenyi	130-090-854	0.00825	1:20
EpCAM	BV-421	Mouse IgG2bκ	BioLegend	324219	0.05	1:800
CD44v6	APC	rec. human IgG1 (REA)	Miltenyi	130-111-425	0.1	1:1000
Isotype	PE-Vio770	rec. human IgG1 (REA)	Miltenyi	130-104-618	0.095	1:1700
Isotype	APC	Mouse IgG2bκ	eBioscience	17-4732-42	0.2	1:500
Isotype	BV-421	Mouse IgG2bκ	BioLegend	400341	0.05	1:800
Isotype	APC	rec. human IgG1 (REA)	Miltenyi	130-104-614	0.02	1:200

After antibody incubation, 400 µL of staining buffer were added to each staining and the cells were centrifuged at 300 × *g* for 5 min at 4 °C. Supernatant was discarded and the cells were resuspended in 400 µL staining buffer. For flow cytometric analysis, 4 µL of 1:10 PI in staining buffer were added to each staining and 150 µL of the solution were measured by a MACSQuant® Analyzer 10 (Miltenyi Biotec GmbH, Bergisch Gladbach, Germany). Data analysis was performed using the software FlowJo™ 10.7.1 (Tree Star Inc., Ashland, USA).

2.2. Mice

All animal experiments were performed with the approval of the ethics and animal care committee Homburg. Mice were purchased from Charles River (Sulzfeld, Germany). They were kept in an assigned mouse cabinet (UniProtect Air Flow Cabinet, Bioscape, Castrop-Rauxel, Germany) in the Institute of Internal Medicine II (Saarland University, Homburg, Germany) under pathogen-free conditions and they had unlimited access to food and water. Food and water supply was checked on a daily basis and the cages (Innocage® mouse cage, Innovive Inc., San Diego, USA) were exchanged weekly. All experimental procedures were performed on male 7-9-week-old wild type C57Bl/6 mice that were fed with standard diet.

2.2.1. Reagents

Roswell Park Memorial Institute (RPMI) 1640 medium: Gibco by Life Technologies, Paisley, UK

Fetal bovine serum (FBS): heat-inactivated, Life Technologies, Carlsbad, USA

Collagenase P:.2 mg/ml, Sigma Aldrich, Steinheim, Germany

DNase-I: Life Technologies, Carlsbad, USA

Dispase: Sigma Aldrich, Steinheim, Germany

Hank's buffered saline solution (HBSS): Gibco by Life Technologies, Paisley, UK

Sodium azide: 10%, Thermo Fisher Scientific, Waltham, Massachusetts, USA

ACK lysing buffer: Gibco by Life Technologies, Paisley, UK

Digestion buffer: RPMI + 1% (v/v) FBS + 0.2 mg/mL collagenase-P + 0.1 mg/mL DNase-I + 0.6 mg/mL dispase

Hu FcR binding inhibitor purified (Fc block): eBioScience Inc., San Diego, USA

Purified anti-CD64 antibody: 0.5 mg/mL, clone X57-5/7.1, BioLegend, San Diego, USA

Propidium iodide (PI): Miltenyi Biotec GmbH, Bergisch Gladbach, Germany

Collection buffer: RPMI + 1% (v/v) FBS

Staining buffer: HBSS + 1% (v/v) FBS + 0.01% (v/v) sodium azide

Fc block mix: 39 µL staining buffer + 10 µL Fc block + 1 µL purified anti-CD64 antibody per staining

2.2.2. Preparation of murine organ single cell suspensions

Dissection of mice and organ removal were performed based on a previously published protocol (Julich-Haertel *et al.* 2017a). Mice were euthanized by using isoflurane followed by cervical dislocation. Subsequently, their abdomen was opened by a mid-line incision from caudal to cranial, followed by Y-incisions towards the limbs. The peritoneum was opened by a mid-line incision from caudal up to the sternum and the intestine was displaced to one side of the mouse. The gallbladder and all liver lobes were removed, while avoiding contamination of the liver tissue by the gallbladder. Subsequently, 1.5-2 cm of the distal colon next to the rectum were removed and were cleaned by repeated rinsing with HBSS. In order to extract the lung the thorax was opened by a mid-line incision and both lungs were removed. All organs were weighed after removal and kept in HBSS on ice until further processing. They were homogeneously cut into small pieces of approximately 2 mm size using a scalpel and the organ pieces were each transferred to separate 15 mL centrifugation tubes after cutting. Subsequently, 2.5 mL prewarmed digestion buffer were added and the tubes were placed in a 37 °C water bath. Tubes were shaken gently after 5, 10 and 15 min to detach and mix the pieces. After 22 min the cell suspensions were gently mixed with a cut 1000 µL pipette tip. Subsequently, the organ pieces were allowed to settle down. After 2 min the supernatant that contained the disseminated cells was transferred through a filter mesh (100 µm) into a fresh 15 mL centrifugation tube containing 3.5 mL of collection buffer and the suspension was kept on ice. The removed supernatant from the digestion tube was replaced with digestion buffer. The procedure of mixing, incubation, supernatant removal and supernatant replacement was repeated every 5 min until the organs were completely digested (typically 60 – 90 min). After the digest the collected cell suspensions were centrifuged at 180 × *g* for 8 min at 4 °C with reduced acceleration and deceleration of the centrifuge. The supernatant was discarded and the cell pellets were resuspended in 1 mL ACK lysing buffer for 1 min at RT to lyse erythrocytes. To stop the reaction, 5 mL of collection buffer were added and the cell suspensions were centrifuged again at 180 × *g* for 8 min at 4 °C with reduced acceleration and deceleration. After discarding the supernatant, cell pellets were resuspended in 3 mL collection buffer and were kept on ice until further processing.

2.2.3. Surface staining of murine single cells for flow cytometric analysis

Staining of murine tissue cells was performed based on a previously published protocol (Julich-Haertel *et al.* 2017a). All steps in this protocol were performed on ice. Depending on the available amount of isolated tissue cells for each organ, 3×10^5 (liver), 4×10^5 (lung), 10^5 (colon) or 10^4 (gallbladder) living cells were used for each staining. After determining the cell count (see 2.1.6 Cell counting), the respective volume for each staining was transferred to a 1.5 mL reaction tube and the cells were centrifuged at 300 × *g* for 3 min at 4 °C.

Tab. 2: Overview of antibodies for surface staining of murine organs. Listed are all used antibodies including information about antigen, conjugated fluorophor, host/isotype, vendor, catalog number, concentration and used dilution for the final staining mix of 100 µL. This table is part of the attached publication Urban *et al.* (2020) that resulted from this project. #: number, c: colon, conc.: concentration, g: gallbladder, li: liver, lu: lung, syr: syrian.

antibody (against mouse)	conjugate	host/isotype	vendor	catalog#	conc. [µg/µl]	dilution
CD45	APC-Cy7	Rat IgG2aκ	BioLegend	103116	0.2	1:200
CD31	AF488	Rat IgG2aκ	BioLegend	102406	0.5	1:200
CD31	PE-Cy7	Rat IgG2aκ	BioLegend	102524	0.2	1:200
gp38	APC	Syr. Hamster IgG	BioLegend	127410	0.2	1:1400
CD133	PE	Rat IgG1	Miltenyi	130-102-210	0.03	1:33
EpCAM	BV-421	Rat IgG2aκ	BioLegend	118225	0.2	1:400 (li) 1:800 (lu) 1:1000 (c) 1.3000 (g)
CD44	PE-Vio770	Rat IgG2bκ	Miltenyi	130-102-904	0.03	1:20 (li) 1:33 (c,g,lu)
Isotype	APC-Cy7	Rat IgG2aκ	BioLegend	400523	0.2	1:200
Isotype	AF488	Rat IgG2aκ	BioLegend	400525	0.5	1:200
Isotype	PE-Cy7	Rat IgG2aκ	BioLegend	400521	0.2	1:200
Isotype	APC	Syr. Hamster IgG	BioLegend	402012	0.2	1:1400
Isotype	PE	Rat IgG1	BioLegend	400407	0.2	1:220
Isotype	BV-421	Rat IgG2aκ	BioLegend	400535	0.05	1:100 (li) 1:200 (lu) 1:250 (c) 1:750 (g)
Isotype	PE-Vio770	Rat IgG2b	Miltenyi	130-103-091	0.03	1:20 (li) 1:33 (c,g,lu)

After discarding the supernatant, each cell pellet was resuspended in 50 µL Fc block mix and the cells were incubated for 5 min on ice. After the incubation 50 µL of diluted antibodies in staining buffer were added to each staining (Tab. 2) and cells were incubated for 15 min on ice in the dark. All antibodies were titrated against their corresponding isotype prior use and isotype dilutions were concentration-matched to the respective antibody. After antibody incubation, 400 µL of staining buffer were added to each staining and the cells were centrifuged at 300 × *g* for 3 min at 4 °C. Supernatant was discarded and the cells were resuspended in 200 µL staining buffer. For flow cytometric analysis, 6 µL of 1:8 PI in staining buffer were added to each staining and 180 µL of the solution were measured by a MACSQuant® Analyzer 10 (Miltenyi Biotec GmbH, Bergisch Gladbach, Germany). Data analysis was performed using the software FlowJo™ 10.7.1 (Tree Star Inc., Ashland, USA).

2.3. Human study cohort

Patient serum for this study was acquired from different Medical Centers throughout Europe. The study was approved by the ethics commissions of the State Chambers of Medicine in Rhineland-Palatinate, Germany (837.151.13 (8836-F); Saarland, Germany (167/11); San Sebastian, Spain (PI2014187); Warsaw, Poland (KB/41/A/2016 and AKB/145/2014) and Cluj-Napoca, Romania (3042/07.03.2018). All patients gave their informed consent to participate. Patients that had received chemotherapy or any other anti-tumor therapy before sample collection were excluded from the study as well as GbCA patients who underwent previous cholecystectomy. Characteristic patient parameters are summarized in Tab. 6, Tab. 16, Supplementary Tab. 1 and Supplementary Tab. 2.

2.4. Preparation of human serum

Human blood was collected in standard a S-Monovette® 7.5 mL, Serum Gel with Clotting Activator (Sarstedt AG & Co., Nümbrecht, Germany) and was allowed to coagulate for 30-60 min at RT. Subsequently, the Monovette was centrifuged at 1500 × *g* for 20 min at RT. The separated serum was collected, aliquoted into 1 mL fractions and stored at -80 °C until further processing.

2.5. Surface analysis of large extracellular vesicles from human serum

Isolation and staining of lEVs was performed based on a previously published protocol (Lukacs-Kornek *et al.* 2017). All involved reagents were either filtered (Steriflip^{TM}, 0.22 µm, Merck, Darmstadt, Germany) or centrifuged (20,000 × *g*, 60 min, 4 °C; supernatant collection) prior use to eliminate interfering protein aggregates or other contaminating particles. Unless stated otherwise, all steps in this protocol were performed on ice.

2.5.1. Reagents

Phosphate buffered saline (PBS): Sigma Aldrich, Steinheim, Germany; filtered

Hu FcR binding inhibitor purified (Fc block): eBioScience Inc., San Diego, USA; filtered

Bovine serum albumine (BSA): 10%, Miltenyi Biotec GmbH, Bergisch Gladbach, Germany; centrifuged

AnnexinV binding buffer: 10x, Miltenyi Biotec GmbH, Bergisch Gladbach, Germany; filtered

AnnexinV-FITC: Miltenyi Biotec GmbH, Bergisch Gladbach, Germany, filtered

Fc block mix: 11.5 µL PBS + 2.5 µL Fc block + 1 µL BSA for each staining

AnnexinV mix: 5 µL AnnexinV binding buffer + 5 µL AnnexinV-FITC for each staining

2.5.2. Isolation of large extracellular vesicles from human serum

After preparation and storage of human serum at -80 °C, the samples were thawed at RT and 1 mL of liquefied serum was transferred to a fresh 2 mL reaction tube. Serum was centrifuged at 2,000 × *g* for 30 min at 4 °C to eliminate larger vesicles and cellular debris. Subsequently, the supernatant (950 µL) was transferred to a fresh 2 mL reaction tube and was centrifuged at 20,000 × *g* for 30 min at 4 °C to pellet lEVs. The supernatant (850 µL) was carefully aspired and discarded. The remaining pellet was resuspended thoroughly in 300 µL PBS, filtered (100 µm pore size) and stored on ice or at -80 °C until further processing.

2.5.3. Surface staining of large extracellular vesicles from human serum for flow cytometric analysis

Freshly isolated lEVs were used for flow cytometric surface analysis. 50 µL of isolated lEVs were transferred to a fresh 1.5 mL reaction tube for each staining. 15 µL of Fc block mix were added to each staining and the samples were incubated for 60 min at 4 °C. After incubation 10 µL of Annexin mix were added to each staining and the samples were incubated for 30 min at 4 °C in the dark. Following this incubation, 25 µL of diluted antibodies in PBS were added to each staining (Tab. 3) and cells were incubated for 20 min at 4 °C in the dark. All antibodies were titrated against their corresponding isotype prior use and isotype dilutions were concentration-matched to the respective antibody.

Tab. 3: Overview of antibodies for surface staining of human serum large EVs. Listed are all used antibodies including information about antigen, conjugated fluorophor, host/isotype, vendor, catalog number, concentration and used dilution for the final staining mix of 100 µL. This table is part of the attached publication Urban *et al.* (2020) that resulted from this project. #: number, conc.: concentration, rec.: recombinant.

antibody (against human)	conjugate	host/isotype	vendor	catalog#	conc. [µg/µL]	dilution
gp38	PE-Vio770	rec. human IgG1 (REA)	Miltenyi	130-106-954	0.0055	1:1000
CD133	PE-Vio615	Mouse IgG2b	Miltenyi	130-107-453	0.011	1:100
EpCAM	VioBlue	Mouse IgG1κ	Miltenyi	130-097-324	0.0825	1:1000
CD44v6	APC	rec. human IgG1 (REA)	Miltenyi	130-111-425	0.1	1:1000
Isotype	PE-Vio770	rec. human IgG1 (REA)	Miltenyi	130-104-618	0.095	1:17000
Isotype	PE-Vio615	Mouse IgG2b	Miltenyi	130-108-348	0.0055	1:50
Isotype	VioBlue	Mouse IgG1κ	Miltenyi	130-094-670	0.055	1:660
Isotype	APC	rec. human IgG1 (REA)	Miltenyi	130-104-614	0.02	1:200

After antibody incubation, 100 µL of PBS were added to each staining and 150 µL were measured with the MACSQuant® Analyzer 10 (Miltenyi Biotec GmbH, Bergisch Gladbach, Germany). Data analysis was performed using the software FlowJo™ 10.7.1 (Tree Star Inc., Ashland, USA).

2.6. Surface analysis of small extracellular vesicles from human serum

Measurement of isolated sEVs from human patient serum was performed by the company NanoView Biosciences (Boston, USA), who provided the raw dataset for further analyses that are included in this thesis.

2.6.1. Reagents

Phosphate buffered saline (PBS): Sigma Aldrich, Steinheim, Germany; filtered (Steriflip™, 0.22 µm, Merck, Darmstadt, Germany)

Solution A: ExoView® Tetraspanin Kit, EV-TETRA-C, NanoView Biosciences, Boston, USA

Solution B: ExoView® Tetraspanin Kit, EV-TETRA-C, NanoView Biosciences, Boston, USA

Blocking Solution: ExoView® Tetraspanin Kit, EV-TETRA-C, NanoView Biosciences, Boston, USA

2.6.2. Isolation of small extracellular vesicles from human serum

Isolation of sEVs was performed by size exclusion chromatography columns (qEV2/35 nm, serial# 10611, Izon Science, Christchurch, New Zealand) in an automated fraction collector (Izon Science, Christchurch, New Zealand). The necessary steps were performed according to the manufacturer's protocol. Briefly, the column was equilibrated with PBS prior use. 1 mL of serum samples were loaded and after automatically discarding the initial 14 mL void volume, 13 2-mL-fractions were collected. Columns were used up to 5 times and were washed with PBS between the individual isolations. For long-term storage, the columns were washed with PBS + 0.05% sodium azide and were kept at 4 °C until the next isolation. The first 4 collected fractions of each isolation contained sEVs and were therefore pooled and concentrated to a total volume of 500 µL using filter spin columns (Amicon Ultra 3 kDa, Merck, Darmstadt, Germany) at 4000 × *g* for up to an hour at 4 °C. The concentrated fractions were stored at -80 °C until further processing.

2.6.3. Surface staining of small extracellular vesicles from human serum for ExoView® analysis

Surface analysis of sEVs was performed with the ExoView® R100 scanner (NanoView Biosciences, Boston, USA) using their ExoView® Tetraspanin Kit (EV-TETRA-C). The supplied ExoView® chips that were coated with CD81, CD63 and CD9 capture antibodies on their surface needed to be pre-scanned before loading them with the sEV samples. Isolated sEVs were thawed on ice and 35 µL were incubated either undiluted (for subsequent staining with CD133 and CD44v6) or diluted 1:750 in 1x solution A (for subsequent staining with CD81, CD63 and CD9) on the pre-scanned chip in a 24-well flat bottom plate for 16 h overnight at RT on a bench free of vibrations (one chip per patient). After incubation 1000 µL of 1x solution A was added and the plate was placed on an orbital shaker at 500 rpm for 3 min. Subsequently, 750 µL were removed and were replaced with fresh 750 µL of 1x solution A. This washing step was repeated three times in total. After the last wash, 750 µL were removed and 250 µL of diluted antibodies in Blocking Solution were added to the chip (Tab. 4). Antibodies were titrated prior use to ensure optimal performance.

Tab. 4: Overview of antibodies for surface staining of human serum small EVs. Listed are all used antibodies including information about antigen, conjugated fluorophor, host/isotype, vendor, catalog number, concentration and used dilution for the staining mix in 250 µL Blocking Solution. #: number, conc.: concentration, n.a.: not available, rec.: recombinant.

antibody (against human)	conjugate	host/isotype	vendor	catalog#	conc. [µg/µL]	dilution
CD81	CF® 555	n.a.	NanoView	EV-TETRA-C Kit	n.a.	1:600
CD63	CF® 647	n.a.	NanoView	EV-TETRA-C Kit	n.a.	1:600
CD9	CF® 488A	n.a.	NanoView	EV-TETRA-C Kit	n.a.	1:600
CD133	PE-Vio615	Mouse IgG2b	Miltenyi	130-107-453	0.011	1:10
CD44v6	APC	rec. human IgG1 (REA)	Miltenyi	130-111-425	0.1	1:50

The plate was placed on an orbital shaker at 500 rpm for 1h in the dark. After incubation, 500 µL of 1x solution A was added to increase the volume. Subsequently, 750 µL were removed and were replaced with fresh 750 µL of 1x solution A. The plate was placed on an orbital shaker at 500 rpm for 3 min in the dark. After removing 750 µL of the liquid,

750 µL of 1x solution B was added and the plate was placed on an orbital shaker at 500 rpm for 3 min in the dark. Washing with 1x solution B was repeated a total of three times. After removing 750 µL for the last time, 750 µL of deionized water was added to the chip and the plate was placed on an orbital shaker at 500 rpm for 3 min in the dark. Subsequently, each chip was individually transferred to a petri dish filled with deionized water. They were moved back and forth horizontally for washing using tweezers and were recovered from the water at a 45° angle, in order to let them dry on absorbent paper. Chips were now ready to be scanned with the ExoView® instrument. Data analysis was performed using the software ExoView® Analyzer 3.0 (NanoView Biosciences, Boston, USA).

2.7. Nanoparticle tracking analysis of large and small EVs

Large and small EVs were isolated as described in sections 2.5.2 and 2.6.2. Isolated EVs were diluted in filtered (0.22 µm) PBS to a particle count between 50 and 200 particles/position (typical dilutions ranged between 1:300 to 1:5000). They were mixed thoroughly and 1 mL of diluted EVs were injected into the chamber of the ZetaView S/N 17-333 (Particle Metrix, Meerbusch, Germany). Measurement was performed at 11 positions in 2 cycles regarding size distribution and particle concentration (sensitivity: 80, shutter: 70, min. brightness: 30, min. size: 5, max. size: 1000). The chamber was washed with 5 mL PBS between each measurement. Data analysis was performed using the software ZetaView Analyze 8.05.11 SP1 (Particle Metrix, Meerbusch, Germany).

2.8. Determining protein concentration of large and small EVs

The protein concentration of large and sEVs was determined by using the well-established bicinchoninic acid (BCA) assay that visualizes total protein concentration by a color change that can be measured with colorimetric techniques.

2.8.1. Reagents

RIPA buffer: Life Technologies, Carlsbad, USA

Halt™ Protease and Phosphatase Inhibitor Cocktail (100X): Thermo Fisher Scientific, Waltham, Massachusetts, USA

RIPA Lysis and Extraction Buffer: Thermo Fisher Scientific, Waltham, Massachusetts, USA

Pierce™ BCA Protein Assay Kit: Thermo Fisher Scientific, Waltham, Massachusetts, USA

2.8.2. Lysis of large and small EVs

Large and small EVs were isolated as described in sections 2.5.2 and 2.6.2. For determining the protein concentration, isolated EVs were lysed with RIPA Lysis and Extraction Buffer supplemented with 1:1000 Protease and Phosphatase Inhibitor Cocktail according to the manufacturer's specifications. Briefly, isolated EVs were mixed with RIPA buffer including protease phosphatase inhibitor in a 1:1 ratio and were incubated for 30 min on ice in the dark. Subsequently, samples were centrifuged at 11,000 × *g* for 15 min at 4 °C. The supernatant (lysate) was transferred to a fresh 1.5 mL reaction tube and either stored on ice or at -80 °C until further processing.

2.8.3. BCA assay of large and small EVs

Determination of the protein concentration of isolated and lysed EVs was performed by using the Pierce™ BCA Protein Assay Kit according to the manufacturer's specifications. Briefly, supplied BSA standard solutions were diluted in RIPA buffer according to the scheme and the supplied BCA Reagent A and BCA Reagent B solutions were mixed in a 50:1 ratio to obtain the working reagent. Subsequently, 25 µL of each standard and lysed EV sample was transferred to a 96-well flat bottom microplate in duplicates. 200 µL of the working reagent were added to each well containing either standard or sample and the plate was incubated for 30 min at 37 °C. After incubation absorbance at 562 nm was measured using the microplate reader Safire^2 (Tecan, Männedorf, Switzerland). Data analysis and calculation of protein concentration was performed using Microsoft Excel 2010 (Microsoft Corporation, Redmond, USA).

2.9. Liquid chromatography-mass spectrometry

Proteomic analysis of cell line-derived EVs by liquid chromatography-mass spectrometry (LC-MS) was performed by our collaboration partner Jesus M. Banales' team (Department of Liver and Gastrointestinal Diseases, Biodonostia Health Research Institute – Donostia

University Hospital, University of the Basque Country (UPV/EHU), San Sebastian, Spain). Samples were acquired and processed as described in a previous publication (Arbelaiz *et al.* 2017). Briefly, the separation of peptides was conducted on a nanoACQUITY UPLC System (Waters Corporation, Milford, USA) connected to an LTQ Orbitrap XL mass spectrometer (Thermo Electron, Waltham, USA). Differential protein expression analysis was conducted with Progenesis LC-MS 4.0 (Nonlinear Dynamics, Newcastle upon Tyne, United Kingdom) and database searches were performed with Mascot search engine 2.1 (Matrix Science, London, United Kingdom). Significance of protein expression changes was tested by analysis of variance (ANOVA) and proteins not satisfying the criteria $p \leq 0.01$ and ratio>2 in either direction were filtered out. Heatmaps were generated with Perseus 1.6 (Max Planck Institute of Biochemistry, Martinsried, Germany).

2.10. Data processing and statistical analysis

All primary data were initially processed with the software indicated in the individual Material and Methods sections. For further data processing and handling of large datasets Microsoft Excel 2010 (Microsoft Corporation, Redmond, USA) was used. Statistical analysis of processed data and creation of graphs was performed with GraphPad Prism 8.0.2 (GraphPad Software, San Diego, USA). Multiple groups (>2) were compared by Kruskal-Wallis non-parametric tests followed by Dunn's multiple comparison post hoc tests, whereas two individual groups were compared by two-tailed Mann-Whitney *U* tests. The corresponding test is indicated in each individual figure legend. Correlations were analyzed by Spearman's rank correlation coefficient in GraphPad Prism. Overall, a *p*-value ≤0.05 was considered statistically significant with $p \leq 0.05$ = *, $p \leq 0.01$ = **, $p \leq 0.001$ = *** and $p \leq 0.0001$ = ****. Diagnostic benchmarks were calculated using GraphPad Prism and Microsoft Excel. Fluorescent images were processed with the free Java-based image processing program ImageJ (National Institutes of Health, Bethesda, USA) and the free and open-source raster graphics editor GIMP 2.8.14. Schematic flowcharts and images were created with BioRender.com as indicated in the individual figure legends. Final figures were prepared with the free and open-source vector graphics editor Inkscape 0.91.

3. Results

The study at hand is separated into three main parts. First, the identification and verification of potential protein biomarkers for EV surface profiling is described. Next, the diagnostic benefit of large EVs with the chosen surface markers and combinations thereof for differential hepatobiliary cancer diagnosis is assessed. Likewise, the diagnostic benefit of small EVs harboring the same surface markers will be investigated in a final evaluation.

3.1. Selecting protein biomarkers for differential hepatobiliary cancer diagnosis

Some proteins on the surface of EVs have been shown to be potent biomarkers for cancer diagnosis (Melo *et al.* 2015, Abbate *et al.* 2017, Julich-Haertel *et al.* 2017b). Additionally, considering the heterogeneity of cancer entities and EV subtypes, it was proposed that instead of investigating only a single marker on the surface of EVs, a combination of several surface antigens on the same EV could lead to higher specificity in terms of differential cancer diagnosis (Urban *et al.* 2018). Therefore, several candidate markers and combinations thereof were screened for this study.

After extensive literature research and consideration of our group's previously published results on lEV-based hepatic cancer diagnosis (Julich-Haertel *et al.* 2017b) that laid the groundwork for this study, epithelial cell adhesion molecule (EpCAM, CD326) and prominin-1 (CD133) were chosen as the first candidate proteins. EpCAM is considered to be one of the most frequently investigated tumor-associated surface antigens known (Baeuerle and Gires 2007). It can be found in a great variety of human epithelial tissues, cancers (including hepatobiliary cancers) as well as in progenitor and stem cells (Prince *et al.* 2008, Munz *et al.* 2009, Yamashita *et al.* 2009, Sulpice *et al.* 2014). Likewise, CD133 is well-established as the most frequently used marker for stem cells and cancer stem cells. It can be found on a wide variety of solid tumors including hepatobiliary cancers (Shi *et al.* 2011, Cai *et al.* 2018, Glumac and LeBeau 2018). Furthermore, CD133 was discovered, in conjunction with podoplanin (gp38), on a subset of liver progenitor cells that have bipotential differentiation capacity and are therefore able to differentiate into either hepatocytes or cholangiocytes (Eckert *et al.* 2016). Therefore, gp38 was included as a candidate marker for this study as well. Another marker of interest was CD44 variant 6 (CD44v6). It can be found in several types of cancers including hepatobiliary carcinomas (Yanagisawa *et al.* 2001, Mima *et al.* 2012, Gu and Jang 2014) and is the most prominent

marker on cancer-initiating cells (CICs) that are responsible for tumor progression and metastasis (Wang *et al.* 2018b). Additionally, CD44v6 was found to be involved in vesicle loading of EVs, underlining the potential importance of the protein in this diagnostic EV study (Wang *et al.* 2018b). A detailed description of the chosen markers in relation to their suitability for differential hepatobiliary cancer diagnosis can be found in the discussion of this thesis.

In a first marker verification step, expression levels of the selected candidate markers EpCAM, CD133, gp38 and CD44v6 were compared *in vitro* on human hepatobiliary tumor cell lines. Unfortunately, no human gallbladder carcinoma (GbCA) cell lines were commercially available at the time this study was conducted, so the analysis was limited to hepatocellular carcinoma (HCC) and cholangiocarcinoma (CCA) cell lines for this line of experiments. Three HCC (HuH7, HepG2 and Hep3B) and three CCA tumor cell lines (TFK-1, EGI-1 and CCC-5) were chosen and their surface protein levels were analyzed by flow cytometry. With these experiments the question was addressed, if the individual markers are expressed on different tumor entities and if they already showed a differential expression pattern on this cellular level *in vitro*. The cells were cultured for several days as described in the Material and Methods section. After growing the cells without FBS for 16-24 h, they were harvested and subsequently stained with antibodies against the selected markers. For flow cytometric measurement a proper gating strategy needed to be established for every cell line and is exemplarily depicted for HuH7 cells (Fig. 4A). In brief, after excluding debris, the analysis was restricted to single cells by comparing signal area (FSC-A) and height (FSC-H). Single cells show a proportional area to height ratio and can thus be separated from cell clusters that display an increased signal area with only slightly enhanced or unchanged signal height. In a following step, the analysis was restricted to living cells. This was achieved by propidium iodide (PI) staining before measurement. PI is a widely used dead cell dye that enters dead cells through holes in the degrading plasma membrane and intercalates into the DNA. Thus, dead cells show a positive signal during flow cytometeric analysis. Cells that were not stained with PI prior to measurement served as negative controls to identify the living cells population. Next, the antibodies against the candidate markers needed to be verified and the proper concentration needed to be titrated on each cell line.

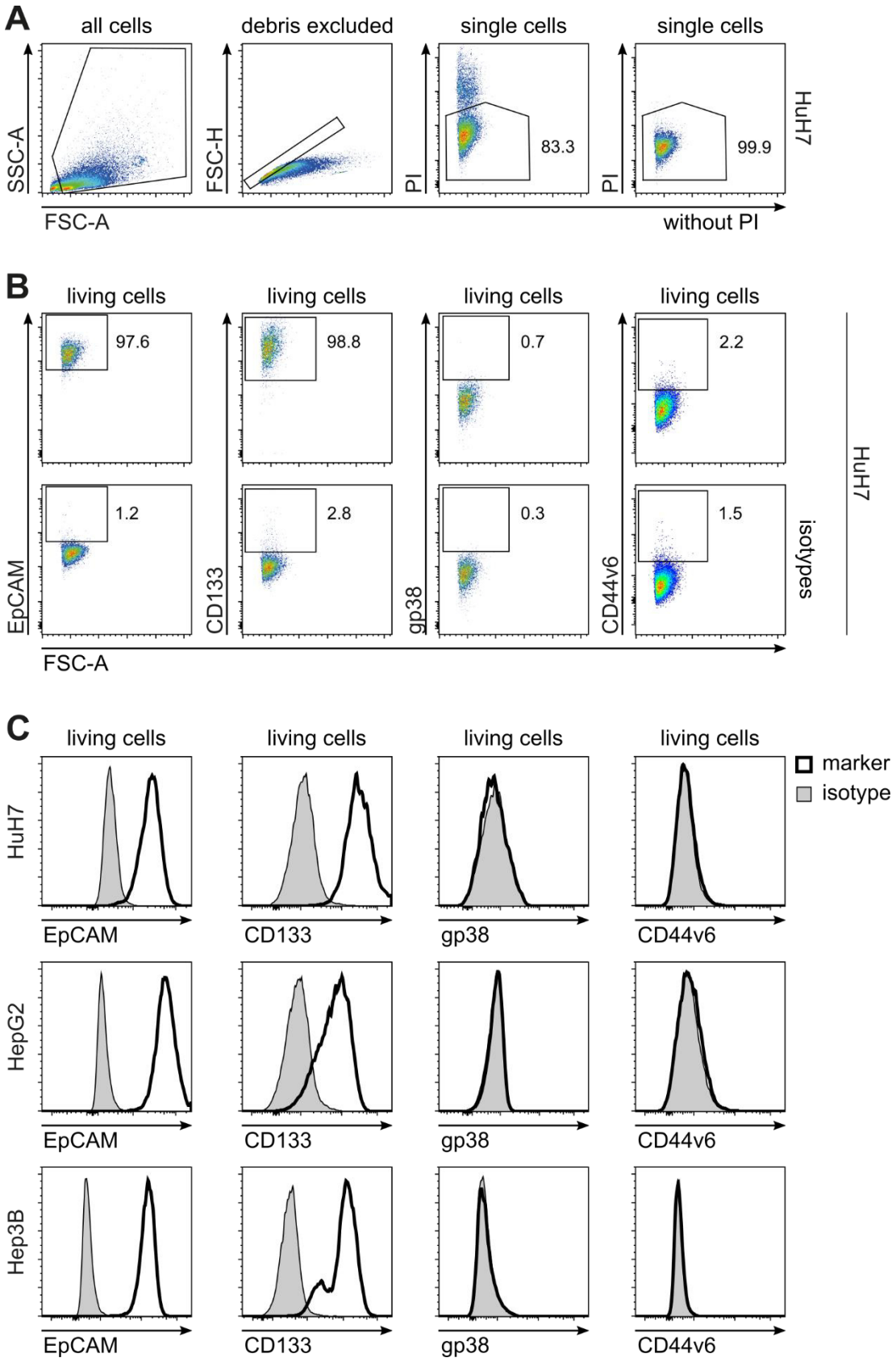

Fig. 4: Candidate markers are differentially expressed on human HCC cell lines. After starving cells from the commercial HCC cell lines HuH7, HepG2 and Hep3B for

16-24 h, cells were harvested and fluorescently stained with antibodies against the candidate markers EpCAM, CD133, gp38 and CD44v6. All depicted dot plots and histograms are representative of at least three independent experiments. **A** The general successive gating strategy applied to all HCC cell lines for flow cytometric analysis is exemplarily depicted for HuH7 cells. After excluding cellular debris and unwanted cell clusters, propidium iodide (PI) was used for dead cell exclusion. Cells without PI staining served as negative controls to identify living cells. Numbers indicate percentage of parent population (single cells). **B** Representative dot plots for each candidate marker (upper panel) and their corresponding isotype controls (lower panel) are exemplarily depicted for HuH7 cells. Numbers indicate percentage of parent population (living cells). **C** shows exemplary histograms of surface expression for each marker as compared to their corresponding isotype control for all three HCC cell lines. The panels **A** and **B** are part of the attached publication Urban *et al.* (2020) that resulted from this project. A: area, FSC: forward scatter, H: height, SSC: sideward scatter.

In Fig. 4B single antibody stainings with their corresponding isotype controls are exemplarily shown for each marker on HuH7 cells. Isotype concentrations were matched to the respective antibody concentrations. The used dilutions for each antibody and cell line can be found in Tab. 1. In Fig. 4C exemplary histograms displaying the marker profile for each HCC cell line (HuH7, HepG2 and Hep3B) are depicted. All three cell lines show a high expression of EpCAM and CD133, whereas the expression of gp38 and CD44v6 is negligible.

The same experimental settings that were used for human HCC cell line expression analysis were applied to the three human CCA cell lines TFK-1, EGI-1 and CCC-5. As described for HCC cell lines, Fig. 5A exemplarily depicts the successive gating strategy applied to all CCA cell lines for TFK-1 cells. Furthermore, single antibody stainings with their concentration-matched isotype controls are exemplarily shown for TFK-1 cells in Fig. 5B, and the candidate marker profile for each CCA cell line is visualized in Fig. 5C. The used dilutions for each antibody and cell line can be found in Tab. 1. In contrast to HCC cell lines, all CCA cells show a high expression of EpCAM and CD44v6. Only EGI-1 cells display increased CD133 expression, whereas, similar to HCC cells, all CCA cell lines show no gp38 expression.

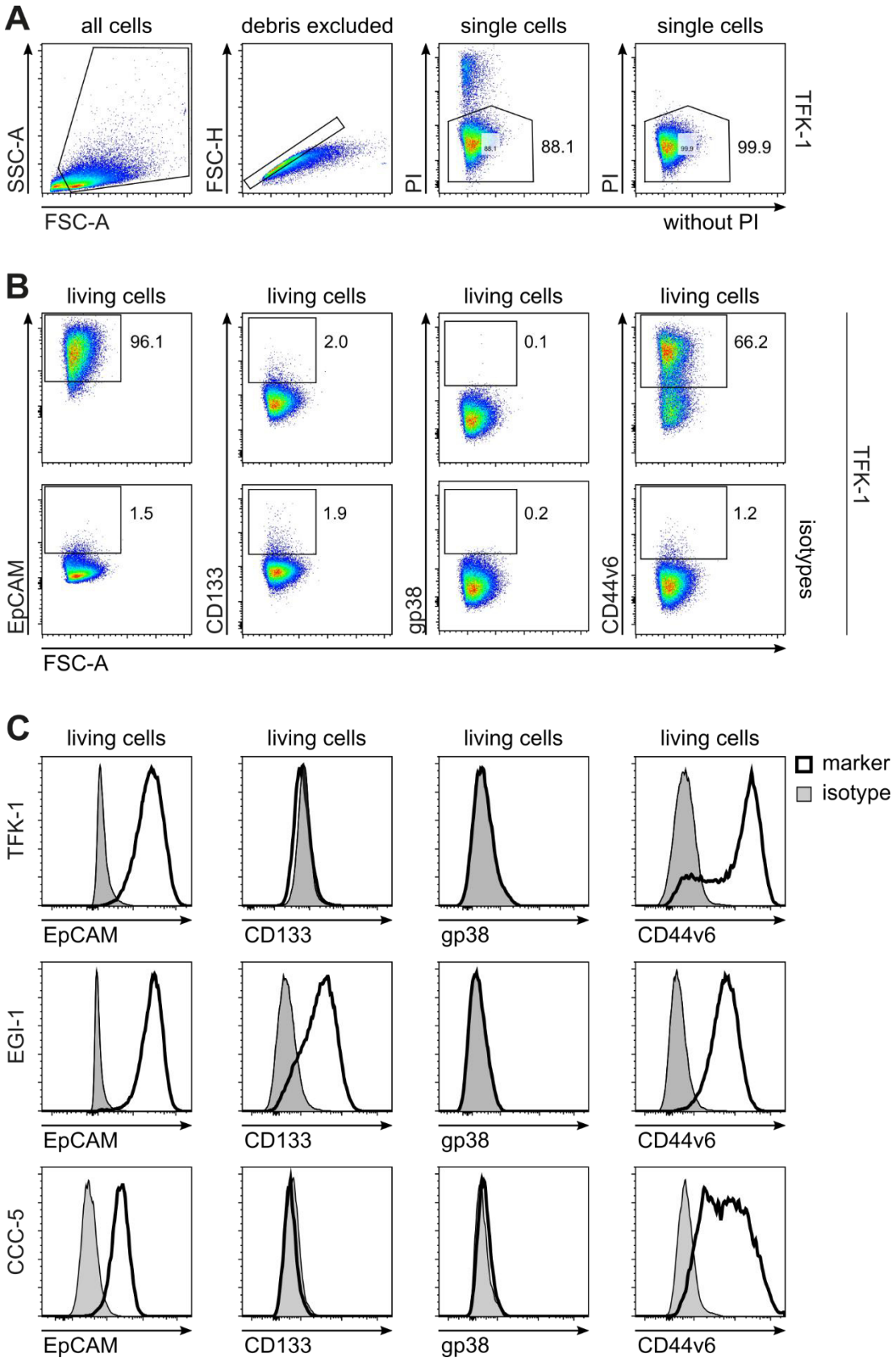

Fig. 5: Candidate markers are differentially expressed on human CCA cell lines. After starving cells from the commercial CCA cell lines TFK-1, EGI-1 and CCC-5 for

16-24 h, cells were harvested and fluorescently stained with antibodies against the candidate markers EpCAM, CD133, gp38 and CD44v6. All depicted dot plots and histograms are representative of at least three independent experiments. **A** The general successive gating strategy applied to all CCA cell lines for flow cytometric analysis is exemplarily depicted for TFK-1 cells. After excluding cellular debris and unwanted cell clusters, propidium iodide (PI) was used for dead cell exclusion. Cells without PI staining served as negative controls to identify living cells. Numbers indicate percentage of parent population (single cells). **B** Representative dot plots for each candidate marker (upper panel) and their corresponding isotype controls (lower panel) are exemplarily depicted for TFK-1 cells. Numbers indicate percentage of parent population (living cells). **C** shows exemplary histograms of surface expression for each marker as compared to their corresponding isotype control for all three CCA cell lines. A: area, FSC: forward scatter, H: height, SSC: sideward scatter.

In Fig. 6 the surface expression profiles of all candidate markers and tumor cell lines are summarized. For this analysis all obtained individual values for HCC and CCA cell lines were combined into one cohort, respectively. EpCAM, as an established epithelial cancer marker, shows high expression in all six tumor cell lines, whereas gp38 cannot be identified on any of the investigated cell lines (Fig. 6A). However, CD133 is almost exclusively expressed on HCC cell lines, whereas CD44v6 is limited to CCA cell lines, indicating possible differential capabilities of these markers. Statistical analysis revealed that except for gp38 all markers were expressed differentially on HCC and CCA cell lines with high significance (Fig. 6B). Even though statistic testing revealed that EpCAM expression is significantly different between HCC and CCA cell lines, the differentiation potential of this marker seems to be rather low, when taking into account that EpCAM expression is very high in both entities (>94% in both cases) and that it is accompanied by stable standard errors. CD133 on the other hand shows an enhanced expression in HCC cell lines as compared to CCA cell lines by 6.7-fold ($p \leq 0.0001$), whereas CD44v6 is increased by 5.0-fold ($p \leq 0.0001$) in CCA cell lines as compared to HCC cell lines. These significant differences in CD133 and CD44v6 expression between HCC and CCA hint at their promising differentiation potential for the two entities in further experiments.

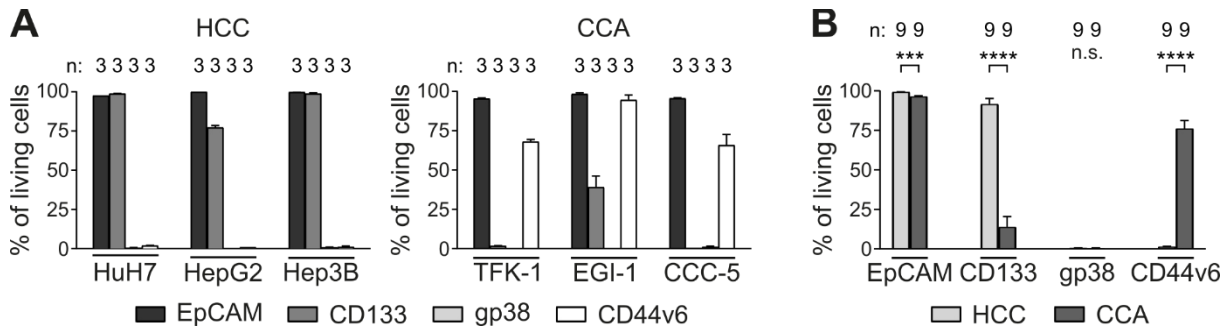

Fig. 6: Human HCC and CCA cell lines show differential expression patterns of the candidate markers. After starving cells from HCC (HuH7, HepG2, Hep3B, each n=3) and CCA (TFK-1, EGI-1, CCC-5, each n=3) cell lines for 16-24 h, cells were harvested and fluorescently stained with antibodies against the candidate markers EpCAM, CD133, gp38 and CD44v6. Surface expression of the markers among living cells was analyzed by flow cytometry and is shown as means with standard error of the mean (SEM) for each HCC and CCA cell line individually (**A**) and for HCC and CCA cell lines combined, respectively (**B**, each n=9). n indicates number of independent replicates. A two-tailed Mann-Whitney *U* test was performed with $p \leq 0.05$ considered statistically significant (* = $p \leq 0.05$, ** = $p \leq 0.01$, *** = $p \leq 0.001$, **** = $p \leq 0.0001$). This figure is part of the attached publication Urban *et al.* (2020) that resulted from this project. n.s.: non-significant.

The results obtained from these *in vitro* tumor cell line experiments were supported by an existing dataset on EVs derived from tumor cell lines and non-malignant primary cells that was already partly published at that time (Arbelaiz *et al.* 2017). Upon request, the team around our collaboration partner Jesus M. Banales kindly analyzed their dataset for the candidate markers and provided us with the results (Fig. 7).

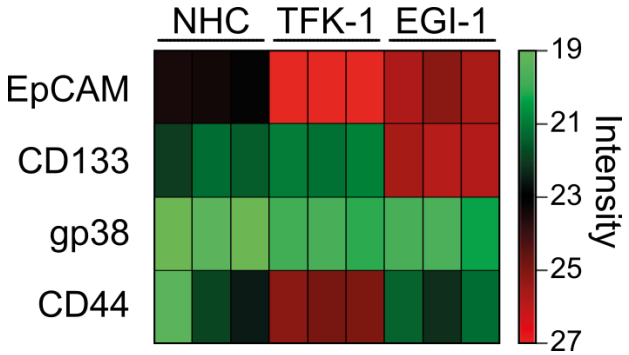

Fig. 7: Heatmap of proteomic data of cell line-derived EVs. EVs from the CCA cell lines EGI-1 and TFK-1 and from normal human cholangiocytes (NHC) were isolated and analyzed with liquid chromatography-mass spectrometry (LC-MS). The abundance (green: low, black: middle, red: high) of the four candidate markers EpCAM, CD133, gp38 and CD44 in and on EVs is depicted. The corresponding statistics can be found in Tab. 5. This figure is part of the attached publication Urban *et al.* (2020) that resulted from this project. The dataset was kindly provided by our collaboration partner Jesus M. Banales.

In brief, EVs were isolated from two human CCA tumor cell lines (TFK-1 and EGI-1) and from normal human primary cholangiocytes (NHC). Their proteomic content and surface composition were analyzed by liquid chromatography-mass spectrometry (LCMS) and the abundance of EpCAM, CD133, gp38 and CD44 was visualized in a heatmap. Expression levels of the markers in TFK-1- and EGI-1-derived EVs were compared to that in NHC-derived EVs and their statistical differences were assessed (Tab. 5). Unfortunately, the analysis of variants of CD44 was not possible retrospectively, so instead of CD44v6 CD44 was included in the evaluation.

Tab. 5: Quantitative protein expression analysis in EVs from CCA cell lines (TFK-1 and EGI-1) as compared to normal human cholangiocytes (NHC). Relative protein quantification and comparison was conducted with the software Progenesis. Only proteins identified with at least two different peptides were included in the evaluation. In order to analyze the significance of the differential results, a *t*-test was performed. This table is part of the attached publication Urban *et al.* (2020) that resulted from this project. The dataset was kindly provided by our collaboration partner Jesus M. Banales. Blue: ratio≥2, green: $p \leq 0.05$, n.a.: not available.

	TFK-1/NHC		EGI-1/NHC	
marker	***p* value**	**ratio**	***p* value**	**ratio**
EpCAM	**3.11×10^{-6}**	**14.89**	**3.17×10^{-4}**	**4.61**
CD133	8.78 E-02	1.50	**6.36×10^{-5}**	**18.19**
gp38	n.a.	n.a.	n.a.	n.a.
CD44	**1.71×10^{-2}**	**9.81**	7.34 E-01	0.96

In accordance with the results from CCA tumor cell lines, EpCAM was significantly more abundant in both TFK-1- and EGI-1-derived EVs by 14.89- and 4.61-fold, respectively, as compared to NHC-derived EVs (compare Fig. 6A, right panel). CD133 was only found to be significantly more abundant in EGI-1-derived EVs by 18.19-fold and was barely enhanced in TFK-1-derived EVs, which also corresponds to the findings on CCA tumor cell lines. CD44 on the other hand was only significantly increased in TFK-1-derived EVs by 9.81-fold and in contrast to the results obtained on CCA tumor cell lines in this thesis, it could barely be detected in EGI-1-derived EVs, which might be caused by the differences in CD44 variants used for the two analyses. Gp38 could not be detected in any evaluated EVs, which concurs with the findings on CCA tumor cell lines.

3.1.1. Identifying possible parental cell populations for EVs in mouse organs

In the course of this study, a multitude of combinations of the candidate markers as well as their single expression on EVs were analyzed in terms of their hepatobiliary differentiation potential. Only the combinations that resulted in meaningful diagnostic separation by EVs are presented in this thesis later on, hence, only the physiological verification of these populations of interest is included in the section at hand.

After investigating the individual expression profiles of the candidate markers on human tumor cells and tumor-derived EVs, the existence of possible physiological cell populations acting as EV-releasing parental cells was evaluated. Since EVs reflect the (surface) composition of their parental cells, cell populations presenting the same markers as EVs could potentially be the cells of origin for these particular EVs. Consequently, in order to identify an EV-based diagnostic biomarker for a specific type of cancer, it is reasonable to evaluate EVs from cells that are associated with the development or progression of this particular cancer in the first place. Therefore, the existence of physiological cell populations that have either been proposed as putative cells of cancer origin or that are involved in tumor progression was investigated in murine liver, gallbladder and other organs *in vivo*. Of note, the following selection of cell populations and their nomenclature is based on an attempt of the author to logically structure the obtained results and to facilitate easier understanding for the reader. The classification only partially reflects the cellular origin or function of the markers and is not to be understood as a strict distinction. The selection of markers and their relation to each other and to putative cells of cancer origin will be elaborated extensively in the discussion of this thesis.

In short, it has been proposed that tissue-specific progenitor cells within one organ can give rise to different cancer subtypes (Banales *et al.* 2020). Accordingly, liver progenitor cells are capable of differentiating into hepatocytes or cholangiocytes and thus might be involved in the development of both HCC and CCA (Rountree *et al.* 2007, Dorrell *et al.* 2011). Recently, a subset of $CD133^+gp38^+$ liver progenitor cells has been described, that was additionally associated with high EpCAM expression (Eckert *et al.* 2016). Therefore, the existence of $CD133^+gp38^+$ and $EpCAM^+CD133^+gp38^+$ subsets was chosen to be investigated. Owing to their progenitor cell origin, these two specific marker combinations will from now on be referred to as “progenitor cell-associated” throughout this thesis. On

the other hand, CD44v6 has been discovered not only as a marker for cancer stem cells but also as a functionally important protein for tumor progression and metastasis (Wang *et al.* 2018b). Additionally, CD44v6 alone and in conjunction with CD133 has been demonstrated to be associated with poor prognosis in several cancers (Chen *et al.* 2014, Wang *et al.* 2018b, Padthaisong *et al.* 2020). Hence, the existence of $CD44v6^+$ and $CD44v6^+CD133^+$ subsets as potential parental cells for EVs was chosen to be investigated in murine organs. According to their involvement in tumor progression and prognosis, these two specific marker combinations will be referred to as “tumor-associated” throughout this thesis.

First, several wild type C57Bl/6J mouse organs were enzymatically digested to single cell suspensions and were subsequently immunofluorescently labelled with a panel of antibodies for flow cytometric evaluation. Antibodies against murine CD45 and CD31 were part of every staining, whereas antibodies against CD133, gp38 and EpCAM were added for analysis of progenitor cell-associated populations and antibodies against CD44 and CD133 were included for analyzing tumor-associated subsets. Unfortunately, no antibody against the splice variant CD44v6 was available to the author that was suitable for flow cytometric analysis in mice, so an antibody against the murine standard form CD44 was employed instead. The investigated murine organs included liver and gallbladder representing origins for HCC, CCA and GbCA, as well as lung and colon as control organs. For flow cytometric measurement, successive gating strategies for every organ were established based on the strategy described for identifying liver progenitor cells (Eckert *et al.* 2016) (Fig. 8A-D). Briefly, similar to analyzing tumor cell lines *in vitro*, debris and cell clusters were first excluded, followed by restricting the analysis to living cells by performing a live/dead cell staining with PI. Out of the living cells, nucleated hematopoietic and endothelial cells were excluded according to their high CD45 and CD31 expression profile, respectively. For analyzing progenitor-associated subsets, mesothelial cells were additionally excluded based on their high gp38 expression. The two parental populations that served as starting point for subsequent analyses of progenitor cell-associated (mesothel excluded, $CD45^-CD31^-gp38^{lower}$) and tumor-associated populations (endothel excluded, $CD45^-CD31^-$) are described in Fig. 8E and will be clearly indicated in every individual figure legend.

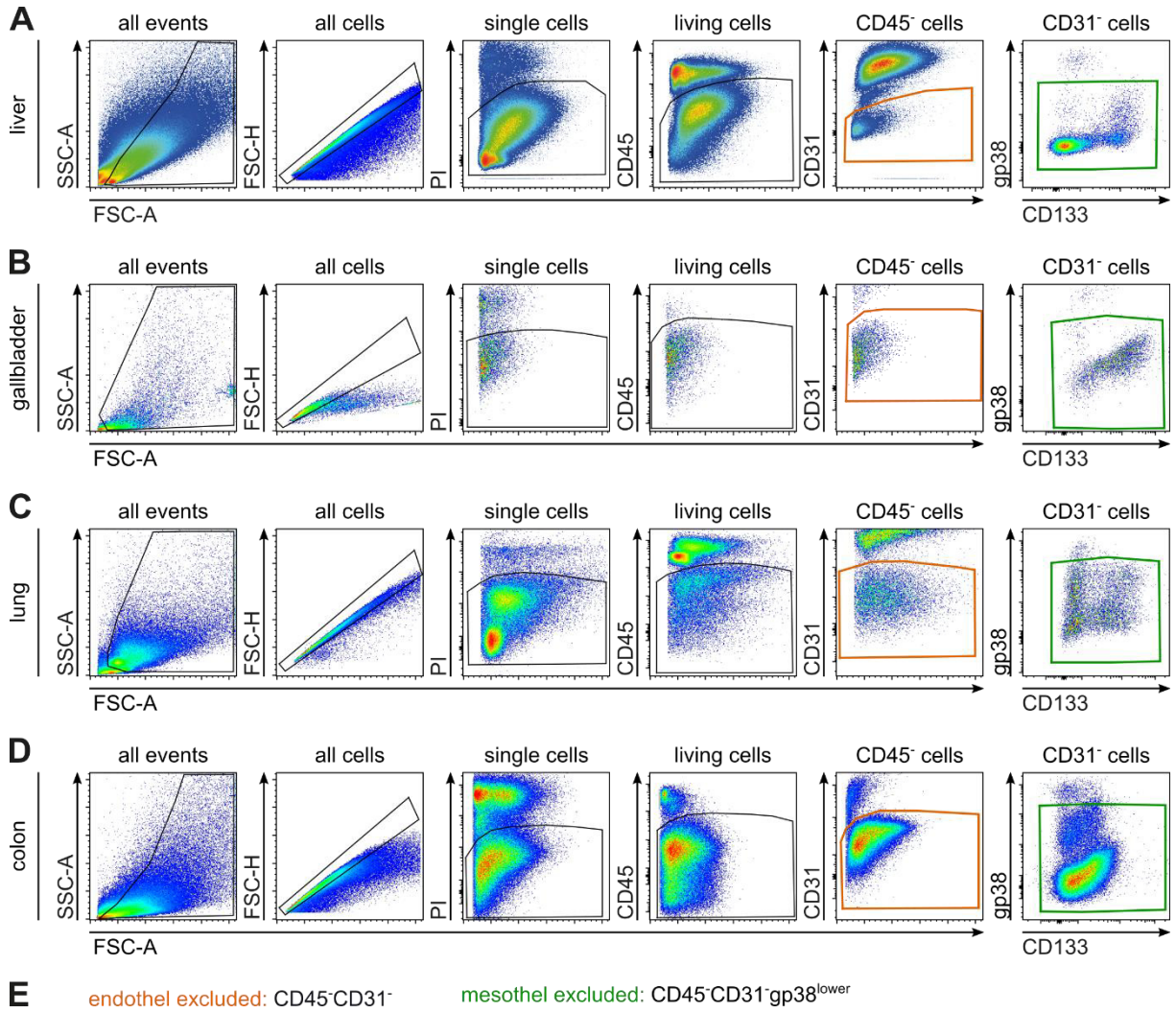

Fig. 8: Gating strategy for several wild type mouse organs. Liver, gallbladder, lung and colon of wild type C57Bl/6J mice were isolated and enzymatically digested to single cell suspensions. For flow cytometry, cells were stained with antibodies against the surface markers CD45 and CD31. For analysis of progenitor cell-associated populations, gp38, CD133 and EpCAM were added to the general antibody mix, whereas CD44 and CD133 were included for analysis of tumor-associated populations. The general successive gating strategy for murine liver (**A**), gallbladder (**B**), lung (**C**) and colon (**D**) is exemplarily depicted. After exclusion of cellular debris and cell clusters, propidium iodide (PI) was used for dead cell exclusion to identify living cells. Subsequently, hematopoietic ($CD45^+$), endothelial ($CD31^+$) and mesothelial ($gp38^{high}$, progenitor cell-associated populations only) cells were excluded. All depicted dot plots are representative of three independent experiments. **E** describes the two parental populations used for subsequent identification of progenitor cell-associated (mesothel excluded, green) and tumor-associated populations (endothel excluded, orange). Parental populations are indicated above the respective scatter plots for each organ in A-D. Panel **A** is part of the attached publication Urban *et al.* (2020) that resulted from this project. A: area, FSC: forward scatter, H: height, SSC: sideward scatter.

For identification of progenitor cell-associated populations, the general gating strategy was expanded by separating the cells according to their gp38 and CD133 expression profile (Fig. 9A). Single $CD133^+$ and $gp38^+$ as well as double positive $CD133^+gp38^+$ and double negative $CD133^-gp38^-$ cells are exemplarily visualized alongside the corresponding isotype controls for each organ. Double positive $CD133^+gp38^+$ cells were additionally tested for EpCAM positivity and their expression compared to the corresponding isotype control is depicted in exemplary histograms for every organ (Fig. 9B). In order to ensure optimal performance of all used antibodies, they were titrated prior use. All isotype concentrations were matched to the respective antibody concentrations. The used dilutions for each antibody and organ can be found in Tab. 2. Interestingly, the surface analysis revealed no $CD133^+$ cells in the colon, consequently, no double positive $CD133^+gp38^+$ or triple positive $EpCAM^+CD133^+gp38^+$ cells could be detected. All other organs showed the presence of double positive $CD133^+gp38^+$ and triple positive $EpCAM^+CD133^+gp38^+$ cells in varying degrees. These findings are reflected in the relative surface expression analysis of three independent experiments of the double and triple positive populations in all investigated organs (Fig. 9C). In order to ensure the comparability among both cell populations, for this relative expression analysis the indicated numbers are relative to the same parental population (mesothel excluded) for both investigated populations (in contrast to the histograms shown in Fig. 9B that display EpCAM positivity out of $CD133^+gp38^+$ cells). It is noticeable that the two populations are expressed in similar levels on the gallbladder, whereas $CD133^+gp38^+$ cells in liver and lung are increased by approximately 2-fold as compared to $EpCAM^+CD133^+gp38^+$ cells. Statistical analysis by Kruskal-Wallis non-parametric test followed by Dunn's multiple comparison post hoc test revealed a significantly higher level of $EpCAM^+CD133^+gp38^+$ cells in gallbladder as compared to the colon ($p \leq 0.05$). All other differences within either $CD133^+gp38^+$ or $EpCAM^+CD133^+gp38^+$ cells were non-significant with $p > 0.5$. Additionally, within each organ, no statistically significant differences could be observed between the abundance of $CD133^+gp38^+$ and $EpCAM^+CD133^+gp38^+$ cells, as tested by two-tailed Mann-Whitney *U* tests.

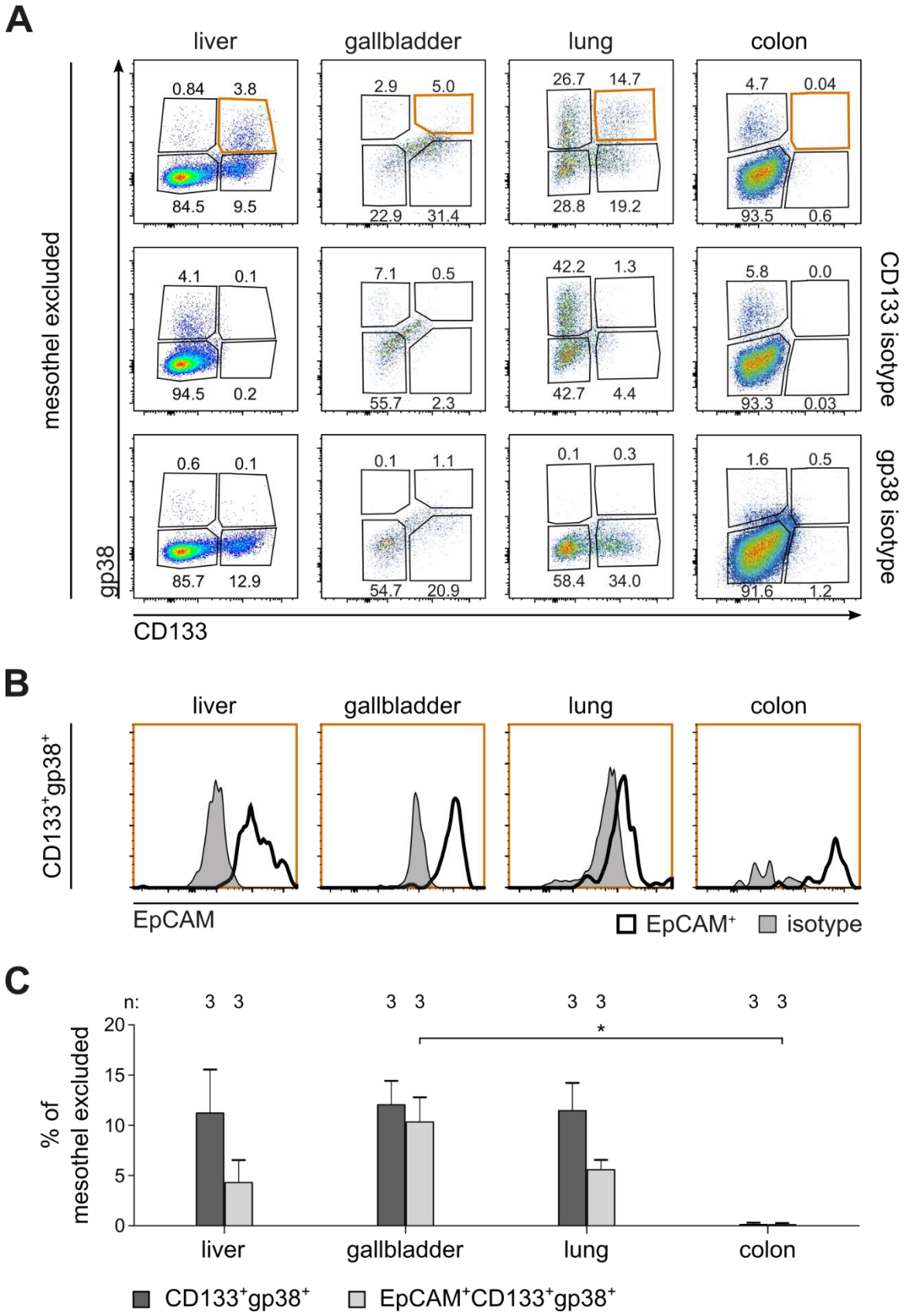

Fig. 9: Progenitor cell-associated population profiles on mouse organs. Liver, gallbladder, lung and colon of wild type C57Bl/6J mice were isolated and enzymatically

digested to single cell suspensions. For flow cytometry, cells were stained with antibodies against the surface markers CD45, CD31, CD133, gp38 and EpCAM. The general gating strategy described in Fig. 8 was applied to all organs. All depicted dot plots and histograms are representative of three independent experiments. **A** The surface marker expression of $CD133^+$, $gp38^+$, $CD133^+gp38^+$ double positive and $CD133^-gp38^-$ double negative cells for each organ (top panel) is shown alongside the isotype controls for CD133 (middle panel) and gp38 (bottom panel). The numbers indicate the percentage relative to the parent population (mesothel excluded). In **B** the double positive $CD133^+gp38^+$ population (highlighted in orange) was additionally tested for EpCAM positivity (white) and compared to its corresponding isotype control (grey) in each organ. **C** summarizes the relative surface expression of the two progenitor cell-associated populations $CD133^+gp38^+$ and $EpCAM^+CD133^+gp38^+$ with "mesothel excluded" serving as parent population for both combinations. The graph shows means with standard error of the mean (SEM) with n=3 for each organ and population, respectively. Statistical significance within the individual populations was assessed by Kruskal-Wallis non-parametric test followed by Dunn's multiple comparison post hoc test, whereas statistical significance within the individual organs was assessed by two-tailed Mann-Whitney *U* tests (* = $p \leq 0.05$, ** = $p \leq 0.01$, *** = $p \leq 0.001$, **** = $p \leq 0.0001$). The panels **A** and **B** are part of the attached publication Urban *et al.* (2020) that resulted from this project.

The same experimental settings that were employed to identify progenitor cell-associated populations were applied to visualize the tumor-associated populations $CD44^+$ and $CD44^+CD133^+$. Here, $CD45^-CD31^-$ cells (endothel excluded) served as parental populations for both combinations. After applying the general gating strategy presented in Fig. 8, cells were first tested for CD44 positivity (Fig. 10A). In order to identify double positive $CD44^+CD133^+$ populations, the cells were subsequently separated based on the expression of these two markers (Fig. 10B). In order to ensure optimal performance of all used antibodies, they were titrated prior use. All isotype concentrations were matched to the respective antibody concentrations. The used dilutions for each antibody and organ can be found in Tab. 2. Single positive $CD44^+$ cells could be detected in low levels in all organs. In contrast to that, double positive $CD44^+CD133^+$ cells were identified in varying degrees in all organs, except for the colon. These findings are reflected in the relative surface expression of three independent experiments of the single and double positive populations in all investigated organs (Fig. 10C). It is noticeable that the expression profiles of liver and gallbladder look similar, with $CD44^+$ cells being increased by approximately 2-fold as compared to $CD44^+CD133^+$ cells. In lung on the other hand, the abundance of both cell populations is generally lower, with $CD44^+$ cells being increased by approximately 4.5-fold as compared to $CD44^+CD133^+$ cells.

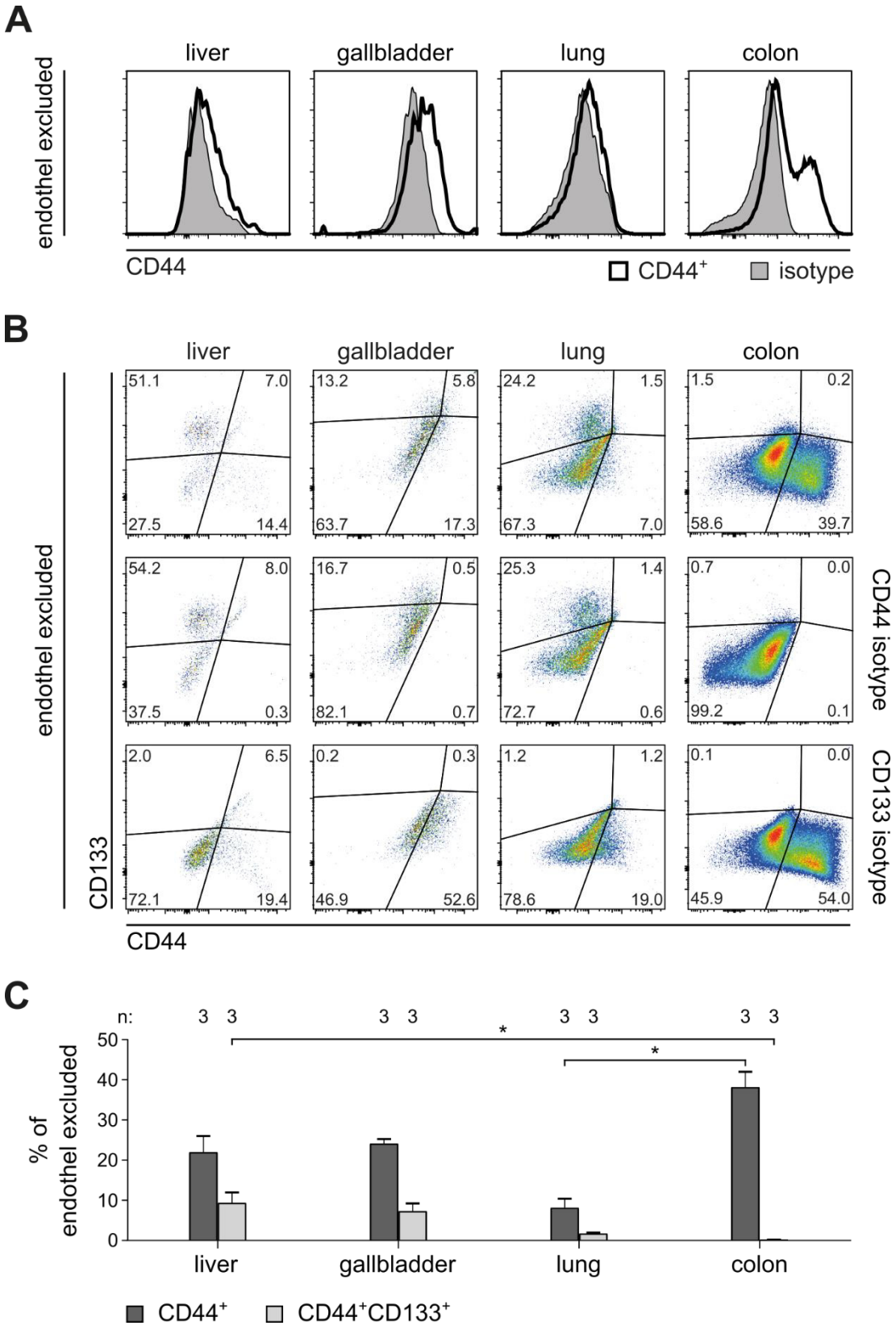

Fig. 10: Tumor-associated population profiles on mouse organs. Liver, gallbladder, lung and colon of wild type C57Bl/6J mice were isolated and enzymatically digested to single cell suspensions. For flow cytometry, cells were stained with antibodies against the

surface markers CD45, CD31, CD133 and CD44. The gating strategy described in Fig. 8 was applied to all organs with “endothel excluded” serving as parent population for both subsequent populations. All depicted dot plots and histograms are representative of three independent experiments. **A** Out of the parent population, histograms of cells expressing CD44 (white) compared to its isotype control (grey) are shown. **B** The surface marker expression of $CD133^+$, $CD44^+$, $CD133^+CD44^+$ double positive and $CD133^-CD44^-$ double negative cells for each organ (top panel) is shown alongside the isotype controls for CD44 (middle panel) and CD133 (bottom panel). The numbers indicate the percentage relative to the parent population. **C** summarizes the relative surface expression of the two tumor-associated populations $CD44^+$ and $CD44^+CD133^+$ with “endothel excluded” serving as parent population for both combinations. The graph shows means with standard error of the mean (SEM) with n=3 for each organ and population, respectively. Statistical significance within the individual populations was assessed by Kruskal-Wallis non-parametric test followed by Dunn’s multiple comparison post hoc test, whereas statistical significance within the individual organs was assessed by two-tailed Mann-Whitney *U* tests (* = $p \leq 0.05$, ** = $p \leq 0.01$, *** = $p \leq 0.001$, **** = $p \leq 0.0001$). The panels **A** and **B** are part of the attached publication Urban *et al.* (2020) that resulted from this project.

The colon presents with the highest expression levels of $CD44^+$ cells (37%) as compared to all other organs, but no expression of $CD44^+CD133^+$ cells could be detected. Statistical analysis by Kruskal-Wallis non-parametric test followed by Dunn’s multiple comparison post hoc test revealed significantly higher levels of $CD44^+CD133^+$ cells in liver as compared to the colon ($p \leq 0.05$) and of $CD44^+$ cells in colon as compared to the lung ($p \leq 0.05$). All other differences within either $CD44^+$ or $CD44^+CD133^+$ cells were non-significant with $p > 0.5$. Additionally, within each organ, no statistically significant differences could be observed between the abundance of $CD44^+$ and $CD44^+CD133^+$ cells, as tested by two-tailed Mann-Whitney *U* tests.

Concluding, physiological populations, that were previously proposed to be either putative cells of cancer origin or to be involved in cancer progression, could be identified in several healthy mouse organs. Furthermore, every organ showed a distinct expression profile of the investigated cell populations. These observations were prerequisites for the following two assumptions: (i) The investigated populations could potentially be parental cell populations of EVs featuring the same marker profile and (ii) if organs have a differing expression profile of the investigated cell populations, tumors originating from these particular organs could have similarly diverse marker distributions. Hence, EVs with the investigated marker combinations on their surface could potentially be used for differential

diagnosis of cancers from different organ origins, which will be evaluated in the following sections.

3.2. Large EVs as biomarkers for differential hepatobiliary cancer diagnosis

After identifying candidate markers and putative physiological parental cells *in vitro* and *in vivo*, the capability of lEVs featuring the established markers and marker combinations on their surface for differential hepatobiliary cancer diagnosis was explored in primary human serum samples. Therefore, human serum was collected from different patient cohorts, lEVs were isolated and their surface marker profile was screened.

3.2.1. The human study cohort for large EV analysis

In total, 327 subjects who gave their informed consent to participate were enrolled in the study (Fig. 11). This pool consisted of healthy individuals (48), patients with liver cirrhosis (54) and patients suffering from various cancerous diseases, comprising 20 colorectal carcinoma (CRC), 32 non-small cell lung carcinoma (NSCLC), 67 hepatocellular carcinoma (HCC), 77 cholangiocarcinoma (CCA) and 29 gallbladder carcinoma (GbCA) patients. As described earlier, the marker combinations characterizing putative EV-releasing cell populations in mice were divided into two groups according to their supposed role in cancer development or tumor progression: the progenitor cell-associated ($CD133^+gp38^+$ or $EpCAM^+CD133^+gp38^+$) and the tumor associated populations ($CD44^+$ or $CD44^+CD133^+$). Consistent with this separation, two studies on lEVs were conducted and their performances in regard to hepatobiliary cancer differentiation were compared to each other. Consequently, the patient cohorts can be divided into two study cohorts, whereby some patients were part of both studies and some only partook in one of them.

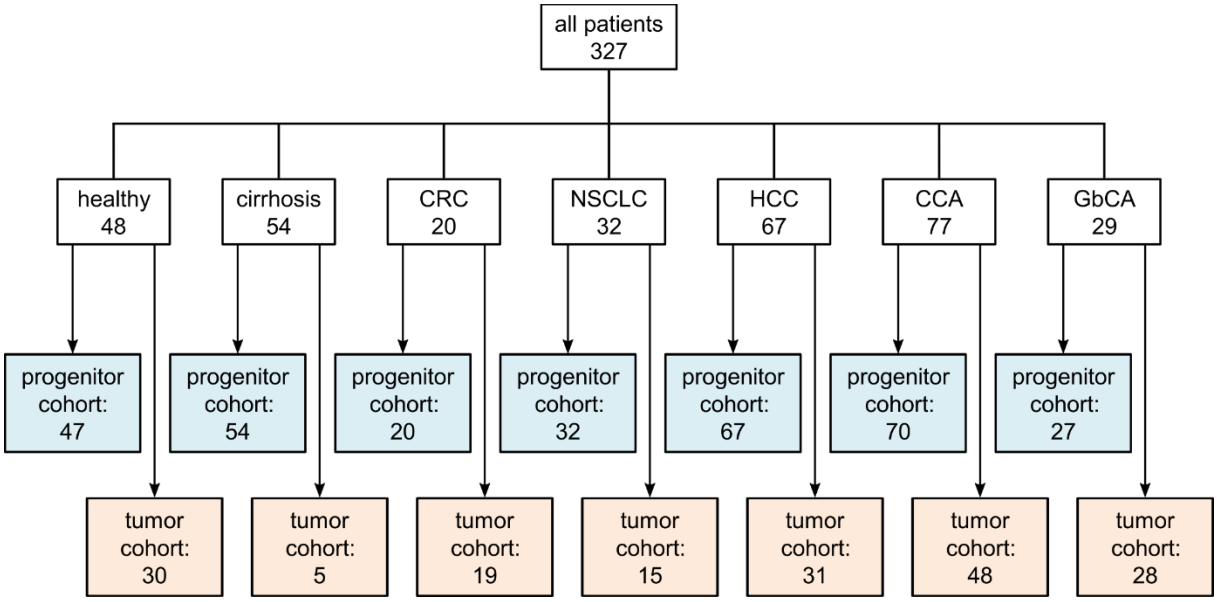

Fig. 11: Distribution of patients in the different study cohorts for large EV analysis. The total amount of enrolled subjects comprised healthy individuals, patients with cirrhosis, colorectal carcinoma (CRC), non-small cell lung carcinoma (NSCLC), hepatocellular carcinoma (HCC), cholangiocarcinoma (CCA) and gallbladder carcinoma (GbCA). Some of these patients were part of both the progenitor cell-associated (blue) and the tumor-associated (orange) study cohort, some were only considered for one of the studies.

A detailed description of key demographic parameters of each individual patient cohort, divided into progenitor cell- and tumor-associated study cohort, is available in Tab. 6, additional biochemical parameters can be found in Supplementary Tab. 1. Out of these values, relative gender, age and BMI distributions among the individual patient cohorts are visualized (Fig. 12). The distributions of these parameters within the patient cohorts differ only slightly between the progenitor cell- and tumor-associated cohorts, so the two study cohorts can be considered comparable.

When comparing the gender distribution in the individual patient cohorts, it is noticeable that most of the participants suffering from diseases were male, with the exception of GbCA patients, which were dominated by female subjects (77%, Fig. 12A). This observation concurs with overall global incidence rates.

Tab. 6: Demographic parameters of the different patient cohorts within the progenitor cell-associated and tumor-associated study cohorts. Age and BMI are given as mean. Additional biochemical parameters of the patients are provided in Supplementary Tab. 1. #: absolute number of patients in each cohort, s.d.: standard deviation.

progenitor cell-associated study cohort							
	healthy	**cirrhosis**	**CRC**	**NSCLC**	**HCC**	**CCA**	**GbCA**
patients [#]	47	54	20	32	67	70	27
female [#]	32	15	5	9	27	30	22
male [#]	15	39	15	23	40	40	5
age [years]	30.8	52.5	69.9	64.4	64.1	63.5	63.0
s.d.	12.4	9.5	13.8	9.6	12.3	10.3	11.4
range	17-75	21-72	33-89	49-81	24-83	32-85	31-77
BMI [kg/m^2]	25.0	26.2	27.6	26.7	26.1	26.3	25.5
s.d.	5.1	4.8	5.7	4.4	3.9	4.0	4.4
range	18.8-38.3	20.0-38.6	20.2-44.5	18.2-36.1	18.9-42.5	18.7-37.5	18.6-36.3
tumor-associated study cohort							
	healthy	**cirrhosis**	**CRC**	**NSCLC**	**HCC**	**CCA**	**GbCA**
patients [#]	30	5	19	15	31	48	28
female [#]	21	2	4	4	12	21	24
male [#]	9	3	15	11	19	27	4
age [years]	27.1	51.3	68.1	67.9	64.0	65.2	62.5
s.d.	6.2	9.4	13.4	7.3	12.7	8.9	11.0
range	17-46	39-60	33-89	56-81	28-82	39-85	31-77
BMI [kg/m^2]	25.9	25.7	27.9	26.1	25.4	27.0	25.7
s.d.	6.6	5.4	5.6	3.7	3.6	4.4	4.2
range	19.9-38.3	21.4-32.9	20.2-44.5	18.9-31.3	18.9-32.5	18.7 -37.5	19.6-36.3

The average age of patients with malignancies ranged from 62.5 to 69.9 years at the point of diagnosis in both study cohorts, whereas patients suffering from liver cirrhosis were younger, with an average of 52.5 years in the progenitor cell-associated and 51.3 years in the tumor-associated study cohort (Tab. 6). Healthy subjects, on the other hand, were considerably younger with a mean age of 30.8 years for the progenitor cell-associated and 27.1 years for the tumor-associated cohort. In both study cohorts, the most frequent age group in CRC patients was 70 to 79 years, whereas in all other cancer patient cohorts the most dominant age group was 60 to 69 years (Fig. 12B). In cirrhosis patients the most frequent age group was 50 to 59 years and healthy subjects were dominated by 20 to 29 year old individuals.

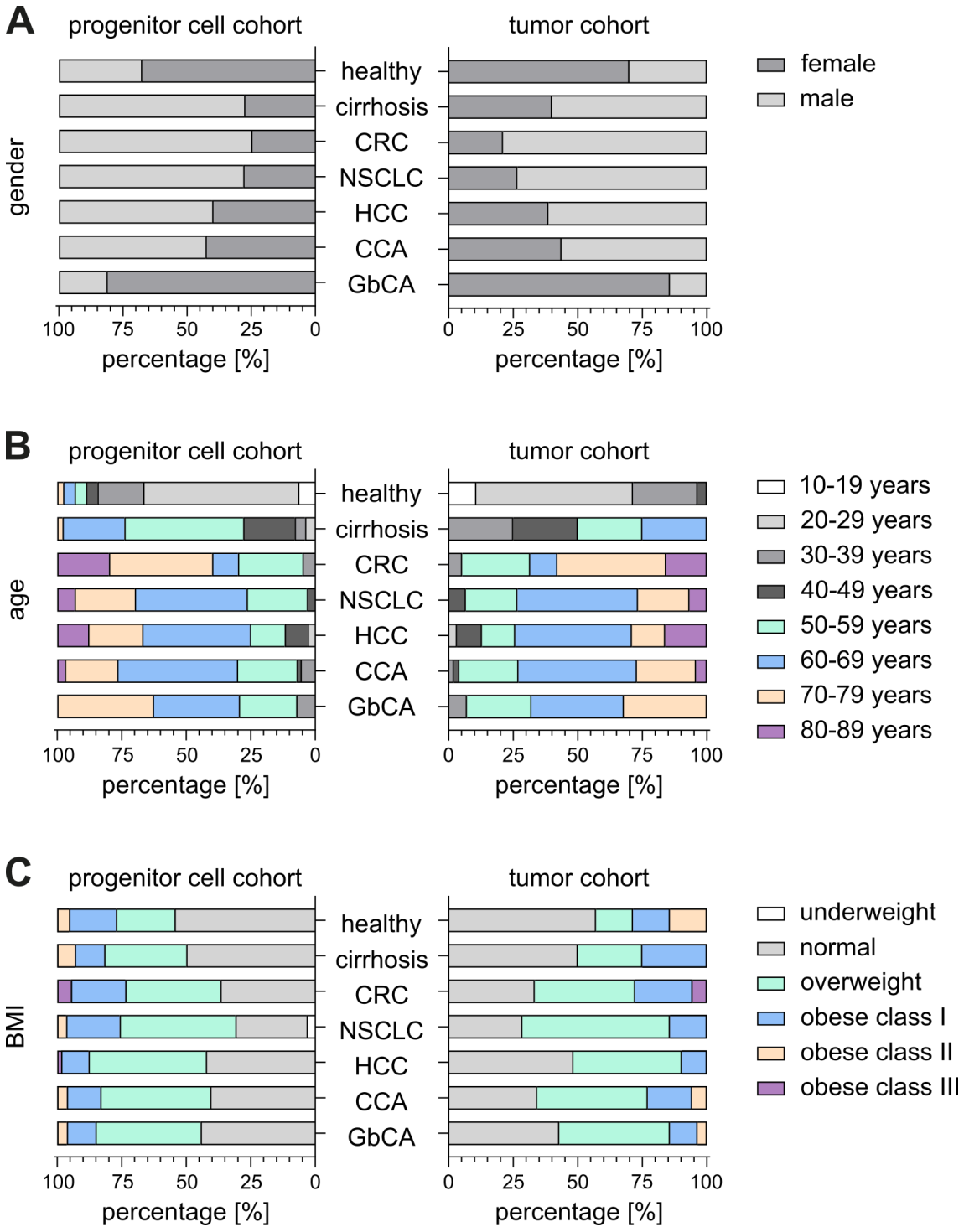

Fig. 12: Distribution of demographic parameters in the different patient cohorts within the progenitor cell-associated and tumor-associated study cohorts. Shown are the percentages of indicated gender (**A**), age (**B**) and BMI (**C**) groups. Corresponding values are displayed in Tab. 6. BMI was classified as follows: underweight: <18.5 kg/m^2, normal weight: 18.5 to <25 kg/m^2, overweight: 25 to <30 kg/m^2, obese class I: 30 to <35 kg/m^2, obese class II: 35 to <40 kg/m^2, obese class III: ≥40 kg/m^2

It is noticeable that the average BMI for all patient cohorts, including healthy subjects, ranged between 25.0 and 27.9 in both study cohorts, which corresponds to overweight (Tab. 6). Most of the cirrhosis patients and healthy individuals showed normal BMIs ranging from 18.5 to <25, whereas the majority of patients with malignancies were overweight with BMIs from 25 to <30 (Fig. 12C). Obese patients could be observed in every patient cohort and were distributed similarly, however, obese class III patients with BMIs above 40 were only present in the CRC and HCC cohorts, concurring with established risk factors of these malignancies. Of note, healthy subjects and GbCA patients tended to be younger and comprised more females, while all other cancer cohorts were dominated be male and older individuals. Cirrhosis patients on the other hand were a mixture, comprising mostly male but generally younger patients highlighting the role of cirrhosis as a preceding disease for later cancer development.

3.2.2. Characterization of isolated large EVs and establishment of flow cytometric measurement methodology

Before the surface of lEVs could be screened in regard to their marker composition, they needed to be isolated from human serum. Therefore, human blood was collected from every patient and serum was isolated by centrifugation (Fig. 13A). Among other blood components, serum contains all EV subtypes. Therefore, lEVs needed to be separated from other subsets as purely as possible. This was performed by sequential centrifugation, starting at lower speed (2,000 × *g*) to eliminate apoptotic bodies and cell debris and continuing with a high speed centrifugation step (20,000 × *g*) of the supernatant to pellet lEVs. Because of their smaller size, sEVs need a much higher centrifugation force to pellet, so they will mainly remain in the supernatant. However, to date, there is no method available that achieves a perfect separation of specific EV subtypes (Théry *et al.* 2018). Depending on the employed purification method, the enrichment of one EV subtype is typically facilitated, but a complete depletion of undesired EV populations is not possible yet. This issue can be addressed by examining the quality of enriched EVs, i.e. by assessing particle size, protein concentration or specific EV protein markers, and by ensuring that undesired EV subtypes do not interfere with the subsequent analysis method.

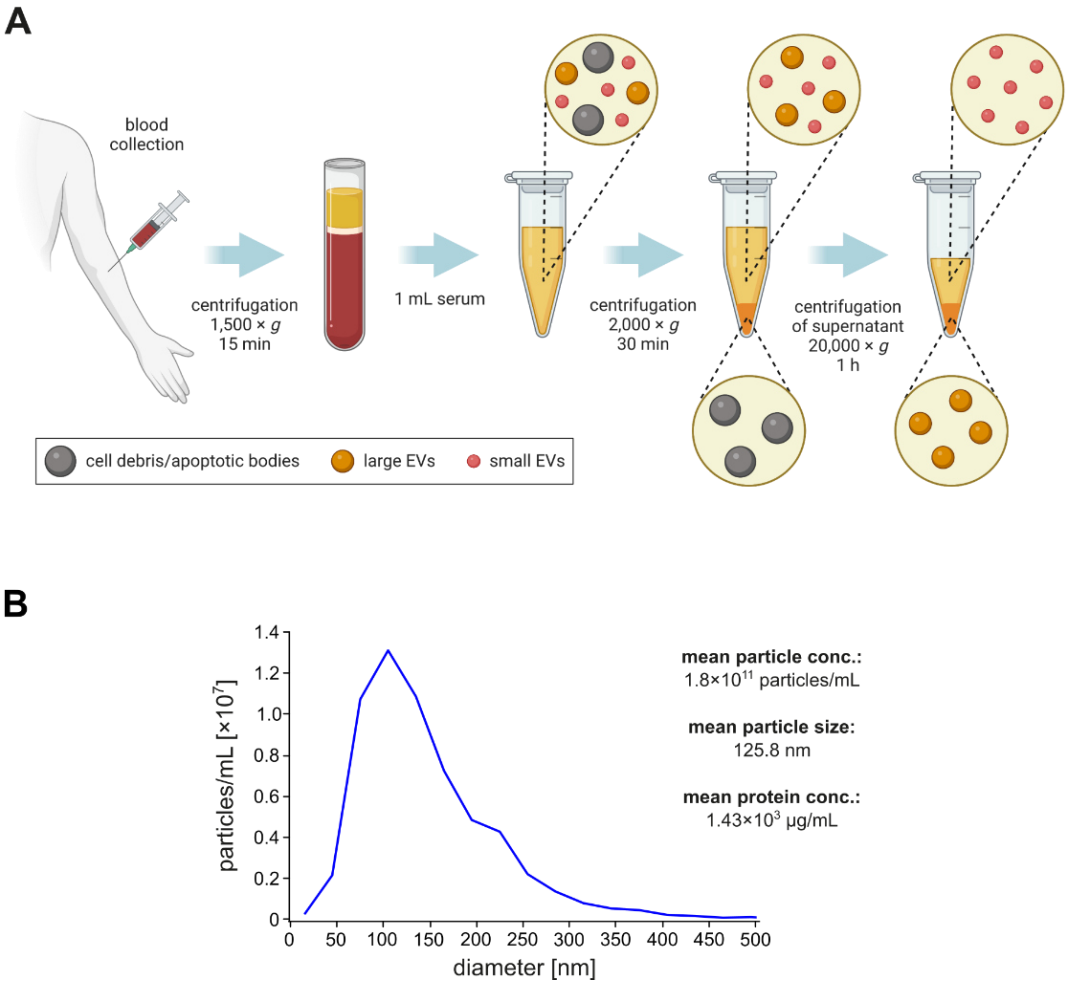

Fig. 13: Characterization of isolated large EVs. A Blood was collected from patients and centrifuged to isolate serum. 1 mL of serum was used for lEV isolation by two sequential centrifugation steps. First, cellular debris and apoptotic bodies were excluded at low speed, afterwards lEVs were pelleted from the remaining supernatant at higher speed. Flowchart was created with BioRender.com. **B** Size distribution of isolated lEVs is visualized. Particle concentration and size was determined by nanoparticle tracking analysis (NTA), protein concentration by BCA assays. Data is shown exemplarily for lEV isolation of a healthy subject. Indicated means are representative of at least four independent experiments.

To further characterize isolated lEVs, size and particle concentration were determined by nanoparticle tracking analysis (NTA). A mean diameter of 125.8 nm was observed, which corresponds to the typical size of lEVs (diameter above 100 nm) (Fig. 13B). Furthermore, a mean particle concentration of 1.8×10^{11} particles/mL and a mean protein concentration of 1.43×10^{3} µg/mL were observed throughout all measured isolations. After characterization of the isolated lEVs, they were stained with a panel of fluorescent components to screen their surface composition by flow cytometric analysis (Fig. 14).

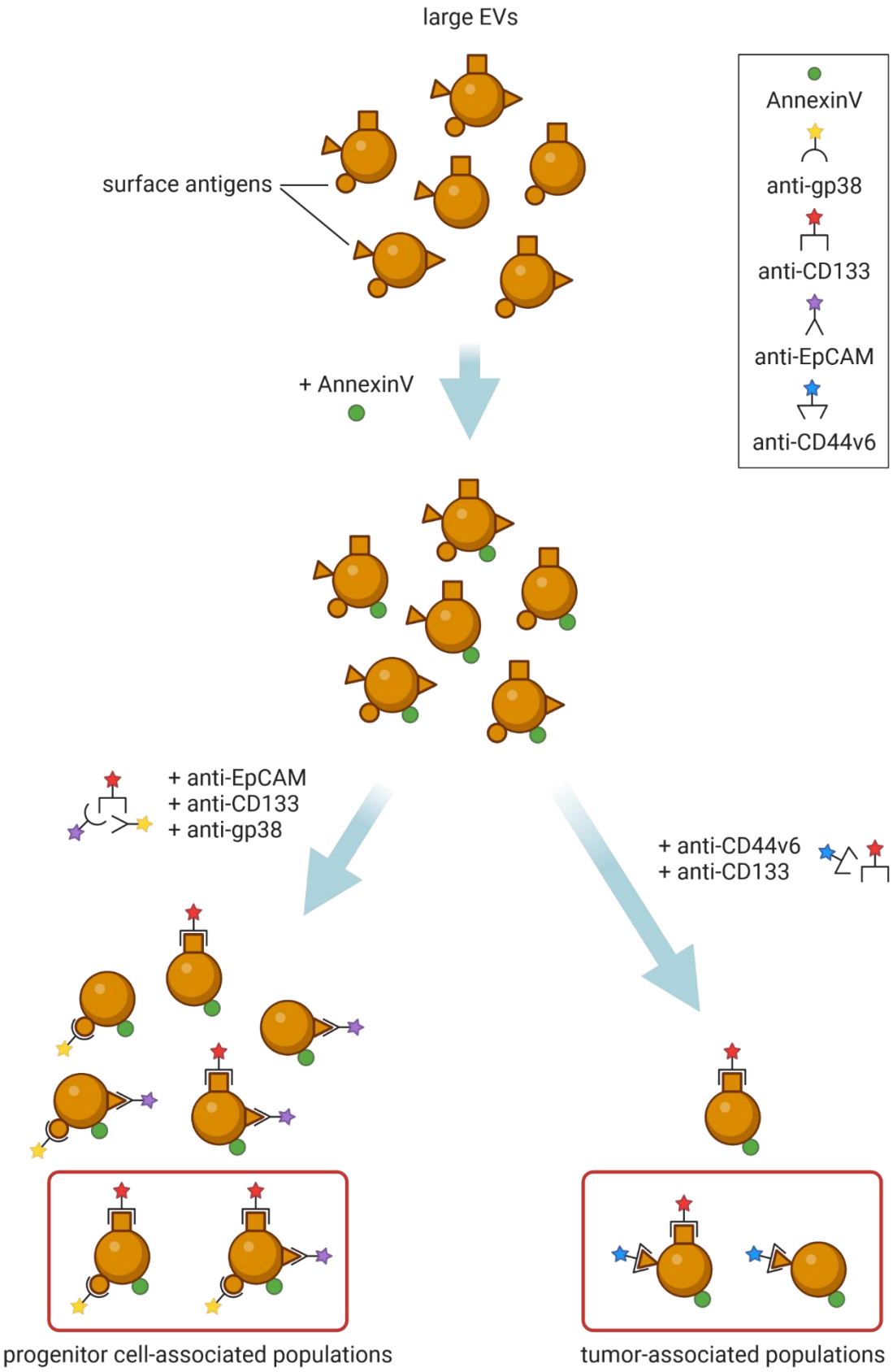

Fig. 14: Schematic overview of antibody staining for flow cytometric measurement of large EVs. After isolation by centrifugation, EVs were first stained with the general EV

marker AnnexinV that binds to exposed phosphatidylserine (PS) in the EV membrane. Afterwards, fluorescent antibodies against the candidate markers were added and the labelled EVs were analyzed by flow cytometry. Out of the pool of possible antibody combinations, the indicated progenitor cell-associated and tumor-associated EV populations were further investigated in this study. Flowchart was created with BioRender.com.

In a first step, lEVs were incubated with fluorescently labelled AnnexinV (AnnV), a common EV marker (Arraud *et al.* 2015, Théry *et al.* 2018). It binds to phosphatidylserine (PS) in the outer leaflet of phospholipid bilayers (van Genderen *et al.* 2008). In living cells, PS distribution is asymmetrical with the majority of the lipid residing in the inner leaflet. This state is maintained by an energy-consuming process. In cells undergoing apoptosis or in extracellular vesicles, asymmetry of the membrane is lost resulting in externalized PS in the outer leaflet to which AnnV can bind in an Ca^{2+}-dependent manner. After incubation of isolated lEVs with AnnV, they were stained with two different sets of antibodies: (i) antibodies against human EpCAM, CD133 and gp38 were used to identify progenitor cell-associated populations and (ii) antibodies against human CD44v6 and CD133 were used to identify tumor-associated populations. Out of all possible staining combinations, only such EVs were of interest that expressed the progenitor cell-associated and tumor-associated marker combinations on their surface.

Subsequently, isolated and stained lEVs were analyzed by flow cytometry. Before conducting any measurements, key parameters for good and reliable flow cytometric practice needed to be established and quality controls needed to be performed. Therefore, a general gating strategy for identifying lEVs was developed (Fig. 15A). Briefly, all events were restricted to include all possible EVs (all lEVs), followed by the exclusion of debris and EV aggregates (debris excluded). This separation was achieved in a similar manner as the exclusion of cell clusters before: single EVs show a defined signal area to height ratio, whereas aggregates and debris diverge from this ideal line. The successful exclusion of debris is visualized in the scatter plot second from the right by applying a backgating step (compare to left panel: all events). The respective parent population is indicated above each graph. Subsequently, the population was restricted to $AnnV^+$ events that represent the general EV population. In order to identify the $AnnV^+$ population, a sample of isolated lEVs without addition of fluorescently labelled AnnV was measured (Fig. 15B, left panel).

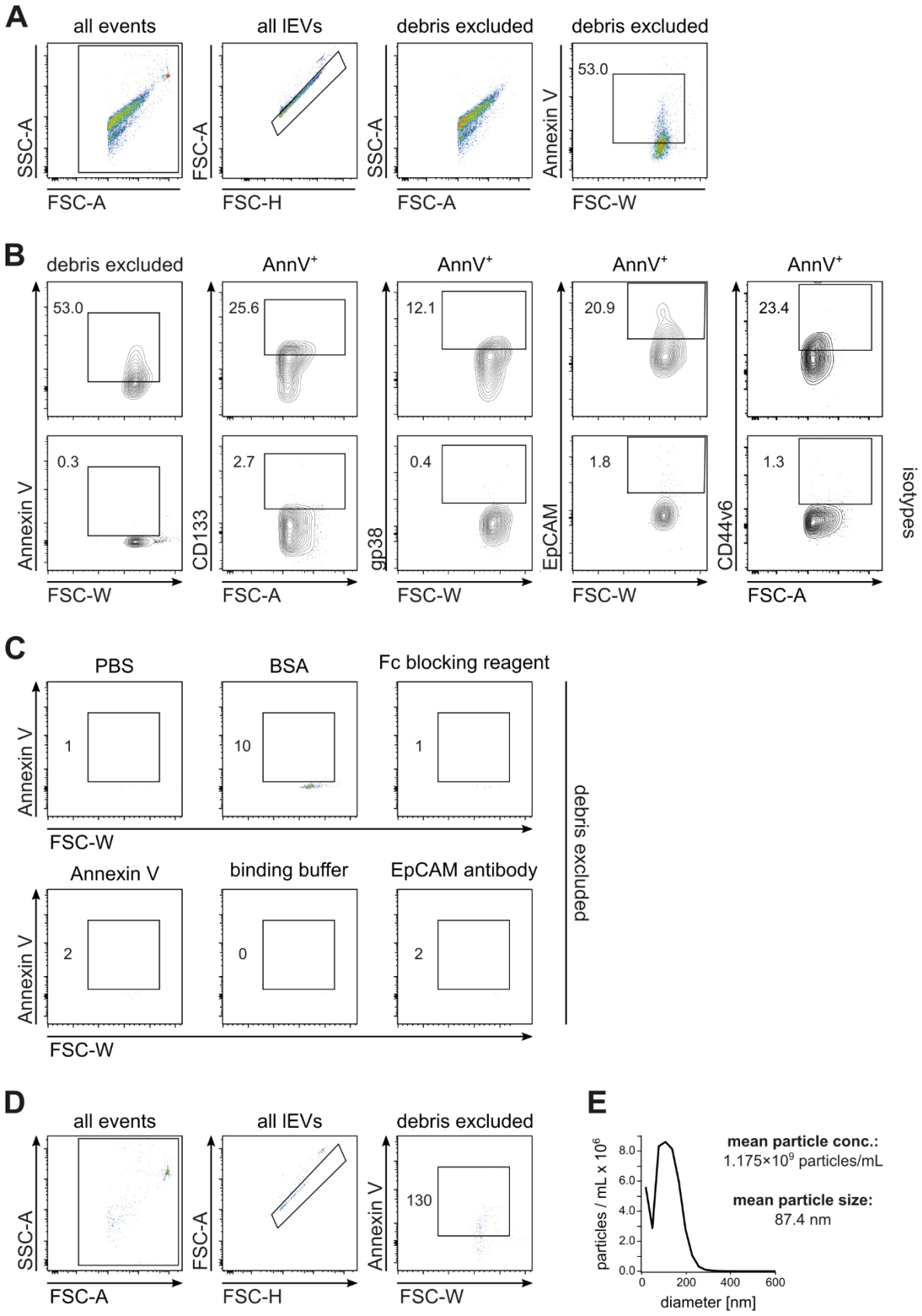

Fig. 15: Establishment of flow cytometric measurement methodology for large EVs. After isolation and immunofluorescent labeling of serum lEVs, they were analyzed by flow

cytometry. **A** exemplarily depicts the successive general gating strategy applied to all lEV measurements: first all events were restricted to the appropriate size range (all lEVs), then to single events in order to exclude debris and aggregates (debris excluded). Afterwards, only AnnexinV$^+$ (AnnV$^+$) lEVs were considered for further analysis. Number represents percentage of parent population (debris excluded). The respective parent population is indicated above each graph. Out of the AnnV$^+$ population **B** shows dot plots of all used antibodies against the candidate markers (upper panel) and their corresponding isotype control (lower panel). All isotype controls were matched to the respective antibody concentration and the used dilutions for each antibody can be obtained from Tab. 3. For AnnV, unstained lEVs were used as negative control. Numbers represent percentage of parent population (debris excluded or AnnV$^+$). **C** Depicted are representative dot plots of each reagent used for lEV profiling. EpCAM antibody is representative for all antibodies applied. The analysis was performed using the same parameters and gating strategy as for normal lEV analysis to identify possible contaminations. Numbers indicate absolute counts of AnnV$^+$ events within the parent population (debris excluded). **D** Serum sEVs were isolated from a colorectal cancer patient and analyzed by flow cytometry with the same settings as used for lEV profiling in order to identify interferences of sEVs. Number indicates absolute count of AnnV$^+$ events within the parent population (debris excluded). The initial number of isolated and subsequently analyzed sEVs as determined by **E** nanoparticle tracking analysis (NTA) was 1.175×10^9. Median diameter of sEVs was 87.4 nm. This figure is part of the attached publication Urban *et al.* (2020) that resulted from this project. A: area, FSC: forward scatter, H: height, SSC: sideward scatter, W: width

Furthermore, positive lEV populations for all employed markers were identified by comparing them to lEVs stained with the respective concentration-matched isotype control (Fig. 15B). Prior use, every antibody was titrated to ensure the best possible performance. The dilutions used for each antibody can be obtained from Tab. 3.

Another important factor that needs to be addressed when developing a reliable flow cytometric measurement methodology is the possible interference of reagents used during the experiment. Therefore, every reagent that was employed for isolation and staining of lEVs was measured with the same settings and concentrations as applied for lEV flow cytometric analysis and their influence on the general EV population (AnnV$^+$) is exemplarily depicted in Fig. 15C. In this case, EpCAM antibody is representative for every used antibody. The numbers given in the scatter plots indicate absolute counts of AnnV$^+$ events within the parent population. Thus, the quality check revealed that no measurable interference of any reagent could be detected. As mentioned before, perfect separation of EV subtypes is nearly impossible and the interference of other EV types in prepared isolations needs to be examined. Therefore, serum sEVs were isolated as described in the Material and Methods section and were subsequently analyzed by flow cytometry with

the same settings as used for lEV profiling (Fig. 15D). The initial number of sEVs, as confirmed by nanoparticle tracking analysis (NTA, Fig. 15E), was 1.175×10^9, out of which only 130 absolute events were positive for AnnV. Thus, for this explicit experimental setting of lEV flow cytometric quantification, any substantial influence of sEV cross-contamination in lEV isolates was successfully ruled out.

After developing a reliable method for flow cytometric analysis of lEVs without interferences of reagents and other EV subtypes, the comparability of lEV quantification between the proposed patient cohorts needed to be assessed in order to conduct a conclusive study. Therefore, lEVs of different patient cohorts were isolated and their total and AnnV$^+$ levels were compared among the cohorts (Fig. 16).

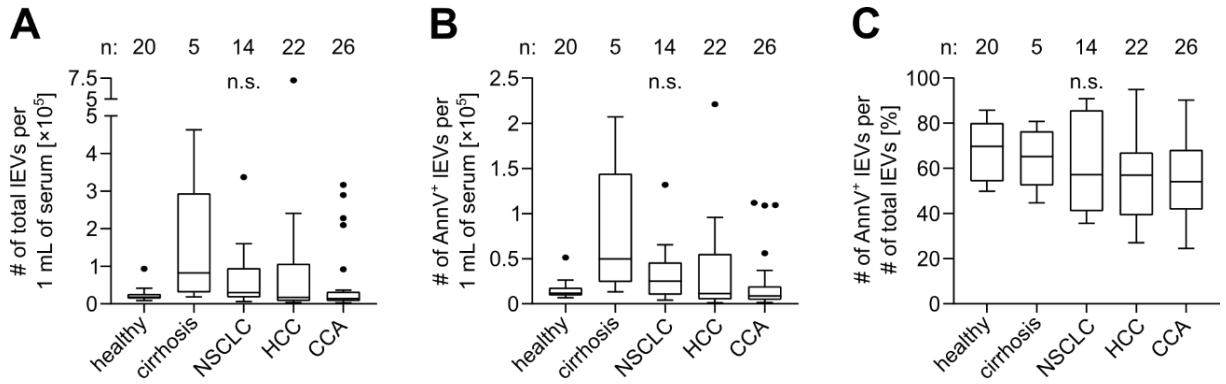

Fig. 16: Large EVs are detectable by flow cytometric analysis and their abundancy is comparable among different patient cohorts. Serum lEVs of the indicated patient cohorts were isolated by centrifugation and stained with AnnV$^+$. Gating was applied as described in Fig. 15A. Data is shown as medians with interquartile range (IQR), whiskers represent 1.5 × IQR (Tukey) with potential outliers plotted as dots. n indicates number of patients. **A** shows the total amount of lEVs per 1 mL of serum, whereas **B** depicts the total amount of AnnV$^+$ lEVs per 1 mL of serum. In **C** AnnV$^+$ lEV numbers were normalized to total lEV numbers. Statistical significance was assessed by Kruskal-Wallis non-parametric test followed by Dunn's multiple comparison post hoc test with $p \leq 0.05$ considered statistically significant. n.s.: non-significant.

In this first pilot evaluation, only parts of the healthy individuals and cirrhosis, NSCLC, HCC and CCA patients were included. Gating was conducted as described in Fig. 15A and total counts were normalized to 1 ml of initial serum. The number of total lEVs corresponds to the events within the "debris excluded" population (Fig. 16A), whereas AnnV positive counts were obtained from the "AnnV$^+$" population (Fig. 16B). Kruskal-Wallis non-parametric tests followed by Dunn's multiple comparison post hoc tests were

performed in order to identify differences among the patient cohorts but revealed no significant variations between the cohorts in both populations (p>0.5). Interestingly, in both populations median lEV counts for cirrhosis patients are slightly enhanced as compared to the other patient cohorts, which might be due to the lower patient number in this cohort. However, when normalizing AnnV$^+$ counts to total lEV numbers, this effect is relativized (Fig. 16C). Consequently, no significant differences could be observed after applying Kruskal-Wallis non-parametric test followed by Dunn's multiple comparison post hoc test (p>0.5) as well.

Taken together, a robust and reliable method for isolation and flow cytometric measurement of lEVs was established that yielded similar numbers of AnnV$^+$ lEVs among the relevant patient cohorts in this study. With this in mind, it was possible to conduct a comparative study that evaluates differences in lEV levels that are not influenced by the used reagents, methodology or the respective patient cohort, but which effects can solely be attributed to pathophysiological differences between the patient cohorts.

3.2.3. Progenitor cell-associated large EV populations can diagnostically differentiate between hepatobiliary cancers

In order to assess the general detecting and differentiating capability of serum lEVs within the established experimental settings, a pilot study involving only progenitor cell-associated lEV populations was conducted. Therefore, lEVs of a restricted number of patients were isolated, immunofluorescently labelled and analyzed by flow cytometry. In addition to the general gating strategy described in Fig. 15A, the gating was successively expanded as depicted in Fig. 17A to identify the two progenitor cell-associated lEV populations AnnV$^+$CD133$^+$gp38$^+$ and AnnV$^+$EpCAM$^+$CD133$^+$gp38$^+$, which are schematically visualized in Fig. 17B. Briefly, AnnV$^+$ lEVs were restricted to CD133$^+$ lEVs, followed by an identification of gp38$^+$ lEVs out of the AnnV$^+$CD133$^+$ lEV pool to obtain the first progenitor cell-associated population AnnV$^+$CD133$^+$gp38$^+$. Subsequently, AnnV$^+$CD133$^+$gp38$^+$ lEVs were limited to EpCAM$^+$ lEVs to obtain the second progenitor cell-associated population AnnV$^+$EpCAM$^+$CD133$^+$gp38$^+$. The gates in this figure correspond to the positive populations that were identified for each marker according to their concentration-matched isotype controls (compare Fig. 15B). The counts for each progenitor cell-associated population were evaluated and normalized to 1000 AnnV$^+$ lEVs

for comparability among samples and cohorts. Median, normalized lEV levels of each individual patient cohort for AnnV⁺CD133⁺gp38⁺ and AnnV⁺EpCAM⁺CD133⁺gp38⁺ are depicted in Fig. 17C and Fig. 17D, respectively.

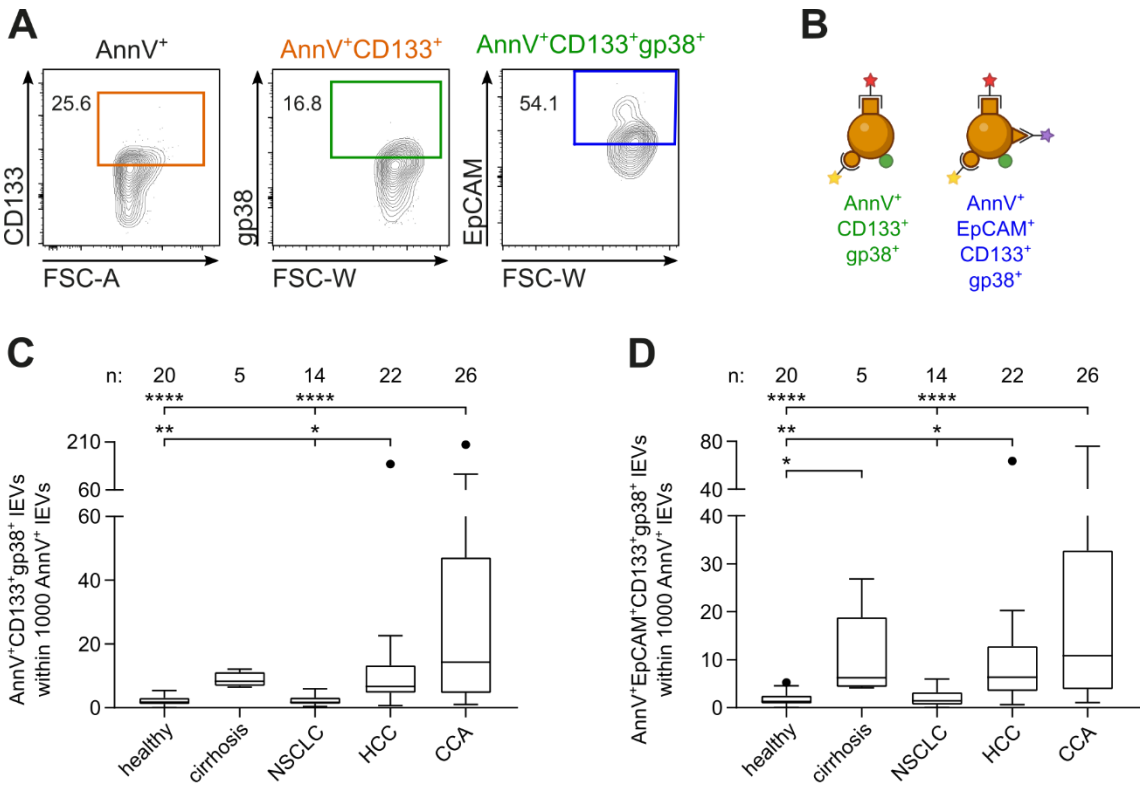

Fig. 17: Pilot results – progenitor cell-associated large EVs are enriched in patients with hepatobiliary diseases. After isolation of serum lEVs and immunofluorescent labelling, they were analysed by flow cytometry. Gating was applied as described in Fig. 15A. **A** exemplarily describes the subsequent successive gating strategy applied to identify the two progenitor cell-associated lEV populations AnnV⁺CD133⁺gp38⁺ (green) and AnnV⁺EpCAM⁺CD133⁺gp38⁺ (blue). In **B** lEVs of the two progenitor cell-associated populations are schematically visualized (created with BioRender.com) referring to the staining protocol described in Fig. 14. lEV values of the two progenitor cell-associated populations AnnV⁺CD133⁺gp38⁺ (**C**) and AnnV⁺EpCAM⁺CD133⁺gp38⁺ (**D**) are shown for healthy individuals, cirrhosis patients and various cancer patient cohorts (NSCLC, HCC, CCA). For this analysis only patients that were measured by the author were included. Data is shown as medians with interquartile range (IQR), whiskers represent 1.5 × IQR (Tukey) with potential outliers plotted as dots. n indicates number of patients. Statistical significance was assessed by Kruskal-Wallis non-parametric test followed by Dunn's multiple comparison post hoc test with $p \leq 0.05$ considered statistically significant (* = $p \leq 0.05$, ** = $p \leq 0.01$, **** = $p \leq 0.0001$). Panel **A** is part of the attached publication Urban *et al.* (2020) that resulted from this project.

In both populations lEV levels for CCA patients are elevated as compared to all other cohorts. Kruskal-Wallis non-parametric test followed by Dunn's multiple comparison post hoc test revealed a significant increase of lEVs in CCA patients as compared to healthy individuals and NSCLC patients in both populations ($p \leq 0.0001$, respectively). Furthermore, lEV levels in HCC patients were significantly increased as compared to healthy individuals ($p \leq 0.01$) and NSCLC patients ($p \leq 0.05$) in both populations as well. For $AnnV^+EpCAM^+CD133^+gp38^+$ lEVs, cirrhosis patients additionally showed significantly increased levels as compared to healthy subjects ($p \leq 0.05$). Of note, all three patient cohorts with elevated lEV levels feature patients with hepatobiliary diseases, hinting at a potential hepatobiliary specificity of the chosen progenitor cell-associated populations. Even though the discrimination of the two cancer entities HCC and CCA had not been possible in this pilot study yet, the tendency of elevated lEV levels in CCA patients became evident. Thus, the results were a first indication of the suitability of lEVs for hepatobiliary cancer detection and differentiation with these marker combinations. Therefore, a follow-up study with all four proposed lEV populations was conducted in a team effort to achieve diagnostically conclusive results with adequate patient cohort sizes. Data acquisition for the progenitor cell-associated as well as the tumor-associated study cohort was conducted independently by three students of the lab: the author herself, Dr. Henrike Julich-Haertel and Hanna Sänger. This way, high numbers of patients could be screened and the reproducibility of the method was ensured, eliminating handling bias. Processing and interpretation of all acquired data was conducted solely by the author and the results are presented herein.

Large EV levels of all patients participating in the progenitor cell-associated study cohort were evaluated and the values for each individual cohort for both progenitor cell-associated populations are visualized in Fig. 18A. A group analysis with Kruskal-Wallis non-parametric test followed by Dunn's multiple comparison post hoc test between biliary cancer entities (CCA and GbCA), non-biliary cancer entities (HCC, CRC and NSCLC), cirrhosis patients and healthy individuals revealed that normalized, median lEV levels were significantly elevated in biliary cancer patients as compared to all control groups in both progenitor cell-associated populations (Fig. 18B).

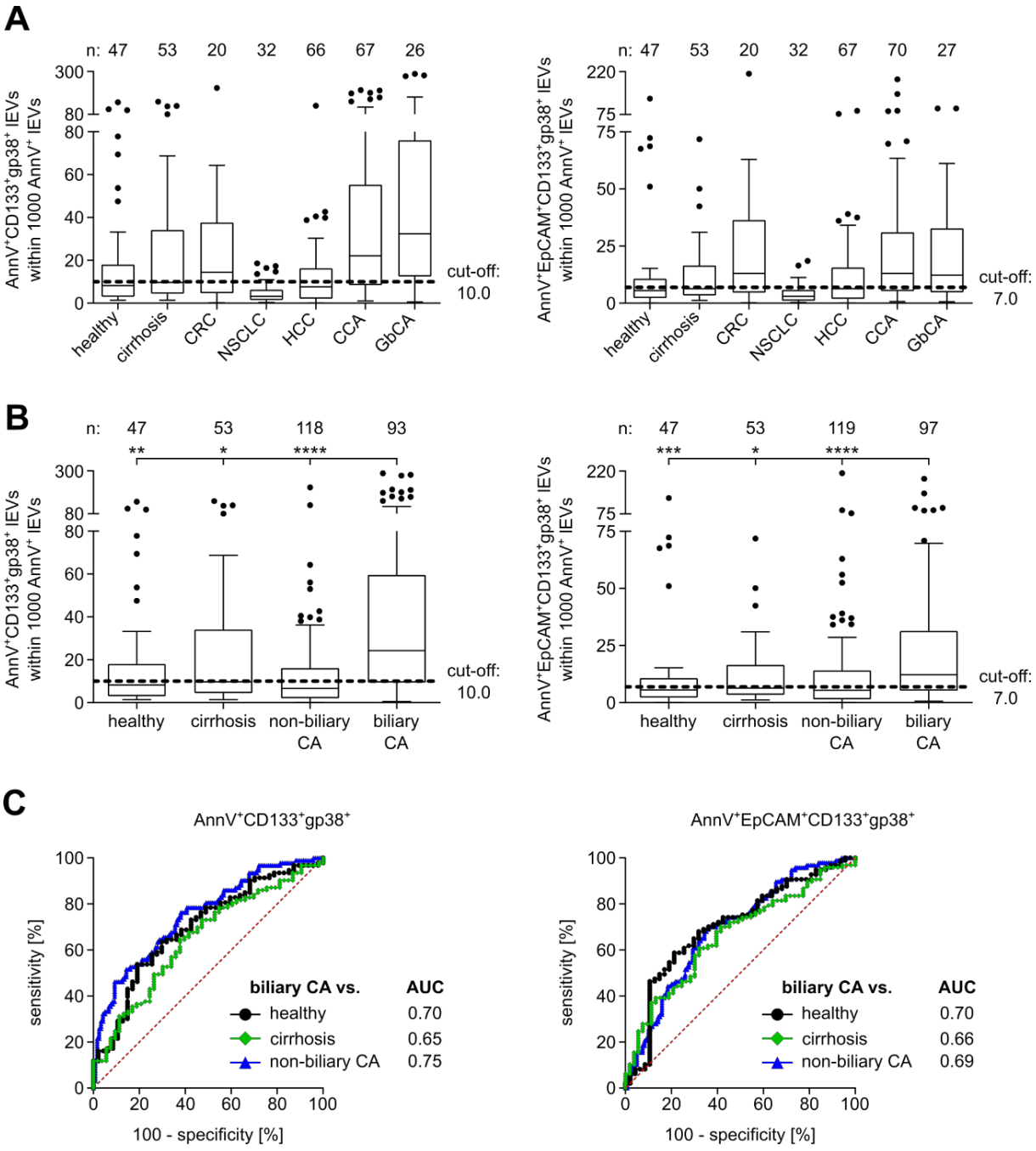

Fig. 18: Progenitor cell-associated large EVs can distinguish biliary cancer patients from controls. After isolation of serum lEVs and immunofluorescent labelling, they were analysed by flow cytometry. Gating was applied as described in Fig. 15A and Fig. 17A. **A** lEV values of the two progenitor cell-associated populations AnnV+CD133+gp38+ (left panel) and AnnV+EpCAM+CD133+gp38+ (right panel) are shown for healthy individuals, cirrhosis patients and various cancer patient cohorts (CRC, NSCLC, HCC, CCA, GbCA). **B** Patient cohorts were summarized to non-biliary carcinomas (non-biliary CA) comprising CRC, NSCLC and HCC patients, and biliary carcinomas (biliary CA) comprising CCA and GbCA patients. AnnV+CD133+gp38+ lEV (left panel) as well as AnnV+EpCAM+CD133+gp38+ lEV (right panel) levels of the combined cohorts are depicted. Data is shown as medians with interquartile range (IQR), whiskers represent

1.5 × IQR (Tukey) with potential outliers plotted as dots. n indicates number of patients. Dotted lines indicate diagnostic cut-offs for discrimination between biliary CA and controls for the respective IEV population (see Tab. 7). Statistical significance was assessed by Kruskal-Wallis non-parametric test followed by Dunn's multiple comparison post hoc test with $p \leq 0.05$ considered statistically significant. **C** Corresponding ROC curves for $AnnV^+CD133^+gp38^+$ IEVs (left panel) and $AnnV^+EpCAM^+CD133^+gp38^+$ IEVs (right panel) for the discrimination between biliary CA and controls (healthy, cirrhosis and non-biliary CA) including AUC values are shown. (* = $p \leq 0.05$, ** = $p \leq 0.01$, *** = $p \leq 0.001$, **** = $p \leq 0.0001$). The panels **A** and **B** are part of the attached publication Urban *et al.* (2020) that resulted from this project.

In detail, $AnnV^+CD133^+gp38^+$ IEV levels of biliary cancer patients were 3.0-fold increased compared to healthy subjects ($p \leq 0.01$), 2.5-fold increased compared to cirrhosis patients ($p \leq 0.05$) and 3.6-fold increased compared to non-biliary cancer patients ($p \leq 0.0001$). $AnnV^+EpCAM^+CD133^+gp38^+$ IEV levels of biliary cancer patients were 2.2-fold increased compared to healthy subjects ($p \leq 0.001$), 1.9-fold increased compared to cirrhosis patients ($p \leq 0.05$) and 2.2-fold increased compared to non-biliary cancer patients ($p \leq 0.0001$). In order to assess the diagnostic relevance of these results, receiver operating characteristic (ROC) curves and associated area under ROC curves (AUC) values were computed for discrimination of biliary cancer patients from each of the three control groups for both progenitor cell-associated populations (Fig. 18C). AUC values can generally range between 0.5, which describes random results with no diagnostic validity, and 1.0, which refers to a perfect diagnostic test with 100% correct predictions. AUC values of $AnnV^+CD133^+gp38^+$ IEVs for discriminating biliary cancer patients from healthy individuals (0.70), cirrhosis patients (0.65) and non-biliary cancer patients (0.75) indicated a good predictive power of the biomarker to varying degrees. AUC values of $AnnV^+EpCAM^+CD133^+gp38^+$ IEVs for discriminating biliary cancer patients from healthy individuals (0.70), cirrhosis patients (0.66) and non-biliary cancer patients (0.69) indicated a slightly lower predictive power than $AnnV^+CD133^+gp38^+$ IEVs. Out of the ROC curve analyses, diagnostic cut-offs and other predictive values for both progenitor cell-associated populations were calculated according to the point of optimal sensitivity and specificity (Tab. 7). For both populations differentiation of biliary cancer from all controls was associated with a good sensitivity of at least 71%. With 73.1% sensitivity, 62.7% specificity, 60.7% positive predictive value (PPV) and 74.8% negative predictive value

(NPV) AnnV$^+$CD133$^+$gp38$^+$ lEVs showed the best diagnostic performance for discrimination of biliary from non-biliary cancer patients.

Tab. 7: Diagnostic performance of progenitor cell-associated large EV populations for biliary cancer diagnosis. Biliary cancers (CCA and GbCA) were compared to healthy controls, cirrhosis patients and non-biliary CA (NSCLC, CRC and HCC) patients. Diagnostic cut-offs are given as number per 10^3 AnnV$^+$ lEVs, whereas sensitivities (sens), specificities (spec) as well as positive (PPV) and negative predictive values (NPV) are given as percentage. n indicates cohort size.

AnnV$^+$CD133$^+$gp38$^+$ lEVs							
	cut-off	**AUC**	***p*-value**	**sens [%]**	**spec [%]**	**PPV [%]**	**NPV [%]**
biliary CA (n=93) vs. **healthy** (n=47)	10.0	0.70	0.0001	73.1	57.5	77.3	51.9
biliary CA (n=93) vs. **cirrhosis** (n=53)	10.0	0.65	0.0027	73.1	52.8	73.1	52.8
biliary CA (n=93) vs**.** **non-biliary CA** (n=118)	10.0	0.75	<0.0001	73.1	62.7	60.7	74.8
AnnV$^+$EpCAM$^+$CD133$^+$gp38$^+$ lEVs							
	cut-off	**AUC**	***p*-value**	**sens [%]**	**spec [%]**	**PPV [%]**	**NPV [%]**
biliary CA (n=97) vs. **healthy** (n=47)	7.0	0.70	<0.0001	71.1	61.7	79.3	50.9
biliary CA (n=97) vs. **cirrhosis** (n=53)	7.0	0.66	0.0011	71.1	54.7	74.2	50.9
biliary CA (n=97) vs**.** **non-biliary CA** (n=119)	7.0	0.69	<0.0001	71.1	59.7	59.0	71.7

This line of experiments showed that progenitor cell-associated lEVs are a marker for biliary cancer and that they can reliably distinguish it from a pool of other malignancies and liver-related diseases.

Furthermore, the differentiation potential of progenitor cell-associated lEVs within the hepatobiliary compartment was of interest. Therefore, normalized median lEV levels for both progenitor cell-associated populations were compared in HCC, CCA and GbCA patients (Fig. 19A).

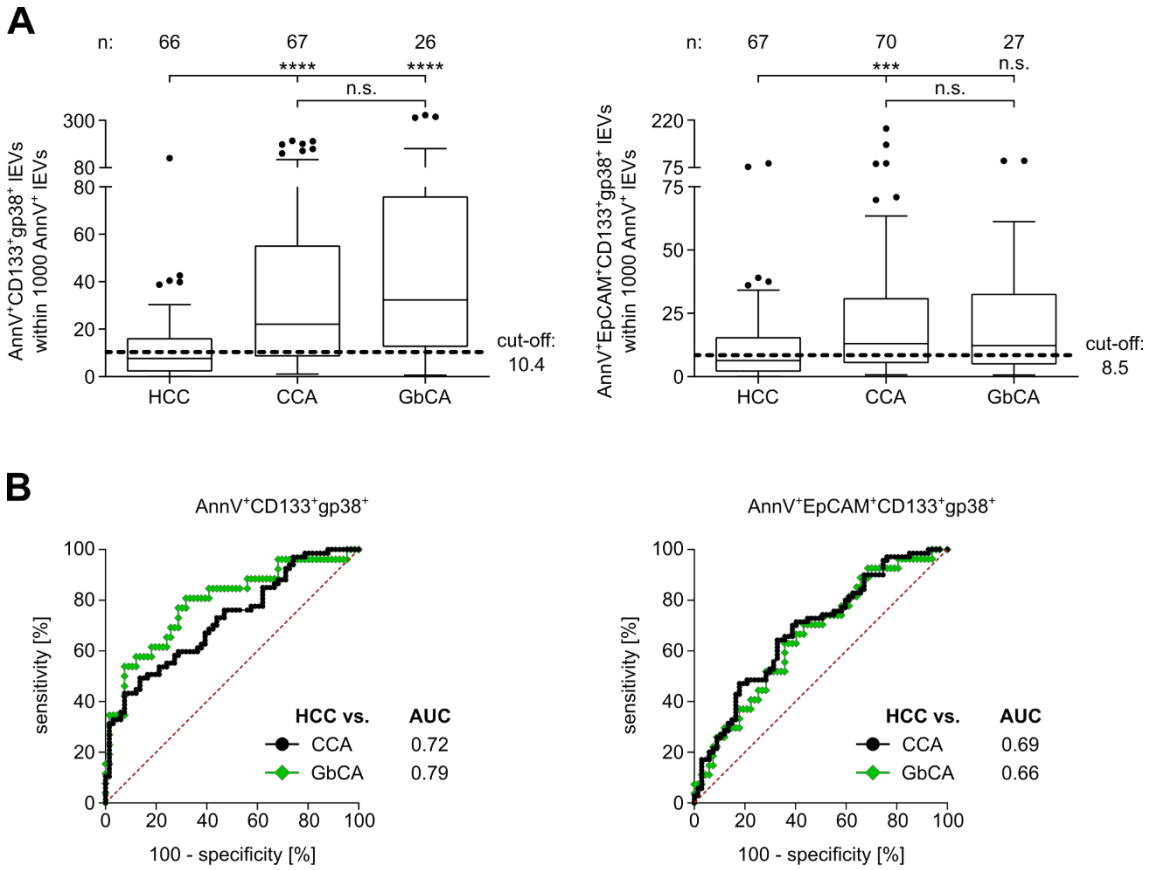

Fig. 19: Progenitor cell-associated large EVs are distributed differentially in hepatobiliary cancer entities. After isolation of serum lEVs and immunofluorescent labelling, they were analysed by flow cytometry. Gating was applied as described in Fig. 15A and Fig. 17A. **A** lEV values of the two progenitor cell-associated populations AnnV+CD133+gp38+ (left panel) and AnnV+EpCAM+CD133+gp38+ (right panel) are shown for HCC, CCA and GbCA patients. Data is shown as medians with interquartile range (IQR), whiskers represent 1.5 × IQR (Tukey) with potential outliers plotted as dots. n indicates number of patients. Dotted lines indicate diagnostic cut-offs for discrimination between HCC and CCA or GbCA for the respective lEV population (see Tab. 8). Statistical significance was assessed by Kruskal-Wallis non-parametric test followed by Dunn's multiple comparison post hoc test with $p \leq 0.05$ considered statistically significant. **B** Corresponding ROC curves for AnnV+CD133+gp38+ lEVs (left panel) and AnnV+EpCAM+CD133+gp38+ lEVs (right panel) for the discrimination between HCC and CCA or GbCA including AUC values are shown. (* = $p \leq 0.05$, ** = $p \leq 0.01$, *** = $p \leq 0.001$, **** = $p \leq 0.0001$). n.s.: non-significant.

Kruskal-Wallis non-parametric test followed by Dunn's multiple comparison post hoc test revealed that lEV levels were significantly elevated in CCA and GbCA patients as compared to HCC patients in both progenitor cell-associated populations, whereas lEV levels in CCA and GbCA patients were similar, without significant differences. In detail, AnnV+CD133+gp38+ lEV levels of CCA patients were 2.9-fold increased ($p \leq 0.0001$) and

levels of GbCA patients were 4.2-fold increased ($p \leq 0.0001$) as compared to HCC patients. AnnV$^+$EpCAM$^+$CD133$^+$gp38$^+$ lEV levels of CCA patients were 2.0-fold increased ($p \leq 0.001$), whereas levels of GbCA patients were not significantly increased ($p > 0.05$) as compared to HCC patients. In order to assess the diagnostic relevance of these results, ROC curves and associated AUC values were computed for discrimination of CCA and GbCA patients from HCC patients (Fig. 19B). AUC values of AnnV$^+$CD133$^+$gp38$^+$ lEVs for discriminating CCA from HCC (0.72) and for distinguishing GbCA from HCC (0.79) indicated a good predictive power of the biomarker. AUC values of AnnV$^+$EpCAM$^+$CD133$^+$gp38$^+$ lEVs for discriminating CCA from HCC (0.69) and for distinguishing GbCA from HCC (0.66) indicated a slightly lower predictive power than AnnV$^+$CD133$^+$gp38$^+$ lEVs. Out of the ROC curve analyses, diagnostic cut-offs and other predictive values for both progenitor cell-associated populations were calculated (Tab. 8).

Tab. 8: Diagnostic performance of progenitor cell-associated large EV populations for hepatobiliary cancer differentiation. CCA and GbCA patients were compared to HCC patients, respectively. Diagnostic cut-offs are given as number per 10^3 AnnV$^+$ lEVs, whereas sensitivities (sens), specificities (spec) as well as positive (PPV) and negative predictive values (NPV) are given as percentage. n indicates cohort size.

AnnV$^+$CD133$^+$gp38$^+$ lEVs							
	cut-off	**AUC**	***p*-value**	**sens [%]**	**spec [%]**	**PPV [%]**	**NPV [%]**
CCA (n=67) vs. **HCC** (n=66)	10.4	0.72	<0.0001	67.2	60.6	63.4	64.5
GbCA (n=26) vs**.** **HCC** (n=66)	11.7	0.79	<0.0001	80.8	68.2	50.0	90.0
AnnV$^+$EpCAM$^+$CD133$^+$gp38$^+$ lEVs							
	cut-off	**AUC**	***p*-value**	**sens [%]**	**spec [%]**	**PPV [%]**	**NPV [%]**
CCA (n=70) vs. **HCC** (n=67)	8.5	0.69	0.0002	70.0	61.2	65.3	66.1
GbCA (n=27) vs**.** **HCC** (n=67)	9.0	0.66	0.0159	63.0	62.7	40.5	80.8

With 80.8% sensitivity, 68.2% specificity, 50.0% PPV and 90.0% NPV AnnV$^+$CD133$^+$gp38$^+$ lEVs showed the best diagnostic performance for discrimination of GbCA from HCC patients, whereas AnnV$^+$EpCAM$^+$CD133$^+$gp38$^+$ lEVs demonstrated the best diagnostic performance for distinguishing CCA from HCC patients with 70.0%

sensitivity, 61.2% specificity, 65.3% PPV and 66.1% NPV. These results showed that progenitor cell-associated lEVs can be employed as a biomarker for reliable differential diagnosis of CCA/GbCA from HCC. A distinction of CCA and GbCA had not been possible with this marker combination.

To address the clinically relevant question of the feasibility of progenitor cell-associated lEVs in HCC/iCCA differentiation, their capability of detecting and differentiating CCA subtypes from each other and from HCC was assessed. Therefore, normalized median lEV levels of HCC, intrahepatic CCA (iCCA) and extrahepatic CCA (eCCA) patients were compared for both progenitor cell-associated populations (Fig. 20A).

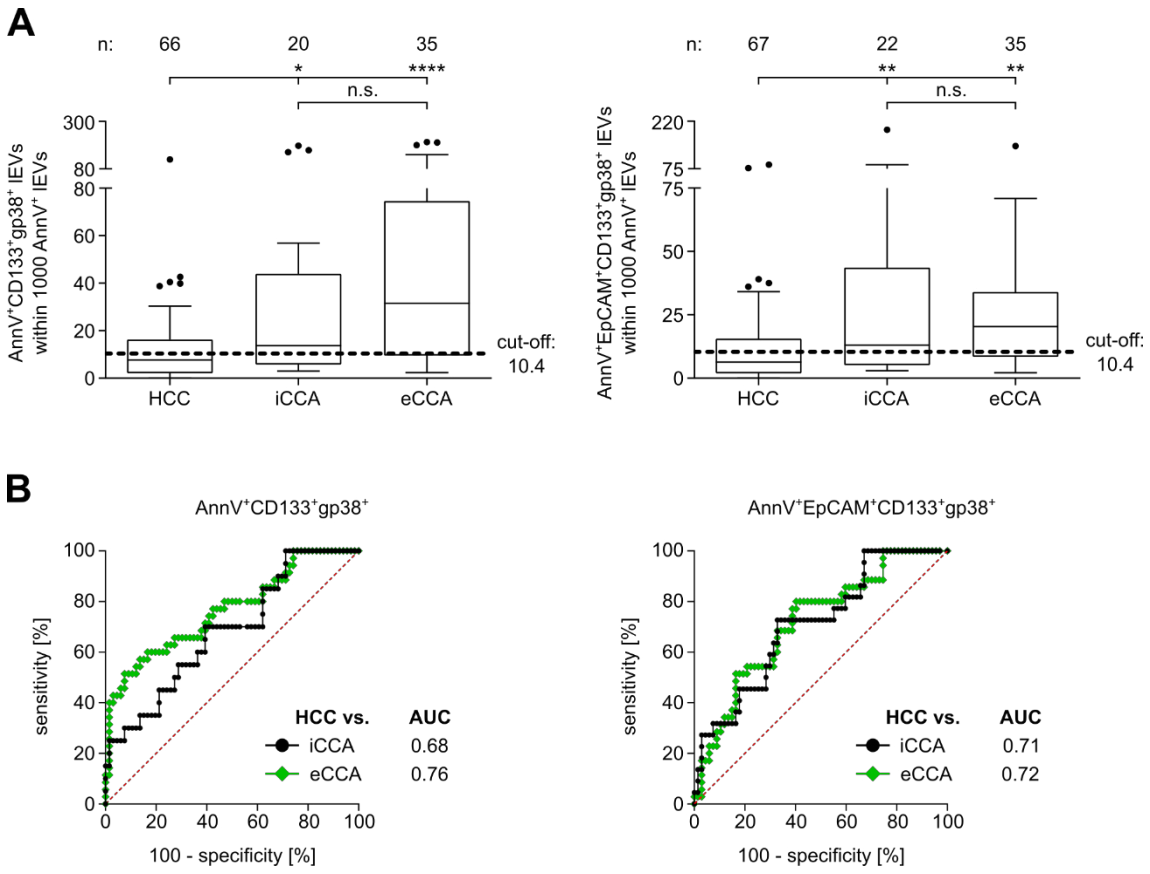

Fig. 20: Progenitor cell-associated large EVs can differentiate between HCC and iCCA. After isolation of serum lEVs and immunofluorescent labelling, they were analyzed by flow cytometry. Gating was applied as described in Fig. 15A and Fig. 17A. **A** lEV values of the two progenitor cell-associated populations AnnV+CD133+gp38+ (left panel) and AnnV+EpCAM+CD133+gp38+ (right panel) are shown for HCC, intrahepatic (iCCA) and extrahepatic (eCCA) CCA patients. Data is shown as medians with interquartile range (IQR), whiskers represent 1.5 × IQR (Tukey) with potential outliers plotted as dots. n indicates number of patients. Dotted lines indicate diagnostic cut-offs for discrimination between HCC and iCCA or eCCA for the respective lEV population (see Tab. 9). Statistical

significance was assessed by Kruskal-Wallis non-parametric test followed by Dunn's multiple comparison post hoc test with $p \leq 0.05$ considered statistically significant. **B** Corresponding ROC curves for AnnV$^+$CD133$^+$gp38$^+$ lEVs (left panel) and AnnV$^+$EpCAM$^+$CD133$^+$gp38$^+$ lEVs (right panel) for the discrimination between HCC and iCCA or eCCA including AUC values are shown. (* = $p \leq 0.05$, ** = $p \leq 0.01$, *** = $p \leq 0.001$, **** = $p \leq 0.0001$). n.s.: non-significant.

Kruskal-Wallis non-parametric test followed by Dunn's multiple comparison post hoc test revealed that lEV levels were significantly elevated in iCCA and eCCA patients as compared to HCC patients in both progenitor cell-associated populations, whereas no significant difference could be observed between the two CCA subtypes. In detail, AnnV$^+$CD133$^+$gp38$^+$ lEV levels of iCCA patients were 1.8-fold increased ($p \leq 0.05$) and levels of eCCA patients were 4.1-fold increased ($p \leq 0.0001$) as compared to HCC patients. AnnV$^+$EpCAM$^+$CD133$^+$gp38$^+$ lEV levels of iCCA patients were 2.0-fold increased ($p \leq 0.01$) and levels of eCCA patients were 3.2-fold increased ($p \leq 0.01$) as compared to HCC patients. In order to assess the diagnostic relevance of these results, ROC curves and associated AUC values were computed for discrimination of iCCA and eCCA patients from HCC patients (Fig. 20B). AUC values of AnnV$^+$CD133$^+$gp38$^+$ lEVs for discriminating iCCA from HCC (0.68) and for distinguishing eCCA from HCC (0.76) indicated a good predictive power of the biomarker. AUC values of AnnV$^+$EpCAM$^+$CD133$^+$gp38$^+$ lEVs for discriminating iCCA from HCC (0.71) and for distinguishing eCCA from HCC (0.72) indicated a similar predictive power as AnnV$^+$CD133$^+$gp38$^+$ lEVs. Out of the ROC curve analyses, diagnostic cut-offs and other predictive values for both progenitor cell-associated populations were calculated (Tab. 9). For iCCA/HCC and eCCA/HCC distinction AnnV$^+$EpCAM$^+$CD133$^+$gp38$^+$ lEVs were superior to AnnV$^+$CD133$^+$gp38$^+$ lEVs in terms of diagnostic performance, with sensitivities of 72.7% and 77.1%, specificities of 67.2% and 61.2%, PPVs of 42.1% and 50.9% and NPVs of 88.2% and 83.7%, respectively.

Tab. 9: Diagnostic performance of progenitor cell-associated large EV populations for differentiation of CCA subtypes from HCC. iCCA and eCCA patients were compared to HCC patients, respectively. Diagnostic cut-offs are given as number per 10^3 $AnnV^+$ lEVs, whereas sensitivities (sens), specificities (spec) as well as positive (PPV) and negative predictive values (NPV) are given as percentage. n indicates cohort size.

$AnnV^+CD133^+gp38^+$ lEVs							
	cut-off	**AUC**	***p*-value**	**sens [%]**	**spec [%]**	**PPV [%]**	**NPV [%]**
iCCA (n=20) vs. **HCC** (n=66)	10.4	0.68	0.0138	70.0	60.6	35.0	87.0
eCCA (n=35) vs**.** **HCC** (n=66)	10.4	0.76	<0.0001	71.4	60.6	49.0	80.0
$AnnV^+EpCAM^+CD133^+gp38^+$ lEVs							
	cut-off	**AUC**	***p*-value**	**sens [%]**	**spec [%]**	**PPV [%]**	**NPV [%]**
iCCA (n=22) vs. **HCC** (n=67)	10.4	0.71	0.0032	72.7	67.2	42.1	88.2
eCCA (n=35) vs**.** **HCC** (n=67)	8.4	0.72	0.0003	77.1	61.2	50.9	83.7

Taken together the results render progenitor cell-associated lEV populations a suitable tool for biliary cancer detection and, more importantly, for differential diagnosis of hepatobiliary cancer entities with the possibility to easily distinguish iCCA from HCC in a diagnostically relevant and uncomplicated manner.

3.2.3.1. Progenitor cell-associated large EVs improve the diagnostic performance of commonly used serum tumor markers

Currently, the serum markers AFP and CA19-9 are widely used to aid in HCC and CCA detection, respectively, even though their diagnostic benefit is debatable and their sole use for diagnosis is not recommended (Bridgewater *et al.* 2014, Galle *et al.* 2018). Nonetheless, they have proven to be diagnostically useful in a multitude of studies, so it was interesting to evaluate if a combination of serum tumor markers with the progenitor cell-associated lEV biomarker established herein led to an improved differentiation capability between HCC and CCA.

As described earlier, human serum for this thesis was obtained from several medical centers across Europe. Due to differing operating procedures, not every center could provide detailed information about all serological parameters. Therefore, the patient

cohorts needed to be adjusted to patients for which lEV values as well as AFP or CA19-9 values were available, leading to smaller cohort sizes as compared to the original progenitor cell-associated study cohort. Additionally, even though the differentiation of HCC from iCCA is of the greatest clinical interest, CCA patients of both subtypes were taken into account for this analysis. This was necessary due to the fact that the number of patients within the cohorts would have been greatly unequal (60 HCC versus 14 iCCA patients), which would have significantly reduced the diagnostic power of the analysis.

In a first step, possible correlations of progenitor cell-associated lEVs with the two serum markers were evaluated in CCA and HCC patients, in order to identify dependencies. Therefore, Spearman's rank correlation coefficients (r) for each progenitor cell-associated lEV population as compared to AFP and CA19-9 were calculated and the distribution was visualized. Spearman's rank correlation coefficient describes if two variables are monotonically related (r=1) and indicates the direction of the association with a positive (both variables increase) or negative (one variable increases, one decreases) algebraic sign. The correlation analysis revealed that neither AFP nor CA19-9 correlated significantly with any progenitor cell-associated lEV population in HCC patients (Fig. 21A) with r values ranging from -0.17 to -0.08. For CCA patients on the other hand, a slight but significant correlation tendency could be observed between $AnnV^+CD133^+gp38^+$ lEVs and AFP (r=-0.35, p=0.01) and between $AnnV^+CD133^+gp38^+$ lEVs and CA19-9 (r=0.39, p=0.002), whereas $AnnV^+EpCAM^+CD133^+gp38^+$ lEVs did not correlate significantly with any serum marker (Fig. 21B). Next, the diagnostic performance of AFP and CA19-9 for HCC and CCA differentiation within the progenitor cell-associated study cohort was evaluated (Fig. 21C and D). Two-tailed Mann-Whitney U tests revealed that AFP levels were significantly elevated ($p \leq 0.0001$) by 12.9-fold in HCC patients as compared to CCA patients. CA19-9 levels on the other hand were significantly elevated ($p \leq 0.0001$) by 14.4-fold in CCA patients as compared to HCC patients.

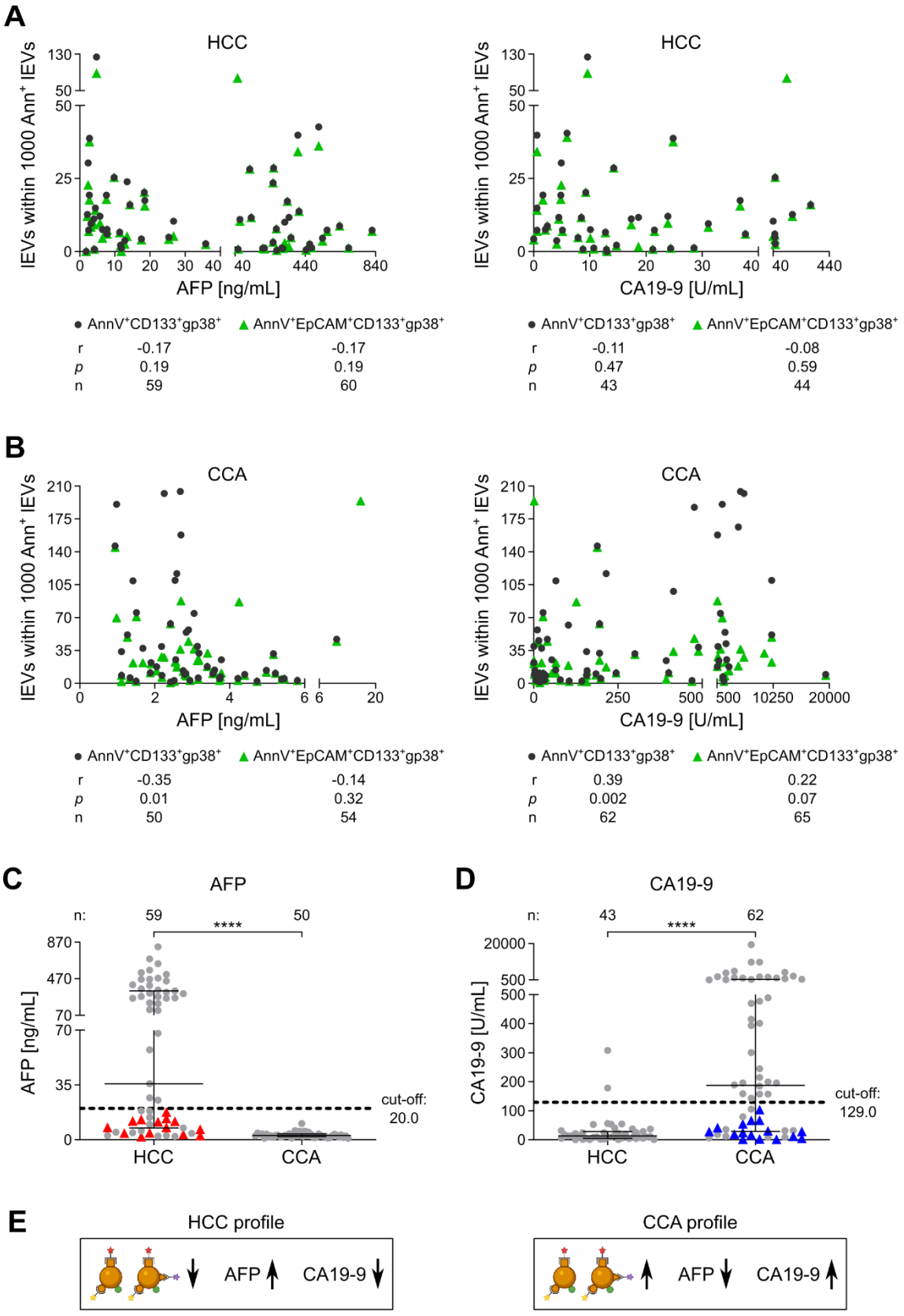

Fig. 21: Progenitor cell-associated large EVs improve the diagnostic performance of AFP and CA19-9. After isolation of serum lEVs and immunofluorescent labelling, they

were analyzed by flow cytometry. Gating was applied as described in Fig. 15A and Fig. 17A. **A** Correlations between lEV levels and AFP (left panel) or CA19-9 (right panel) of HCC patients for the two progenitor cell-associated populations are depicted. **B** Correlations between lEV levels and AFP (left panel) or CA19-9 (right panel) of CCA patients are shown. Spearman's correlation (r), *p*-values and cohort sizes (n) are indicated for each individual population and patient cohort. In **C** AFP values of HCC and CCA patients are displayed. Indicated in red are patients that based on AFP levels are not classified as HCC patients (AFP < 20 ng/mL) but can positively be identified as HCC by $AnnV^+EpCAM^+CD133^+gp38^+$ lEVs < 8.5 (see Tab. 8). In **D** CA19-9 values of HCC and CCA patients are displayed. Indicated in blue are patients that based on CA19-9 levels are not classified as CCA patients (CA19-9 < 129 U/mL) but can positively be identified as CCA by $AnnV^+EpCAM^+CD133^+gp38^+$ lEVs > 8.5 (see Tab. 8). Data is shown as scatter plots including median with interquartile range. n indicates number of patients. Dotted lines indicate recommended diagnostic cut-off of 20 ng/mL for AFP and 129 U/mL for CA19-9. Statistical significance was assessed by two-tailed Mann-Whitney *U* tests with $p \leq 0.05$ considered statistically significant. (* = $p \leq 0.05$, ** = $p \leq 0.01$, *** = $p \leq 0.001$, **** = $p \leq 0.0001$). In **E** the diagnostic profile for HCC detection (left panel) with low progenitor cell-associated lEV levels, high AFP and low CA19-9 values is schematically visualized. *Vice versa*, the diagnostic profile for CCA detection is shown in the right panel. Profiles were created with BioRender.com. The panels **A** (left panel), **B** (left panel) and **C** are part of the attached publication Urban *et al.* (2020) that resulted from this project research.

Out of the displayed AFP and CA19-9 levels in HCC and CCA patients associated predictive values were computed (Tab. 10). Cut-offs of 20 ng/mL for AFP and 129 U/mL for CA19-9 were chosen, which refer to the suggested diagnostic cut-offs in the respective international guidelines for HCC and CCA management, respectively (Valle *et al.* 2016, Galle *et al.* 2018). With 100% sensitivity and 54.2% specificity AFP as a sole biomarker displayed a good diagnostic reliability for HCC and CCA differentiation in the progenitor cell-associated study cohort, whereas CA19-9 showed slightly lower predictive power with 58.7% sensitivity and 95.3% specificity. When adding the previous findings of this thesis of progenitor cell-associated lEVs as biomarkers to sole AFP and CA19-9 evaluation, a distinct diagnostic improvement becomes evident. In Fig. 21C those HCC patients are highlighted in red that based on AFP levels are not classified as HCC (AFP < 20 ng/mL) but that can positively be identified as HCC by $AnnV^+EpCAM^+CD133^+gp38^+$ lEVs < 8.5 (see cut-off Tab. 8). *Vice versa*, in Fig. 21D those CCA patients are exemplarily highlighted in blue that based on CA19-9 levels are not classified as CCA (CA19-9 < 129 U/mL) but that can positively be identified as CCA by $AnnV^+EpCAM^+CD133^+gp38^+$ lEVs > 8.5. After adding the patients that were correctly identified by progenitor cell-associated lEVs to the already identified patients by AFP or CA19-9, corresponding adjusted predictive values

could be calculated accordingly (Tab. 10). Both progenitor cell-associated lEV biomarkers markedly increased the diagnostic performance of AFP, whereby the combination with AnnV$^+$EpCAM$^+$CD133$^+$gp38$^+$ lEVs resulted in the highest diagnostic values with 100% sensitivity, 78.0% specificity, 79.4% PPV and 100% NPV. Similarly, the diagnostic performance of CA19-9 could considerably be enhanced by both progenitor cell-associated populations. Again, the combination with AnnV$^+$EpCAM$^+$CD133$^+$gp38$^+$ lEVs showed the best results with 84.1% sensitivity, 95.3% specificity, 96.4% PPV and 80.4% NPV.

Tab. 10: Diagnostic performance of AFP and CA19-9 individually and combined with progenitor cell-associated large EV populations in HCC/CCA differentiation. CCA patients were compared to HCC patients. Diagnostic cut-offs are given as number per 10^3 AnnV$^+$ lEVs for lEV populations, as ng/mL for AFP and as U/mL for CA19-9. Sensitivities (sens), specificities (spec) as well as positive (PPV) and negative predictive values (NPV) are given as percentage. n indicates cohort size.

AFP					
CCA: n=50, HCC: n=59	**cut-off**	**sens [%]**	**spec [%]**	**PPV [%]**	**NPV [%]**
AFP	20	100	54.2	64.9	100
AFP or AnnV$^+$CD133$^+$gp38$^+$	20 or 10.4	100	76.3	78.1	100
AFP or AnnV$^+$EpCAM$^+$CD133$^+$gp38$^+$	20 or 8.5	**100**	**78.0**	**79.4**	**100**
CA19-9					
CCA: n=63, HCC: n=43	**cut-off**	**sens [%]**	**spec [%]**	**PPV [%]**	**NPV [%]**
CA19-9	129	58.7	95.3	94.9	61.2
CA19-9 or AnnV$^+$CD133$^+$gp38$^+$	129 or 10.4	82.5	95.3	96.3	78.8
CA19-9 or AnnV$^+$EpCAM$^+$CD133$^+$gp38$^+$	129 or 8.5	**84.1**	**95.3**	**96.4**	**80.4**

In summary, combining the currently used serum biomarkers AFP and CA19-9 with the novel progenitor cell-associated lEV biomarkers established in this study led to an almost perfect separation of CCA from HCC patients. With these insights it was possible to generate a specific and highly relevant diagnostic profile for HCC and CCA patients for potential future uncomplicated differential diagnosis that is based solely on serum biomarkers (Fig. 21E): Thus, patients presenting with low progenitor cell-associated lEV, high AFP and low CA19-9 values might easily be identified as HCC patients, whereas,

vice versa, high progenitor cell-associated lEV, low AFP and high CA19-9 values might be characteristic for CCA patients.

3.2.4. Tumor-associated large EV populations can diagnostically differentiate between hepatobiliary cancers

Since this thesis investigated the role of lEVs in hepatobiliary cancer management for two study cohorts, the benefit of tumor-associated lEV populations will be evaluated and compared to progenitor cell-associated lEV populations in the upcoming chapters. As for progenitor cell-associated populations, lEVs of several patient cohorts were isolated, immunofluorescently labelled and analyzed by flow cytometry. In addition to the general gating strategy described in Fig. 15A, the gating was successively expanded as depicted in Fig. 22A to identify the two tumor-associated lEV populations $AnnV^+CD44v6^+$ and $AnnV^+CD44v6^+CD133^+$, which are schematically visualized in Fig. 22B. Briefly, $AnnV^+$ lEVs were restricted to $CD44v6^+$ lEVs to obtain the first tumor-associated population $AnnV^+CD44v6^+$. To obtain the second tumor-associated population $AnnV^+CD44v6^+CD133^+$, $AnnV^+$ lEVs were limited to $CD133^+$ lEVs, followed by an identification of $CD44v6^+$ lEVs out of the $AnnV^+CD133^+$ lEV pool. The gates in this figure correspond to the positive populations that were identified for each marker according to their concentration-matched isotype controls (compare Fig. 15B). The counts for each tumor-associated population were evaluated and normalized to 1000 $AnnV^+$ lEVs for comparability among samples and cohorts. Median, normalized lEV levels of all patients participating in the tumor-associated study cohort were evaluated and the values for each individual cohort for both tumor-associated populations are visualized in Fig. 22C. A group analysis with Kruskal-Wallis non-parametric test followed by Dunn's multiple comparison post hoc test between biliary cancer entities (CCA and GbCA), non-biliary cancer entities (HCC, CRC and NSCLC), cirrhosis patients and healthy individuals revealed that lEV levels were significantly elevated in biliary cancer patients as compared to healthy subjects and non-biliary cancer patients in both tumor-associated populations (Fig. 22D).

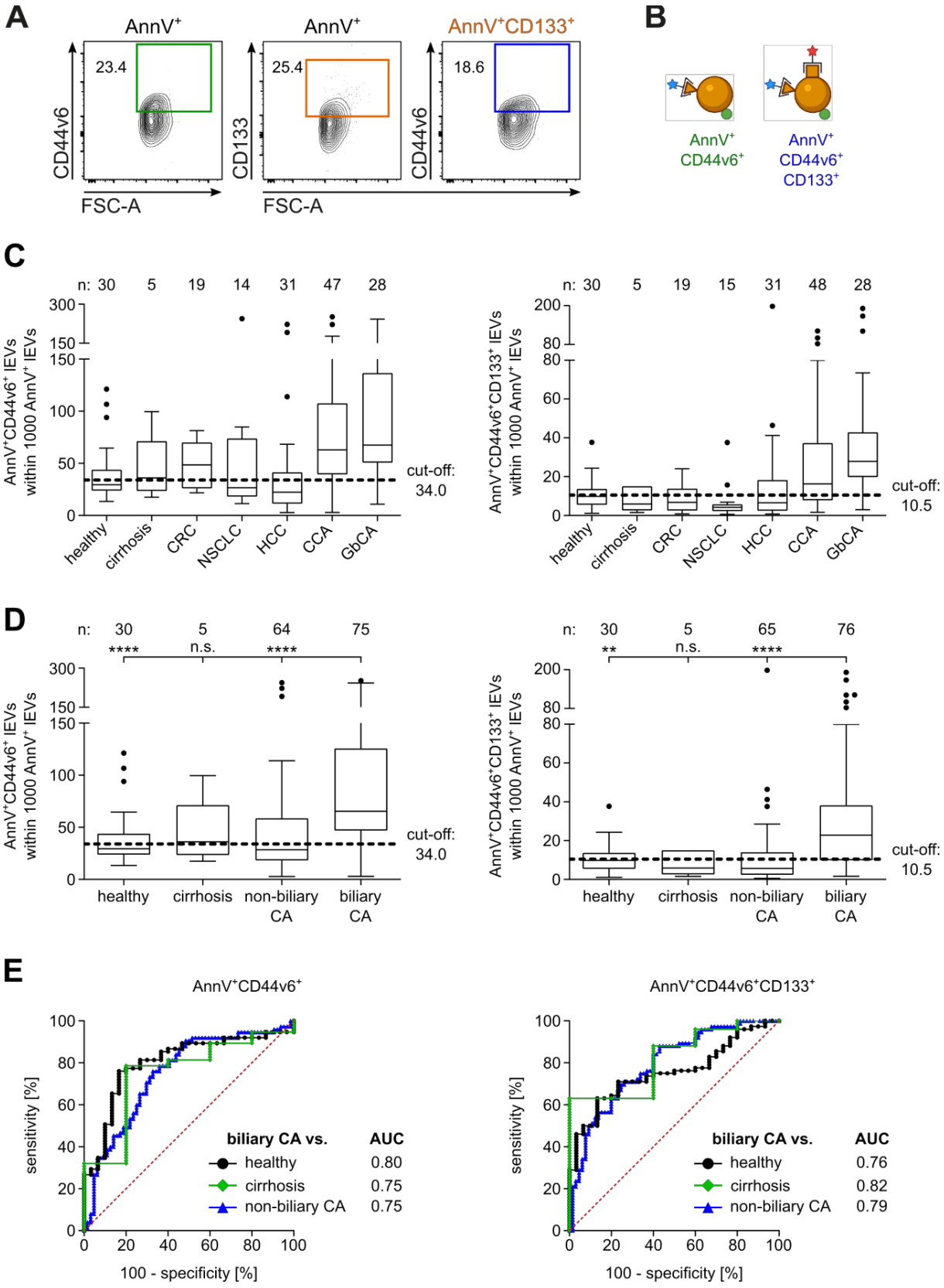

Fig. 22: Tumor-associated large EVs can distinguish biliary cancer patients from controls. After isolation of serum lEVs and immunofluorescent labelling, they were

analyzed by flow cytometry. Gating was applied as described in Fig. 15A. **A** exemplarily describes the subsequent successive gating strategy applied to identify the two tumor-associated lEV populations AnnV$^+$CD44v6$^+$ (green) and AnnV$^+$CD44v6$^+$CD133$^+$ (blue). In **B** lEVs of the two tumor-associated populations are schematically visualized (created with BioRender.com) referring to the staining protocol described in Fig. 14. **C** lEV values of the two tumor-associated populations AnnV$^+$CD44v6$^+$ (left panel) and AnnV$^+$CD44v6$^+$CD133$^+$ (right panel) are shown for healthy individuals, cirrhosis patients and various cancer patient cohorts (CRC, NSCLC, HCC, CCA, GbCA). **D** Patient cohorts were summarized to non-biliary carcinomas (non-biliary CA) comprising CRC, NSCLC and HCC patients, and biliary carcinomas (biliary CA) comprising CCA and GbCA patients. AnnV$^+$CD44v6$^+$ lEV (left panel) as well as AnnV$^+$CD44v6$^+$CD133$^+$ lEV (right panel) levels of the combined cohorts are depicted. Data is shown as medians with interquartile range (IQR), whiskers represent 1.5 × IQR (Tukey) with potential outliers plotted as dots. n indicates number of patients. Dotted lines indicate diagnostic cut-offs for discrimination between biliary CA and controls for the respective lEV population (see Tab. 11). Statistical significance was assessed by Kruskal-Wallis non-parametric test followed by Dunn's multiple comparison post hoc test with $p \leq 0.05$ considered statistically significant. **E** Corresponding ROC curves for AnnV$^+$CD44v6$^+$ lEVs (left panel) and AnnV$^+$CD44v6$^+$CD133$^+$ lEVs (right panel) for the discrimination between biliary CA and controls (healthy, cirrhosis and non-biliary CA) including AUC values are shown. (* = $p \leq 0.05$, ** = $p \leq 0.01$, *** = $p \leq 0.001$, **** = $p \leq 0.0001$). The panels **A**, **C** and **D** are part of the attached publication Urban *et al.* (2020) that resulted from this project. n.s.: non-significant.

In detail, AnnV$^+$CD44v6$^+$ lEV levels of biliary cancer patients were 2.2-fold increased compared to healthy subjects ($p \leq 0.0001$) and 2.3-fold increased compared to non-biliary cancer patients ($p \leq 0.0001$). AnnV$^+$CD44v6$^+$CD133$^+$ lEV levels of biliary cancer patients were 2.3-fold increased compared to healthy subjects ($p \leq 0.01$) and 4.0-fold increased compared to non-biliary cancer patients ($p \leq 0.0001$). No significant difference ($p > 0.5$) could be observed between biliary cancer versus cirrhosis patients in both tumor-associated populations. ROC curves and associated AUC values were computed for discrimination of biliary cancer patients from each of the three control groups for both tumor-associated populations (Fig 22E). AUC values of AnnV$^+$CD44v6$^+$ lEVs for discriminating biliary cancer patients from healthy individuals (0.80), cirrhosis (0.75) and non-biliary cancer patients (0.75) indicated a good predictive power of the biomarker to varying degrees. AUC values of AnnV$^+$CD44v6$^+$CD133$^+$ lEVs for discriminating biliary cancer patients from healthy individuals (0.76), cirrhosis (0.82) and non-biliary cancer patients (0.79) indicated a similar predictive power as for AnnV$^+$CD44v6$^+$ lEVs. Out of the ROC curve analyses, diagnostic cut-offs and other predictive values for both tumor-associated populations were calculated (Tab. 11).

Tab. 11: Diagnostic performance of tumor-associated large EV populations for biliary cancer diagnosis. Biliary cancers (CCA and GbCA) were compared to healthy controls, cirrhosis patients and non-biliary CA (NSCLC, CRC and HCC) patients. Diagnostic cut-offs are given as number per 10^3 AnnV$^+$ lEVs, whereas sensitivities (sens), specificities (spec) as well as positive (PPV) and negative predictive values (NPV) are given as percentage. n indicates cohort size.

AnnV$^+$CD44v6$^+$ lEVs							
	cut-off	**AUC**	**p-value**	**sens [%]**	**spec [%]**	**PPV [%]**	**NPV [%]**
biliary CA (n=75) vs. **healthy** (n=30)	34	0.80	<0.0001	84.0	63.3	85.1	61.3
biliary CA (n=75) vs. **cirrhosis** (n=5)	34	0.75	0.0603	84.0	40.0	95.5	14.3
biliary CA (n=75) vs**. non-biliary CA** (n=64)	34	0.75	<0.0001	84.0	56.3	69.2	75.0
AnnV$^+$CD44v6$^+$CD133$^+$ lEVs							
	cut-off	**AUC**	**p-value**	**sens [%]**	**spec [%]**	**PPV [%]**	**NPV [%]**
biliary CA (n=75) vs. **healthy** (n=30)	10.5	0.76	<0.0001	74.7	56.7	81.2	47.2
biliary CA (n=75) vs. **cirrhosis** (n=5)	10.5	0.82	0.0167	74.7	60.0	96.6	13.6
biliary CA (n=75) vs**. non-biliary CA** (n=65)	10.5	0.79	<0.0001	74.7	66.2	71.8	69.4

For both populations, differentiation of biliary cancer from all controls was associated with a good sensitivity of at least 74.7%. AnnV$^+$CD44v6$^+$ lEVs achieved the best diagnostic values with 84.0% sensitivity, 63.3% specificity, 85.1% PPV and 61.3% NPV for discrimination of biliary cancer patients from healthy individuals. AnnV$^+$CD44v6$^+$CD133$^+$ lEVs on the other hand showed slightly lower predictive power than AnnV$^+$CD44v6$^+$ lEVs, with 74.7% sensitivity, 66.2% specificity, 71.8% PPV and 69.4% NPV for distinguishing biliary from non-biliary cancer patients. Of note, since only five cirrhosis patients could be included in this analysis, the cohort sizes were extremely unequal (as compared to 75 biliary cancer patients), so the significance and comparability of the results might be impaired and should be interpreted with care in case of differential diagnosis of biliary cancers from cirrhosis. Compared to the progenitor cell-associated lEV populations, the tumor-associated lEV populations showed an overall better diagnostic performance (see Tab. 7), with AnnV$^+$CD44v6$^+$ lEVs revealing to be the most promising population for general biliary cancer diagnosis and differentiation out of a pool of other malignancies and

liver-related diseases. As for progenitor cell-associated lEV populations, the differentiation potential of both tumor-associated populations within the hepatobiliary compartment was assessed. Therefore, normalized median lEV levels for both tumor-associated populations were evaluated in HCC, CCA and GbCA patients (Fig. 23A).

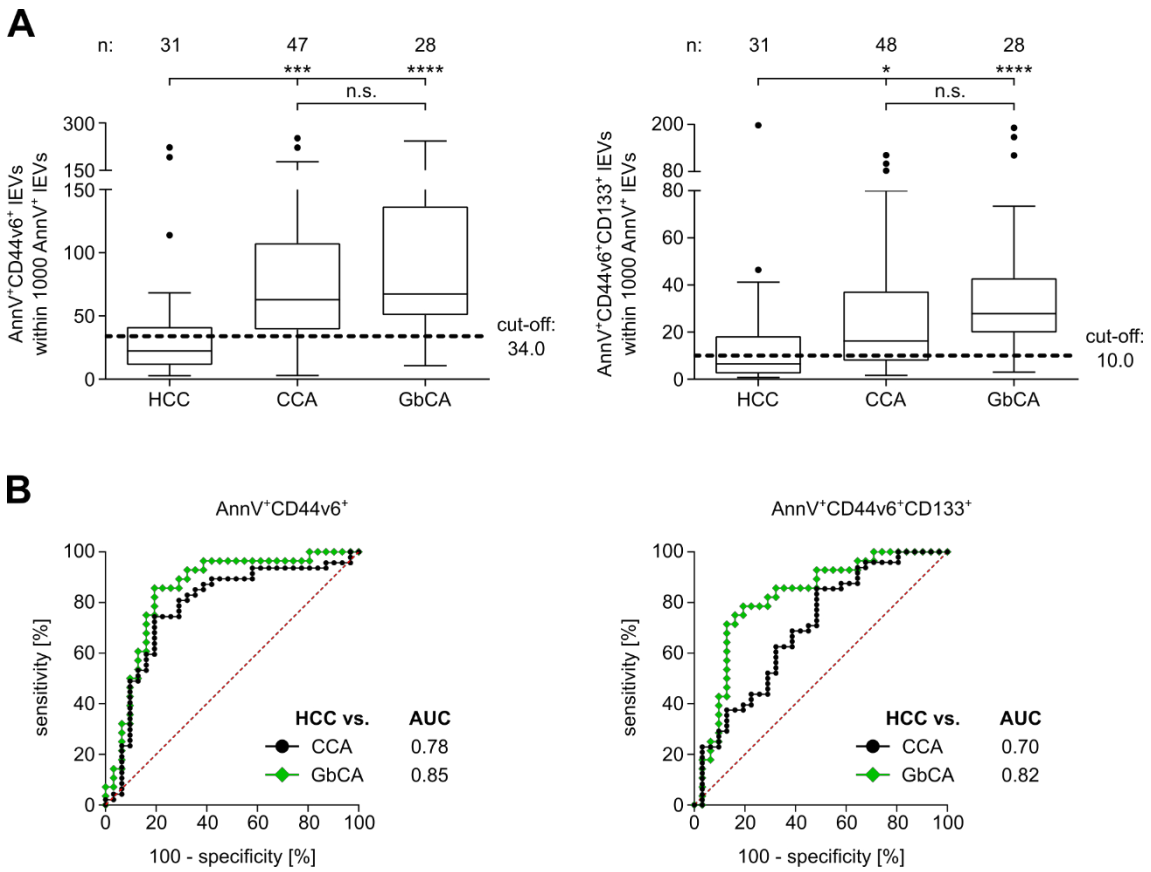

Fig. 23: Tumor-associated large EVs are distributed differentially in hepatobiliary cancer entities. After isolation of serum lEVs and immunofluorescent labelling, they were analysed by flow cytometry. Gating was applied as described in Fig. 15A and Fig. 22A. **A** lEV values of the two tumor-associated populations AnnV$^+$CD44v6$^+$ (left panel) and AnnV$^+$CD44v6$^+$CD133$^+$ (right panel) are shown for HCC, CCA and GbCA patients. Data is shown as medians with interquartile range (IQR), whiskers represent 1.5 × IQR (Tukey) with potential outliers plotted as dots. n indicates number of patients. Dotted lines indicate diagnostic cut-offs for discrimination between HCC and CCA or GbCA for the respective lEV population (see Tab. 12). Statistical significance was assessed by Kruskal-Wallis non-parametric test followed by Dunn's multiple comparison post hoc test with $p \leq 0.05$ considered statistically significant. **B** Corresponding ROC curves for AnnV$^+$CD44v6$^+$ (left panel) and AnnV$^+$CD44v6$^+$CD133$^+$ lEVs (right panel) for the discrimination between HCC and CCA or GbCA including AUC values are shown. (* = $p \leq 0.05$, ** = $p \leq 0.01$, *** = $p \leq 0.001$, **** = $p \leq 0.0001$). n.s.: non-significant.

Kruskal-Wallis non-parametric test followed by Dunn's multiple comparison post hoc test revealed that lEV levels were significantly elevated in CCA and GbCA patients as compared to HCC patients in both tumor-associated populations, whereas lEV levels in CCA and GbCA patients were similar, without significant differences. In detail, AnnV$^+$CD44v6$^+$ lEV levels of CCA patients were 2.8-fold increased ($p \leq 0.001$) and levels of GbCA patients were 3.0-fold increased ($p \leq 0.0001$) as compared to HCC patients. AnnV$^+$CD44v6$^+$CD133$^+$ lEV levels of CCA patients were 2.5-fold increased ($p \leq 0.05$), and levels of GbCA patients were 4.3-fold increased ($p \leq 0.0001$) as compared to HCC patients. In order to assess the diagnostic relevance of these results, ROC curves and associated AUC values were computed for discrimination of CCA and GbCA patients from HCC patients (Fig. 23B). AUC values of AnnV$^+$CD44v6$^+$ lEVs for discriminating CCA from HCC (0.78) and for distinguishing GbCA from HCC (0.85) indicated a very good predictive power of the biomarker. AUC values of AnnV$^+$CD44v6$^+$CD133$^+$ lEVs for discriminating CCA from HCC (0.70) and for distinguishing GbCA from HCC (0.82) indicated a slightly lower predictive power than AnnV$^+$CD133$^+$gp38$^+$ lEVs. Out of the ROC curve analyses, diagnostic cut-offs and other predictive values for both tumor-associated populations were calculated (Tab. 12). AnnV$^+$CD44v6$^+$ lEVs were superior in differentiation of CCA from HCC as well as GbCA from HCC and showed a powerful predictive power, especially for GbCA/HCC differentiation with 89.3% sensitivity, 71.0% specificity, 73.5% PPV and 88.0% NPV. Nonetheless, for CCA/HCC differentiation AnnV$^+$CD44v6$^+$ lEVs achieved 80.9% sensitivity, 71.0% specificity, 80.9% PPV and 71.0% NPV and can thus be considered as the lEV population that showed the best results for HCC/CCA discrimination out of all four investigated populations. The diagnostic performance of AnnV$^+$CD44v6$^+$CD133$^+$ lEVs for HCC/CCA differentiation with 68.8% sensitivity, 61.3% specificity, 73.3% PPV and 55.9% NVP is similar to that of the progenitor cell-associated lEV populations and cannot surpass them.

Tab. 12: Diagnostic performance of tumor-associated large EV populations for hepatobiliary cancer differentiation. CCA and GbCA patients were compared to HCC patients, respectively. Diagnostic cut-offs are given as number per 10^3 $AnnV^+$ lEVs, whereas sensitivities (sens), specificities (spec) as well as positive (PPV) and negative predictive values (NPV) are given as percentage. n indicates cohort size.

$AnnV^+CD44v6^+$ lEVs							
	cut-off	**AUC**	***p*-value**	**sens [%]**	**spec [%]**	**PPV [%]**	**NPV [%]**
CCA (n=47) vs. **HCC** (n=31)	34	0.78	<0.0001	80.9	71.0	80.9	71.0
GbCA (n=28) vs**.** **HCC** (n=31)	34	0.85	<0.0001	89.3	71.0	73.5	88.0
$AnnV^+CD44v6^+CD133^+$ lEVs							
	cut-off	**AUC**	***p*-value**	**sens [%]**	**spec [%]**	**PPV [%]**	**NPV [%]**
CCA (n=48) vs. **HCC** (n=31)	10.0	0.70	0.0028	68.8	61.3	73.3	55.9
GbCA (n=28) vs**.** **HCC** (n=31)	13.8	0.82	<0.0001	85.7	67.7	70.6	84.0

As observed for progenitor cell-associated lEV populations, these results showed that tumor-associated lEVs can be employed as a biomarker for reliable differential diagnosis of CCA or GbCA from HCC, whereas a distinction of CCA and GbCA had not been possible with this marker combination.

To address the clinically relevant question of the feasibility of tumor-associated lEVs in HCC/iCCA differentiation, their capability of detecting and differentiating CCA subtypes from each other and from HCC was assessed. Therefore, normalized median lEV levels of HCC, intrahepatic CCA (iCCA) and extrahepatic CCA (eCCA) patients were compared for both tumor-associated populations (Fig. 24A).

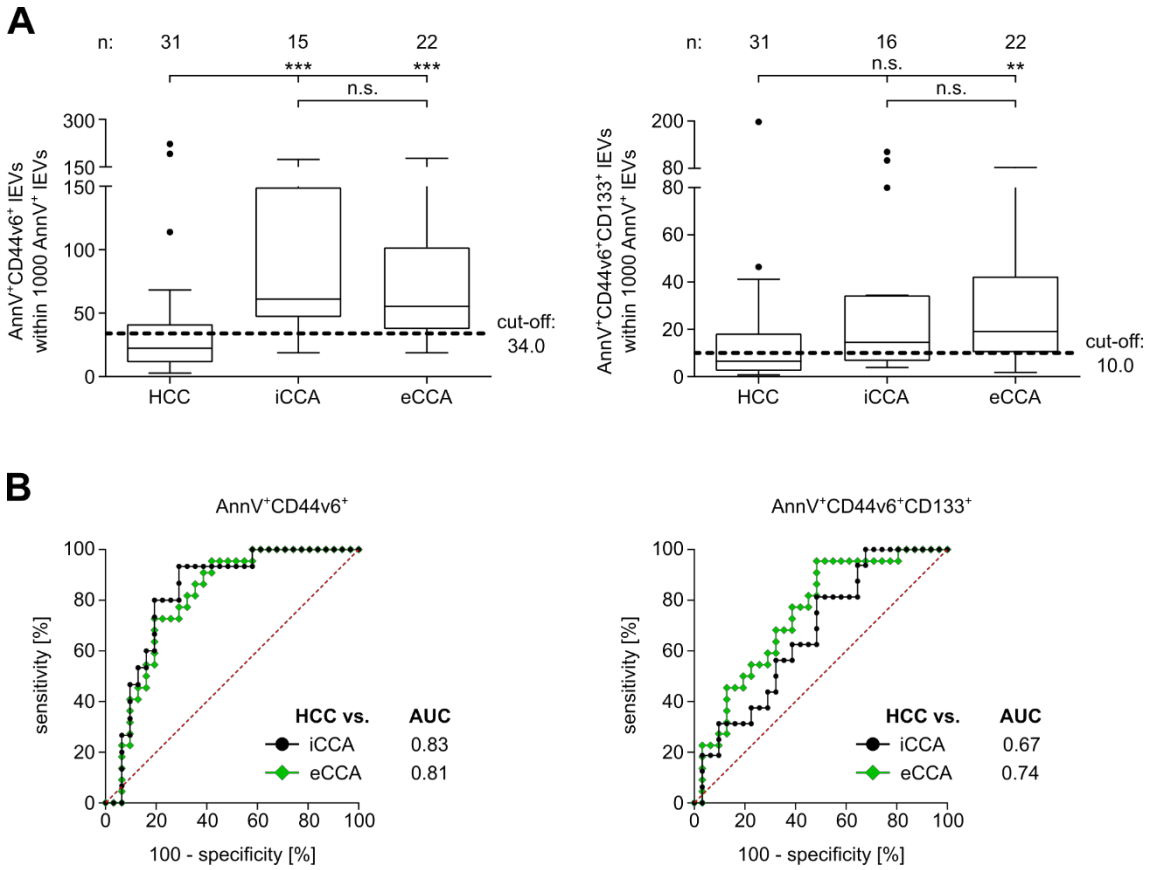

Fig. 24: Tumor-associated large EVs can differentiate between HCC and iCCA. After isolation of serum lEVs and immunofluorescent labelling, they were analysed by flow cytometry. Gating was applied as described in Fig. 15A and Fig. 22A. **A** lEV values of the two tumor-associated populations AnnV$^+$CD44v6$^+$ (left panel) and AnnV$^+$CD44v6$^+$CD133$^+$ (right panel) are shown for HCC, intrahepatic (iCCA) and extrahepatic (eCCA) CCA patients. Data is shown as medians with interquartile range (IQR), whiskers represent 1.5 × IQR (Tukey) with potential outliers plotted as dots. n indicates number of patients. Dotted lines indicate diagnostic cut-offs for discrimination between HCC and iCCA or eCCA for the respective lEV population (see Tab. 13). Statistical significance was assessed by Kruskal-Wallis non-parametric test followed by Dunn's multiple comparison post hoc test with $p \leq 0.05$ considered statistically significant. **B** Corresponding ROC curves for AnnV$^+$CD44v6$^+$ lEVs (left panel) and AnnV$^+$CD44v6$^+$CD133$^+$ lEVs (right panel) for the discrimination between HCC and iCCA or eCCA including AUC values are shown. (* = $p \leq 0.05$, ** = $p \leq 0.01$, *** = $p \leq 0.001$, **** = $p \leq 0.0001$). n.s.: non-significant.

Kruskal-Wallis non-parametric test followed by Dunn's multiple comparison post hoc test revealed that lEV levels were significantly elevated in iCCA and eCCA patients as compared to HCC patients in both tumor-associated populations, whereas no significant difference could be observed between the two CCA subtypes. In detail, AnnV$^+$CD44v6$^+$ lEV levels of iCCA patients were 2.7-fold increased ($p \leq 0.001$) and levels of eCCA patients

were 2.5-fold increased ($p \leq 0.001$) as compared to HCC patients. AnnV$^+$CD44v6$^+$CD133$^+$ lEV levels of iCCA patients were not significantly increased ($p > 0.05$), whereas levels of eCCA patients were 3.0-fold increased ($p \leq 0.01$) as compared to HCC patients. In order to assess the diagnostic relevance of these results, ROC curves and associated AUC values were computed for discrimination of iCCA and eCCA patients from HCC patients (Fig. 24B). AUC values of AnnV$^+$CD44v6$^+$ lEVs for discriminating iCCA from HCC (0.83) and for distinguishing eCCA from HCC (0.81) indicated a good predictive power of the biomarker. AUC values of AnnV$^+$CD44v6$^+$CD133$^+$ lEVs for discriminating iCCA from HCC (0.67) and for distinguishing eCCA from HCC (0.74) indicated a slightly lower predictive power as AnnV$^+$CD44v6$^+$ lEVs. Out of the ROC curve analyses, diagnostic cut-offs and other predictive values for both tumor-associated populations were calculated (Tab. 13).

Tab. 13: Diagnostic performance of tumor-associated large EV populations for differentiation of CCA subtypes from HCC. iCCA and eCCA patients were compared to HCC patients, respectively. Diagnostic cut-offs are given as number per 10^3 AnnV$^+$ lEVs, whereas sensitivities (sens), specificities (spec) as well as positive (PPV) and negative predictive values (NPV) are given as percentage. n indicates cohort size.

AnnV$^+$CD44v6$^+$ lEVs							
	cut-off	**AUC**	**p-value**	**sens [%]**	**spec [%]**	**PPV [%]**	**NPV [%]**
iCCA (n=15) vs. **HCC** (n=31)	34	0.83	0.0004	93.3	71.0	60.9	95.7
eCCA (n=22) vs. **HCC** (n=31)	31.3	0.81	0.0002	81.8	67.7	64.3	84.0
AnnV$^+$CD44v6$^+$CD133$^+$ lEVs							
	cut-off	**AUC**	**p-value**	**sens [%]**	**spec [%]**	**PPV [%]**	**NPV [%]**
iCCA (n=16) vs. **HCC** (n=31)	10.0	0.67	0.0564	62.5	61.3	45.5	76.0
eCCA (n=22) vs. **HCC** (n=31)	10.0	0.74	0.0026	77.3	61.3	58.6	79.2

AnnV$^+$CD44v6$^+$ lEVs showed a very good predictive power for discriminating iCCA from HCC with 93.3% sensitivity, 71.0% specificity, 60.9% PPV and 95.7% NPV, whereas the diagnostic performance for discriminating eCCA from HCC was slightly lower with 81.8% sensitivity, 67.7% specificity, 64.3% PPV and 84.0% NPV. With only 62.5% sensitivity, AnnV$^+$CD44v6$^+$CD133$^+$ lEVs show the lowest predictive power of all four populations for

iCCA/HCC differentiation, while discrimination between eCCA and HCC, with 77.3% sensitivity, is associated with similar diagnostic relevancy as the progenitor cell-associated lEV populations. As observed for progenitor cell-associated lEV populations, tumor-associated lEV populations are a suitable tool for biliary cancer detection and, more importantly, for differential diagnosis of hepatobiliary cancer entities with the possibility to easily distinguish CCA from HCC in a diagnostically relevant and uncomplicated manner. Again, $AnnV^+CD44v6^+$ lEVs were found to be the most promising population in this study setting.

3.2.4.1. Tumor-associated large EVs improve the diagnostic performance of commonly used serum tumor markers

As evaluated for progenitor cell-associated lEV populations, it was of interest if combination of the serum tumor markers AFP or CA19-9 with the tumor-associated lEV biomarker established herein led to an improved differentiation capability between HCC and CCA. Again, due to inconsistent information availability about serum marker levels, the patient cohorts needed to be adjusted to patients, for which lEV values as well as AFP or CA19-9 values were available, leading to slightly lower cohort sizes as compared to the original tumor-associated study cohort. Additionally, as for progenitor cell-associated populations, CCA patients of both subtypes combined were taken into account for this analysis. Indeed, with 29 HCC and 10 iCCA patients the cohort sizes would not have been as unequal as for progenitor cell-associated populations but combining both CCA subtypes for analysis of the tumor-associated populations as well ensured the comparability of both study arms.

In a first step, possible correlations of tumor-associated lEVs with the two serum markers were evaluated in CCA and HCC patients, in order to identify dependencies. Therefore, Spearman's rank correlation coefficients (r) for each tumor-associated lEV population as compared to AFP and CA19-9 were calculated and the distribution was visualized. The correlation analysis revealed that, while r values ranged from -0.12 to 0.34, neither AFP nor CA19-9 correlated significantly ($p \leq 0.05$) with any tumor-associated lEV population in neither HCC nor CCA patients (Fig. 25A and B).

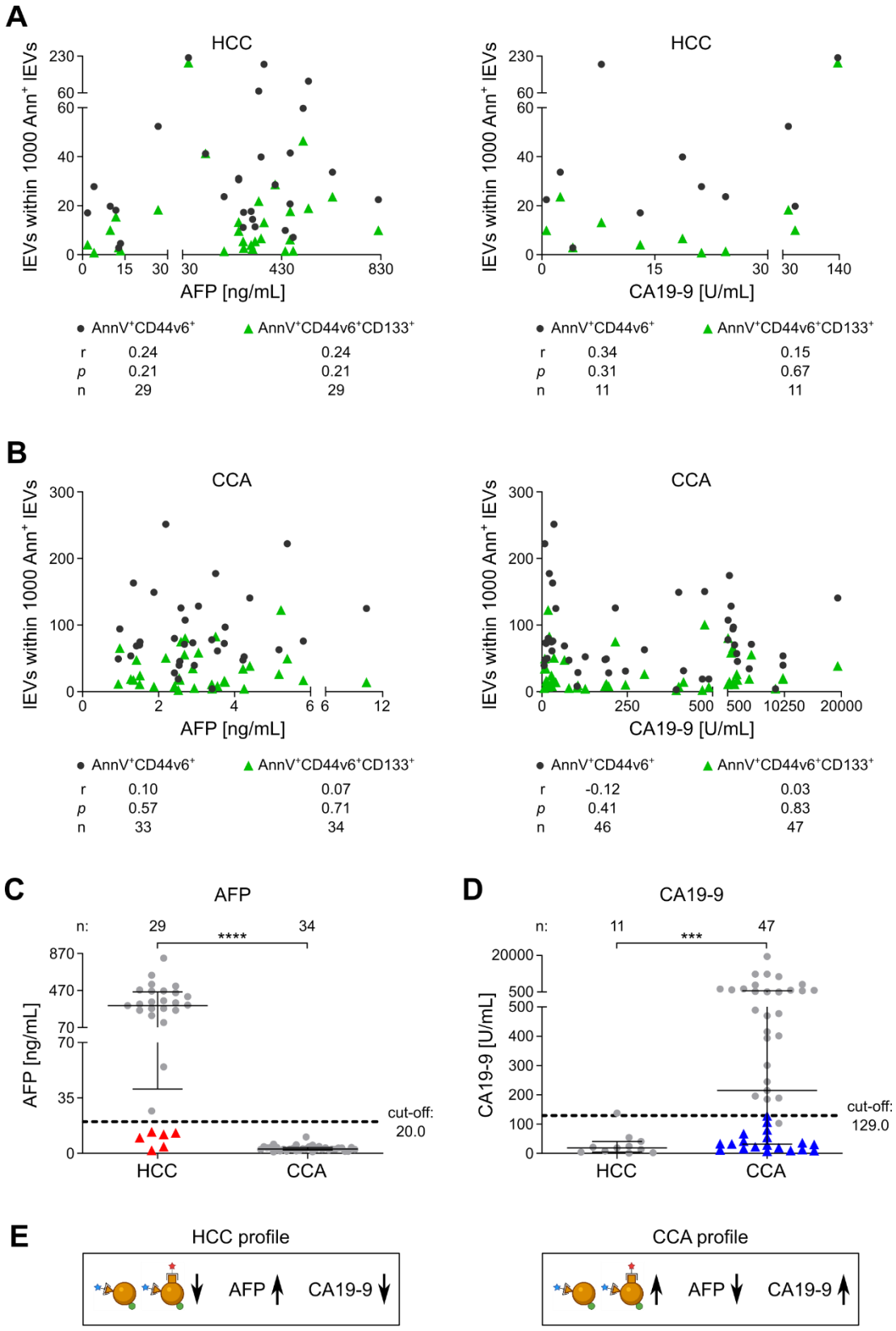

Fig. 25: Tumor-associated large EVs improve the diagnostic performance of AFP and CA19-9. After isolation of serum lEVs and immunofluorescent labelling, they were analysed by flow cytometry. Gating was applied as described in Fig. 15A and Fig. 22A.

A Correlations between lEV levels and AFP (left panel) or CA19-9 (right panel) of HCC patients for the two tumor-associated populations are depicted. **B** Correlations between lEV levels and AFP (left panel) or CA19-9 (right panel) of CCA patients are shown. Spearman's correlation (r), *p*-values and cohort sizes (n) are indicated for each individual population and patient cohort. In **C** AFP values of HCC and CCA patients are displayed. Indicated in red are patients that based on AFP levels are not classified as HCC patients (AFP < 20 ng/mL) but can positively be identified as HCC by AnnV$^+$CD44v6$^+$ lEVs < 34 (see Tab. 12). In **D** CA19-9 values of HCC and CCA patients are displayed. Indicated in blue are patients that based on CA19-9 levels are not classified as CCA patients (CA19-9 < 129 U/mL) but can positively be identified as CCA by AnnV$^+$CD44v6$^+$ gp38$^+$ lEVs > 34 (see Tab. 12). Data is shown as scatter plots including median with interquartile range. n indicates number of patients. Dotted lines indicate recommended diagnostic cut-off of 20 ng/mL for AFP and 129 U/mL for CA19-9. Statistical significance was assessed by two-tailed Mann-Whitney *U* tests with $p \leq 0.05$ considered statistically significant. (* = $p \leq 0.05$, ** = $p \leq 0.01$, *** = $p \leq 0.001$, **** = $p \leq 0.0001$). In **E** the diagnostic profile for HCC detection (left panel) with low tumor-associated lEV levels, high AFP and low CA19-9 values is visualized. *Vice versa*, the diagnostic profile for CCA detection is shown in the right panel. Diagnostic profiles were created with BioRender.com. The panels **A**, **B** and **C** are part of the attached publication Urban *et al.* (2020) that resulted from this project.

Next, the diagnostic performance of AFP and CA19-9 for HCC and CCA differentiation within the tumor-associated study cohort was evaluated (Fig. 25C and D). Two-tailed Mann-Whitney *U* tests revealed that AFP levels were significantly elevated ($p \leq 0.0001$) by 110-fold in HCC patients as compared to CCA patients. CA19-9 levels on the other hand were significantly elevated ($p \leq 0.001$) by 11.5-fold in CCA patients as compared to HCC patients. Out of the displayed AFP and CA19-9 levels in HCC and CCA patients associated predictive values were computed (Tab. 14). As for progenitor cell-associated lEVs, cut-offs of 20 ng/mL for AFP and 129 U/mL for CA19-9 were chosen, which correspond to the suggested diagnostic cut-offs in the respective international guidelines for HCC and CCA management, respectively (Valle *et al.* 2016, Galle *et al.* 2018). With 100% sensitivity and 79.3% specificity AFP as a sole biomarker displayed a good diagnostic reliability for HCC and CCA differentiation in the tumor-associated study cohort, whereas CA19-9 showed lower predictive power with 57.4% sensitivity and 90.9% specificity. When adding the previous findings of this thesis of tumor-associated lEVs as biomarkers to AFP and CA19-9 evaluation, a distinct diagnostic improvement becomes evident. In Fig. 25C those HCC patients are exemplarily highlighted in red that based on AFP levels are not classified as HCC (AFP < 20 ng/mL) but that can positively be identified as HCC by AnnV$^+$CD44v6$^+$ lEVs < 34 (see cut-off Tab. 12). *Vice versa*, in Fig. 25D those

CCA patients are exemplarily highlighted in blue that based on CA19-9 levels are not classified as CCA (CA19-9 < 129 U/mL) but that can positively be identified as CCA by AnnV$^+$CD44v6$^+$ lEVs > 34. After adding the patients that were correctly identified by tumor-associated lEVs to the already identified patients by AFP or CA19-9, corresponding adjusted predictive values could be calculated accordingly (Tab. 14). Both tumor-associated lEV biomarkers markedly increased the diagnostic performance of AFP, whereby the combination with AnnV$^+$CD44v6$^+$ lEVs resulted in a perfect diagnostic separation of HCC and CCA with 100% sensitivity, 100% specificity, 100% PPV and 100% NPV. Similarly, the diagnostic performance of CA19-9 could considerably be enhanced by both tumor-associated populations. Again, the combination with AnnV$^+$CD44v6$^+$ lEVs showed the best results with 97.9% sensitivity, 90.9% specificity, 97.9% PPV and 90.9% NPV.

Tab. 14: Diagnostic performance of AFP and CA19-9 individually and combined with tumor-associated large EV populations in HCC/CCA differentiation. CCA patients were compared to HCC patients. Diagnostic cut-offs are given as number per 10^3 AnnV$^+$ lEVs for lEV populations, as ng/mL for AFP and as U/mL for CA19-9. Sensitivities (sens), specificities (spec) as well as positive (PPV) and negative predictive values (NPV) are given as percentage. n indicates cohort size.

AFP					
CCA: n=34, HCC: n=29	**cut-off**	**sens [%]**	**spec [%]**	**PPV [%]**	**NPV [%]**
AFP	20	100	79.3	85.0	100
AFP or AnnV$^+$CD44v6$^+$	20 or 34	**100**	**100**	**100**	**100**
AFP or AnnV$^+$CD44v6$^+$CD133$^+$	20 or 10	100	96.6	97.1	100
CA19-9					
CCA: n=47, HCC: n=11	**cut-off**	**sens [%]**	**spec [%]**	**PPV [%]**	**NPV [%]**
CA19-9	129	57.4	90.9	96.4	33.3
CA19-9 or AnnV$^+$CD44v6$^+$	129 or 34	**97.9**	**90.9**	**97.9**	**90.9**
CA19-9 or AnnV$^+$CD44v6$^+$CD133$^+$	129 or 10	85.1	90.9	97.6	58.8

In summary, combining the currently used serum biomarkers AFP and CA19-9 with the novel tumor-associated lEV biomarkers established in this study led to a perfect separation of CCA from HCC. Both tumor-associated lEV populations exceeded the diagnostic performance observed for progenitor cell-associated lEV populations with

AnnV$^+$CD44v6$^+$ lEVs being the most promising lEV biomarker. With these insights it was possible to generate a specific and highly relevant diagnostic profile for HCC and CCA patients for potential future uncomplicated differential diagnosis that is based solely on serum biomarkers (Fig. 25E). Thus, patients presenting with low tumor-associated lEV, high AFP and low CA19-9 values might easily be identified as HCC patients, whereas, *vice versa*, high tumor-associated lEV, low AFP and high CA19-9 values might be characteristic for CCA patients.

3.2.5. Large EV levels are independent of demographic and disease-related parameters in hepatobiliary cancer entities

In regard to the study cohort for lEV assessment described earlier, lEV levels can additionally be correlated with relevant factors to identify dependencies or tendencies that could influence the obtained results for hepatobiliary differentiation or could lead to additional insights concerning the characteristics of the tumors. Therefore, the distribution of all four lEV populations in relation to the demographic parameters gender, age and BMI were evaluated for the three hepatobiliary cancer entities HCC, CCA and GbCA. Additionally, it was investigated if lEV levels showed any correlation tendency with advancing tumor severity or with the occurrence of distant metastases, lymph node nodules or precancerous chronic liver cirrhosis. The results of these assessments are summarized in Tab. 15, whereas the corresponding figures can be obtained from the appendix. All four lEV populations showed no significantly different levels (p>0.05, Mann-Whitney U test) between female and male study participants in the three patient cohorts, thus eliminating any potential gender bias of the differential results obtained earlier (Supplementary Fig. 1). Spearman's rank correlation coefficients of lEV values compared to age distribution revealed a heterogeneous composition in all four populations and patient cohorts, with only AnnV$^+$CD44v6$^+$CD133$^+$ lEVs showing a significant but slight correlation (r=0.40, p=0.005) in CCA patients (Supplementary Fig. 2). Similarly, Spearman's rank correlation coefficients of lEV values compared to BMI distribution revealed that only AnnV$^+$CD44v6$^+$CD133$^+$ lEVs correlated significantly in HCC patients (r=0.46, p=0.009), while all other investigated lEV populations and patient groups showed no significant correlation (Supplementary Fig. 3). Thus, the effects of patient age and BMI do not seem to influence lEV differentiation of hepatobiliary cancers.

Tab. 15: Summary of correlation analysis of IEV levels with demographic and disease-related parameters in hepatobiliary cancer entities. All four IEV populations were correlated with each parameter in HCC, CCA and GbCA patients and summarized significance results are depicted. Depending on the investigated parameter, statistical significance was either assessed by Mann-Whitney *U* test, Kruskal-Wallis non-parametric test or Spearman's rank correlation with $p \leq 0.05$ overall considered statistically significant. The employed test is indicated in the corresponding individual figure legends (* = $p \leq 0.05$, ** = $p \leq 0.01$, *** = $p \leq 0.001$, **** = $p \leq 0.0001$). n.a.: not available, n.s.: non-significant

	IEV population	HCC	CCA	GbCA	reference
gender	AnnV$^+$CD133$^+$gp38$^+$	n.s.	n.s.	n.s.	Supplement. Fig. 1
	AnnV$^+$EpCAM$^+$CD133$^+$gp38$^+$	n.s.	n.s.	n.s.	
	AnnV$^+$CD44v6$^+$	n.s.	n.s.	n.s.	
	AnnV$^+$CD44v6$^+$CD133$^+$	n.s.	n.s.	n.s.	
age	AnnV$^+$CD133$^+$gp38$^+$	n.s.	n.s.	n.s.	Supplement. Fig. 2
	AnnV$^+$EpCAM$^+$CD133$^+$gp38$^+$	n.s.	n.s.	n.s.	
	AnnV$^+$CD44v6$^+$	n.s.	n.s.	n.s.	
	AnnV$^+$CD44v6$^+$CD133$^+$	n.s.	**	n.s.	
BMI	AnnV$^+$CD133$^+$gp38$^+$	n.s.	n.s.	n.s.	Supplement. Fig. 3
	AnnV$^+$EpCAM$^+$CD133$^+$gp38$^+$	n.s.	n.s.	n.s.	
	AnnV$^+$CD44v6$^+$	n.s.	n.s.	n.s.	
	AnnV$^+$CD44v6$^+$CD133$^+$	**	n.s.	n.s.	
tumor stage	AnnV$^+$CD133$^+$gp38$^+$	n.s.	n.s.	n.s.	Supplement. Fig. 4
	AnnV$^+$EpCAM$^+$CD133$^+$gp38$^+$	*	n.s.	n.s.	
	AnnV$^+$CD44v6$^+$	n.s.	n.s.	n.s.	
	AnnV$^+$CD44v6$^+$CD133$^+$	*	n.s.	n.s.	
distant metastases	AnnV$^+$CD133$^+$gp38$^+$	n.s.	n.s.	n.s.	Supplement. Fig. 5
	AnnV$^+$EpCAM$^+$CD133$^+$gp38$^+$	n.s.	n.s.	n.s.	
	AnnV$^+$CD44v6$^+$	n.s.	n.s.	n.s.	
	AnnV$^+$CD44v6$^+$CD133$^+$	n.s.	n.s.	n.s.	
lymph node nodules	AnnV$^+$CD133$^+$gp38$^+$	n.s.	n.s.	n.s.	Supplement. Fig. 6
	AnnV$^+$EpCAM$^+$CD133$^+$gp38$^+$	n.s.	n.s.	n.s.	
	AnnV$^+$CD44v6$^+$	n.s.	n.s.	n.s.	
	AnnV$^+$CD44v6$^+$CD133$^+$	n.s.	n.s.	n.s.	
cirrhotic background	AnnV$^+$CD133$^+$gp38$^+$	n.s.	n.s.	n.a.	Supplement. Fig. 7
	AnnV$^+$EpCAM$^+$CD133$^+$gp38$^+$	n.s.	n.s.	n.a.	
	AnnV$^+$CD44v6$^+$	n.s.	n.s.	n.a.	
	AnnV$^+$CD44v6$^+$CD133$^+$	n.s.	n.s.	n.a.	

$AnnV^+EpCAM^+CD133^+gp38^+$ and $AnnV^+CD44v6^+CD133^+$ lEV levels showed a tendency to increase with advancing tumor stages in HCC patients ($p \leq 0.05$, Kruskal-Wallis non-parametric test), while all other lEV populations remained unobtrusive in every patient cohort (Supplementary Fig. 4). These findings indicate that hepatobiliary cancer differentiation by lEVs is independent of tumor progression and might be feasible throughout all tumor stages. These assumptions are further reinforced by the observation that the occurrence of distant metastases and lymph node nodules as a measure of tumor progression and severity do not significantly correlate ($p > 0.05$; Mann-Whitney *U* and Kruskal-Wallis non-parametric test, respectively) with lEV levels in any patient cohort (Supplementary Fig. 5 and Supplementary Fig. 6). Finally, HCC and CCA patients with underlying chronic liver cirrhosis show no significant elevation of lEV levels in any population ($p > 0.05$; Mann-Whitney *U* test), indicating the independency of lEVs as a serum biomarker for hepatobiliary cancer differentiation from this precancerous condition (Supplementary Fig. 7).

3.3. Small EVs as biomarkers for differential hepatobiliary cancer diagnosis

After successfully conducting a study on the benefit of lEVs in hepatobiliary cancer differentiation, the role of sEVs was evaluated in the same regard. In order to particularly address the clinical issue of challenging HCC/iCCA differentiation, the investigated patient cohorts were restricted to HCC and iCCA patients as well as healthy individuals in this consecutive study. Since CD44v6 and CD133 showed the best diagnostic performance for differential hepatobiliary cancer detection in lEVs, they were selected as candidate markers for evaluating the differential capability of sEVs in this study. This way, the comparability between the two studies on large and sEVs was ensured and possible advantages or disadvantages could directly be compared.

Human serum was collected from the patient cohorts, sEVs were isolated and their surface was screened on single sEV basis according to their single and combined CD44v6 and CD133 expression.

3.3.1. The human study cohort for small EV analysis

In total, 20 subjects, who gave their informed consent to participate, were enrolled in the sEV study (Fig. 26A). This pool consisted of 4 healthy subjects, 8 HCC and 8 iCCA patients. A detailed description of key demographical parameters of the individual patient cohorts is available in Tab. 16, additional biochemical parameters can be found in Supplementary Tab. 2. Out of these values, relative gender, age and BMI distributions among the individual patient cohorts are visualized (Fig. 26B). Unfortunately, no demographic parameters were available for healthy individuals.

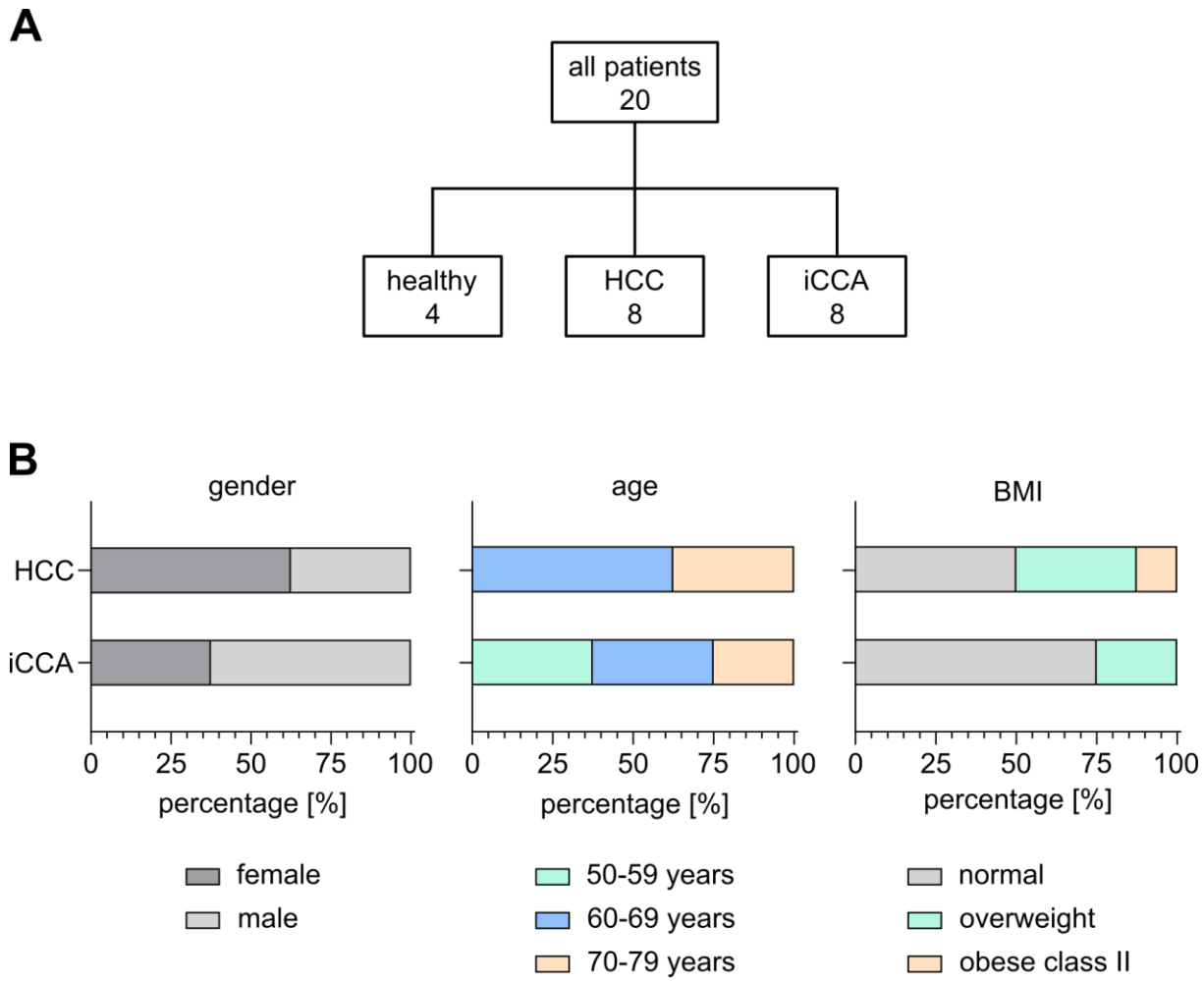

Fig. 26: Distribution of patients and demographic parameters in the different study cohorts for small EV analysis. A The total amount of enrolled subjects comprised hepatocellular carcinoma (HCC) and intracellular cholangiocarcinoma (iCCA) patients. **B** Shown are the percentages of indicated gender, age and BMI groups. Corresponding values are displayed in Tab. 16. BMI was classified as follows: underweight: <18.5 kg/m^2, normal weight: 18.5 to <25 kg/m^2, overweight: 25 to <30 kg/m^2, obese class I: 30 to <35 kg/m^2, obese class II: 35 to <40 kg/m^2, obese class III: ≥40 kg/m^2

An almost equal gender distribution can be observed in the participating patient cohorts. 62.5% of all HCC patients were male, whereas 62.5% of all iCCA patients were female. With an average of 68.8 years, HCC patients were slightly older than iCCA patients (63.8 years). In contrast to iCCA, no patient younger than 61 years was enrolled in the HCC group. Furthermore, HCC patients presented with higher overall BMI than iCCA patients (26.3 vs. 23.0 kg/m^2, respectively). The majority (75%) of iCCA patients showed normal BMIs (18.5 to <25 kg/m^2) with the remaining 25% being overweight (25 to <30 kg/m^2). In contrast, 50% of HCC patients classified as overweight or obese class II (35 to <40 kg/m^2), while no patients classified as obese class I.

Tab. 16: Demographic parameters of the different patient cohorts for small EV analysis. Age and BMI are given as mean. Additional biochemical parameters of the patients are provided in Supplementary Tab. 2. #: absolute number of patients in each cohort, n.a.: not available, s.d.: standard deviation.

	healthy	**HCC**	**iCCA**
patients [#]	4	8	8
female [#]	n.a.	5	3
male [#]	n.a.	3	5
age [years]		68.8	63.8
s.d.	n.a.	6.3	8.0
range		61-77	52-76
BMI [kg/m^2]		26.3	23.0
s.d.	n.a.	4.6	2.3
range		22.3-36.4	18.9-26.7

Compared to the study cohorts for lEV evaluation, HCC patients show similar age and BMI distributions, while BMI for iCCA patients is higher in both the progenitor cell-associated and tumor-associated study cohort and corresponds to the “overweight” category with 26.3 and 27.0 kg/m^2, respectively (compare Tab. 6).

3.3.2. Characterization of isolated small EVs

In a first step, sEVs were isolated from 1 mL of patient serum by size exclusion chromatography (SEC) columns (Fig. 27A). These columns are filled with a matrix (stationary phase) that consists of spherical porous beads. Particles in the mobile phase diffuse through these pores according to their molecular size differences. The smaller the

particles, the easier they can enter the beads through the pores and the more they interact with the inner surface of the beads, resulting in a delayed passage through the column. Larger particles, on the other hand, are less likely to enter the beads or they pass around them completely leading to an earlier elution (lower retention time) than smaller particles (Fekete *et al.* 2014). Thus, separation of the vesicles by molecular size is achieved, while simultaneously depleting protein contaminants. The resulting fractions were collected and their protein as well as particle concentration was determined.

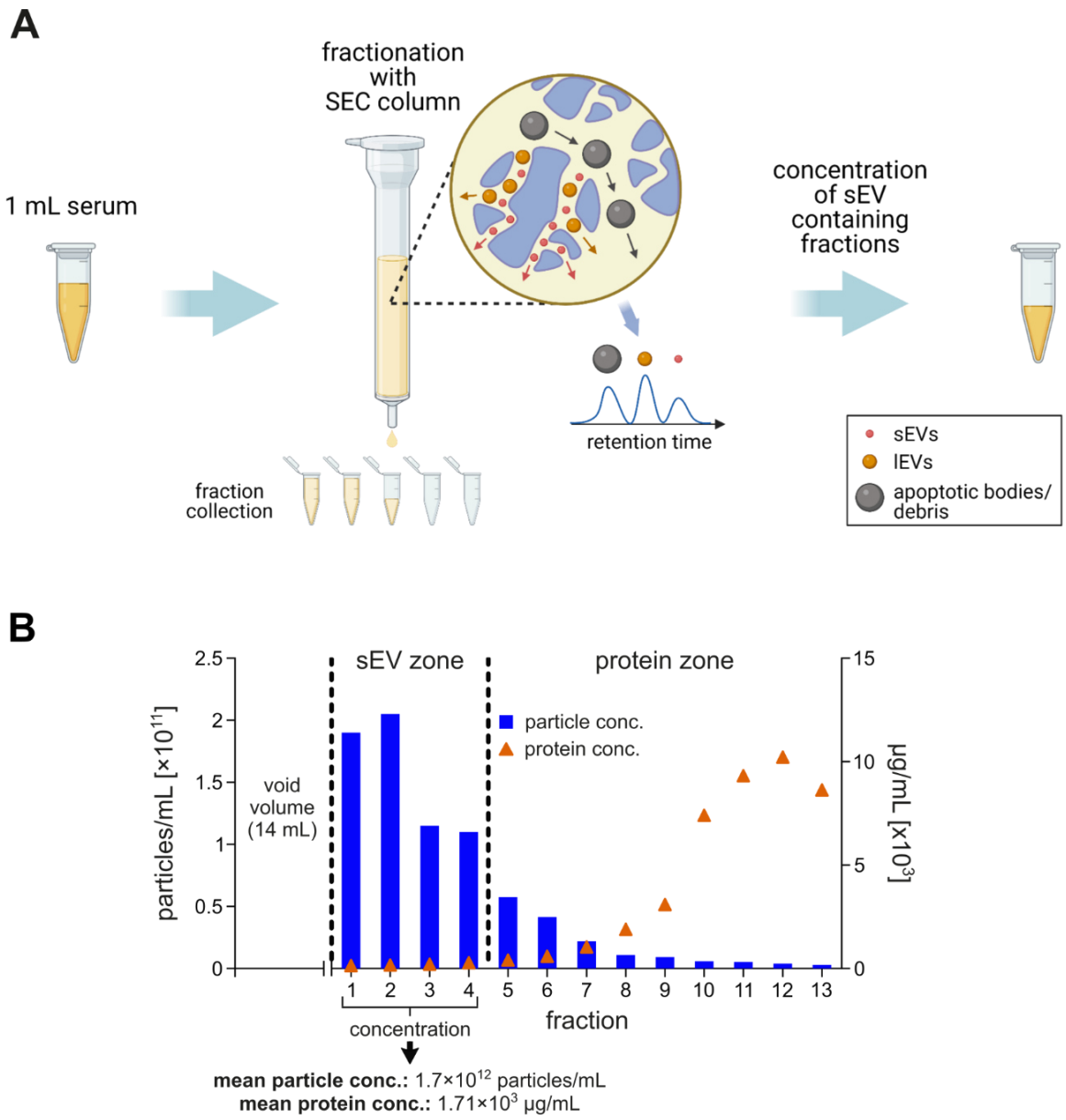

Fig. 27: Characterization of isolated small EVs. A 1 mL of human patient serum was used for sEV isolation by size exclusion chromatography (SEC) columns, that separate particles passing through according to their sizes. Due to less surface interactions with

the columns, larger particles elute earlier than smaller ones (retention time). Collected fractions containing sEVs were pooled and concentrated for further processing. Flowchart was created with BioRender.com. **B** Particle concentration of all collected fractions was determined by nanoparticle tracking analysis (NTA), whereas protein concentration was assessed by BCA assays. Data is shown exemplarily for sEV isolation of a healthy subject. Indicated means are representative of three independent experiments.

The fractions containing sEVs were pooled and concentrated for further processing. Since, in accordance with the manufacturer's protocol, the initial 14 mL of the elution contain debris and larger particles (void volume), the first fractions were collected after discarding the respective initial volume. The profile of particle and protein concentrations in the collected fractions is exemplarily shown in Fig. 27B for sEV isolation of a healthy subject. The manufacturer's specifications for the columns suggest that the first four collected fractions contain the desired sEVs. As determined by nanoparticle tracking analysis (NTA), the first four collected fractions contained considerably more particles than the remaining ones, while simultaneously showing low protein concentrations, as confirmed by BCA assays. Consequently, these fractions were pooled and concentrated for further sEV analysis. Concentrated sEVs showed a mean particle concentration of 1.7×10^{12} particles/mL and a mean protein concentration of 1.71×10^{3} µg/mL.

In contrast to lEVs, sEVs, with diameters typically below 100 nm, cannot be analyzed with commonly available flow cytometers on a single EV basis. Therefore, a new platform for single sEV surface analysis needed to be established. We chose to analyze single sEVs by a newly developed system operated by the company NanoView Biosciences (Boston, USA), who isolated and measured sEVs from human patient serum and provided us with the raw data. The principle of this technique is based on immobilizing single sEVs to the surface of a chip, followed by immunofluorescent labelling of the bound sEVs with antibodies against the target proteins (Fig. 28). By exciting the fluorophores of the bound antibodies with different wavelengths, sEVs can be quantified and their surface composition can be evaluated. In addition, the size of sEVs can be analyzed by interferometric imaging, which is a microscopic technique based on assembling multiple wavelength-divided partial images into a composite image to enhance the optical resolution limit (Kuznetsova *et al.* 2007). The individual capture spots on the chips are pre-coated with antibodies against one of the three tetraspanins CD81, CD63 and CD9. These three proteins are the most frequently identified proteins in EVs and are thus

considered as classical EV markers. However, even sEV subtypes themselves comprise heterogeneous vesicle populations which are, among other differences, characterized by differing tetraspanin proportions on their surface (Andreu and Yáñez-mó 2014). Since each capture spot on the chip is pre-coated with only one of the three tetraspanins, three different sEV subpopulations ($CD81^+$, $CD63^+$ and $CD9^+$) can be evaluated simultaneously in one measurement. Each capture spot is measured in triplicates.

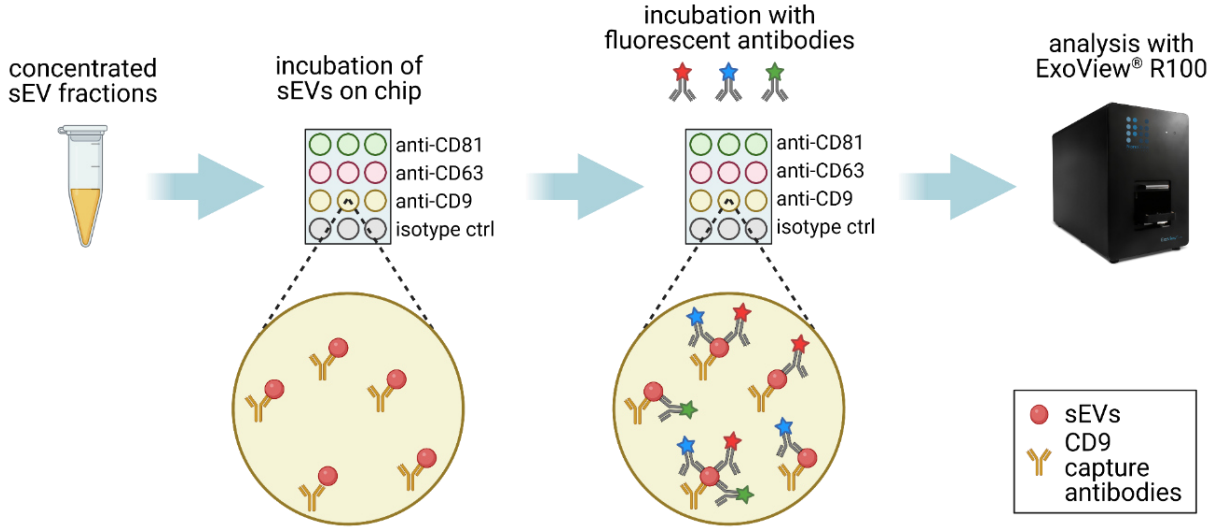

Fig. 28: Schematic overview of small EV processing. After isolation of sEVs from human serum by SEC columns, concentrated sEVs were incubated on the ExoView® chip overnight and were allowed to bind to the capture spots that were pre-coated with tetraspanin capture antibodies. After an immunofluorescent counterstain with antibodies against the desired target proteins, chips were scanned with the ExoView® R100 scanner. Image of the ExoView® R100 was obtained from the official NanoView Biosciences web page (www.nanoviewbio.com). Flowchart was created with BioRender.com.

In order to confirm that sEVs were enriched in isolates obtained by SEC columns from human serum, the size distribution of the isolated and subsequently concentrated sEVs was analyzed by interferometric imaging by the ExoView® scanner in a first step. Fig. 29A. exemplarily visualizes the size distribution of $CD81^+$, $CD63^+$ and $CD9^+$ sEV subpopulations for one individual patient of each cohort. Even though sEV sizes and total particle counts differ among the three subpopulations, the observed profile is consistent for every patient cohort (Fig. 29B). Accordingly, no significant difference ($p>0.5$) can be detected in mean sEV sizes between the patient cohorts for all three subpopulations, as assessed by Kruskal-Wallis non-parametric test followed by Dunn's multiple comparison

post hoc test. Interestingly, the mean sizes of CD81⁺ sEVs range from 56.5 nm to 60.6 nm among the patient cohorts, whereas CD63⁺ sEVs are larger with mean sizes ranging from 62.0 nm to 66.9 nm. CD9⁺ sEVs, however, are the largest in all patient cohorts with sizes ranging from 66.7 nm to 73.0 nm.

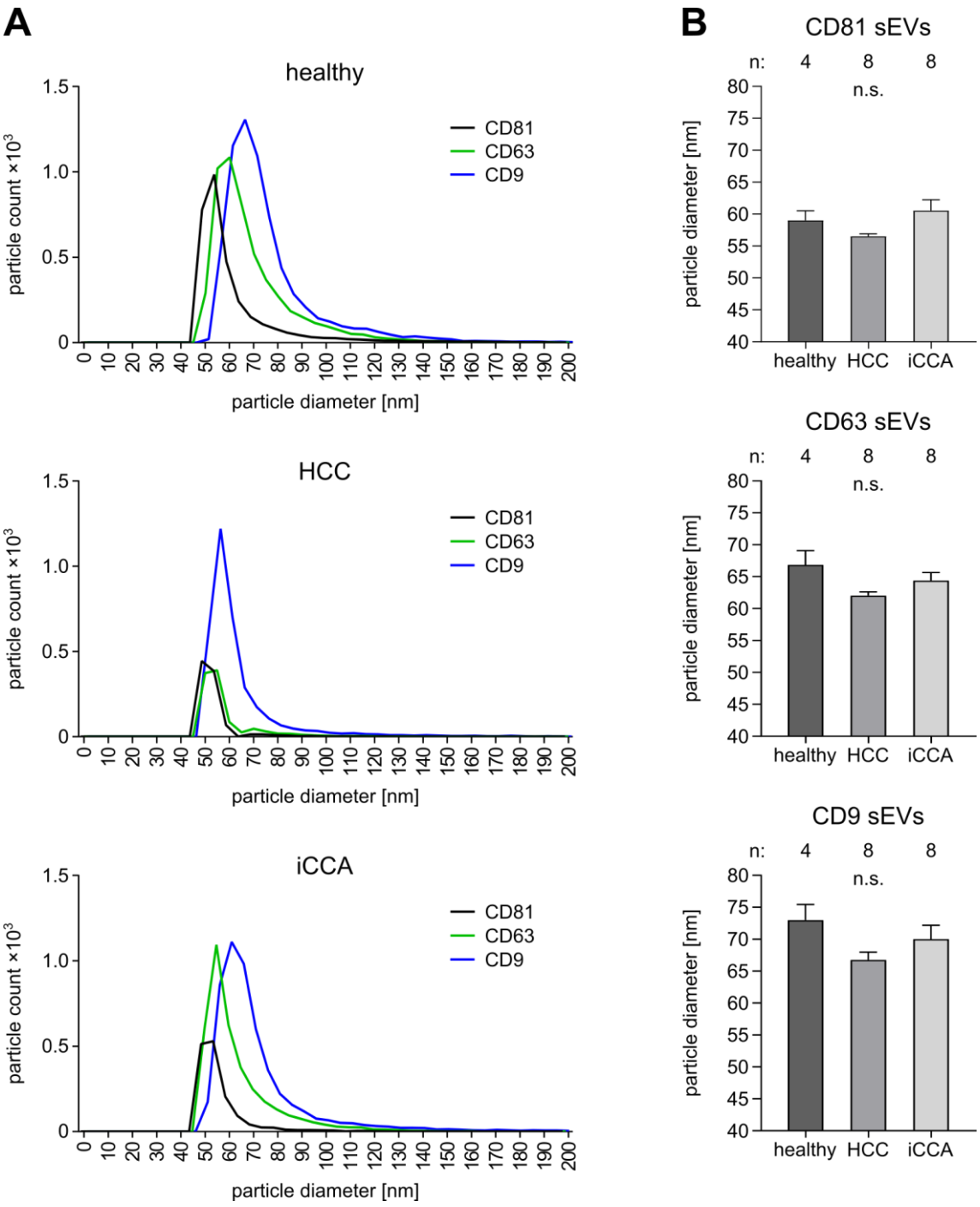

Fig. 29: Size distribution of small EVs among the patient cohorts is comparable but shows differences between different small EV subpopulations. Small EVs were

isolated by SEC columns and incubated on ExoView® chips pre-coated with CD81, CD63 and CD9 capture antibodies. By interferometric imaging sEV sizes were analyzed. **A** The size distribution of CD81$^+$, CD63$^+$ and CD9$^+$ sEVs is exemplarily shown for one healthy individual, one HCC and one iCCA patient. **B** The average sizes of sEVs among the patient cohorts for CD81$^+$, CD63$^+$ and CD9$^+$ sEVs are depicted. Data is shown as mean with standard error of the mean (SEM). n indicates cohort size. Statistical significance was assessed by Kruskal-Wallis non-parametric test followed by Dunn's multiple comparison post hoc test with $p \leq 0.05$ considered statistically significant. n.s.: non-significant.

Taken together, sEV isolation by SEC columns yields three distinct sEV subpopulations (CD81$^+$, CD63$^+$ and CD9$^+$ sEVs) with classical EV markers on their surface and with diameters in range of sEVs (40-100 nm). For each subpopulation, mean sEV sizes are comparable between the patient cohorts, which indicates that possible effects in differentiation are not due to different sEV sizes but can rather be attributed to pathophysiological differences between the patient cohorts.

3.3.3. Different small EV subpopulations can diagnostically differentiate between iCCA and HCC

The particle concentration of the three sEV subpopulations in the different patient cohorts was assessed in respect to their differential capability and in order to ensure comparability among the cohorts for subsequent evaluation of the putative differential markers CD44v6 and CD133. ExoView® chips were scanned prior loading of isolated sEVs from human serum and after loading. As exemplarily shown for an iCCA patient, single bound and immobilized sEVs of all three subpopulations (CD81$^+$, CD63$^+$ and CD9$^+$ sEVs) can be detected on the individual capture spots after loading (Fig. 30A). MIgG corresponds to the respective antibody isotype of all three capture antibodies against human CD81, CD63 and CD9 that is coated to the chip surface in an additional capture spot and serves as a negative control to identify unspecific binding of sEVs and subsequent antibodies. After loading with sEVs, the chips were incubated with fluorescent antibodies against the tetraspanins CD81, CD63 and CD9. The optimal concentrations for both sEV starting material and employed antibodies were titrated prior use to ensure optimal performance and can be obtained from the Materials and Methods section 2.6.3.

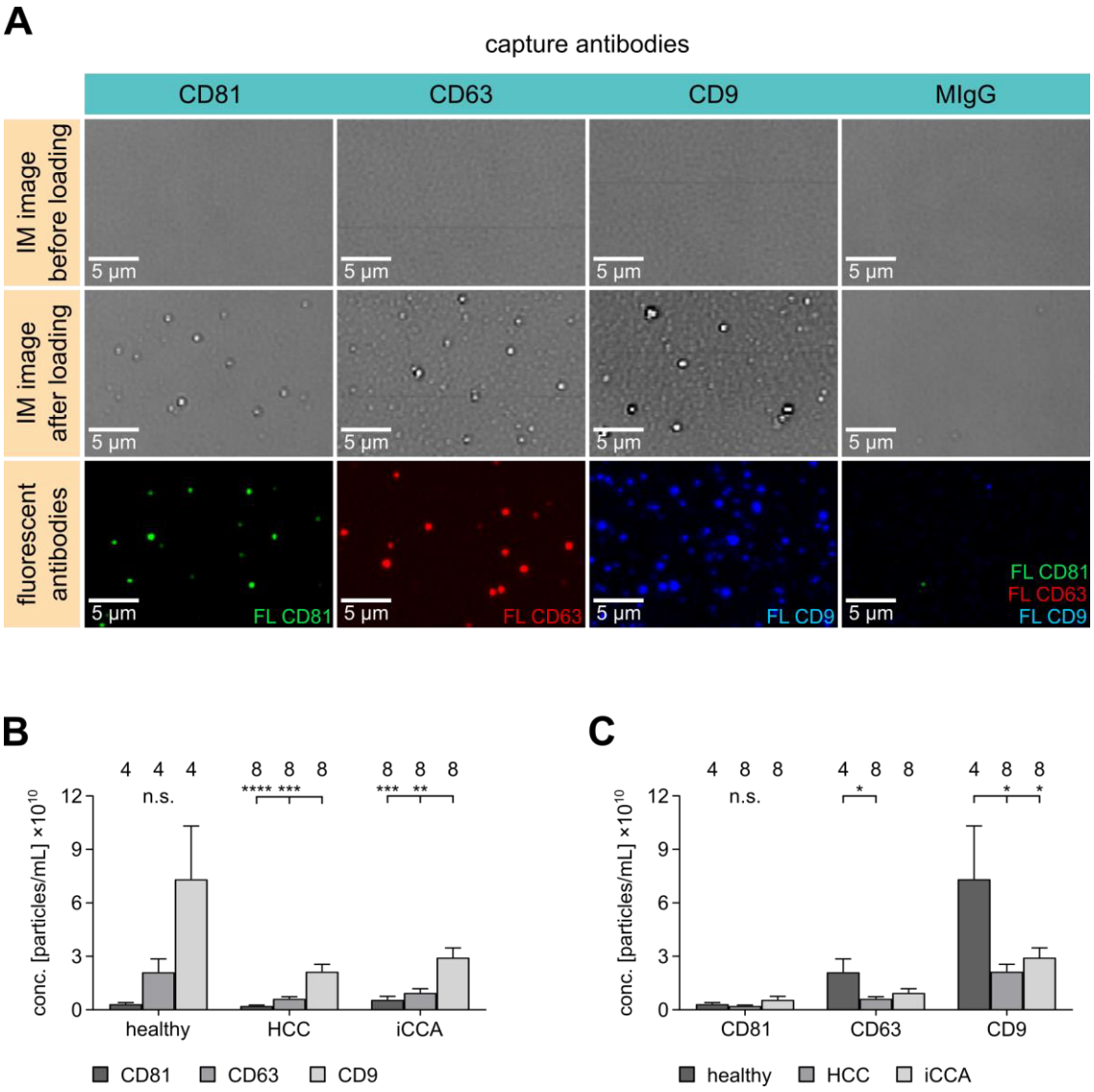

Fig. 30: Small EV subpopulations are characterized by differing tetraspanin expression levels. Small EVs were isolated by SEC columns and incubated on ExoView® chips pre-coated with CD81, CD63 and CD9 capture antibodies. After counterstaining with the aforementioned fluorescent antibodies, the sEV concentration was measured by the ExoView® R100 scanner. **A** exemplarily shows interferometric (IM) images of the individual capture spots on the chip coated with CD81, CD63, CD9 or their isotype control (MIgG) before loading with sEVs (upper panel) and after loading (middle panel) of an iCCA patient. In the lower panel the counterstains with fluorescent (FL) antibodies against CD81, CD63 and CD9, respectively, are shown. **B** depicts the differences in concentration of the patient cohorts (healthy individuals, HCC and iCCA patients) among the $CD81^+$, $CD63^+$ and $CD9^+$ sEV subpopulations, whereas **C** displays the differences of the aforementioned subpopulations among the patient cohorts. Data is shown as mean with standard error of the mean (SEM). n indicates cohort size. Statistical significance was assessed by Kruskal-Wallis non-parametric test followed by Dunn's multiple comparison post hoc test with $p \leq 0.05$ considered statistically significant. (* = $p \leq 0.05$, ** = $p \leq 0.01$, *** = $p \leq 0.001$, **** = $p \leq 0.0001$). n.s.: non-significant.

The fluorescent images of the capture spots revealed distinct expression profiles of CD81$^+$, CD63$^+$ and CD9$^+$ sEVs in the different patient cohorts. It is noticeable that CD9$^+$ sEVs are most abundant in every patient cohort, followed by CD63$^+$ and CD81$^+$ sEVs in decreasing order (Fig. 30B). In detail, within HCC patients, CD9$^+$ sEVs are significantly elevated as compared to both CD81$^+$ ($p \leq 0.0001$) and CD63$^+$ sEVs ($p \leq 0.001$) by 9.7-fold and 3.5-fold, respectively. Similarly, within iCCA patients CD9$^+$ sEV levels are significantly increased as compared to both CD81$^+$ ($p \leq 0.001$) and CD63$^+$ levels ($p \leq 0.01$) by 5.2-fold and 3.1-fold, respectively. Even though the differences between the three sEV subpopulations in healthy subjects appear substantial, no significant variation was observed ($p > 0.05$). This might be due to the low cohort size of only four healthy individuals. Interestingly, particle size and concentration seem to correlate, with CD9$^+$ sEVs being the largest as well as most abundant of all three subpopulations in all cohorts, followed decreasingly by CD63 and CD81 (compare Fig. 29).

While CD81$^+$ sEV levels are comparable among all cohorts with no significant differences ($p > 0.5$), CD63$^+$ sEV levels of healthy individuals are significantly elevated by 3.4-fold as compared to HCC patients ($p \leq 0.05$) (Fig. 30C). Similarly, within CD9$^+$ sEVs, healthy individuals show significantly increased levels as compared to both HCC and iCCA patients (both $p \leq 0.05$) by 3.4-fold and 2.5-fold, respectively. Importantly, sEV levels of all three subpopulations show no significant variation between HCC and iCCA patients demonstrating that tetraspanins by themselves are not sufficient as a differential marker for HCC/iCCA distinction. Hence, the potentially differential markers CD44v6 and CD133 were added to the basis sEV subpopulations CD81$^+$, CD63$^+$ and CD9$^+$. In order to achieve diagnostically relevant results with additional markers, it is a prerequisite that the amounts of the basis sEV subpopulations are comparable among the cohorts. Otherwise, differential effects observed by the addition of markers cannot exclusively be allocated to them. Although the concentration of CD81$^+$ sEVs was comparable among the patient cohorts with no distinct variation observed, levels were overall very low indicating poor diagnostic significance of CD81$^+$ sEVs (compare Fig. 30C). Furthermore, CD63$^+$ and CD9$^+$ sEV levels were only comparable among HCC and iCCA patients indicating that healthy subjects might not reliably be differentiated from patients with malignancies by assessing CD63$^+$ and CD9$^+$ sEV levels.

For assessing the diagnostic relevance of sEV subpopulations with additional markers, isolated sEVs from human serum were incubated on ExoView® chips and stained with fluorescent antibodies against the two candidate markers CD133 and CDD44v6. The fluorescent images of the capture spots revealed that both CD133 and CD44v6 could be detected individually on all three basis sEV subpopulations, as exemplarily shown for an iCCA patient (Fig. 31A). Colocalisations of both markers on one single sEV, on the other hand, could not be observed in any subpopulation. These observations are reflected in the summarized results, in which distinct sEV marker distribution profiles for each of the three basis sEV subpopulations and patient cohorts become apparent (Fig. 31B).

In $CD81^+$ sEVs, high concentrations of CD133 as compared to CD44v6 could be observed in healthy subjects and iCCA patients, while both markers were expressed similarly in HCC patients. In contrast to that, in $CD63^+$ sEVs, CD44v6 could be detected in considerably higher amounts than CD133 in all three patient cohorts. In $CD9^+$ sEVs, on the other hand, both individual markers are expressed in similar amounts in all cohorts. While no significant difference in expression levels could be detected between the single markers in any sEV basis subpopulation, the fact that almost no double positive $CD133^+CD44v6^+$ sEVs could be observed in any sEV basis population or patient cohort resulted in significantly different levels between the single markers and the double positive sEV population. In detail, $CD81^+CD133^+$ sEV levels were 56.0-fold ($p \leq 0.05$) and $CD81^+CD44v6^+$ sEV levels were 81.4-fold ($p \leq 0.001$) elevated as compared to $CD81^+CD44v6^+CD133^+$ sEV levels in HCC patients. In iCCA patients, $CD81^+CD133^+$ sEV levels were increased by 59.4-fold ($p \leq 0.001$) and $CD81^+CD44v6^+$ sEV levels were increased by 22.1-fold ($p \leq 0.05$) as compared to $CD81^+CD44v6^+CD133^+$ sEV levels. Similarly, $CD63^+CD133^+$ sEV levels were 32.9-fold ($p \leq 0.05$) and $CD63^+CD44v6^+$ sEV levels were 123.5-fold ($p \leq 0.001$) elevated as compared to $CD63^+CD44v6^+CD133^+$ sEV levels in HCC patients. In iCCA patients, $CD63^+CD133^+$ sEV levels were increased by 17.4-fold ($p \leq 0.05$) and $CD63^+CD44v6^+$ sEV levels were increased by 47.4-fold ($p \leq 0.05$) as compared to $CD63^+CD44v6^+CD133^+$ sEV levels. Finally, $CD9^+CD133^+$ sEV levels were 58.9-fold ($p \leq 0.001$) and $CD9^+CD44v6^+$ sEV levels were 64.0-fold ($p \leq 0.01$) elevated as compared to $CD9^+CD44v6^+CD133^+$ sEV levels in HCC patients. In iCCA patients, only $CD9^+CD133^+$ sEV levels were increased by 24.8-fold ($p \leq 0.01$), while $CD9^+CD44v6^+$ sEV levels were not elevated significantly as compared to $CD9^+CD44v6^+CD133^+$ sEV levels.

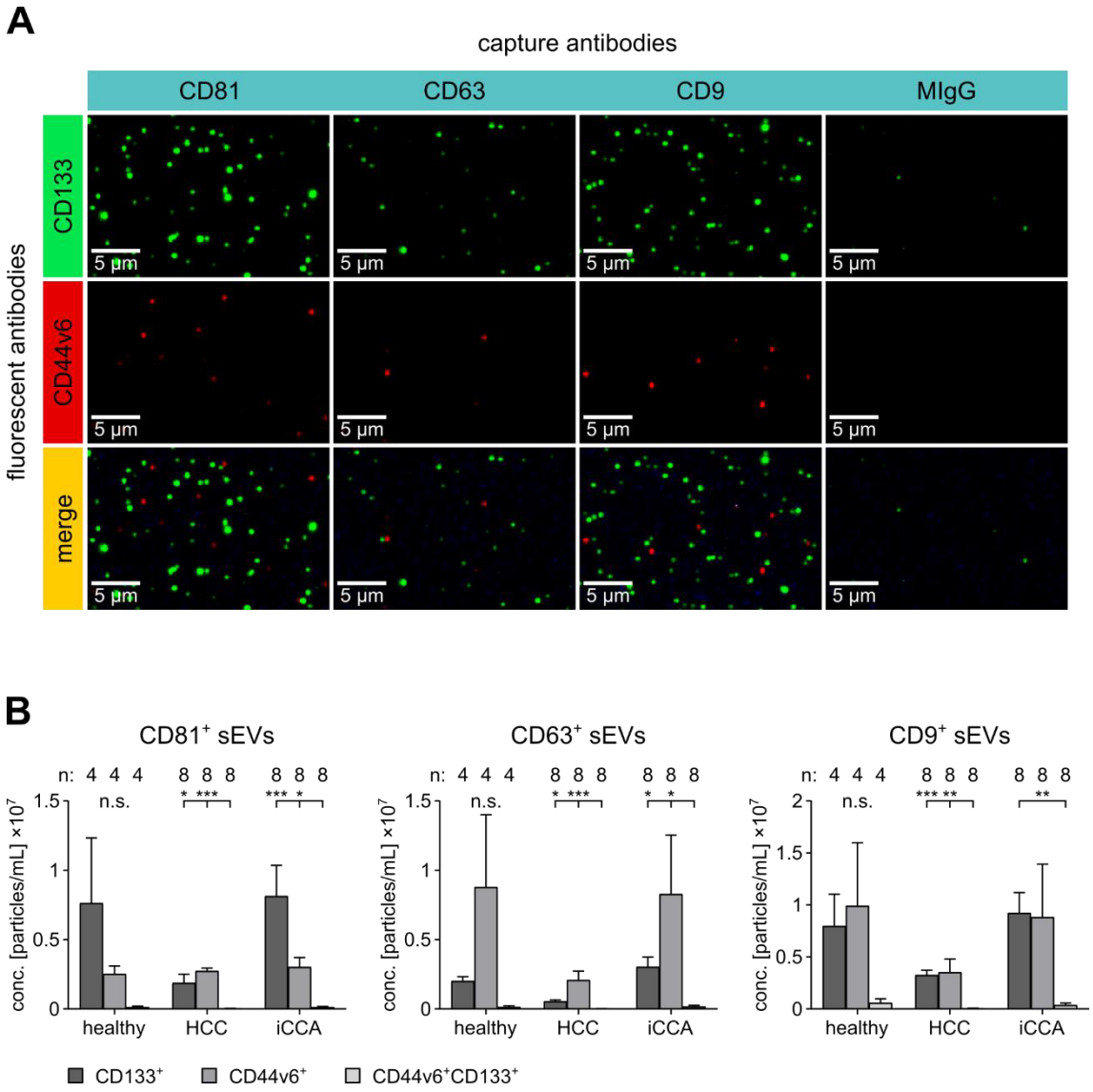

Fig. 31: CD133 and CD44v6 are differentially distributed on small EVs among the patient cohorts. Small EVs were isolated by SEC columns and incubated on ExoView® chips pre-coated with CD81, CD63 and CD9 capture antibodies. After counterstaining with fluorescent antibodies against CD133 and CD44v6, the sEV concentration was measured by the ExoView® R100 scanner. **A** exemplarily shows fluorescence microscopic images of the individual capture spots on the chip coated with CD81, CD63, CD9 or their isotype control (MIgG) of an iCCA patient. In the upper and middle panel the counterstains with the two fluorescent (FL) antibodies are shown individually, whereas the lower panel depicts a merged image of both antibody stainings. In **B** for each sEV subpopulation ($CD81^+$, $CD63^+$ and $CD9^+$, respectively) the differences among the patient cohorts (healthy individuals, HCC and iCCA patients) of the single positive $CD133^+$ and $CD144v6^+$ or double positive $CD44v6^+CD133^+$ populations are displayed. Data is shown as mean with standard error of the mean (SEM). n indicates cohort size. Statistical significance was assessed by Kruskal-Wallis non-parametric test followed by Dunn's multiple comparison post hoc test with $p \leq 0.05$ considered statistically significant. (* = $p \leq 0.05$, ** = $p \leq 0.01$, *** = $p \leq 0.001$, **** = $p \leq 0.0001$). n.s.: non-significant.

As observed earlier, even though the differences between sEV levels within the healthy cohort appear substantial in every sEV basis subpopulation, there were no significant variations (p>0.05). Again, this might be an effect of the low healthy cohort size that can be responsible for insignificant statistical tests. Importantly, both CD133 and CD44v6 show a tendency to be elevated in iCCA as compared to HCC patients in all three basis sEV subpopulations, hinting at their potential differentiation capability, which will be explored in the subsequent analysis.

As mentioned earlier, the particle concentration of all three basis sEV subpopulations displays no notable differences among HCC and iCCA patients, so these cohorts can therefore be considered suitable for subsequent diagnostic evaluation with the additional markers CD44v6 and CD133. Considering the observed incomparability of healthy subjects to the other cohorts and the fact that the main clinical challenge is distinguishing HCC from iCCA, the following diagnostic assessment was limited to these two cohorts.

Therefore, median levels of the three basis sEV subpopulations additionally expressing CD44v6 and CD133 individually or in combination on their surface were compared among HCC and iCCA patients. Single positive CD44v6$^+$ sEVs as well as double positive CD44v6$^+$CD133$^+$ sEVs were associated with low diagnostic relevancy in all three basis sEV subpopulations for differentiating HCC and iCCA patients and are consequently not shown in this thesis. However, good diagnostic separations were achieved with CD133 in all three basis sEV subpopulations (Fig. 32, left panels). In detail, two-tailed Mann-Whitney U tests revealed that median CD63$^+$CD133$^+$ sEV levels in iCCA patients were significantly elevated by 6.5-fold as compared to HCC patients (p≤0.01). Similarly, median CD9$^+$CD133$^+$ sEV levels were significantly increased by 3.6-fold and median CD81$^+$CD133$^+$ sEV levels showed a significant elevation by 9.7-fold in iCCA patients as compared to HCC patients (both p≤0.05). In order to assess the diagnostic relevance of sEVs as a biomarker, ROC curves and associated AUC values were computed for discrimination of iCCA from HCC patients (Fig. 32, right panels). AUC values of 0.89 (CD63$^+$CD133$^+$), 0.83 (CD9$^+$CD133$^+$) and 0.80 (CD81$^+$CD133$^+$) describe a good predictive power of the three biomarkers, with CD63$^+$CD133$^+$ sEVs being the most promising.

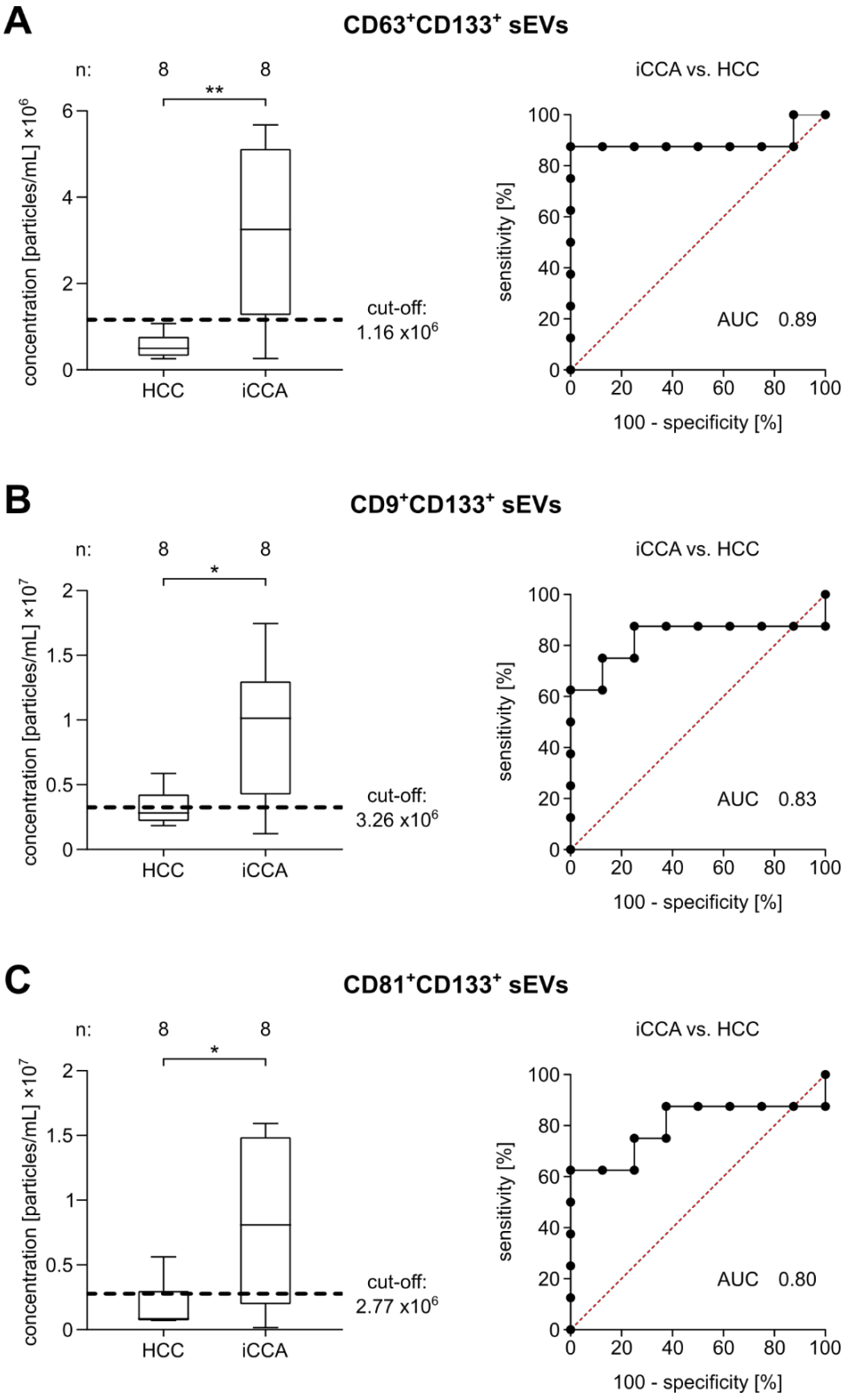

Fig. 32: Small EV populations are diagnostically relevant for iCCA differentiation from HCC. Small EVs were isolated by SEC columns and incubated on ExoView® chips pre-coated with CD81, CD63 and CD9 capture antibodies. After counterstaining with fluorescent antibodies against CD133 and CD44v6, the sEV concentration was measured by an ExoView® R100 scanner. sEV values of the three subpopulations $CD63^+CD133^+$

(**A**, left panel), $CD9^+CD133^+$ (**B**, left panel) and $CD81^+CD133^+$ (**C**, left panel) are shown for HCC and iCCA patients. Data is shown as medians with interquartile range (IQR), whiskers represent 1.5 × IQR (Tukey) with potential outliers plotted as dots. n indicates number of patients. Dotted lines indicate diagnostic cut-offs for discrimination between iCCA and HCC for the respective sEV population (see Tab. 17). Statistical significance was assessed by two-tailed Mann-Whitney *U* tests with $p \leq 0.05$ considered statistically significant (* = $p \leq 0.05$, ** = $p \leq 0.01$, *** = $p \leq 0.001$, **** = $p \leq 0.0001$). Corresponding ROC curves for the respective sEV populations for the discrimination between iCCA and HCC including AUC values are shown in the right panels.

Out of the ROC curve analyses, diagnostic cut-offs and other predictive values were calculated according to the point of optimal sensitivity and specificity (Tab. 17). With 87.5% sensitivity, 100% specificity, 100% PPV and 88.9% NPV $CD63^+CD133^+$ sEVs can be considered as the best-performing sEV subpopulation for discrimination of iCCA from HCC. When taking the diagnostic performance of the best lEV population (Tab. 13, $AnnV^+CD44v6^+$ lEVs) into account, it becomes evident that even though $CD63^+CD133^+$ sEVs showed a slightly lower sensitivity (87.5% as compared to 93.3%) and NPV (88.9% as compared to 95.7%) for iCCA/HCC distinction, the specificity and PPV are considerably higher than for $AnnV^+CD44v6^+$ lEVs (100% as compared to 71.0% and 100% as compared to 60.9%, respectively).

Tab. 17: Diagnostic performance of selected small EV populations for iCCA/HCC differentiation. Diagnostic cut-offs are given as total sEV counts per mL, whereas sensitivities (sens), specificities (spec) as well as positive (PPV) and negative predictive values (NPV) are given as percentage. n indicates cohort size.

iCCA: n=8, HCC: n=8	**cut-off**	**AUC**	***p*-value**	**sens [%]**	**spec [%]**	**PPV [%]**	**NPV [%]**
$CD63^+CD133^+$	1162000	0.89	0.0087	87.5	100	100	88.9
$CD9^+CD133^+$	3257500	0.83	0.0274	87.5	62.5	70.0	83.3
$CD81^+CD133^+$	2774000	0.80	0.0460	75.0	75.0	75.0	75.0

In summary, as observed for lEVs in the study before, sEVs proved to be a valuable and diagnostically relevant biomarker that could potentially be used for hepatic cancer differentiation.

3.3.4. Small EVs improve the diagnostic performance of commonly used serum tumor markers

As evaluated for lEV populations, it was of interest if the diagnostic performance of sEV subpopulations as a biomarker could be improved by combining them with the two serum biomarkers AFP and CA19-9 that are currently used to facilitate HCC and CCA detection, respectively. Thus, their differentiation capability in this specific experimental setting alone and in combination with the sEV biomarkers established herein was evaluated. In a first step, possible correlations of the identified diagnostically relevant sEV subpopulations with the two serum markers were evaluated in iCCA and HCC patients, in order to identify dependencies. Therefore, Spearman's rank correlation coefficients (r) for each sEV subpopulation as compared to AFP (Fig. 33A) and CA19-9 (Fig. 33B) were calculated for HCC and iCCA patients and the distribution was visualized. The correlation analysis revealed that, even though r values ranged from -0.45 to 0.66, neither AFP nor CA19-9 correlated significantly ($p \leq 0.05$) with any sEV subpopulation in neither HCC nor iCCA patients.

Next, the diagnostic performance of AFP and CA19-9 individually and combined with sEV populations for HCC and iCCA differentiation was evaluated and associated predictive values were computed (Tab. 18). Cut-offs of 20 ng/mL for AFP and 129 U/mL for CA19-9 were chosen, which are the suggested diagnostic cut-offs in the respective international guidelines for HCC and CCA management, respectively (Valle *et al.* 2016, Galle *et al.* 2018). With 87.5% sensitivity and 50.0% specificity AFP displayed a moderate diagnostic reliability as a sole biomarker for HCC and CCA differentiation. Moreover, CA19-9 showed an even lower predictive power with 37.5% sensitivity and 75.0%% specificity. As analysed in lEVs before (compare Fig. 21 and Fig. 25), after including those patients into the evaluation that based on AFP or CA19-9 levels were not classified as HCC (AFP < 20 ng/mL or CA19-9 > 129 U/mL) or iCCA patients (AFP > 20 ng/mL or CA19-9 < 129 U/mL), but that could correctly be identified as such by sEV subpopulations (HCC: sEV levels < cut-off, CCA: sEV levels > cut-off; Tab. 17), a distinct diagnostic improvement becomes evident.

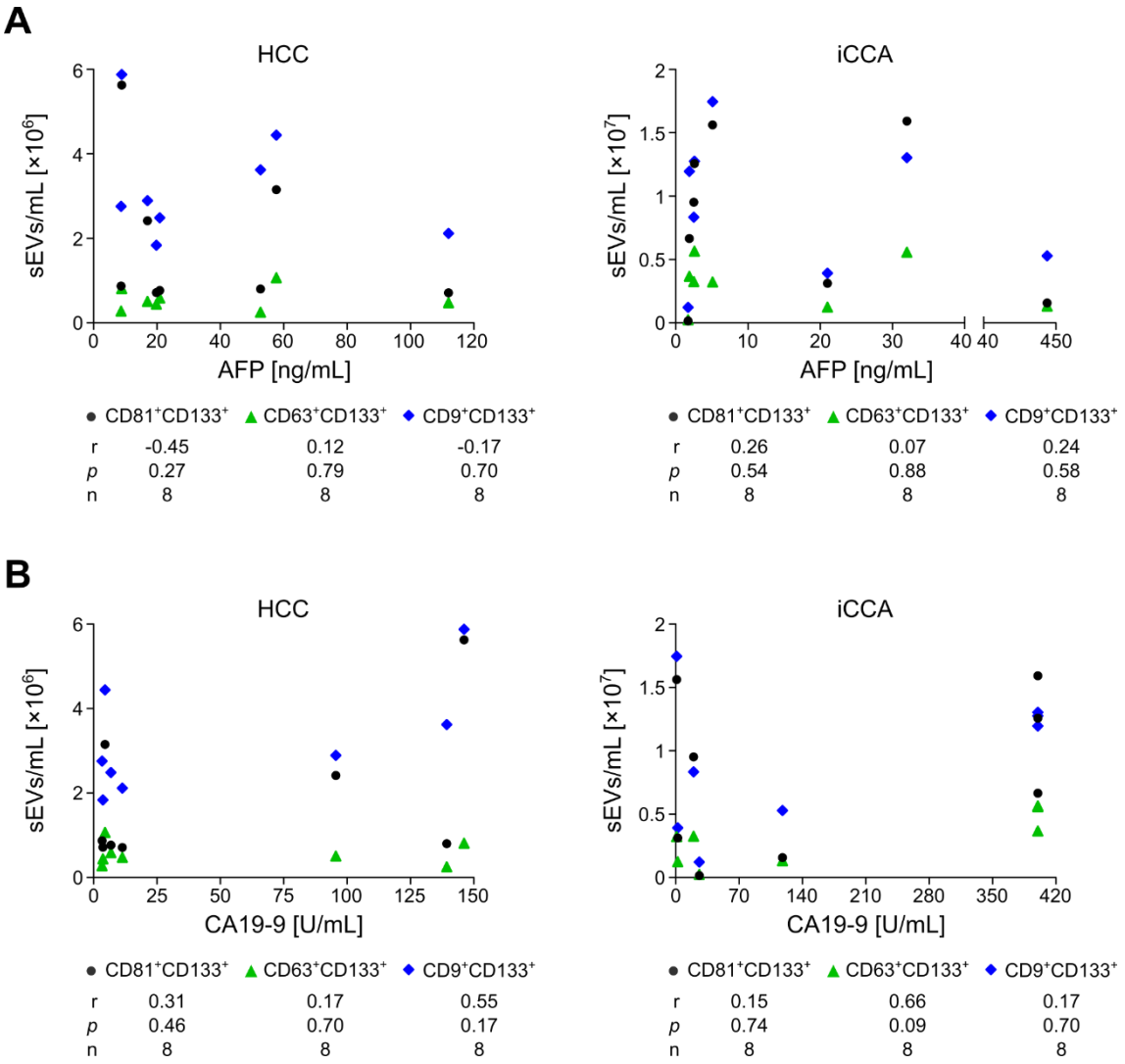

Fig. 33: Small EVs improve the diagnostic performance of AFP and CA19-9. Small EVs were isolated by SEC columns and incubated on ExoView® chips pre-coated with CD81, CD63 and CD9 capture antibodies. After counterstaining with fluorescent antibodies against CD133 and CD44v6, the sEV concentration was measured by the ExoView® R100 scanner. **A** Correlations between sEV levels and AFP of HCC and iCCA patients for the three sEV subpopulations $CD81^+CD133^+$, $CD63^+CD133^+$ and $CD9^+CD133^+$ are depicted. **B** Correlations between sEV levels and CA19-9 of HCC and iCCA patients for the three sEV subpopulations $CD81^+CD133^+$, $CD63^+CD133^+$ and $CD9^+CD133^+$ are shown. Spearman's correlation (r), *p*-values and cohort sizes (n) are indicated for each individual population and patient cohort.

All three sEV subpopulations increased the diagnostic performance of AFP, whereby the combination with $CD9^+CD133^+$ sEVs was associated with the best predictive values for HCC/iCCA separation with 100% sensitivity, 87.5% specificity, 88.9% PPV and 100% NPV (Tab. 18). Similarly, the diagnostic performance of CA19-9 could considerably be

enhanced by all three sEV subpopulations, whereby the combination with CD63$^+$CD133$^+$ sEVs showed the best results in this case with 87.5% sensitivity, 100% specificity, 100% PPV and 88.9% NPV. In contrast to lEVs, with which a perfect separation of HCC and iCCA patients could be achieved by combining AFP with AnnV$^+$CD44v6$^+$ lEVs, all sEV subpopulations displayed a very good, but slightly lower diagnostic power in this combinational approach.

Tab. 18: Diagnostic performance of AFP and CA19-9 individually and combined with small EV populations. iCCA patients were compared to HCC patients. Diagnostic cut-offs are given as total sEV counts per mL, as ng/mL for AFP and as U/mL for CA19-9. Sensitivities (sens), specificities (spec) as well as positive (PPV) and negative predictive values (NPV) are given as percentage. n indicates cohort size.

AFP					
CCA: n=8, HCC: n=8	**cut-off**	**sens [%]**	**spec [%]**	**PPV [%]**	**NPV [%]**
AFP	20	87.5	50.0	63.6	80.0
AFP or CD63$^+$CD133$^+$	20 or 1162000	87.5	100	100	88.9
AFP or CD9$^+$CD133$^+$	20 or 3257500	100	87.5	88.9	100
AFP or CD81$^+$CD133$^+$	20 or 2774000	87.5	87.5	87.5	87.5
CA19-9					
CCA: n=8, HCC: n=8	**cut-off**	**sens [%]**	**spec [%]**	**PPV [%]**	**NPV [%]**
CA19-9	129	37.5	75.0	60.0	54.5
CA19-9 or CD63$^+$CD133$^+$	129 or 1162000	87.5	100	100	88.9
AFP or CD9$^+$CD133$^+$	129 or 3257500	87.5	75.0	77.8	85.7
AFP or CD81$^+$CD133$^+$	129 or 2774000	75.0	87.5	85.7	77.8

All in all, combining sEV levels of the three subpopulations with the serum markers AFP and CA19-9 did not lead to a considerable improvement of HCC/iCCA differentiation in diagnostic terms. Sole evaluation of CD63$^+$CD133$^+$ sEVs (Tab. 17) achieved exactly the same predictive values as the combined approach of this sEV subpopulation with AFP. Even though CD9$^+$CD133$^+$ sEVs combined with AFP scored higher sensitivity and NPV with 100% each, they lack in specificity and PPV as compared to CD63$^+$CD133$^+$ sEVs and can therefore be considered equally suitable for minimal-invasive HCC/iCCA differentiation.

4. Discussion

In this section the feasibility of the experimental as well as of the study design will be explored and the gain of knowledge obtained from the findings in this thesis will be discussed and set into relation to currently employed diagnostic measures for hepatobiliary cancer diagnosis.

4.1. Selection of surface markers and their relation to putative cells of cancer origin

The overall aim of this study was to identify EV populations that could aid in differential diagnosis of hepatobiliary cancers, especially between HCC and iCCA. In the course of this project it was found that EVs expressing the markers CD133, gp38, EpCAM and CD44v6 or combinations thereof could distinguish between HCC and CCA with very good diagnostic accuracy. Since it is widely acknowledged that EVs reflect the composition and physiological state of their parental cells on many levels, it is reasonable to assume that these vesicles likely originated from cells carrying the same markers on their surface (Van Niel *et al.* 2018). This leads to the hypothesis that an increased release of EVs with certain surface marker profiles into the bloodstream of cancer patients indicates that their parental cells might be involved in carcinogenesis or cancer promotion. Identifying these cells of potential cancer-driving origin opens new possibilities for early cancer development interference and novel treatment options. Therefore, potential cells of cancer origin that are characterized by the same surface marker expression as observed on EVs in the serum of cancer patients were investigated in this thesis.

4.1.1. Progenitor cells as putative origin for differential EVs

The putative cellular origin of HCC and CCA is highly debated. While some evidence suggests that HCC arises from transformed mature hepatocytes, other theories postulate hepatic progenitor cells as a possible origin (Sia *et al.* 2017, Llovet *et al.* 2021). Similarly, among others, cholangiocytes, transdifferentiated hepatocytes and hepatic or biliary tree progenitor cells have been suggested as potential cells of origin for CCA development (Lu *et al.* 2015, Wei *et al.* 2016, Raven *et al.* 2018, Wang *et al.* 2018a). However, growing evidence supports the hypothesis that specific cells within an organ, typically tissue-specific stem or progenitor cells, can give rise to different subspecies of cancer (Visvader

2011, Hoadley *et al.* 2018, Lytle *et al.* 2018). In the liver, so called oval cells have been identified that expand during liver injury and that have bipotential differentiation capacity, enabling them to give rise to both hepatocytes and cholangiocytes *in vitro* and *in vivo* (Tanimizu *et al.* 2003, Rountree *et al.* 2007, Dorrell *et al.* 2011, Shin *et al.* 2011). Considering that both of these cell types are putative cellular origins for HCC and CCA, respectively, the theory arises that disturbances in the differentiation process of these common precursors into hepatocytes or cholangiocytes could predispose these cells for future HCC or CCA development (Sia *et al.* 2017, Lytle *et al.* 2018). In the course of this thesis it became evident that EVs with typical progenitor cell markers on their surface showed a differential expression profile in HCC and CCA patients with high abundancies in CCA and almost no occurrence in HCC. Besides the diagnostic value of this finding, it could indicate that indeed liver progenitor cells as a common precursor for both hepatocytes and cholangiocytes rather than mature hepatocytes or cholangiocytes themselves might play a critical role in primary liver tumor development, especially in CCA carcinogenesis.

In this regard, all of the chosen candidate markers in this thesis (EpCAM, CD133, gp38 and CD44v6) have been found to be associated with (cancer) stem/progenitor cells in a great variety of studies before. While CD133 is one of the most-studied markers for (cancer) stem cells of multiple normal tissue and cancer origins (Ren *et al.* 2013, Glumac and LeBeau 2018, Barzegar Behrooz *et al.* 2019), gp38 (also called podoplanin/PDPN) was originally described as a marker for lymphatic endothelial cells (Breiteneder-Geleff *et al.* 1999, Hirakawa *et al.* 2003). However, its association with progenitor cells, especially but not exclusively in a hepatic context, has been observed lately (Konishi *et al.* 2011, Jain *et al.* 2015, Eckert *et al.* 2016). In this thesis, $CD133^+gp38^+$ cells were detected in murine liver, gallbladder and lung (Fig. 9). This observation is consistent with literature, in which $CD133^+$, $gp38^+$ and $CD133^+gp38^+$ liver stromal cells with progenitor cell characteristics were identified in mice (Dollé *et al.* 2010, Konishi *et al.* 2011, Eckert *et al.* 2016). Interestingly, in the lung, gp38 is highly expressed in alveolar type I cells, which were shown to retain plasticity during alveolar injury, exhibiting stem cell-like behavior (Barth *et al.* 2010, Jain *et al.* 2015). This is consistent with our finding of high amounts of $gp38^+$ cells in murine lungs that are similar to the levels observed in murine liver. Furthermore, we identified $EpCAM^+CD133^+gp38^+$ cells in murine liver, gallbladder and

lung, which corresponds to the study by Eckert *et al.,* in which $CD133^+gp38^+$ liver progenitor cells were additionally shown to be associated with high EpCAM expression (Eckert *et al.* 2016). EpCAM is a very well-characterized protein that can be considered the most studied tumor-associated marker. While it can be found in a wide variety of human normal epithelium, it is frequently overexpressed in epithelial tumors (Baeuerle and Gires 2007, Schnell *et al.* 2013). Moreover, its association with stem cells has been reported (Ng *et al.* 2010) and it has been found to be part of a population of hepatic stem/progenitor cells that are able to differentiate into either hepatocytes or cholangiocytes (Safarikia *et al.* 2020). Furthermore, $EpCAM^+$ liver progenitor cells have been identified in several other studies and their role as potential tumor-initiating cells has been described (Yamashita *et al.* 2009, Safarikia *et al.* 2020). Moreover, multipotent endodermal stem/progenitor cells that could give rise, among others, to hepatocytes and cholangiocytes have been identified in human gallbladder as being positive for EpCAM (Carpino *et al.* 2012, 2014). In this thesis, almost all $CD133^+gp38^+$ cells in murine gallbladder were additionally positive for EpCAM (Fig. 9), possibly corresponding to the aforementioned progenitor cell population identified by Carpino *et al.*. While research concerning gp38 in GbCA is scarce, CD133 positive cells were reported to exhibit self-renewal ability and tumorigenicity in GbCA (Shi *et al.* 2011). Moreover, cells that were positive for both CD133 and CD44 showed cancer stem cell-like characteristics in GbCA as well (Shi *et al.* 2010). CD44 and its various variant isoforms, including CD44v6, are adhesion molecules that have been described as most prominent function-relevant cancer stem cell markers, that are associated with carcinogenesis, tumor migration and metastasis in a wide variety of cancers (Jijiwa *et al.* 2011, Todaro *et al.* 2014, Wang *et al.* 2018b, Ma *et al.* 2019). As a side note, at the time the experiments were performed for this thesis no antibody against murine CD44v6 was available to our group, so CD44 was used as a substitute. Therefore, when interpreting the results one has to keep in mind that, even though they are very similar, these two proteins might not behave completely interchangeably. Nonetheless, in this thesis, CD44 was most dominantly expressed in murine colon as compared to all other organs (Fig. 10). Accordingly, slightly elevated $AnnV^+CD44v6^+$ lEV levels in CRC patients as compared to all other control groups were observed later on (Fig. 22). It has previously been shown that especially intestinal cancer stem cells often exhibit high CD44/CD44v6 expression (Todaro *et al.* 2014), which could

explain these observations. In the liver, precancerous $CD133^+CD44^+$ cells were identified in a rat liver carcinogenesis model, that could be allocated to the hepatic oval cell fraction that exhibits bipotential differentiation capability (Zheng *et al.* 2014). Accordingly, high amounts of $CD133^+CD44^+$ and $CD44^+/CD44v6^+$ stem/progenitor cells could be observed in human HCC and CCA, respectively (Zhu *et al.* 2009, Padthaisong *et al.* 2020), and the presence of these cell populations in murine liver was detected in this thesis as well (Fig. 10).

4.1.2. Tumorous origin of differential EVs

In contrast to our obtained *in vivo* murine data, where gp38 could be detected in every investigated organ, the presence of the protein could not be observed on human HCC or CCA cancer cell lines *in vitro* (Fig. 6). The absence of gp38 on HCC and CCA cells is consistent with histological reports that explored the expression pattern of gp38 in normal liver tissue and various liver cancer entities. Among the seven investigated liver cancer entities, gp38 could only be detected on epithelioid hemangioendothelioma, but was absent on HCC as well as on iCCA (Fujii *et al.* 2008). Moreover, hepatocytes and biliary epithelial cells, both possible cells for HCC and CCA origin, respectively, were found to be completely negative for gp38 in the same study. Nonetheless, $gp38^+$ lEVs were identified in this thesis. This gives rise to the following hypothesis: EVs detected in patient serum might not be originating from the tumors themselves but rather from adjacent cells promoting tumor development and progression via EV release. EV-mediated interactions between the tumor and stromal cells in the tumor microenvironment have been studied intensely in the last decades uncovering a complex communication network. Hence, tumor-released EVs were found to stimulate surrounding cells to secrete factors supporting almost every step necessary for invasive progression including inflammation, ECM remodelling, angiogenesis and neovascularization, loss of tumor cell adhesion, formation of the metastatic niche and establishing tumor tolerance and chemoresistance (Skog *et al.* 2008, Webber *et al.* 2010, Becker *et al.* 2016, Lapitz *et al.* 2018, Wang *et al.* 2018b). Importantly, *vice versa*, it has also been shown that EVs released by tumor-surrounding cells can influence tumor progression. In this regard, EVs secreted by cancer-associated fibroblasts have been reported to promote tumor motility, invasion and dissemination in breast cancer (Luga *et al.* 2012). Even though the mechanisms by which

healthy stromal cells are triggered to support malignant behavior remain to be fully elucidated, it highlights the bi-directional nature of EV-mediated communication. Accordingly, progenitor cells, as a type of cells within the tumor microenvironment, could not only act as direct cells of cancer origin but might also be potential EV-secreting key drivers for cancer development, which could thus be another possible explanation for increased levels of EVs featuring progenitor-associated surface markers in cancer patients.

In contrast to gp38, expression of the markers CD133, EpCAM and CD44v6 could be detected directly on the surface of human HCC as well as CCA cell lines and their presence on human CCA cell line-derived EVs was verified (Fig. 6 and Fig. 7, respectively). This supports a directly tumorous origin of EVs with these particular markers on their surface instead of originating from tumor-promoting stromal cells. Especially CD133 and CD44v6 were interesting in this setting, since they showed a differential expression pattern with high amounts of CD133 present on the surface of HCC cells and CD44v6 being predominantly expressed on CCA cells, indicating a possible differential capability already at the cellular level. Both of these antigens subsequently proved their relevance for EV-based HCC/iCCA differentiation in this thesis with CD44v6 being particularly useful in large EV diagnosis, whereas CD133 proved to be the most relevant marker in small EV differentiation. Up to date, a clear distinction of HCC and iCCA by comparing expression patterns of CD133, CD44v6 or their combination on cells or EVs has not been achieved. This might partially be due to the great heterogeneity within the respective tumor entities which leads to enormous variations in detectable protein levels. Immunohistologically, CD133 and CD44v6 expression has been identified in human tumorous HCC (Yun *et al.* 2002, Song *et al.* 2008, Mima *et al.* 2012, Sung *et al.* 2016) and CCA (Yun *et al.* 2002, Leelawat *et al.* 2011, Cai *et al.* 2018, Padthaisong *et al.* 2020) tissues in multiple studies, although the degree of identified CD133 and CD44v6 positive tumors varies considerably for both HCC and CCA among the reports. Similarly, EpCAM expression can be observed in histopathological stainings of both HCC (Spizzo *et al.* 2011, Sung *et al.* 2016) and CCA (Komuta *et al.* 2012, Sulpice *et al.* 2014, Padthaisong *et al.* 2020) to varying degrees. Even though EpCAM had been found to be highly expressed in most tumors of the gastrointestinal tract, HCC was frequently negative (Spizzo *et al.* 2011). Nonetheless, an association of EpCAM positivity and advanced HCC

tumor stage has previously been observed (Bae *et al.* 2012) and is partially reflected in this thesis by the finding that the amount of EpCAM positive lEVs ($AnnV^+CD133^+gp38^+EpCAM^+$) in the serum of HCC patients but not of other tumor patients tends to correlate with advanced tumor stage (see Supplementary Fig. 4 and Tab. 15). Interestingly, there is evidence that CD44v6 defines a population of circulating tumor cells that is independent of simultaneous EpCAM expression (Belthier *et al.* 2021), which corroborates the division of the present lEV study into two seperate study arms: one assessing the differentiation capacity of lEVs involving EpCAM, while the other investigates the role of CD44v6 positive EVs in HCC/iCCA differentiation.

In conclusion, it can only be speculated about the explicit origins of the differential EVs identified in this study. Even though discovering their origin was not an integral component of this thesis, discussing different options provides helpful insights into possible reasons for their differential capability and assists in evaluating the feasibility of EVs as a measure for addressing the pressing clinical issue of reliable HCC/iCCA differentiation. Therefore, since possible parental cell populations were successfully identified *in vitro* and *in vivo* that express marker combinations corresponding to relevant differential EVs later on, the selection of markers and their combinations within the experimental setting of this thesis can be considered reasonable to address the main objectives of this project.

4.2. The differences of large and small EVs in hepatobiliary cancer differentiation

In the course of this study it became evident that EVs as serum biomarkers can be valuable assets in hepatobiliary cancer diagnosis and differentiation. They proved especially useful in specific and minimal invasive HCC/iCCA differentiation, which up until today poses an unmet clinical challenge. To tackle this important issue and to achieve a comprehensive overview of the overall feasibility of EVs for hepatobiliary cancer diagnosis, two main subtypes of EVs, large and small EVs, were isolated and their diagnostic performance in relation to their specific surface marker composition was compared.

According to their surface marker profile, lEVs were further divided into two subgroups, progenitor cell-associated and tumor-associated lEVs, each representing cellular populations that were identified as putative EV parental populations and as potentially

diagnostically relevant for hepatobiliary cancer diagnosis and differentiation earlier (Fig. 6, Fig. 7, Fig. 9 and Fig. 10). Generally, it was noticable that tumor-associated lEVs, comprising the surface marker combinations AnnV$^+$CD44v6$^+$ and AnnV$^+$CD44v6$^+$CD133$^+$, performed superiorly than progenitor cell-associated lEVs, comprising the marker combinations AnnV$^+$CD133$^+$gp38$^+$ and AnnV$^+$EpCAM$^+$CD133$^+$gp38$^+$. Within the tumor-associated lEV populations AnnV$^+$CD44v6$^+$ predominantly presented with the best diagnostic performance in most analyses. Nonetheless, all investigated lEV populations were proven to act as reliable serum biomarkers for biliary cancers (CCA and GbCA combined) by successfully discriminating them from other malignancies (including HCC), cirrhosis and healthy individuals with good diagnostic accuracy (Fig. 18, Tab. 7, Fig. 22 and Tab. 11). With an AUC value of 0.80, 84.0% sensitivity, 63.3% specificity, 85.1% positive predictive value (PPV) and 61.3% negative predictive value (NPV) AnnV$^+$CD44v6$^+$ lEVs proved to be the most useful population for detecting biliary cancers out of a pool of healthy individuals. This setting reflects a scenario, in which a suspicion of biliary cancer could be raised as part of a routine screening without showing any symptoms of malignancies or liver-related diseases beforehand. Since the majority of iCCA cases arise in the absence of known risk factors and are therefore predominantly detected by cross-sectional imaging performed for other indications (Sirica *et al.* 2019, Banales *et al.* 2020), early detection as part of an uncomplicated screening by EVs might be of great value. Naturally, the screening result would have to be verified in a subsequent examination for definitive diagnosis. In addition to identifying biliary cancers out of a heterogeneous pool of maladies, all lEV populations reliably distinguished between CCA (all subtypes combined) and HCC with AnnV$^+$CD44v6$^+$ lEVs showing the best diagnostic performance again (AUC: 0.78, sensitivity: 80.9%, specificity: 71.0%, PPV: 80.9%, NPV: 71.0%) (Fig. 19, Tab. 8, Fig. 23 and Tab. 12). Even more important in a clinical context, all lEV populations were capable of reliably discriminating iCCA from HCC with good diagnostic accuracy, again with AnnV$^+$CD44v6$^+$ lEVs being in the lead in terms of diagnostic performance (AUC: 0.83, sensitivity: 93.3%, specificity: 71.0%, PPV: 60.9%, NPV: 95.7.0%) (Fig. 20, Tab. 9, Fig. 24 and Tab. 13). Moreover, as one of the most important results of this thesis, it was shown that the diagnostic performances of the two serum biomarkers AFP and CA19-9 were considerably improved by implementing lEVs, leading to a perfect, 100% accurate diagnostic separation of 29 CCA and 34 HCC

patients, when combining AFP and AnnV$^+$CD44v6$^+$ lEVs in a pooled analysis (Tab. 14). These results could be of great clinical value for accurately identifying iCCA that can be notoriously difficult to distinguish from HCC owing to their similar and hard to access location within the liver parenchyma, while simultaneously requiring highly diverse treatment regimen (Valle *et al.* 2016, Banales *et al.* 2020).

When analysing the diagnostic capability of sEVs in this important issue, some distinct differences to lEVs became evident. First of all, colocalization of the two markers CD133 and CD44v6 could not be observed on any sEV subpopulation, making an assessment of double positive sEVs impossible (Fig. 31). Secondly, in contrast to lEVs, sEVs bearing CD133 on their surface performed superiorly in all analysed subpopulations as compared to sEVs harboring CD44v6 on their surface. In this context CD63$^+$CD133$^+$ sEVs showed the best diagnostic performance in differentiating iCCA from HCC with an AUC value of 0.89, 87.5% sensitivity, 100% specificity, 100% PPV and 88.9% NPV (Fig. 32 and Tab. 17). Hence, sole assessment of CD63$^+$CD133$^+$ sEVs led to higher specificity and PPV than sole assessment of the best performing lEV population AnnV$^+$CD44v6$^+$ (compare: 0.83 AUC, 93.3% sensitivity, 71.0% specificity, PPV: 60.9% PPV, 95.7.0% NPV). Lastly, even though combining CD133$^+$ sEV subpopulations with the serum markers AFP and CA19-9 improved the respective diagnostic capacity of the individual serum marker, it did not lead to overall better diagnostic separation of iCCA from HCC than sole assessment of sEV subpopulations (Tab. 18).

4.2.1. The different characteristics of isolated large and small EVs

The reasons for the observed diagnostic differences in large and small EVs can be manifold. Importantly, one has to keep in mind that the cohort sizes for the two EV studies in this thesis varied considerably. While 67 HCC and 22 iCCA patients could be analysed for their lEV profile, only 8 HCC and iCCA patients each were available for sEV analysis. Therefore, the statistical and diagnostical power of the sEV study is limited and it should rather be considered as an exploratory pilot study that needs further validation with bigger cohort sizes for definitive predictions. Nonetheless, especially when considering that due to the rarity of the diseases only a limited number of CCA patients are available and that the majority of studies is conducted on equally low or only slightly bigger cohort sizes, the results are promising and give reason to expect a potential clinical utility of sEVs for

HCC/iCCA differentiation in the future. Another important factor that might influence the diagnostic differences observed among the two EV subtypes is based on the enormous complexity of the research field itself that is faced with a multitude of challenges, especially in terms of EV classification and standardization of isolation methods (Théry *et al.* 2018). These issues are mostly due to the fact that EVs display a tremendous level of multiparameter heterogeneity. This way, in addition to different modes of biogenesis, the parameters size, content, functional impact on recipient cells and cellular origin should be considered for appropriate subclassification, adding another level of complexity to EV research (Kalluri and LeBleu 2020). Moreover, even if several parameters are considered, isolation of pure EV subpopulations of interest is nearly impossible (Bobrie *et al.* 2012, Gould and Raposo 2013). To tackle these limitations and to ensure an appropriate characterization of different isolated subtypes and subpopulations of EVs in this thesis, numerous quality controls and precautional measures were performed while establishing the respective isolation protocols (Fig. 13, Fig. 15, Fig. 16, Fig. 27, Fig. 29 and Fig. 30). First, EVs were purified according to their size. Depending on the implemented method, a certain subtype of EVs will be enriched, while other subtypes will still be present in the isolate to a certain extent. For lEV enrichment from patient serum a sequential centrifugational method was chosen that led to pelletation of larger EVs at speeds of 10,000 × *g* (see section 2.5.2). Size determination by NTA showed that indeed the majority of isolated EVs had a mean diameter of around 125.8 nm (Fig. 13). Small EVs on the other hand were enriched by so called size exclusion chromatography (SEC) columns that were optimized for isolation of smaller particles (see section 2.6.2). Indeed, size determination by ExoView® scanning confirmed a mean diameter ranging between 56.5 to 73.0 nm for isolated sEVs, depending on the respective subpopulation (Fig. 29), verifying their smaller size as compared to lEVs isolated by sequential centrifugation. Importantly, characteristics such as size or density alone are not sufficient as strict criteria to define small and large EVs, since both vesicle types may be produced by the same cell and since both modes of biogenesis, plasma membrane budding and endomembraneous invagination, might lead to similar sized vesicles (Heijnen *et al.* 1999, Booth *et al.* 2006, Andreu and Yáñez-mó 2014). Therefore, in a concerted effort leading EV experts tried to standardize EV research by identifying criteria for isolation and classification of EVs leading to the publication of a position paper on “Minimal information for studies of

extracellular vesicles" (MISEV) (Théry *et al.* 2018). Based on their recommendation, in addition to size determination of EV isolates, characteristic EV protein markers should be evaluated in a quantitative and qualitative manner to further classify isolated EVs and to exclude other co-isolated particles (e.g. lipoproteins or protein aggregates) of the same sizes. Due to limited resources in terms of funding and availability of infrastructure not all of the suggested analyses were possible during the experimental phase of this thesis. Nevertheless, protein verification of isolated EVs was conducted to verify successful EV isolation and to further classify them.

For lEV analysis, flow cytometric quantification of AnnexinV (AnnV) was incorporated as a general EV marker after isolation by sequential centrifugation. AnnV binds to externalized phosphatidylserine (PS) on EV membranes and can thus be considered as an indirect EV marker. Even though AnnV is not a completely exclusive marker for lEV identification, it is a very widely used and accepted method for general EV detection (Théry *et al.* 2018). Therefore, the combination of a) the presence of the indirect EV protein marker AnnV bound to PS in the plasma membrane of EVs and b) a confirmed mean diameter of 125.8 nm of isolated EVs were considered sufficient criteria to verify lEV isolation. Furthermore, based on light scattering the lower detection limit of conventional flow cytometers, which was the primary analysis modality for assessing lEV levels, lies at around 300-500 nm (Botha *et al.* 2021). However, incorporating fluorescence triggering by fluorescently labelled AnnV, as was performed in this thesis, was shown to lower the detection limit to 100-150 nm, which corresponds to the size of lEVs (Arraud *et al.* 2015). Flow cytometric analysis of smaller EVs is very difficult, if not impossible. Accordingly, as visualized in Fig. 15D and E, out of initially 1.175×10^9 sEV particles only a negligible number of 130 absolute events were detectable by flow cytometric analysis. This corroborates that only lEVs were included in the analysis of the diagnostic profiles within the lEV study arm of this thesis since sEVs could not be measured by flow cytometric analysis. Moreover, all reagents for isolation as well as for flow cytometric analysis were filtered prior use (0.02 µm filters), so the presence of possible contaminating particles introduced by these reagents was prohibited as validated by the absence of measurable particles in the flow cytometric analysis (Fig. 15C). The presence of other co-isolated biological particles in the lEV isolate with similar sizes to lEVs (e.g. lipoproteins or protein aggregates) could not be completely excluded with all these incorporated measures.

However, while functional analysis of EVs requires an isolation and characterization of the isolated particles as well as possible in order to attribute specific functional effects to them, the focus of this thesis was not on functional analysis of EVs. Instead, a diagnostically useful, easily applicable test should be established, so potential contaminations can be disregarded as long as the diagnostic capability is conclusive and reproducible. To this end, the diagnostic utility of lEVs could be demonstrated to an impressive extent in the course of this thesis.

As recommended by the MISEV guidelines, characteristic protein markers needed to be identified on isolated sEVs to further classify them. Therefore, after isolation of sEVs by SEC columns, levels of the three tetraspanins CD9, CD63 and CD81 were analysed on the sEV surface. Tetraspanins are widely used and well-accepted markers for EVs (Andreu and Yáñez-mó 2014, Théry *et al.* 2018). However, the sole implementation of tetraspanins for classification of EV subtypes is controversial, since they are widely spread in the plasma membrane and may also be present in vesicles budding from the plasma membrane (Andreu and Yáñez-mó 2014, Willms *et al.* 2018). Therefore, additional size verification is crucial, which revealed a mean diameter of 56.5 to 73.0 nm depending on sEV subpopulation confirming their size to be in range of sEVs (below 100 nm) and to be smaller than the mean diameter of isolated lEVs in this thesis (125.8 nm) (Fig. 29). Hence, the combination of size verification and tetraspanin profile can be considered conclusive for successful sEV isolation. Small EVs with different tetraspanin profiles have been shown to exhibit quite differing functional behavior (e.g. vesicle loading and binding affinity to cells) in a multitude of studies previously, highlighting the enormous heterogeneity within this EV subtype (Giebel 2017, Van Niel *et al.* 2018, Kalluri and LeBleu 2020). Therefore, a distinct assessment of several sEV subpopulations rather than a bulk analysis added a considerable value to the diagnostic approach in this thesis which was ultimately confirmed by the diagnostic differences observed between the different sEV subpopulations harboring different tetraspanin profiles (Fig. 31 and Fig. 32). Interestingly, characteristic differences between the different sEV subpopulations could not only be observed on a diagnostic level, since $CD9^+$ sEVs tended to be the subpopulation with the largest particles in size, followed by $CD63^+$ and $CD81^+$ sEVs (Fig. 29). Furthermore, $CD9^+$ sEVs were not only the largest sEVs but also the ones that showed the highest particle concentrations in all three patient cohorts, again followed by $CD63^+$ and $CD81^+$ sEVs

(Fig. 30). As mentioned before, these findings reflect the great heterogeneity of sEVs and corroborate their division into different subpopulations for comprehensive diagnostic analysis in hepatobiliary cancers.

4.3. The diagnostic utility of EVs in hepatobiliary cancer diagnosis

The overall goal of this project was a comprehensive assessment of the diagnostic value of EVs in hepatobiliary cancer management. In the course of this thesis EVs manifested themselves on the one hand as valuable minimal invasive markers for biliary cancers and on the other hand as extremely useful markers for the critical differentiation between the hard to distinguish entities iCCA and HCC.

4.3.1. The diagnostic utility of EVs as markers for biliary cancer

In contrast to some forms of HCC for which radiological criteria exist that are considered sufficient for definitive diagnosis without histological confirmation, no such non or minimal-invasive methods are available for definitive CCA or GbCA diagnosis. Therefore, up to date, a biopsy followed by histopathological evaluation is mandatory for reliable diagnosis of biliary cancer entities (Bridgewater *et al.* 2014, Banales *et al.* 2016). However, the sensitivity of biopsies highly depends upon location and size of the tumor as well as upon operator expertise (Bridgewater *et al.* 2014, Ney *et al.* 2021). Several different sampling techniques exist with endoscopic retrograde cholangiopancreatography (ERCP) being the primary modality of choice (Valle *et al.* 2016, Ney *et al.* 2021). While pooled specificities for this sampling technique are usually between 98-100% for diagnosing CCA from a benign setting, corresponding pooled sensitivities are limited ranging only between 6-65% (Avadhani *et al.* 2017). Additionally, for GbCA diagnosis ERCP-guided biopsies only achieved an accuracy of 46-88% (Tong *et al.* 2022). Considering this low diagnostic yield, endoscopic ultrasound fine needle aspiration (EUS-FNA) has gained popularity increasing the pooled sensitivity to 80% with simultaneous pooled specificity of 97% for CCA diagnosis (Sadeghi *et al.* 2016). For GbCA diagnosis EUS-FNA could even be shown to be associated with 95% sensitivity and 100% specificity (Tong *et al.* 2022). Another sampling technique for diagnosing biliary cancers is single operator cholangioscopy (SOC) with cholangioscopy-guided biopsy which was reported to have pooled sensitivities

and specificities ranging from 66-72% and 98-99% for CCA diagnosis, respectively (Navaneethan *et al.* 2015, Badshah *et al.* 2019). Importantly, there exist some concerns regarding FNA which can lead to needle tract seeding of the tumor or other adverse events following biopsies in biliary cancer patients (Levy *et al.* 2010, Minaga *et al.* 2017). The overall risk ranges between approximately 2-4% but the impact on disease progression and overall survival remains unclear (Micames *et al.* 2003, Minaga *et al.* 2017, Yane *et al.* 2020). Overall, independent of the chosen sampling technique, biopsies are associated with high specificities, while often lacking in sensitivity. This means that while a positive biopsy will certainly establish a diagnosis (high positive predictive value), a negative result does not exclude the presence of a tumor (low negative predictive value) (Bridgewater *et al.* 2014). To address the issue of low negative predictive values of biopsies, for patients with negative histological results a follow-up screening is suggested. There are several options for follow-up assessments including a second biopsy, various imaging procedures, serum proteins or different kinds of liquid biopsies including extracellular vesicles.

Since both CCA as well as GbCA displayed similarly elevated lEV levels and were undistinguishable from one another within each investigated lEV subpopulation in this thesis, they were combined to a comprehensive “biliary cancer” cohort and the diagnostic potential of lEVs as a biliary cancer marker was evaluated. With 84% sensitivity, 63% specificity, 85% PPV and 61% NPV (Tab. 11) $AnnV^+CD44v6^+$ lEVs displayed an even greater sensitivity for discriminating biliary cancer patients from healthy controls than any aforementioned type of biopsy for CCA diagnosis. However, one has to keep in mind that the clinical challenge lies within differential diagnosis from other malignant and underlying diseases. To this end, $AnnV^+CD44v6^+$ lEVs were able to differentiate biliary from non-biliary cancers (including HCC, NSCLC and CRC) with 84% sensitivity, 56% specificity, 69% PPV and 75% NPV in a large patient cohort (n=75 and n=64, respectively). Again, the sensitivity exceeded the values of all biopsies and was accompanied by a very good negative predictive value that was even higher than for discrimination from healthy subjects and that is a hallmark with which biopsies often struggle. During the experimental phase of this thesis, unfortunately no PSC patients were available to our group, so the differential capability of lEVs to discriminate biliary cancers from this important predisposing condition was not possible. However, patients displaying liver cirrhosis, defining another risk-group especially in terms of CCA, were available, for which a

diagnostic separation by progenitor cell-associated lEVs was achieved with 71-73% sensitivity, 53-55% specificity, 73-74% PPV and 51-53% NPV (Tab. 7). Even though $AnnV^+CD44v6^+$ lEVs show very good and higher sensitivity and PPV than progenitor cell-associated lEVs with 84% and 96%, respectively, for discrimination of biliary cancer from cirrhosis patients, these values have to be interpreted with care, since the patient cohorts in the tumor-associated study arm were greatly unequal due to limited access to cirrhosis patients for this part of the study (n=75 and n=5, respectively). Despite the limited diagnostic power for discrimination of biliary cancers from benign diseases, lEV surface profiling could be a very useful tool to augment the diagnosis of biliary cancers. Especially if their high diagnostic conclusiveness for discriminating biliary cancers from healthy subjects and patients with other malignancies as well as the methodological advantages are considered: lEV surface profiling only requires a blood sample which is a minimal-invasive procedure that is easily accessible, accepted by patients and leaves almost no room for operator-dependency.

Currently, various imaging procedures are employed if biliary cancer is suspected and they can be of great benefit in establishing a diagnosis by augmenting biopsies and in developing a following treatment plan. Unfortunately, since no distinct radiological criteria exist, differential diagnosis of biliary cancers solely by imaging is difficult and can not be relied upon (Beuers *et al.* 2009, Bridgewater *et al.* 2014). Thus, since a complete surgical resection of the tumor is the only potentially curative treatment, the primary role of imaging is the characterization of the tumor to determine possible surgical candidates as well as the extent of the surgery (Hennedige *et al.* 2014, Joo *et al.* 2018). Multidetector computed tomography (CT) has emerged as the standard imaging method for diagnosis, staging and resectability assessment and is associated with a high negative predictive value of 85-100% for advanced diseases, but only shows limited sensitivity for detecting small intrahepatic and distant metastases (Vilgrain 2008). However, no single imaging modality can yield a comprehensive evaluation of biliary cancers, therefore, multimodality approaches, e.g. including MRI with MRCP or PET are recommended (Vijayakumar *et al.* 2013, Hennedige *et al.* 2014, Joo *et al.* 2018).

The observed negative predictive values for multidetector CT exceed the ones obtained by lEV profiling in this thesis but are only valid for detecting advanced diseases with bigger tumors. Accordingly, currently applied imaging procedures tend to have difficulties to

reliably detect tumors below 10-20 mm of size resulting in low sensitivities (Forner *et al.* 2008). In terms of this critical early detection of small tumors, lEV profiling might be of significant advantage. Even though the usefulness of lEV surface profiling for early detection of small biliary tumors was not the focus of the study at hand and has consequently not been investigated, a study previously published by our group showed a close correlation of liver tumor size (HCC and CCA combined) and lEV levels bearing various combinations of the surface markers EpCAM, ASGPR1 and CD133 (Julich-Haertel *et al.* 2017b). The smallest tumor available for this study was 11 mm in size which could confidently be detected by lEV surface profiling. Due to the unavailability of tumors smaller than 11 mm, the lower detection limit of lEVs might not have been explored fully yet and might only be restricted by the stage of vascularization of the tumor, since access of the tumor to the bloodstream is a prerequisite for lEVs being detectable in the serum of patients. Vascularization usually starts at tumor diameters of roughly 2 mm indicating the potential of lEVs as an early screening tool for very small tumors (McDougall *et al.* 2006). Current serum or bile tumor markers (e.g. CA19-9 or CEA) are not specific to establish a diagnosis for any biliary cancer entity since they have significant overlap with other benign and malignant diseases and display low sensitivity for early stage disease which hampers their diagnostic utility. This way, even though CA19-9 is elevated in up to 85% of CCA patients, it is frequently elevated in PSC patients as well leading to low sensitivities of 40-70%, specificities of 50-80% and positive predictive values of 16-40% for CCA diagnosis, depending on the cut-off value (Hultcrantz *et al.* 1999, Gores 2000, Patel *et al.* 2000). However, CA19-9 might be of prognostic value since patients with unresectable CCA typically display elevated levels and persistently raised levels after decompression were found to be indicative of malignancy (Patel *et al.* 2000, Abbas and Lindor 2009, Valle *et al.* 2010). In GbCA elevated CA19-9 levels were associated wich advanced-stage tumors and metastases, also highlighting the prognostic relevance for this serum tumor marker (Sachan *et al.* 2020).

In comparison to CA19-9 in CCA patients, $AnnV^+CD44v6^+$ lEVs for discriminating biliary cancer patients from healthy subjects were associated with higher sensitivity and more than twice as high PPV, while simultaneously displaying equal specificity (Tab. 11). For discriminating biliary from non-biliary cancer patients, the diagnostic performance of $AnnV^+CD44v6^+$ lEVs was comparable to that for distinguishing biliary cancer patients from

healthy subjects with slightly lower sensitivity and PPV but higher NPV. Therefore, even though routine implementation of lEV surface profiling might be more challenging than serum CA19-9 assessment, considering the superior diagnostic performance, the diagnostic benefit of lEV profiling becomes evident. Since the overall focus of this thesis was to investigate EV profiling as a means for iCCA/HCC differentiation, a direct comparison of the diagnostic performances of EVs and CA19-9 within the study group of this thesis in terms of their usefulness as a biliary cancer marker was not evaluated. Instead, CA19-9 levels were evaluated later on in the context of iCCA/HCC differentiation. In general, considering that cancer represents an ever-increasing health issue, liquid biopsies as a promising, minimal-invasive diagnostic tool are an emerging research field, so it is not surprising that a multitude of studies exist that investigate the usefulness of many different liquid biopsy approaches for detection of any kind of cancer including biliary malignancies. Several approaches have been shown inefficient or insensitive for biliary cancer diagnosis or need further validation such as the evaluation of circulating tumor cells or cell-free DNA in the blood of patients (Al Ustwani *et al.* 2012, Goyal *et al.* 2017). Other approaches are promising: In terms of serum proteins CYFRA 21-1 has been shown to be significantly upregulated in biliary malignancies (including iCCA, pCCA, dCCA and GbCA). However, with an associated sensitivity of 75% and specificity of 85% they were less sensitive but more specific than $AnnV^{+}CD44v6^{+}$ lEVs in this thesis (Huang *et al.* 2015). In another study, Arbelaiz *et al.* investigated the differential protein content of serum EVs from CCA and PSC patients and found that the protein FCN2 was significantly elevated in early stage CCA (stage I and II) as compared to PSC (Arbelaiz *et al.* 2017). Associated diagnostic values reached 100% sensitivity and 81% specificity. However, the cohort size of 13 CCA and 30 PSC patients was rather small and needs further validation. In contrast to the aforementioned studies that were conducted on proteins or EVs derived from patient serum, bile can be an important source for biliary cancer diagnosis. This way, a miRNA panel (miR-9, miR-302c, miR-199a-3p and miR-222) derived from bile EVs was found to be associated with 89% sensitivity and 100% specificity for differentiating biliary malignancies (CCA and GbCA combined) from benign choledolithiasis patients (Shigehara *et al.* 2011). Even though the diagnostic performance was better than that of lEVs in this thesis, the cohort sizes were rather small and included only 9 choledolithiasis and 9 malignant specimens (CCA and GbCA combined) rendering the results promising

but decreasing the power of the study, especially when compared to the 75 biliary cancer patients and 30-64 control subjects in this thesis. Additionally, one has to keep in mind that in contrast to serum, bile is harder to obtain from patients involving a more invasive process than drawing a blood sample, which might reduce the willingness of patients to undergo such a procedure, especially if the procedure is planned as part of a routine screening, when there is no apparent indication of any disease or malignancy yet. In another interesting study, Severino *et al.* found that total EVs in bile were elevated in malignant common bile duct stenoses (pancreatic cancer and CCA combined) versus non-malignant stenoses and they could be discriminated with 100% accuracy (Severino *et al.* 2017). Again, cohort sizes of only 15 patients per group might limit the diagnostic power of this study. In contrast to CCA, for GbCA diagnosis, the total EV count from bile could not be confirmed to be indicative of malignancy (Turpati *et al.* 2020). This is in line with some studies that suggest that evaluation of total EV counts in biological fluids might only be of limited power, since the majority of EVs within the circulation is not of tumorous origin which leads to high background noises (Reátegui *et al.* 2018). Therefore, instead of total EV counts, EVs with tumor- or progenitor cell-associated markers on their surface were analysed in this thesis.

4.3.2. The diagnostic utility of EVs for differential diagnosis of iCCA and HCC

In addition to EVs being useful markers for biliary cancer, they proved especially beneficial for the clinically challenging differential diagnosis of iCCA and HCC in this thesis. Since these two entities involve considerably different treatment strategies and prognoses, the differential diagnosis of iCCA from HCC is critical (Valle *et al.* 2016, Banales *et al.* 2020). Currently, no completely reliable non or minimal invasive procedure exists for definitive differentiation leaving biopsy followed by histopathological evaluation as the only method to establish a definitive differential diagnosis (Bridgewater *et al.* 2014, Joo *et al.* 2018, Banales *et al.* 2020). Imaging differentiation of iCCA and HCC remains difficult since they share common risk factors (e.g. liver cirrhosis) and can mimic each other by exhibiting atypical imaging features with iCCA mimicking HCC more frequently than the other way round (Kim *et al.* 2011, Huang *et al.* 2016, Joo *et al.* 2018). Given that in high risk patients HCC can be diagnosed based on imaging criteria without the requirement of subsequent histopathological confirmation (Galle *et al.* 2018, Marrero *et al.* 2018), imaging-based

misdiagnosis of iCCA as HCC may cause physicians to skip the histological confirmation step thus leading to improper treatment. Considering these concerns other options for differential iCCA/HCC diagnosis need to be explored and are currently under investigation in order to facilitate treatment decisions and to ultimately improve patient survival.

All lEV populations investigated in this thesis were capable of reliably discriminating iCCA from HCC with good diagnostic accuracy. $AnnV^+CD44v6^+$ lEVs even achieved diagnostic values as high as 93.3% sensitivity, 71.0% specificity, 60.9% PPV and 95.7% NPV (AUC: 0.83), greatly emphasizing their promising clinical potential for iCCA/HCC differentiation (Fig. 24 and Tab. 13). Notably, a differential diagnosis of the two subtypes iCCA and eCCA could not be achieved with any lEV population. While sEVs harboring CD44v6 on their surface did not lead to any conclusive differential results, $CD63^+CD133^+$ sEVs on the other hand showed the best diagnostic performance out of all sEV subpopulations in differentiating iCCA from HCC with an AUC value of 0.89, 87.5% sensitivity, 100% specificity, 100% PPV and 88.9% NPV (Fig. 32 and Tab. 17). Hence, sole assessment of $CD63^+CD133^+$ sEVs led to higher specificity and PPV than sole assessment of the best performing lEV population $AnnV^+CD44v6^+$, while higher sensitivity and NPV were achieved by $AnnV^+CD44v6^+$ lEVs. The diagnostic differences observed between small and large EVs supports the initial hypothesis of this thesis that a comprehensive analysis of different EV subtypes might be beneficial for evaluating the whole potential of EVs as diagnostic markers for hepatobiliary cancers.

Several attempts for minimal-invasive iCCA/HCC differentiation are currently under investigation including a panel of 4 serum metabolites (glycine, aspartic acid, SM(42:3), and SM(43:2)) that were found to be associated with 75% sensitivity and 90% specificity (AUC: 0.89) for differentiating iCCA from HCC (Banales *et al.* 2019). In another approach the differential expression of serum EV-derived proteins was assessed revealing a differential capability of the protein FIBG that discriminated iCCA from HCC with 83% sensitivity and 90% specificity (AUC: 0.894) (Arbelaiz *et al.* 2017). However, in terms of sensitivity, the diagnostic performances of EVs in this thesis surpassed the results obtained from both of these studies, indicating the great potential of surface EV profiling for iCCA/HCC differentiation.

AFP is the most widely studied serum biomarker in terms of HCC surveillance, diagnosis and prognosis (Galle *et al.* 2018, Marrero *et al.* 2018, Benson *et al.* 2021). It has been

shown that AFP can be helpful for identifying at-risk populations as persistently high AFP levels are a risk factor for HCC development (Tsukuma *et al.* 1993). This way, elevated AFP levels above the recommended cut-off of 20 ng/mL were shown to be associated with 62% sensitivity, 89% specificity, 85% PPV and 69% NPV for HCC diagnosis (Trevisani *et al.* 2001). Consequently, AFP levels have also been investigated in terms of their usefulness for iCCA/HCC differentiation displaying 91% sensitivity and 55% specificity (Tao *et al.* 2010). While the sensitivity is comparable to that of $AnnV^+CD44v6^+$ lEVs and $CD63^+CD133^+$ sEVs in this thesis, the specificity is significantly lower, highlighting EVs as a more promising means for iCCA/HCC differentiation than AFP. This corroborates the assumption that AFP might not be the ideal marker for differentiation of iCCA from HCC since its usefulness might be hampered by the fact that AFP was found to be elevated frequently in other cancers including iCCA as well as in pregnancy (Gregory and Finlay 1999, Bruix and Sherman 2011). Furthermore, only 10-20% of early stage HCC present with abnormal AFP serum levels, rendering it less efficient for critical early diagnosis (Galle *et al.* 2018). In addition to AFP, CA19-9 has been investigated for iCCA/HCC differentiation, which revealed only 62% sensitivity and 63% specificity (Tao *et al.* 2010). Even though the diagnostic values for these single serum markers are considerably lower as compared to $AnnV^+CD44v6^+$ lEVs and to $CD63^+CD133^+$ sEVs, a combinational approach involving AFP, CA19-9 and EV populations to further improve the diagnostic capability for iCCA/HCC differentiation seemed promising.

As none of the EV subpopulations showed any correlation with AFP or CA19-9 levels in iCCA or HCC patients (Fig. 21, Fig. 25 and Fig. 33), EVs can be considered as independent biomarkers, which is a prerequisite for implementing them in an additive model in order to achieve added diagnostic value in a combined analysis. Consequently, as one of the most important results of this thesis, it could be shown that the diagnostic performances of both AFP and CA19-9 were considerably improved by implementing lEVs, leading to a perfect, 100% accurate diagnostic separation of 29 CCA and 34 HCC patients, when combining AFP and $AnnV^+CD44v6^+$ lEVs in a pooled analysis (Tab. 14). Of note, the results obtained in this thesis surpass all the aforementioned studies on other diagnostic measures undertaken for hepatobiliary cancer diagnosis. Since we only had limited information as to AFP and CA19-9 levels in iCCA patients in the lEV study arm, both CCA subtypes were combined in this analysis to achieve diagnostically conclusive

cohort size and to ensure the comparability between the two study arms. However, since a 100% correct distinction of both CCA subtypes combined from HCC was achieved, the correct identification of all iCCA patients is warranted as well. Interestingly, even though combining $CD133^+$ sEV subpopulations with the serum markers AFP and CA19-9 improved the respective diagnostic capacity of the individual serum marker, it did not lead to overall better diagnostic separation of iCCA from HCC than sole assessment of sEV subpopulations (Tab. 18). Based on the results obtained in this thesis, we propose a specific diagnostic profile that could greatly aid in establishing an uncomplicated differential diagnosis of iCCA and HCC in the future and that is solely based on serum biomarkers: High $AnnV^+CD44v6^+$ lEV, low AFP and high CA19-9 levels (above/below the respective cut-offs) are characteristic for CCA patients, whereas, *vice versa*, low $AnnV^+CD44v6^+$ lEV, high AFP and low CA19-9 levels represent HCC patients. According to this profile a perfect differential diagnosis of iCCA and HCC was possible in this thesis (sensitivity, specificity, PPV and NPV all at 100%), which highlights the tremendous potential of this minimal invasive approach for future routine clinical application.

4.4. Conclusion

Within the course of this thesis, EV surface profiling proved to be of considerable value for differential hepatobiliary cancer diagnosis. Large EVs, especially $AnnV^+CD44v6^+$ lEVs, represent diagnostically powerful markers for biliary cancer detection as well as for the clinically enormously challenging differential diagnosis of iCCA from HCC. Most impressively, the combination of $AnnV^+CD44v6^+$ lEVs with the serum tumor marker AFP led to a 100% correct identification of all 63 investigated CCA and HCC patients highlighting the potential clinical relevance of this marker combination. In contrast to lEVs, even though sEV profiling was associated with very good diagnostic capability for iCCA/HCC differentiation, their sole as well as combined assessment with AFP did not reach 100% rendering $AnnV^+CD44v6^+$ lEVs the most relevant and exciting marker identified in this study. Thus, $AnnV^+CD44v6^+$ lEVs (with and without AFP) have an enormous potential and could be of great value to complement current surveillance and diagnosis procedures for hepatobiliary cancers as part of a multiparameter diagnostic approach.

Considering the respective limitations of a) biopsies, which are invasive with associated risks and have a low NPV, b) imaging procedures, which are cost-intensive and in many cases not sufficient to establish a differential diagnosis alone, and c) current tumor biomarkers, which are not specific or sensitive enough to establish a diagnosis, the gap and need for more diagnostic options for differential hepatobiliary cancer detection becomes evident. As a minimal-invasive liquid biopsy, lEV profiling compensates all of these limitations and offers an easily accessible and applicable tool that is low in cost and risk and is at the same time highly sensitive and specific. These advantages highlight the enormous potential and value of lEV profiling to augment informed decision-making during the clinically tremendously challenging management of hepatobiliary cancers, thus maximizing best patient care and overall patient survival.

All in all, the ultimate goal of minimal-invasive cancer diagnosis research is the development of a diagnostic modality that is sufficient for specific differential cancer detection without the need to employ additional invasive procedures. With the results obtained in this thesis, an important step towards minimal-invasive differential hepatobiliary cancer diagnosis has been undertaken to come closer to this vision.

4.5. Perspectives

Large EV profiling showed considerable diagnostic potential for hepatobiliary cancers and the first steps towards a possible clinical implementation seem to be made. To this end, lEVs could be of great aid in decision-making during the diagnostic process in order to avoid invasive biopsies. If a liver malignancy is suspected based on imaging procedures, $AnnV^+CD44v6^+$ lEV as well as AFP levels of the respective patient could be determined. According to the specific patient profiles observed in this study, CCA might be confidentally identified and differentiated by high lEV and low AFP levels without the necessity of performing a subsequent invasive biopsy for definitive diagnosis. This offers the possibility of an uncomplicated, minimal-invasive diagnosis and differentiation of iCCA from HCC. As drawing blood samples is easily applicable, low in risk and a generally well-accepted procedure by patients, the determination of $AnnV^+CD44v6^+$ lEV and AFP levels could furthermore possibly be implemented as part of recurrent surveillance screenings of high risk patients but also in patients who display no indication of disease yet in order

to identify potential changes towards hepatobiliary malignancies as early as possible. However, if the assessment of $AnnV^+CD44v6^+$ lEV levels is feasible for the proposed screening or prognostic purposes in the context of hepatobiliary cancers needs to be elucidated further but based on the results in this thesis and previous studies their potential is evident.

While the differential diagnosis of iCCA from HCC is without question an enormous clinical challenge, there are other differential settings, in which easy minimal-invasive diagnosis would be of great benefit. To this end, identification of CCA development out of a benign PSC background, which is a common predisposing condition for CCA but is hard to distinguish, would be very helpful, so the differential diagnostic capacity of $AnnV^+CD44v6^+$ lEVs in this regard could be analysed in a subsequent study to address this clinical issue. Furthermore, a differential diagnosis of other primary liver tumors and liver metastases based on lEV profiling is of great interest and could be investigated in a subsequent study. In this setting, especially combined HCC CCA should be mentioned, since, even though it represents a rare entity, this cancer shares common histologic and imaging characteristics of both HCC and CCA, complicating its diagnosis. A potential differentiation of combined HCC CCA from HCC and CCA based on lEV profiling would thus be relevant and of great value. Moreover, with the lEV surface marker combinations investigated in this thesis a discrimination between CCA and GbCA as well as between the individual CCA subtypes was not achievable, since all of these entitites were associated with similarly elevated lEV levels. However, incorporating other or additional surface markers could be helpful and might lead to possible EV-based differentiation of these cancers. Last but not least, the potential of sEV profiling has not been explored to the full extent in this thesis yet due to very limited cohort sizes. Nonetheless, their diagnostic capacity and heterogeneous distribution seemed promising, so a subsequent validation of the obtained results as well as exploring the feasibility of sEVs in the aforementioned finer differentiations between more hepatobiliary cancer entities is compelling.

All in all, there remains a lot of work to fully establish EV-based profiling as a conclusive minimal-invasive tool for differential hepatobiliary diagnosis. Nonetheless, with the results obtained in this thesis, a possible translation of lEV profiling into clinical practice might be in reach one day.

5. Abstract

Cancer is a global health problem that will intensify in the upcoming years and decades. Hepatobiliary cancers, comprising hepatocellular carcinoma (HCC), cholangiocarcinoma (CCA) and gallbladder carcinoma (GbCA), are among the most fatal types of cancers, owing to their commonly late-stage discovery and resulting bad prognoses with 5-year survival rates of 5-20%. Patient survival could considerably be improved if hepatobiliary cancers, especially biliary cancers (CCA and GbCA), were discovered and treated at earlier stages. Hepatobiliary cancers are a very heterogeneous group of tumors with considerably diverse treatment regimen. However, especially the distinction of HCC and iCCA remains an extremely difficult challenge that requires an invasive tissue biopsy for definitive diagnosis. Nonetheless, the distinction is crucial for following treatment decisions to ensure best patient care and survival. To date, no reliable serum biomarker exists for completely accurate detection and differentiation of these cancers. Extracellular vesicles (EVs), as a type of liquid biopsy, might offer the opportunity to not only discover hepatobiliary cancers at an earlier stage but also to differentiate between these cancer entities in an uncomplicated and easily applicable manner. EVs are phospholipid bilayer-enclosed vesicles that are released by every cell type including tumor cells. According to their size and mode of biogenesis, they can be classified into endosome-derived small EVs (40-100 nm) and plasma membrane-budding large EVs (100-1000 nm). They reflect the intracellular and surface composition of their parental cells and their potential as biomarkers for diseases has been demonstrated in a wide variety of studies.

Here, the capability of EVs as biomarkers for differential diagnosis of hepatobiliary cancers, especially between HCC and iCCA, is assessed, in order to optimize patient care. In contrast to most biomarker studies on EVs that either focus on only one subtype or on the entirety of all EVs without specifying their molecular characteristics, this study comprehensively evaluates both large and small EVs separately in terms of their differential diagnostic capacity for hepatobiliary cancers.

In this regard, the surface markers EpCAM, CD133, gp38 and CD44v6, that are all associated with carcinogenesis or cancer progression, were observed to be differentially expressed on human HCC and CCA tumor cell lines. Likewise, possible parental cell populations for EVs with combinations of the aforementioned markers on their surface were identified and showed a distinct expression pattern in several mouse organs,

including liver and gallbladder. Large EVs (lEVs) featuring the corresponding surface marker combinations were isolated from peripheral patient blood, including HCC, CCA, GbCA, colorectal carcinoma (CRC), non-small cell lung carcinoma (NSCLC) and cirrhosis patients as well as healthy individuals. Flow cytometric analysis revealed that all investigated lEV populations served as biomarkers for biliary cancer with $AnnV^+CD44v6^+$ lEVs showing the best diagnostic performance (AUC: 0.80, sensitivity: 84.0%, specificity: 63.3%, PPV: 85.1%, NPV: 61.3%) for detecting biliary cancers out of a pool of healthy individuals. Furthermore, $AnnV^+CD44v6^+$ lEVs also displayed the best diagnostic capability for distinguishing between HCC and iCCA patients (AUC: 0.83, sensitivity: 93.3%, specificity: 71.0%, PPV: 60.9%, NPV: 95.7%). Importantly, when combining $AnnV^+CD44v6^+$ lEVs with the serum tumor marker AFP, a perfect separation of HCC and CCA was achieved with sensitivity, specificity, PPV and NPV all reaching 100%. Similarly, evaluation of several small EV (sEV) subtypes, characterized by CD9, CD63 or CD81 expression on their surface, by ExoView® scanning revealed a good diagnostic separation of HCC and iCCA patients with $CD63^+CD133^+$ sEVs showing the best diagnostic capability (AUC: 0.89, sensitivity: 87.5%, specificity: 100%, PPV: 100%, NPV: 88.9%). Even though small EVs achieved a similar diagnostic power for separation of HCC and iCCA than large EVs alone, the addition of APF in a combinational approach did not result in any diagnostically relevant improvement in this case.

All in all, lEV profiling, especially $AnnV^+CD44v6^+$ lEVs, was proven to represent a diagnostically powerful marker for biliary cancers as well as for the clinically challenging differential diagnosis of iCCA and HCC that could be of great aid in complementing currently performed diagnostic procedures. As a minimal-invasive liquid biopsy, lEV profiling offers an easily accessible and applicable tool that is low in cost and risk and at the same time highly sensitive and specific. These advantages highlight the enormous potential of lEV profiling to improve informed decision-making during the challenging management of hepatobiliary cancers, thus maximizing best patient care and overall patient survival.

6. List of Figures

7. List of Tables

8. References

Abbas G, Lindor KD. Cholangiocarcinoma in Primary Sclerosing Cholangitis. J Gastrointest Cancer. 2009;40(1–2):19–25.

Abbate V, Marcantoni M, Giuliante F, Vecchio FM, Gatto I, Mele C, Saviano A, Arciuolo D, Gaetani E, Ferrari MC, Giarretta I, Ardito F, Riccardi L, Nicoletti A, Ponziani FR, Gasbarrini A, Pompili M, Pola R. HepPar1-positive circulating microparticles are increased in subjects with hepatocellular carcinoma and predict early recurrence after liver resection. Int J Mol Sci. 2017;18(5):1–11.

Aden DP, Fogel A, Plotkin S, Damjanov I, Knowles BB. Controlled synthesis of HBsAg in a differentiated human liver carcinoma-derived cell line. Nature. 1979;282(5739):615–6.

Akinyemiju T, Abera S, Ahmed M, Alam N, Alemayohu MA, Allen C, Al-Raddadi R, Alvis-Guzman N, Amoako Y, Artaman A, Ayele TA, Barac A, Bensenor I, Berhane A, Bhutta Z, Castillo-Rivas J, Chitheer A, Choi J-Y, Cowie B, Dandona L, Dandona R, Dey S, Dicker D, Phuc H, Ekwueme DU, Zaki MES, Fischer F, Fürst T, Hancock J, Hay SI, Hotez P, Jee SH, Kasaeian A, Khader Y, Khang Y-H, Kumar A, Kutz M, Larson H, Lopez A, Lunevicius R, Malekzadeh R, McAlinden C, Meier T, Mendoza W, Mokdad A, Moradi-Lakeh M, Nagel G, Nguyen Q, Nguyen G, Ogbo F, Patton G, Pereira DM, Pourmalek F, Qorbani M, Radfar A, Roshandel G, Salomon JA, Sanabria J, Sartorius B, Satpathy M, Sawhney M, Sepanlou S, Shackelford K, Shore H, Sun J, Mengistu DT, Topór-Mądry R, Tran B, Ukwaja KN, Vlassov V, Vollset SE, Vos T, Wakayo T, Weiderpass E, Werdecker A, Yonemoto N, Younis M, Yu C, Zaidi Z, Zhu L, Murray CJL, Naghavi M, Fitzmaurice C. The Burden of Primary Liver Cancer and Underlying Etiologies From 1990 to 2015 at the Global, Regional, and National Level: Results From the Global Burden of Disease Study 2015. JAMA Oncol. 2017;3(12):1683–91.

Akpe V, Kim TH, Brown CL, Cock IE. Circulating tumour cells: a broad perspective. J R Soc Interface. 2020;17(168):20200065.

Alvaro D, Bragazzi MC, Benedetti A, Fabris L, Fava G, Invernizzi P, Marzioni M, Nuzzo G, Strazzabosco M, Stroffolini T, AISF “Cholangiocarcinoma” committee. Cholangiocarcinoma in Italy: A national survey on clinical characteristics, diagnostic modalities and treatment. Results from the “Cholangiocarcinoma” committee of the

Italian Association for the Study of Liver disease. Dig Liver Dis. 2011;43(1):60–5.

Andersen RF, Jakobsen A. Screening for circulating RAS/RAF mutations by multiplex digital PCR. Clin Chim Acta. 2016;458:138–43.

Andrén-Sandberg A. Diagnosis and management of gallbladder polyps. N Am J Med Sci. 2012;4(5):203–11.

Andreu Z, Yáñez-mó M. Tetraspanins in extracellular vesicle formation and function. Front Immunol. 2014;5:1–12.

Arbelaiz A, Azkargorta M, Krawczyk M, Santos-Laso A, Lapitz A, Perugorria MJ, Erice O, Gonzalez E, Jimenez-Agüero R, Lacasta A, Ibarra C, Sanchez-Campos A, Jimeno JP, Lammert F, Milkiewicz P, Marzioni M, Macias RIR, Marin JJG, Patel T, Gores GJ, Martinez I, Elortza F, Falcon-Perez JM, Bujanda L, Banales JM. Serum extracellular vesicles contain protein biomarkers for primary sclerosing cholangitis and cholangiocarcinoma. Hepatology. 2017;66(4):1125–43.

Arraud N, Gounou C, Linares R, Brisson AR. A simple flow cytometry method improves the detection of phosphatidylserine-exposing extracellular vesicles. J Thromb Haemost. 2015;13(2):237–47.

Avadhani V, Hacihasanoglu E, Memis B, Pehlivanoglu B, Hanley KZ, Krishnamurti U, Krasinskas AM, Osunkoya AO, Daniels LM, Freedman AA, Goodman M, Adsay V, Reid MD. Cytologic predictors of malignancy in bile duct brushings: a multi-reviewer analysis of 60 cases. Mod Pathol. 2017;30(9):1273–86.

Awasthi NP, Kumari S, Neyaz A, Gupta S, Agarwal A, Singhal A, Husain N. EpCAM-based Flow Cytometric Detection of Circulating Tumor Cells in Gallbladder Carcinoma Cases. Asian Pac J Cancer Prev. 2017;18(12):3429–37.

Badshah MB, Vanar V, Kandula M, Kalva N, Badshah MB, Revenur V, Bechtold ML, Forcione DG, Donthireddy K, Puli SR. Peroral cholangioscopy with cholangioscopy-directed biopsies in the diagnosis of biliary malignancies: a systemic review and meta-analysis. Eur J Gastroenterol Hepatol. 2019;31(8):935–40.

Bae JS, Noh SJ, Jang KY, Park HS, Chung MJ, Park CK, Moon WS. Expression and role of epithelial cell adhesion molecule in dysplastic nodule and hepatocellular carcinoma. Int J Oncol. 2012;41(6):2150–8.

Baeuerle PA, Gires O. EpCAM (CD326) finding its role in cancer. Br J Cancer. England; 2007;96(3):417–23.

Bailey A, Shah SA. Screening high risk populations for cancer: Hepatobiliary. J Surg Oncol. 2019;120(5):847–50.

Banales JM, Cardinale V, Carpino G, Marzioni M, Andersen JB, Invernizzi P, Lind GE, Folseraas T, Forbes SJ, Fouassier L, Geier A, Calvisi DF, Mertens JC, Trauner M, Benedetti A, Maroni L, Vaquero J, Macias RIR, Raggi C, Perugorria MJ, Gaudio E, Boberg KM, Marin JJG, Alvaro D. Expert consensus document: Cholangiocarcinoma: current knowledge and future perspectives consensus statement from the European Network for the Study of Cholangiocarcinoma (ENS-CCA). Nat Rev Gastroenterol Hepatol. 2016;13(5):261–80.

Banales JM, Iñarrairaegui M, Arbelaiz A, Milkiewicz P, Muntané J, Muñoz-Bellvis L, La Casta A, Gonzalez LM, Arretxe E, Alonso C, Martínez-Arranz I, Lapitz A, Santos-Laso A, Avila MA, Martínez-Chantar ML, Bujanda L, Marin JJG, Sangro B, Macias RIR. Serum Metabolites as Diagnostic Biomarkers for Cholangiocarcinoma, Hepatocellular Carcinoma, and Primary Sclerosing Cholangitis. Hepatology. 2019;70(2):547–62.

Banales JM, Marin JJG, Lamarca A, Rodrigues PM, Khan SA, Roberts LR, Cardinale V, Carpino G, Andersen JB, Braconi C, Calvisi DF, Perugorria MJ, Fabris L, Boulter L, Macias RIR, Gaudio E, Alvaro D, Gradilone SA, Strazzabosco M, Marzioni M, Coulouarn C, Fouassier L, Raggi C, Invernizzi P, Mertens JC, Moncsek A, Rizvi S, Heimbach J, Koerkamp BG, Bruix J, Forner A, Bridgewater J, Valle JW, Gores GJ. Cholangiocarcinoma 2020: the next horizon in mechanisms and management. Nat Rev Gastroenterol Hepatol. Springer US; 2020;17(9):557–88.

Barth K, Bläsche R, Kasper M. T1α/Podoplanin Shows Raft-Associated Distribution in Mouse Lung Alveolar Epithelial E10 Cells. Cell Physiol Biochem. 2010;25(001):103–12.

Barzegar Behrooz A, Syahir A, Ahmad S. CD133: beyond a cancer stem cell biomarker. J Drug Target. 2019;27(3):257–69.

Becker A, Thakur BK, Weiss JM, Kim HS, Peinado H, Lyden D. Extracellular Vesicles in Cancer: Cell-to-Cell Mediators of Metastasis. Cancer Cell. 2016;30(6):836–48.

Bellingham SA, Guo BB, Coleman BM, Hill AF. Exosomes: Vehicles for the Transfer of Toxic Proteins Associated with Neurodegenerative Diseases? Front Physiol. 2012;3.

Belthier G, Homayed Z, Grillet F, Duperray C, Vendrell J, Krol I, Bravo S, Boyer J-C,

Villeronce O, Vitre-Boubaker J, Heaug-Wane D, Macari-Fine F, Smith J, Merlot M, Lossaint G, Mazard T, Portales F, Solassol J, Ychou M, Aceto N, Mamessier E, Bertucci F, Pascussi JM, Samalin E, Hollande F, Pannequin J. CD44v6 Defines a New Population of Circulating Tumor Cells Not Expressing EpCAM. Cancers (Basel). 2021;13(19):4966.

Benson AB, Abrams TA, Ben-Josef E, Bloomston PM, Botha JF, Clary BM, Covey A, Curley SA, D'Angelica MI, Davila R, Ensminger WD, Gibbs JF, Laheru D, Malafa MP, Marrero J, Meranze SG, Mulvihill SJ, Park JO, Posey JA, Sachdev J, Salem R, Sigurdson ER, Sofocleous C, Vauthey J-N, Venook AP, Goff LW, Yen Y, Zhu AX. Hepatobiliary Cancers, NCCN Clinical Practice Guidelines in Oncology. J Natl Compr Cancer Netw. 2009;7(4):350–91.

Benson AB, D'Angelica MI, Abbott DE, Anaya DA, Anders R, Are C, Bachini M, Borad M, Brown D, Burgoyne A, Chahal P, Chang DT, Cloyd J, Covey AM, Glazer ES, Goyal L, Hawkins WG, Iyer R, Jacob R, Kelley RK, Kim R, Levine M, Palta M, Park JO, Raman S, Reddy S, Sahai V, Schefter T, Singh G, Stein S, Vauthey JN, Venook AP, Yopp A, McMillian NR, Hochstetler C, Darlow SD. Hepatobiliary Cancers, Version 2.2021, NCCN Clinical Practice Guidelines in Oncology. JNCCN J Natl Compr Cancer Netw. 2021;19(5):541–65.

Bertuccio P, Malvezzi M, Carioli G, Hashim D, Boffetta P, El-Serag HB, La Vecchia C, Negri E. Global trends in mortality from intrahepatic and extrahepatic cholangiocarcinoma. J Hepatol. 2019;71(1):104–14.

Beuers U, Boberg KM, Chapman RW, Chazouillères O, Invernizzi P, Jones DE, Lammert F, Parès A, Trauner M. EASL Clinical Practice Guidelines: Management of cholestatic liver diseases. J Hepatol. 2009;51(2):237–67.

Bobrie A, Colombo M, Krumeich S, Raposo G, Théry C. Diverse subpopulations of vesicles secreted by different intracellular mechanisms are present in exosome preparations obtained by differential ultracentrifugation. J Extracell Vesicles. 2012;1(1):18397.

Booth AM, Fang Y, Fallon JK, Yang J-M, Hildreth JEK, Gould SJ. Exosomes and HIV Gag bud from endosome-like domains of the T cell plasma membrane. J Cell Biol. 2006;172(6):923–35.

Botha J, Pugsley HR, Handberg A. Conventional, High-Resolution and Imaging Flow

Cytometry: Benchmarking Performance in Characterisation of Extracellular Vesicles. Biomedicines. 2021;9(2):124.

Brar G, Greten TF, Graubard BI, McNeel TS, Petrick JL, McGlynn KA, Altekruse SF. Hepatocellular Carcinoma Survival by Etiology: A SEER-Medicare Database Analysis. Hepatol Commun. 2020;4(10):1541–51.

Breiteneder-Geleff S, Soleiman A, Kowalski H, Horvat R, Amann G, Kriehuber E, Diem K, Weninger W, Tschachler E, Alitalo K, Kerjaschki D. Angiosarcomas Express Mixed Endothelial Phenotypes of Blood and Lymphatic Capillaries. Am J Pathol. 1999;154(2):385–94.

Bridgewater J, Galle PR, Khan SA, Llovet JM, Park JW, Patel T, Pawlik TM, Gores GJ. Guidelines for the diagnosis and management of intrahepatic cholangiocarcinoma. J Hepatol. European Association for the Study of the Liver; 2014;60:1268–89.

Bruix J, Sherman M. Management of hepatocellular carcinoma: An update. Hepatology. 2011;53(3):1020–2.

Cai X, Li J, Yuan X, Xiao J, Dooley S, Wan X, Weng H, Lu L. CD133 expression in cancer cells predicts poor prognosis of non-mucin producing intrahepatic cholangiocarcinoma. J Transl Med. BioMed Central; 2018;16(1):1–7.

Caldwell JC. Toward A Restatement of Demographic Transition Theory. Popul Dev Rev. 1976;2(3/4):321.

Carpino G, Cardinale V, Folseraas T, Overi D, Grzyb K, Costantini D, Berloco PB, Di Matteo S, Karlsen TH, Alvaro D, Gaudio E. Neoplastic Transformation of the Peribiliary Stem Cell Niche in Cholangiocarcinoma Arisen in Primary Sclerosing Cholangitis. Hepatology. 2019;69(2):622–38.

Carpino G, Cardinale V, Gentile R, Onori P, Semeraro R, Franchitto A, Wang Y, Bosco D, Iossa A, Napoletano C, Cantafora A, D'Argenio G, Nuti M, Caporaso N, Berloco P, Venere R, Oikawa T, Reid L, Alvaro D, Gaudio E. Evidence for multipotent endodermal stem/progenitor cell populations in human gallbladder. J Hepatol. 2014;60(6):1194–202.

Carpino G, Cardinale V, Onori P, Franchitto A, Berloco PB, Rossi M, Wang Y, Semeraro R, Anceschi M, Brunelli R, Alvaro D, Reid LM, Gaudio E. Biliary tree stem/progenitor cells in glands of extrahepatic and intraheptic bile ducts: an anatomical in situ study yielding evidence of maturational lineages. J Anat. 2012;220(2):186–99.

Center MM, Jemal A, Lortet-Tieulent J, Ward E, Ferlay J, Brawley O, Bray F. International variation in prostate cancer incidence and mortality rates. Eur Urol. 2012;61(6):1079–92.

Chalmin F, Ladoire S, Mignot G, Vincent J, Bruchard M, Remy-Martin J-P, Boireau W, Rouleau A, Simon B, Lanneau D, De Thonel A, Multhoff G, Hamman A, Martin F, Chauffert B, Solary E, Zitvogel L, Garrido C, Ryffel B, Borg C, Apetoh L, Rébé C, Ghiringhelli F. Membrane-associated Hsp72 from tumor-derived exosomes mediates STAT3-dependent immunosuppressive function of mouse and human myeloid-derived suppressor cells. J Clin Invest. 2010;

Chang M-H, You S-L, Chen C-J, Liu C-J, Lai M-W, Wu T-C, Wu S-F, Lee C-M, Yang S-S, Chu H-C, Wang T-E, Chen B-W, Chuang W-L, Soon M-S, Lin C-Y, Chiou S-T, Kuo H-S, Chen D-S, Taiwan Hepatoma Study Group. Long-term Effects of Hepatitis B Immunization of Infants in Preventing Liver Cancer. Gastroenterology. 2016;151(3):472-480.e1.

Chen K, Li Z, Jiang P, Zhang X, Zhang Y, Jiang Y, He Y, Li X. Co-expression of CD133, CD44v6 and human tissue factor is associated with metastasis and poor prognosis in pancreatic carcinoma. Oncol Rep. 2014;32(2):755–63.

Cheng Y, Luo L, Zhang J, Zhou M, Tang Y, He G, Lu Y, Wang Z, Pan M. Diagnostic Value of Different Phenotype Circulating Tumor Cells in Hepatocellular Carcinoma. J Gastrointest Surg. 2019;23(12):2354–61.

Del Conde I, Shrimpton CN, Thiagarajan P, L??pez J a. Tissue-factor-bearing microvesicles arise from lipid rafts and fuse with activated platelets to initiate coagulation. Blood. 2005;106(5):1604–11.

Correa-Gallego C, Maddalo D, Doussot A, Kemeny N, Kingham TP, Allen PJ, D'Angelica MI, DeMatteo RP, Betel D, Klimstra D, Jarnagin WR, Ventura A. Circulating Plasma Levels of MicroRNA-21 and MicroRNA-221 Are Potential Diagnostic Markers for Primary Intrahepatic Cholangiocarcinoma. Dadras SS, editor. PLoS One. 2016;11(9):e0163699.

Costa-Silva B, Aiello NM, Ocean AJ, Singh S, Zhang H, Thakur BK, Becker A, Hoshino A, Mark MT, Molina H, Xiang J, Zhang T, Theilen TM, García-Santos G, Williams C, Ararso Y, Huang Y, Rodrigues G, Shen TL, Labori KJ, Lothe IMB, Kure EH, Hernandez J, Doussot A, Ebbesen SH, Grandgenett PM, Hollingsworth MA, Jain M,

Mallya K, Batra SK, Jarnagin WR, Schwartz RE, Matei I, Peinado H, Stanger BZ, Bromberg J, Lyden D. Pancreatic cancer exosomes initiate pre-metastatic niche formation in the liver. Nat Cell Biol. 2015;17(6):816–26.

Dasgupta P, Henshaw C, Youlden DR, Clark PJ, Aitken JF, Baade PD. Global Trends in Incidence Rates of Primary Adult Liver Cancers: A Systematic Review and Meta-Analysis. Front Oncol. 2020;10(February):1–17.

Deatherage BL, Cookson BT. Membrane Vesicle Release in Bacteria, Eukaryotes, and Archaea: a Conserved yet Underappreciated Aspect of Microbial Life. Andrews-Polymenis HL, editor. Infect Immun. 2012;80(6):1948–57.

DeSantis CE, Bray F, Ferlay J, Lortet-Tieulent J, Anderson BO, Jemal A. International Variation in Female Breast Cancer Incidence and Mortality Rates. Cancer Epidemiol Biomarkers Prev. 2015;24(10):1495–506.

Dollé L, Best J, Mei J, Al Battah F, Reynaert H, van Grunsven LA, Geerts A. The quest for liver progenitor cells: A practical point of view. J Hepatol. 2010;52(1):117–29.

Donato F, Gelatti U, Tagger A, Favret M, Ribero ML, Callea F, Martelli C, Savio A, Trevisi P, Nardi G. Intrahepatic cholangiocarcinoma and hepatitis C and B virus infection, alcohol intake, and hepatolithiasis: a case-control study in Italy. Cancer causes Control. 2001;12(10):959–64.

Dorrell C, Erker L, Schug J, Kopp JL, Canaday PS, Fox AJ, Smirnova O, Duncan AW, Finegold MJ, Sander M, Kaestner KH, Grompe M. Prospective isolation of a bipotential clonogenic liver progenitor cell in adult mice. Genes Dev. 2011;25(11):1193–203.

Duffy AG, Greten TF. Treating Hepatobiliary Cancer: The Immunologic Approach. Dig Dis. 2017;35(4):390–6.

Van Dyke AL, Shiels MS, Jones GS, Pfeiffer RM, Petrick JL, Beebe-Dimmer JL, Koshiol J. Biliary tract cancer incidence and trends in the United States by demographic group, 1999-2013. Cancer. 2019;125(9):1489–98.

Eckert C, Kim YO, Julich H, Heier E-C, Klein N, Krause E, Tschernig T, Kornek M, Lammert F, Schuppan D, Lukacs-Kornek V. Podoplanin discriminates distinct stromal cell populations and a novel progenitor subset in the liver. Am J Physiol Liver Physiol. 2016;310(1):G1–12.

Estes C, Razavi H, Loomba R, Younossi Z, Sanyal AJ. Modeling the epidemic of

nonalcoholic fatty liver disease demonstrates an exponential increase in burden of disease. Hepatology. 2018;67(1):123–33.

Fekete S, Beck A, Veuthey J-L, Guillarme D. Theory and practice of size exclusion chromatography for the analysis of protein aggregates. J Pharm Biomed Anal. 2014;101:161–73.

Florio AA, Ferlay J, Znaor A, Ruggieri D, Alvarez CS, Laversanne M, Bray F, McGlynn KA, Petrick JL. Global trends in intrahepatic and extrahepatic cholangiocarcinoma incidence from 1993 to 2012. Cancer. 2020;126(11):2666–78.

Forner A, Vidili G, Rengo M, Bujanda L, Ponz-Sarvisé M, Lamarca A. Clinical presentation, diagnosis and staging of cholangiocarcinoma. Liver Int. 2019;39 Suppl 1:98–107.

Forner A, Vilana R, Ayuso C, Bianchi L, Solé M, Ayuso JR, Boix L, Sala M, Varela M, Llovet JM, Brú C, Bruix J. Diagnosis of hepatic nodules 20 mm or smaller in cirrhosis: Prospective validation of the noninvasive diagnostic criteria for hepatocellular carcinoma. Hepatology. 2008;47(1):97–104.

Fujii T, Zen Y, Sato Y, Sasaki M, Enomae M, Minato H, Masuda S, Uehara T, Katsuyama T, Nakanuma Y. Podoplanin is a useful diagnostic marker for epithelioid hemangioendothelioma of the liver. Mod Pathol. 2008;21(2):125–30.

Galle PR, Forner A, Llovet JM, Mazzaferro V, Piscaglia F, Raoul J-L, Schirmacher P, Vilgrain V. EASL Clinical Practice Guidelines: Management of hepatocellular carcinoma. J Hepatol. 2018;69(1):182–236.

Gatti S, Bruno S, Deregibus MC, Sordi A, Cantaluppi V, Tetta C, Camussi G. Microvesicles derived from human adult mesenchymal stem cells protect against ischaemia-reperfusion-induced acute and chronic kidney injury. Nephrol Dial Transplant. 2011;26(5):1474–83.

van Genderen HO, Kenis H, Hofstra L, Narula J, Reutelingsperger CPM. Extracellular annexin A5: Functions of phosphatidylserine-binding and two-dimensional crystallization. Biochim Biophys Acta - Mol Cell Res. 2008;1783(6):953–63.

Giebel B. On the function and heterogeneity of extracellular vesicles. Ann Transl Med. 2017;5(6):5–7.

Gill S, Catchpole R, Forterre P. Extracellular membrane vesicles in the three domains of life and beyond. FEMS Microbiol Rev. 2019;43(3):273–303.

GLOBOCAN 2020. Global Cancer Observatory by the International Agency for Research on Cancer (IARC). 2020.

Glumac PM, LeBeau AM. The role of CD133 in cancer: a concise review. Clin Transl Med. 2018;7(1):1–14.

Goetze TO. Gallbladder carcinoma: Prognostic factors and therapeutic options. World J Gastroenterol. 2015;21(43):12211–7.

Goodman MT, Yamamoto J. Descriptive study of gallbladder, extrahepatic bile duct, and ampullary cancers in the United States, 1997-2002. Cancer Causes Control. 2007;18(4):415–22.

Gores GJ. Early detection and treatment of cholangiocarcinoma. Liver Transplant. 2000;6(6B):s30–4.

Gould SJ, Raposo G. As we wait: coping with an imperfect nomenclature for extracellular vesicles. J Extracell vesicles. 2013;2.

Goyal L, Saha SK, Liu LY, Siravegna G, Leshchiner I, Ahronian LG, Lennerz JK, Vu P, Deshpande V, Kambadakone A, Mussolin B, Reyes S, Henderson L, Sun JE, Van Seventer EE, Gurski JM, Baltschukat S, Schacher-Engstler B, Barys L, Stamm C, Furet P, Ryan DP, Stone JR, Iafrate AJ, Getz G, Porta DG, Tiedt R, Bardelli A, Juric D, Corcoran RB, Bardeesy N, Zhu AX. Polyclonal Secondary FGFR2 Mutations Drive Acquired Resistance to FGFR Inhibition in Patients with FGFR2 Fusion–Positive Cholangiocarcinoma. Cancer Discov. 2017;7(3):252–63.

Gregory JJ, Finlay JL. Alpha-Fetoprotein and Beta-Human Chorionic Gonadotropin: Their Clinical Significance as Tumour Markers. Drugs. 1999;57(4):463–7.

Gu MJ, Jang BI. Clinicopathologic significance of Sox2, CD44 and CD44v6 expression in intrahepatic cholangiocarcinoma. Pathol Oncol Res. 2014;20(3):655–60.

Heijnen HF, Schiel AE, Fijnheer R, Geuze HJ, Sixma JJ. Activated platelets release two types of membrane vesicles: microvesicles by surface shedding and exosomes derived from exocytosis of multivesicular bodies and alpha-granules. Blood. 1999;94(11):3791–9.

Hennedige TP, Neo WT, Venkatesh SK. Imaging of malignancies of the biliary tract- an update. Cancer Imaging. 2014;14:14.

Hirakawa S, Hong Y-K, Harvey N, Schacht V, Matsuda K, Libermann T, Detmar M. Identification of Vascular Lineage-Specific Genes by Transcriptional Profiling of

Isolated Blood Vascular and Lymphatic Endothelial Cells. Am J Pathol. 2003;162(2):575–86.

Hoadley KA, Yau C, Hinoue T, Wolf DM, Lazar AJ, Drill E, Shen R, Taylor AM, Cherniack AD, Thorsson V, Akbani R, Bowlby R, Wong CK, Wiznerowicz M, Sanchez-Vega F, Robertson AG, Schneider BG, Lawrence MS, Noushmehr H, Malta TM, Stuart JM, Benz CC, Laird PW, Caesar-Johnson SJ, Demchok JA, Felau I, Kasapi M, Ferguson ML, Hutter CM, Sofia HJ, Tarnuzzer R, Wang Z, Yang L, Zenklusen JC, Zhang J (Julia), Chudamani S, Liu J, Lolla L, Naresh R, Pihl T, Sun Q, Wan Y, Wu Y, Cho J, DeFreitas T, Frazer S, Gehlenborg N, Getz G, Heiman DI, Kim J, Lawrence MS, Lin P, Meier S, Noble MS, Saksena G, Voet D, Zhang H, Bernard B, Chambwe N, Dhankani V, Knijnenburg T, Kramer R, Leinonen K, Liu Y, Miller M, Reynolds S, Shmulevich I, Thorsson V, Zhang W, Akbani R, Broom BM, Hegde AM, Ju Z, Kanchi RS, Korkut A, Li J, Liang H, Ling S, Liu W, Lu Y, Mills GB, Ng K-S, Rao A, Ryan M, Wang J, Weinstein JN, Zhang J, Abeshouse A, Armenia J, Chakravarty D, Chatila WK, de Bruijn I, Gao J, Gross BE, Heins ZJ, Kundra R, La K, Ladanyi M, *et al.* Cell-of-Origin Patterns Dominate the Molecular Classification of 10,000 Tumors from 33 Types of Cancer. Cell. 2018;173(2):291-304.e6.

Horgan AM, Amir E, Walter T, Knox JJ. Adjuvant therapy in the treatment of biliary tract cancer: a systematic review and meta-analysis. J Clin Oncol. 2012;30(16):1934–40.

Huang B, Wu L, Lu X-Y, Xu F, Liu C-F, Shen W-F, Jia N-Y, Cheng H-Y, Yang Y-F, Shen F. Small Intrahepatic Cholangiocarcinoma and Hepatocellular Carcinoma in Cirrhotic Livers May Share Similar Enhancement Patterns at Multiphase Dynamic MR Imaging. Radiology. 2016;281(1):150–7.

Huang H-L. Proteomic identification of tumor biomarkers associated with primary gallbladder cancer. World J Gastroenterol. 2014;20(18):5511.

Huang L, Chen W, Liang P, Hu W, Zhang K, Shen S, Chen J, Zhang Z, Chen B, Han Y, Meng F, DeMorrow S, Yin X, Lai J, Liang L. Serum CYFRA 21-1 in Biliary Tract Cancers: A Reliable Biomarker for Gallbladder Carcinoma and Intrahepatic Cholangiocarcinoma. Dig Dis Sci. 2015;60(5):1273–83.

Hultcrantz R, Olsson R, Danielsson Å, Järnerot G, Lööf L, Ryden BO, Wahren B, Broomé U. A 3-year prospective study on serum tumor markers used for detecting cholangiocarcinoma in patients with primary sclerosing cholangitis. J Hepatol.

1999;30(4):669–73.

Ikeda C, Haga H, Makino N, Inuzuka T, Kurimoto A, Ueda T, Matsuda A, Kakizaki Y, Ishizawa T, Kobayashi T, Sugahara S, Tsunoda M, Suda K, Ueno Y. Utility of Claudin-3 in extracellular vesicles from human bile as biomarkers of cholangiocarcinoma. Sci Rep. 2021;11(1):1195.

Jain R, Barkauskas CE, Takeda N, Bowie EJ, Aghajanian H, Wang Q, Padmanabhan A, Manderfield LJ, Gupta M, Li D, Li L, Trivedi CM, Hogan BLM, Epstein JA. Plasticity of Hopx+ type I alveolar cells to regenerate type II cells in the lung. Nat Commun. 2015;6(1):6727.

Jiao J, Watt GP, Stevenson HL, Calderone TL, Fisher-Hoch SP, Ye Y, Wu X, Vierling JM, Beretta L. Telomerase reverse transcriptase mutations in plasma DNA in patients with hepatocellular carcinoma or cirrhosis: Prevalence and risk factors. Hepatol Commun. 2018;2(6):718–31.

Jijiwa M, Demir H, Gupta S, Leung C, Joshi K, Orozco N, Huang T, Yildiz VO, Shibahara I, de Jesus JA, Yong WH, Mischel PS, Fernandez S, Kornblum HI, Nakano I. CD44v6 Regulates Growth of Brain Tumor Stem Cells Partially through the AKT-Mediated Pathway. Lesniak MS, editor. PLoS One. 2011;6(9):e24217.

Johnstone RM, Adam M, Hammond JR, Orr L, Turbide C. Vesicle formation during reticulocyte maturation. Association of plasma membrane activities with released vesicles (exosomes). J Biol Chem. 1987;262(19):9412–20.

Joo I, Lee JM, Yoon JH. Imaging Diagnosis of Intrahepatic and Perihilar Cholangiocarcinoma: Recent Advances and Challenges. Radiology. 2018;288(1):7–13.

Julich-Haertel H, Tiwari M, Mehrfeld C, Krause E, Kornek M, Lukacs-Kornek V. Isolation and Enrichment of Liver Progenitor Subsets Identified by a Novel Surface Marker Combination. J Vis Exp. 2017a;(120):e55284–e55284.

Julich-Haertel H, Urban SK, Krawczyk M, Willms A, Jankowski K, Patkowski W, Kruk B, Krasnodebski M, Ligocka J, Schwab R, Richardsen I, Schaaf S, Klein A, Gehlert S, Sänger H, Casper M, Banales JM, Schuppan D, Milkiewicz P, Lammert F, Krawczyk M, Lukacs-Kornek V, Kornek M. Cancer-associated circulating large extracellular vesicles in cholangiocarcinoma and hepatocellular carcinoma. J Hepatol. 2017b;67(2):282–92.

Kalluri R. The biology and function of exosomes in cancer. J Clin Invest. 2016;126(4):1208–15.

Kalluri R, LeBleu VS. The biology, function, and biomedical applications of exosomes. Science (80-). 2020;367(6478).

Kamsa-Ard S, Luvira V, Suwanrungruang K, Kamsa-Ard S, Luvira V, Santong C, Srisuk T, Pugkhem A, Bhudhisawasdi V, Pairojkul C. Cholangiocarcinoma Trends, Incidence, and Relative Survival in Khon Kaen, Thailand From 1989 Through 2013: A Population-Based Cancer Registry Study. J Epidemiol. 2019;29(5):197–204.

Khan SA, Davidson BR, Goldin RD, Heaton N, Karani J, Pereira SP, Rosenberg WMC, Tait P, Taylor-Robinson SD, Thillainayagam A V., Thomas HC, Wasan H. Guidelines for the diagnosis and treatment of cholangiocarcinoma: An update. Gut. 2012;61(12):1657–69.

Khan SA, Tavolari S, Brandi G. Cholangiocarcinoma: Epidemiology and risk factors. Liver Int. 2019;39(February):19–31.

Kim SA, Lee JM, Lee KB, Kim SH, Yoon SH, Han JK, Choi BI. Intrahepatic Mass-forming Cholangiocarcinomas: Enhancement Patterns at Multiphasic CT, with Special Emphasis on Arterial Enhancement Pattern—Correlation with Clinicopathologic Findings. Radiology. 2011;260(1):148–57.

Kishimoto T, Eguchi H, Nagano H, Kobayashi S, Akita H, Hama N, Wada H, Kawamoto K, Tomokuni A, Tomimaru Y, Umeshita K, Doki Y, Mori M. Plasma miR-21 is a novel diagnostic biomarker for biliary tract cancer. Cancer Sci. 2013;104(12):1626–31.

Komuta M, Govaere O, Vandecaveye V, Akiba J, Van Steenbergen W, Verslype C, Laleman W, Pirenne J, Aerts R, Yano H, Nevens F, Topal B, Roskams T. Histological diversity in cholangiocellular carcinoma reflects the different cholangiocyte phenotypes. Hepatology. 2012;55(6):1876–88.

Komuta M, Spee B, Borght S Vander, De Vos R, Verslype C, Aerts R, Yano H, Suzuki T, Matsuda M, Fujii H, Desmet VJ, Kojiro M, Roskams T. Clinicopathological study on cholangiolocellular carcinoma suggesting hepatic progenitor cell origin. Hepatology. 2008;47(5):1544–56.

Konishi S, Yasuchika K, Ishii T, Fukumitsu K, Kamo N, Fujita N, Ikai I, Uemoto S. A transmembrane glycoprotein, gp38, is a novel marker for immature hepatic progenitor cells in fetal mouse livers. *In vitro* Cell Dev Biol Anim. 2011;47(1):45–53.

Kucharzewska P, Christianson HC, Welch JE, Svensson KJ, Fredlund E, Ringner M, Morgelin M, Bourseau-Guilmain E, Bengzon J, Belting M. Exosomes reflect the hypoxic status of glioma cells and mediate hypoxia-dependent activation of vascular cells during tumor development. Proc Natl Acad Sci. 2013;110(18):7312–7.

Kumari S, Tewari S, Husain N, Agarwal A, Pandey A, Singhal A, Lohani M. Quantification of Circulating Free DNA as a Diagnostic Marker in Gall Bladder Cancer. Pathol Oncol Res. 2017;23(1):91–7.

Kuznetsova Y, Neumann A, Brueck SR. Imaging interferometric microscopy–approaching the linear systems limits of optical resolution. Opt Express. 2007;15(11):6651.

Kwo L, Aronson J. The Promise of Liquid Biopsies for Cancer Diagnosis. Evidence-Based Oncol. 2021;27(7):SP261–2.

Labgaa I, Villanueva A, Dormond O, Demartines N, Melloul E. The role of liquid biopsy in hepatocellular carcinoma prognostication. Cancers (Basel). 2021;13(4):1–17.

Lapitz A, Arbelaiz A, Olaizola P, Aranburu A, Bujanda L, Perugorria MJ, Banales JM. Extracellular vesicles in hepatobiliary malignancies. Front Immunol. 2018;9:1–12.

Leelawat K, Thongtawee T, Narong S, Subwongcharoen S, Treepongkaruna S. Strong expression of CD133 is associated with increased cholangiocarcinoma progression. World J Gastroenterol. 2011;17(9):1192.

Letelier P, Riquelme I, Hernández A, Guzmán N, Farías J, Roa J. Circulating MicroRNAs as Biomarkers in Biliary Tract Cancers. Int J Mol Sci. 2016;17(5):791.

Levy MJ, Gleeson FC, Campion MB, Caudill JL, Clain JE, Halling K, Rajan E, Topazian MD, Wang KK, Wiersema MJ, Clayton A. Prospective Cytological Assessment of Gastrointestinal Luminal Fluid Acquired During EUS: A Potential Source of False-Positive FNA and Needle Tract Seeding. Am J Gastroenterol. 2010;105(6):1311–8.

Lin X-J, Chong Y, Guo Z-W, Xie C, Yang X-J, Zhang Q, Li S-P, Xiong Y, Yuan Y, Min J, Jia W-H, Jie Y, Chen M-S, Chen M-X, Fang J-H, Zeng C, Zhang Y, Guo R-P, Wu Y, Lin G, Zheng L, Zhuang S-M. A serum microRNA classifier for early detection of hepatocellular carcinoma: a multicentre, retrospective, longitudinal biomarker identification study with a nested case-control study. Lancet Oncol. 2015;16(7):804–15.

Lindnér P, Rizell M, Hafström L. The impact of changed strategies for patients with cholangiocarcinoma in this millenium. HPB surg. 2015;2015:736049.

Llovet JM, Kelley RK, Villanueva A, Singal AG, Pikarsky E, Roayaie S, Lencioni R, Koike K, Zucman-Rossi J, Finn RS. Hepatocellular carcinoma. Nat Rev Dis Prim. Springer US; 2021;7(1).

Lu W-Y, Bird TG, Boulter L, Tsuchiya A, Cole AM, Hay T, Guest R V., Wojtacha D, Man TY, Mackinnon A, Ridgway RA, Kendall T, Williams MJ, Jamieson T, Raven A, Hay DC, Iredale JP, Clarke AR, Sansom OJ, Forbes SJ. Hepatic progenitor cells of biliary origin with liver repopulation capacity. Nat Cell Biol. 2015;17(8):971–83.

Ludwig A-K, Giebel B. Exosomes: Small vesicles participating in intercellular communication. Int J Biochem Cell Biol. 2012;44(1):11–5.

Luga V, Zhang L, Viloria-Petit AM, Ogunjimi AA, Inanlou MR, Chiu E, Buchanan M, Hosein AN, Basik M, Wrana JL. Exosomes Mediate Stromal Mobilization of Autocrine Wnt-PCP Signaling in Breast Cancer Cell Migration. Cell. 2012;151(7):1542–56.

Lukacs-Kornek V, Julich-Haertel H, Urban SK, Kornek M. Multi-Surface Antigen Staining of Larger Extracellular Vesicles. In: Hill AF, editor. Methods Mol Biol Exosomes Microvesicles. Humana Press; 2017. p. 201–8.

Lytle NK, Barber AG, Reya T. Stem cell fate in cancer growth, progression and therapy resistance. Nat Rev Cancer. 2018;18(11):669–80.

Ma L, Dong L, Chang P. CD44v6 engages in colorectal cancer progression. Cell Death Dis. 2019;10(1):30.

Mack M, Kleinschmidt A, Brühl H, Klier C, Nelson PJ, Cihak J, Plachý J, Stangassinger M, Erfle V, Schlöndorff D. Transfer of the chemokine receptor CCR5 between cells by membrane-derived microparticles: A mechanism for cellular human immunodeficiency virus 1 infection. Nat Med. 2000;6(7):769–75.

Marrero JA, Kulik LM, Sirlin CB, Zhu AX, Finn RS, Abecassis MM, Roberts LR, Heimbach JK. Diagnosis, Staging, and Management of Hepatocellular Carcinoma: 2018 Practice Guidance by the American Association for the Study of Liver Diseases. Hepatology. 2018;68(2):723–50.

Mathieu M, Martin-Jaular L, Lavieu G, Théry C. Specificities of secretion and uptake of exosomes and other extracellular vesicles for cell-to-cell communication. Nat Cell Biol. Springer US; 2019;21(1):9–17.

McDougall SR, Anderson ARA, Chaplain MAJ. Mathematical modelling of dynamic adaptive tumour-induced angiogenesis: clinical implications and therapeutic

targeting strategies. J Theor Biol. England; 2006;241(3):564–89.

McGlynn KA, Petrick JL, London WT. Global epidemiology of hepatocellular carcinoma: an emphasis on demographic and regional variability. Clin Liver Dis. 2015;19(2):223–38.

Melo S a., Luecke LB, Kahlert C, Fernandez AF, Gammon ST, Kaye J, Lebleu VS, Mittendorf E a., Weitz J, Rahbari N, Reissfelder C, Pilarsky C, Fraga MF, Piwnica-Worms D, Kalluri R. Glypican-1 identifies cancer exosomes and detects early pancreatic cancer. Nature. 2015;523(7559):177–82.

Micames C, Jowell PS, White R, Paulson E, Nelson R, Morse M, Hurwitz H, Pappas T, Tyler D, McGrath K. Lower frequency of peritoneal carcinomatosis in patients with pancreatic cancer diagnosed by EUS-guided FNA vs. percutaneous FNA. Gastrointest Endosc. 2003;58(5):690–5.

Mima K, Okabe H, Ishimoto T, Hayashi H, Nakagawa S, Kuroki H, Miyake K, Takamori H, Beppu T, Baba H. The expression levels of CD44v6 are correlated with the invasiveness of hepatocellular carcinoma *in vitro*, but do not appear to be clinically significant. Oncol Lett. 2012;3(5):1047–51.

Minaga K, Takenaka M, Katanuma A, Kitano M, Yamashita Y, Kamata K, Yamao K, Watanabe T, Maguchi H, Kudo M. Needle Tract Seeding: An Overlooked Rare Complication of Endoscopic Ultrasound-Guided Fine-Needle Aspiration. Oncology. 2017;93(Suppl. 1):107–12.

Munz M, Baeuerle P a., Gires O. The emerging role of EpCAM in cancer and stem cell signaling. Cancer Res. 2009;69(14):5627–9.

Nakabayashi H, Taketa K, Miyano K, Yamane T, Sato J. Growth of human hepatoma cells lines with differentiated functions in chemically defined medium. Cancer Res. 1982;42(9):3858–63.

Navaneethan U, Njei B, Lourdusamy V, Konjeti R, Vargo JJ, Parsi MA. Comparative effectiveness of biliary brush cytology and intraductal biopsy for detection of malignant biliary strictures: a systematic review and meta-analysis. Gastrointest Endosc. 2015;81(1):168–76.

Ney A, Garcia-Sampedro A, Goodchild G, Acedo P, Fusai G, Pereira SP. Biliary Strictures and Cholangiocarcinoma – Untangling a Diagnostic Conundrum. Front Oncol. 2021;11(September):1–19.

Ng VY, Ang SN, Chan JX, Choo ABH. Characterization of Epithelial Cell Adhesion Molecule as a Surface Marker on Undifferentiated Human Embryonic Stem Cells. Stem Cells. 2010;28(1):29–35.

Van Niel G, D'Angelo G, Raposo G. Shedding light on the cell biology of extracellular vesicles. Nat Rev Mol Cell Biol. Nature Publishing Group; 2018;19(4):213–28.

Omran AR. The Epidemiologic Transition: A Theory of the Epidemiology of Population Change. Milbank Mem Fund Q. 1971;49(4):509.

Padthaisong S, Thanee M, Namwat N, Phetcharaburanin J, Klanrit P, Khuntikeo N, Titapun A, Sungkhamanon S, Saya H, Loilome W. Overexpression of a panel of cancer stem cell markers enhances the predictive capability of the progression and recurrence in the early stage cholangiocarcinoma. J Transl Med. 2020;18(1):64.

Pan American Health Organization. Noncommunicable Diseases. 2021.

Parikh AR, Leshchiner I, Elagina L, Goyal L, Levovitz C, Siravegna G, Livitz D, Rhrissorrakrai K, Martin EE, Van Seventer EE, Hanna M, Slowik K, Utro F, Pinto CJ, Wong A, Danysh BP, de la Cruz FF, Fetter IJ, Nadres B, Shahzade HA, Allen JN, Blaszkowsky LS, Clark JW, Giantonio B, Murphy JE, Nipp RD, Roeland E, Ryan DP, Weekes CD, Kwak EL, Faris JE, Wo JY, Aguet F, Dey-Guha I, Hazar-Rethinam M, Dias-Santagata D, Ting DT, Zhu AX, Hong TS, Golub TR, Iafrate AJ, Adalsteinsson VA, Bardelli A, Parida L, Juric D, Getz G, Corcoran RB. Liquid versus tissue biopsy for detecting acquired resistance and tumor heterogeneity in gastrointestinal cancers. Nat Med. 2019;25(9):1415–21.

Patel AH, Harnois DM, Klee GG, LaRusso NF, Gores GJ. The utility of CA 19-9 in the diagnoses of cholangiocarcinoma in patients without primary sclerosing cholangitis. Am J Gastroenterol. 2000;95(1):204–7.

Petrick JL, McGlynn KA. The Changing Epidemiology of Primary Liver Cancer. Curr Epidemiol Reports. 2019;6(2):104–11.

van der Pol CB, Lim CS, Sirlin CB, McGrath TA, Salameh J-P, Bashir MR, Tang A, Singal AG, Costa AF, Fowler K, McInnes MDF. Accuracy of the Liver Imaging Reporting and Data System in Computed Tomography and Magnetic Resonance Image Analysis of Hepatocellular Carcinoma or Overall Malignancy-A Systematic Review. Gastroenterology. 2019;156(4):976–86.

Prince S, Zeidman A, Dekel Y, Ram E, Koren R. Expression of Epithelial Cell Adhesion

Molecule in Gallbladder Carcinoma and Its Correlation With Clinicopathologic Variables. Am J Clin Pathol. 2008;129(3):424–9.

Raposo G, Stoorvogel W. Extracellular vesicles: Exosomes, microvesicles, and friends. J Cell Biol. 2013;200(4):373–83.

Ratajczak J, Miekus K, Kucia M, Zhang J, Reca R, Dvorak P, Ratajczak MZ. Embryonic stem cell-derived microvesicles reprogram hematopoietic progenitors: evidence for horizontal transfer of mRNA and protein delivery. Leukemia. 2006;20(5):847–56.

Raven A, Lu W-Y, Man TY, Ferreira-Gonzalez S, O'Duibhir E, Dwyer BJ, Thomson JP, Meehan RR, Bogorad R, Koteliansky V, Kotelevtsev Y, Ffrench-Constant C, Boulter L, Forbes SJ. Corrigendum: Cholangiocytes act as facultative liver stem cells during impaired hepatocyte regeneration. Nature. 2018;555(7696):402–402.

Reátegui E, van der Vos KE, Lai CP, Zeinali M, Atai NA, Aldikacti B, Floyd FP, H. Khankhel A, Thapar V, Hochberg FH, Sequist L V., Nahed B V., S. Carter B, Toner M, Balaj L, T. Ting D, Breakefield XO, Stott SL. Engineered nanointerfaces for microfluidic isolation and molecular profiling of tumor-specific extracellular vesicles. Nat Commun. 2018;9(1):175.

Ren F, Sheng W-Q, Du X. CD133: A cancer stem cells marker, is used in colorectal cancers. World J Gastroenterol. 2013;19(17):2603.

Rizvi S, Khan SA, Hallemeier CL, Kelley RK, Gores GJ. Cholangiocarcinoma - evolving concepts and therapeutic strategies. Nat Rev Clin Oncol. 2018;15(2):95–111.

Rompianesi G, Di Martino M, Gordon-Weeks A, Montalti R, Troisi R. Liquid biopsy in cholangiocarcinoma: Current status and future perspectives. World J Gastrointest Oncol. 2021;13(5):332–50.

Rountree CB, Barsky L, Ge S, Zhu J, Senadheera S, Crooks GM. A CD133-Expressing Murine Liver Oval Cell Population with Bilineage Potential. Stem Cells. 2007;25(10):2419–29.

Sachan A, Saluja SS, Nekarakanti PK, Nimisha, Mahajan B, Nag HH, Mishra PK. Raised CA19–9 and CEA have prognostic relevance in gallbladder carcinoma. BMC Cancer. 2020;20(1):826.

Sadeghi A, Mohamadnejad M, Islami F, Keshtkar A, Biglari M, Malekzadeh R, Eloubeidi MA. Diagnostic yield of EUS-guided FNA for malignant biliary stricture: a systematic review and meta-analysis. Gastrointest Endosc. 2016;83(2):290-298.e1.

Safarikia S, Carpino G, Overi D, Cardinale V, Venere R, Franchitto A, Onori P, Alvaro D, Gaudio E. Distinct EpCAM-Positive Stem Cell Niches Are Engaged in Chronic and Neoplastic Liver Diseases. Front Med. 2020;7(September):1–12.

Saijyo S, Kudo T, Suzuki M, Katayose Y, Shinoda M, Muto T, Fukuhara K, Suzuki T, Matsuno S. Establishment of a new extrahepatic bile duct carcinoma cell line, TFK-1. Tohoku J Exp Med. 1995;177(1):61–71.

Sapisochin G, Facciuto M, Rubbia-Brandt L, Marti J, Mehta N, Yao FY, Vibert E, Cherqui D, Grant DR, Hernandez-Alejandro R, Dale CH, Cucchetti A, Pinna A, Hwang S, Lee SG, Agopian VG, Busuttil RW, Rizvi S, Heimbach JK, Montenovo M, Reyes J, Cesaretti M, Soubrane O, Reichman T, Seal J, Kim PTW, Klintmalm G, Sposito C, Mazzaferro V, Dutkowski P, Clavien PA, Toso C, Majno P, Kneteman N, Saunders C, Bruix J, iCCA International Consortium. Liver transplantation for “very early” intrahepatic cholangiocarcinoma: International retrospective study supporting a prospective assessment. Hepatology. 2016;64(4):1178–88.

Scherdin U, Garbrecht M, Klouche M. *In vitro* interaction of á-difluoromethylornithine (DFMO) and human recombinant interferon-a (rIFN-a) on human cancer cell lines. Immunobiology. 1987;175:1–143.

Schnell U, Cirulli V, Giepmans BNG. EpCAM: Structure and function in health and disease. Biochim Biophys Acta - Biomembr. 2013;1828(8):1989–2001.

Severino V, Dumonceau J-M, Delhaye M, Moll S, Annessi-Ramseyer I, Robin X, Frossard J-L, Farina A. Extracellular Vesicles in Bile as Markers of Malignant Biliary Stenoses. Gastroenterology. 2017;153(2):495-504.e8.

Shaib YH, El-Serag HB, Davila JA, Morgan R, McGlynn KA. Risk factors of intrahepatic cholangiocarcinoma in the United States: a case-control study. Gastroenterology. 2005;128(3):620–6.

Shi C-J, Gao J, Wang M, Wang X, Tian R, Zhu F, Shen M, Qin RY. Cd133+ gallbladder carcinoma cells exhibit self-renewal ability and tumorigenicity. World J Gastroenterol. 2011;17(24):2965–71.

Shi C, Tian R, Wang M, Wang X, Jiang J, Zhang Z, Li X, He Z, Gong W, Qin R. CD44+ CD133+ population exhibits cancer stem cell-like characteristics in human gallbladder carcinoma. Cancer Biol Ther. 2010;10(11):1182–90.

Shigehara K, Yokomuro S, Ishibashi O, Mizuguchi Y, Arima Y, Kawahigashi Y, Kanda T,

Akagi I, Tajiri T, Yoshida H, Takizawa T, Uchida E. Real-Time PCR-Based Analysis of the Human Bile MicroRNAome Identifies miR-9 as a Potential Diagnostic Biomarker for Biliary Tract Cancer. Gaetano C, editor. PLoS One. 2011;6(8):e23584.

Shin S, Walton G, Aoki R, Brondell K, Schug J, Fox A, Smirnova O, Dorrell C, Erker L, Chu AS, Wells RG, Grompe M, Greenbaum LE, Kaestner KH. Foxl1-Cre-marked adult hepatic progenitors have clonogenic and bilineage differentiation potential. Genes Dev. 2011;25(11):1185–92.

Shroff RT, Kennedy EB, Bachini M, Bekaii-Saab T, Crane C, Edeline J, El-Khoueiry A, Feng M, Katz MHG, Primrose J, Soares HP, Valle J, Maithel SK. Adjuvant Therapy for Resected Biliary Tract Cancer: ASCO Clinical Practice Guideline. J Clin Oncol. 2019;37(12):1015–27.

Sia D, Villanueva A, Friedman SL, Llovet JM. Liver Cancer Cell of Origin, Molecular Class, and Effects on Patient Prognosis. Gastroenterology. 2017;152(4):745–61.

Siegel R, Desantis C, Jemal A. Colorectal cancer statistics, 2014. CA Cancer J Clin. 2014;64(2):104–17.

Siegel RL, Miller KD, Jemal A. Cancer Statistics , 2017. CA Cancer J Clin. 2017;67(1):7–30.

Silva MA, Hegab B, Hyde C, Guo B, Buckels JAC, Mirza DF. Needle track seeding following biopsy of liver lesions in the diagnosis of hepatocellular cancer: a systematic review and meta-analysis. Gut. 2008;57(11):1592–6.

Singal AG, Lampertico P, Nahon P. Epidemiology and surveillance for hepatocellular carcinoma: New trends. J Hepatol. European Association for the Study of the Liver; 2020;72(2):250–61.

Sirica AE, Gores GJ, Groopman JD, Selaru FM, Strazzabosco M, Wei Wang X, Zhu AX. Intrahepatic Cholangiocarcinoma: Continuing Challenges and Translational Advances. Hepatology. 2019;69(4):1803–15.

Skog J, Würdinger T, van Rijn S, Meijer DH, Gainche L, Curry WT, Carter BS, Krichevsky AM, Breakefield XO. Glioblastoma microvesicles transport RNA and proteins that promote tumour growth and provide diagnostic biomarkers. Nat Cell Biol. 2008;10(12):1470–6.

Song W, Li H, Tao K, Li R, Song Z, Zhao Q, Zhang F, Dou K. Expression and clinical significance of the stem cell marker CD133 in hepatocellular carcinoma. Int J Clin

Pract. 2008;62(8):1212–8.

Spizzo G, Fong D, Wurm M, Ensinger C, Obrist P, Hofer C, Mazzoleni G, Gastl G, Went P. EpCAM expression in primary tumour tissues and metastases: an immunohistochemical analysis. J Clin Pathol. 2011;64(5):415–20.

Stewart B, Wild C. World Cancer Report 2014, WHO. Lyon: International Agency for Research on Cancer; 2014.

Strijker M, Belkouz A, van der Geest LG, van Gulik TM, van Hooft JE, de Meijer VE, Haj Mohammad N, de Reuver PR, Verheij J, de Vos-Geelen J, Wilmink JW, Groot Koerkamp B, Klümpen H-J, Besselink MG, Dutch Pancreatic Cancer Group. Treatment and survival of resected and unresected distal cholangiocarcinoma: a nationwide study. Acta Oncol. 2019;58(7):1048–55.

Sulpice L, Rayar M, Turlin B, Boucher E, Bellaud P, Desille M, Meunier B, Clément B, Boudjema K, Coulouarn C. Epithelial cell adhesion molecule is a prognosis marker for intrahepatic cholangiocarcinoma. J Surg Res. 2014;192(1):117–23.

Sung JJ, Noh SJ, Bae JS, Park HS, Jang KY, Chung MJ, Moon WS. Immunohistochemical Expression and Clinical Significance of Suggested Stem Cell Markers in Hepatocellular Carcinoma. J Pathol Transl Med. 2016;50(1):52–7.

Tan Y, Ma S-Y, Wang F-Q, Meng H-P, Mei C, Liu A, Wu H-R. Proteomic-based analysis for identification of potential serum biomarkers in gallbladder cancer. Oncol Rep. 2011;26(4):853–9.

Tanimizu N, Nishikawa M, Saito H, Tsujimura T, Miyajima A. Isolation of hepatoblasts based on the expression of Dlk/Pref-1. J Cell Sci. 2003;116(Pt 9):1775–86.

Tanos R, Thierry AR. Clinical relevance of liquid biopsy for cancer screening. Transl Cancer Res. 2018;7(S2):S105–29.

Tao LY, Cai L, He XD, Liu W, Qu Q. Comparison of serum tumor markers for intrahepatic cholangiocarcinoma and hepatocellular carcinoma. Am Surg. 2010;76(11):1210–3.

Théry C, Witwer KW, Aikawa E, Alcaraz MJ, Anderson JD, Andriantsitohaina R, Antoniou A, Arab T, Archer F, Atkin-Smith GK, Ayre DC, Bach JM, Bachurski D, Baharvand H, Balaj L, Baldacchino S, Bauer NN, Baxter AA, Bebawy M, Beckham C, Bedina Zavec A, Benmoussa A, Berardi AC, Bergese P, Bielska E, Blenkiron C, Bobis-Wozowicz S, Boilard E, Boireau W, Bongiovanni A, Borràs FE, Bosch S, Boulanger CM, Breakefield X, Breglio AM, Brennan M, Brigstock DR, Brisson A, Broekman MLD,

Bromberg JF, Bryl-Górecka P, Buch S, Buck AH, Burger D, Busatto S, Buschmann D, Bussolati B, Buzás EI, Byrd JB, Camussi G, Carter DRF, Caruso S, Chamley LW, Chang YT, Chaudhuri AD, Chen C, Chen S, Cheng L, Chin AR, Clayton A, Clerici SP, Cocks A, Cocucci E, Coffey RJ, Cordeiro-da-Silva A, Couch Y, Coumans FAW, Coyle B, Crescitelli R, Criado MF, D'Souza-Schorey C, Das S, de Candia P, De Santana EF, De Wever O, del Portillo HA, Demaret T, Deville S, Devitt A, Dhondt B, Di Vizio D, Dieterich LC, Dolo V, Dominguez Rubio AP, Dominici M, Dourado MR, Driedonks TAP, Duarte F V., Duncan HM, Eichenberger RM, Ekström K, EL Andaloussi S, Elie-Caille C, Erdbrügger U, Falcón-Pérez JM, Fatima F, Fish JE, Flores-Bellver M, *et al.* Minimal information for studies of extracellular vesicles 2018 (MISEV2018): a position statement of the International Society for Extracellular Vesicles and update of the MISEV2014 guidelines. J Extracell Vesicles. 2018;7(1).

Todaro M, Gaggianesi M, Catalano V, Benfante A, Iovino F, Biffoni M, Apuzzo T, Sperduti I, Volpe S, Cocorullo G, Gulotta G, Dieli F, De Maria R, Stassi G. CD44v6 is a marker of constitutive and reprogrammed cancer stem cells driving colon cancer metastasis. Cell Stem Cell. Elsevier Inc.; 2014;14(3):342–56.

Tong T, Tian L, Deng M-Z, Chen X-J, Fu T, Ma K-J, Xu J-H, Wang X-Y. The efficacy and safety of endoscopic ultrasound-guided fine-needle biopsy in gallbladder masses. Hepatobiliary Pancreat Dis Int. 2022;In Press.

Torre L, Siegel R, Islami F, Bray F, Jemal A. Worldwide Burden of and Trends in Mortality From Gallbladder and Other Biliary Tract Cancers. Clin Gastroenterol Hepatol. 2018;16(3):427–37.

Trevisani F, D'Intino PE, Morselli-Labate AM, Mazzella G, Accogli E, Caraceni P, Domenicali M, De Notariis S, Roda E, Bernardi M. Serum α-fetoprotein for diagnosis of hepatocellular carcinoma in patients with chronic liver disease: influence of HBsAg and anti-HCV status. J Hepatol. 2001;34(4):570–5.

Trinchet J-C, Bourcier V, Chaffaut C, Ait Ahmed M, Allam S, Marcellin P, Guyader D, Pol S, Larrey D, De Lédinghen V, Ouzan D, Zoulim F, Roulot D, Tran A, Bronowicki J-P, Zarski J-P, Goria O, Calès P, Péron J-M, Alric L, Bourlière M, Mathurin P, Blanc J-F, Abergel A, Serfaty L, Mallat A, Grangé J-D, Buffet C, Bacq Y, Wartelle C, Dao T, Benhamou Y, Pilette C, Silvain C, Christidis C, Capron D, Thiefin G, Hillaire S, Di Martino V, Nahon P, Chevret S, ANRS CO12 CirVir Group. Complications and

competing risks of death in compensated viral cirrhosis (ANRS CO12 CirVir prospective cohort). Hepatology. 2015;62(3):737–50.

Tsukuma H, Hiyama T, Tanaka S, Nakao M, Yabuuchi T, Kitamura T, Nakanishi K, Fujimoto I, Inoue A, Yamazaki H, Kawashima T. Risk Factors for Hepatocellular Carcinoma among Patients with Chronic Liver Disease. N Engl J Med. 1993;328(25):1797–801.

Turpati MV, Duvvur NR, Ramchandani M, Ketavarapu V, Mitnala S. 51P Role of biliary extracellular vesicles in diagnosing various pancreatobiliary malignancies. Ann Oncol. 2020;31:S260.

Tyson GL, El-Serag HB. Risk factors for cholangiocarcinoma. Hepatology. 2011;54(1):173–84.

Urban SK, Krawczyk M, Willms A, Sänger H, Lammert F, Banales JM, Milkiewicz P, Lukacs-Kornek V, Kornek M. Reply to: “Diagnostic and prognostic role of circulating microparticles in hepatocellular carcinoma.” J Hepatol. 2018;68(1):203–4.

Urban SK, Sänger H, Krawczyk M, Julich-Haertel H, Willms A, Ligocka J, Azkargorta M, Mocan T, Kahlert C, Kruk B, Jankowski K, Patkowski W, Krawczyk M, Zieniewicz K, Hołówko W, Krupa Ł, Rzucidło M, Gutkowski K, Wystrychowski W, Król R, Raszeja-Wyszomirska J, Słomka A, Schwab R, Wöhler A, Gonzalez-Carmona MA, Gehlert S, Sparchez Z, Banales JM, Strassburg CP, Lammert F, Milkiewicz P, Kornek M. Synergistic effects of extracellular vesicle phenotyping and AFP in hepatobiliary cancer differentiation. Liver Int. 2020;40(12):3103–16.

Al Ustwani O, Iancu D, Yacoub R, Iyer R. Detection of circulating tumor cells in cancers of biliary origin. J Gastrointest Oncol. 2012;3(2):97–104.

Valle J, Wasan H, Palmer DH, Cunningham D, Anthoney A, Maraveyas A, Madhusudan S, Iveson T, Hughes S, Pereira SP, Roughton M, Bridgewater J. Cisplatin plus Gemcitabine versus Gemcitabine for Biliary Tract Cancer. N Engl J Med. 2010;362(14):1273–81.

Valle JW, Borbath I, Khan SA, Huguet F, Gruenberger T, Arnold D, On behalf of the ESMO Guidelines Committee. Biliary cancer: ESMO clinical practice guidelines for diagnosis, treatment and follow-up. Ann Oncol. 2016;27(May):v28–37.

Vijayakumar A, Vijayakumar A, Patil V, Mallikarjuna MN, Shivaswamy BS. Early Diagnosis of Gallbladder Carcinoma: An Algorithm Approach. ISRN Radiol. 2013;2013:1–6.

Vilgrain V. Staging cholangiocarcinoma by imaging studies. HPB. 2008;10(2):106–9.

Villanueva A. Hepatocellular Carcinoma. N Engl J Med. 2019;380(15):1450–62.

Visvader JE. Cells of origin in cancer. Nature. 2011;469(7330):314–22.

Wang J, Dong M, Xu Z, Song X, Zhang S, Qiao Y, Che L, Gordan J, Hu K, Liu Y, Calvisi DF, Chen X. Notch2 controls hepatocyte-derived cholangiocarcinoma formation in mice. Oncogene. 2018a;37(24):3229–42.

Wang W, Li H, Zhou Y, Jie S. Peripheral blood microvesicles are potential biomarkers for hepatocellular carcinoma. Cancer Biomarkers. 2013;13(5):351–7.

Wang Z, Zhao K, Hackert T, Zöller M. CD44/CD44v6 a Reliable Companion in Cancer-Initiating Cell Maintenance and Tumor Progression. Front Cell Dev Biol. 2018b;6.

Webber J, Steadman R, Mason MD, Tabi Z, Clayton A. Cancer Exosomes Trigger Fibroblast to Myofibroblast Differentiation. Cancer Res. 2010;70(23):9621–30.

Wei M, Lü L, Lin P, Chen Z, Quan Z, Tang Z. Multiple cellular origins and molecular evolution of intrahepatic cholangiocarcinoma. Cancer Lett. 2016;379(2):253–61.

Wild C, Weiderpass E, Stewart B. World Cancer Report 2020, WHO. Lyon: International Agency for Research on Cancer; 2020.

Willms E, Cabañas C, Mäger I, Wood MJA, Vader P. Extracellular vesicle heterogeneity: Subpopulations, isolation techniques, and diverse functions in cancer progression. Front Immunol. 2018;9(APR).

www.nanoviewbio.com. Official NanoView Biosciences web page.

Yamashita T, Ji J, Budhu A, Forgues M, Yang W, Wang H, Jia H, Ye Q, Qin L, Wauthier E, Reid LM, Minato H, Honda M, Kaneko S, Tang Z, Wang XW. EpCAM-Positive Hepatocellular Carcinoma Cells Are Tumor-Initiating Cells With Stem/Progenitor Cell Features. Gastroenterology. 2009;136(3):1012–24.

Yanagisawa N, Mikami T, Mitomi H, Saegusa M, Koike M, Okayasu I. CD44 variant overexpression in gallbladder carcinoma associated with tumor dedifferentiation. Cancer. 2001;91(2):408–16.

Yane K, Kuwatani M, Yoshida M, Goto T, Matsumoto R, Ihara H, Okuda T, Taya Y, Ehira N, Kudo T, Adachi T, Eto K, Onodera M, Sano I, Nojima M, Katanuma A. Non-negligible rate of needle tract seeding after endoscopic ultrasound-guided fine-needle aspiration for patients undergoing distal pancreatectomy for pancreatic cancer. Dig Endosc. 2020;32(5):801–11.

Yáñez-Mó M, Siljander PR-M, Andreu Z, Bedina Zavec A, Borràs FE, Buzas EI, Buzas K, Casal E, Cappello F, Carvalho J, Colás E, Cordeiro-da Silva A, Fais S, Falcon-Perez JM, Ghobrial IM, Giebel B, Gimona M, Graner M, Gursel I, Gursel M, Heegaard NHH, Hendrix A, Kierulf P, Kokubun K, Kosanovic M, Kralj-Iglic V, Krämer-Albers E-M, Laitinen S, Lässer C, Lener T, Ligeti E, Linē A, Lipps G, Llorente A, Lötvall J, Manček-Keber M, Marcilla A, Mittelbrunn M, Nazarenko I, Nolte-'t Hoen ENM, Nyman TA, O'Driscoll L, Olivan M, Oliveira C, Pállinger É, del Portillo HA, Reventós J, Rigau M, Rohde E, Sammar M, Sánchez-Madrid F, Santarém N, Schallmoser K, Stampe Ostenfeld M, Stoorvogel W, Stukelj R, Van der Grein SG, Helena Vasconcelos M, Wauben MHM, De Wever O. Biological properties of extracellular vesicles and their physiological functions. J Extracell Vesicles. 2015;4(1):27066.

Yang JD, Campion MB, Liu MC, Chaiteerakij R, Giama NH, Ahmed Mohammed H, Zhang X, Hu C, Campion VL, Jen J, Venkatesh SK, Halling KC, Kipp BR, Roberts LR. Circulating tumor cells are associated with poor overall survival in patients with cholangiocarcinoma. Hepatology. 2016;63(1):148–58.

Yun KJ, Yoon KH, Han WC. Immunohistochemical Study for CD44v6 in Hepatocellular Carcinoma and Cholangiocarcinoma. Cancer Res Treat. 2002;34(3):170–4.

Zach S, Grün J, Bauer AT, Pilarsky C, Grützmann R, Weng H, Dooley S, Wilhelm TJ, Gaiser T, Rückert F. CCC-5, a new primary cholangiocellular cell line. Int J Clin Exp Pathol. 2017;10(2):2451–60.

Zheng Y-W, Tsuchida T, Shimao T, Li B, Takebe T, Zhang R-R, Sakurai Y, Ueno Y, Sekine K, Ishibashi N, Imajima M, Tanaka T, Taniguchi H. The CD133+ CD44+ Precancerous Subpopulation of Oval Cells Is a Therapeutic Target for Hepatocellular Carcinoma. Stem Cells Dev. 2014;23(18):2237–49.

Zhou Y-M, Yin Z-F, Yang J-M, Li B, Shao W-Y, Xu F, Wang Y-L, Li D-Q. Risk factors for intrahepatic cholangiocarcinoma: a case-control study in China. World J Gastroenterol. 2008;14(4):632–5.

Zhu Z, Hao X, Yan M, Yao M, Ge C, Gu J, Li J. Cancer stem/progenitor cells are highly enriched in CD133 + CD44 + population in hepatocellular carcinoma. Int J Cancer. 2009;1269:2067–78.

9. Acknowledgements

An dieser Stelle möchte ich mich als erstes bei meiner Doktormutter Prof. Veronika Lukacs-Kornek und meinem Gruppenleiter und Betreuer Dr. Miroslaw Kornek bedanken, die immer an mich geglaubt haben, auch wenn ich es selbst nicht getan habe. Ihr habt mir Vieles ermöglicht, was ich oft erst im Nachhinein zu schätzen gelernt habe und für diese Unterstützung bin ich euch sehr dankbar.

Weiterhin gilt mein Dank Prof. Bernd Giebel für die freundliche Übernahme der Zweitkorrektur sowie Prof. Christian Strassburg und Dr. Maria Gonzalez-Carmona für die Beteiligung in meinem Dissertationskomitee. Ebenso möchte ich mich bei Prof. Frank Lammert für die Unterstützung in Homburg bedanken.

Ein riesengroßes Dankeschön geht an meine Freunde, allen voran Catrin, Mathilde, Vera, Bianca, Christina und Steffi. Ihr seid eine unvorstellbar große Stütze in meinem Leben und ich bin so stolz darauf und glücklich darüber, dass ich euch habe. Auch wenn ich mir immer wieder dachte “OMG, INMFTG!”, habt ihr mich wieder eingefangen, mich zum Lachen gebracht und mir Hoffnung gegeben.

Meiner (auch erweiterten) Familie kann ich gar nicht genug danken für ihre bedingungslose Unterstützung und ihre unendliche Geduld, Liebe und Akzeptanz. Es ist geschafft. Promoviert – besser wird’s nicht. Jetzt können wir endlich unser lang ersehntes Essen verwirklichen, das für mich zu einem Symbol dieser Promotion geworden ist. Ihr seid wunderbar! Danke, dass ihr immer für mich da wart und es immer noch seid.

Mein allergrößter Dank geht an Raphael, der fest an meiner Seite steht, sitzt und liegt und der mich durch diese Promotion getragen hat. Du lässt mir Flügel wachsen, wenn ich ziellos im Wald umherirre und du verankerst mich fest im Boden, wenn ich mich verliere. Ein einfaches Dankeschön ist dafür nicht genug und das weißt du auch. Daher gebe ich mein Bestes, dir die gleiche Stütze zu sein wie du mir. Wir schaffen das und es wird großartig!

“I open at the close.”

10. Publications and conference presentations

Publications

1. Słomka A, […], **Urban SK**, […]: EVs as potential new therapeutic tool/target in gastrointestinal cancer and HCC. Cancers (**IF 6.1**). doi: 10.3390/cancers12103019, **Oct 2020**
2. **Urban SK** *et al.*: Synergistic effects of extracellular vesicle phenotyping and AFP in hepatobiliary cancer differentiation. Liver Int (**IF 5.5**). doi: 10.1111/liv.14585, **Jul 2020**
3. Macias RIR, […], **Urban S**, […]: Diagnostic and prognostic biomarkers in cholangiocarcinoma. Liver Int (**IF 5.5**). doi: 10.1111/liv.14090, **Mar 2019**
4. **Urban SK** *et al.*: Extracellular Vesicles in Liver Diseases: Diagnostic, Prognostic, and Therapeutic Application. Semin Liver Dis (**IF 3.5**). doi: 10.1055/s-0038-1676122, **Feb 2019**
5. Słomka A, **Urban SK**, […]: Large Extracellular Vesicles: Have We Found the Holy Grail of Inflammation? Front Immunol (**IF 4.7**). doi: 10.3389/fimmu.2018.02723, **Dec 2018**
6. **Urban SK** *et al.*: Reply: Diagnostic and Prognostic Role of Circulating Microparticles in Hepatocellular Carcinoma. J Hepatol (**IF 18.9**). doi: 10.1016/j.jhep.2017.08.022, **Sep 2017**
7. Julich-Haertel H*, **Urban SK***, […]: Cancer-associated circulating large extracellular vesicles in cholangiocarcinoma and hepatocellular carcinoma. J Hepatol (**IF 18.9**). doi: 10.1016/j.jhep.2017.02.024, **Aug 2017**, *geteilter Erstautor
8. Lukacs-Kornek V, […], **Urban SK** […]: Multi-Surface Antigen Staining of Larger Extracellular Vesicles. Methods Mol Biol (**book chapter**). doi: 10.1007/978-1-4939-7253-1_16, **Aug 2017**
9. Holzmann C, […], **Urban SK**, […]: Transient receptor potential melastatin 4 channel contributes to migration of androgen-insensitive prostate cancer cells. Oncotarget (**IF 5.2**). doi: 10.18632/oncotarget.6157, **Dec 2015**
10. Schorr S, […], **Urban SK**, […]: Co-chaperone Specificity in Gating of the Polypeptide Conducting Channel in the Membrane of the Human Endoplasmic Reticulum. J Biol Chem (**IF 4.1**). doi: 10.1074/jbc.M115.636639, **Jul 2015**

Conferences – oral presentations

1. **II Biennal Congress of ENS-CCA, Rom, 2018:** Liquid biopsy for the identification and differentiation between CCA and HCC – can it be done?
2. **The International Society for Extracellular Vesicles, Annual Meeting, Toronto, 2017:** Circulating tumor-associated microparticles in HCC and CCA
3. **The International Liver Congress by EASL, Amsterdam, 2017:** Circulating tumour-associated microparticles in liver cancer: a question of tumour diameter and volume?

Conferences – poster presentations

1. **The International Liver Congress by EASL, Paris, 2018:** gp38* hepatic progenitor cell-derived large extracellular vesicles in biliary cancers - a novel liquid biopsy marker?
2. **HCC Summit, Genf, 2018:** gp38* hepatic progenitor cell-derived large extracellular vesicles in HCC and biliary cancer - a novel liquid biopsy marker?
3. **EASL Monothematic Conference, Oslo, 2017:** Circulating cancer-associated large extracellular vesicles in cholangiocarcinoma (CCA)
4. **The International Liver Congress by EASL, Amsterdam, 2017:** Circulating tumour-associated microparticles in liver cancer: a question of tumour diameter and volume?

11. Appendix

11.1. Supplementary Figures

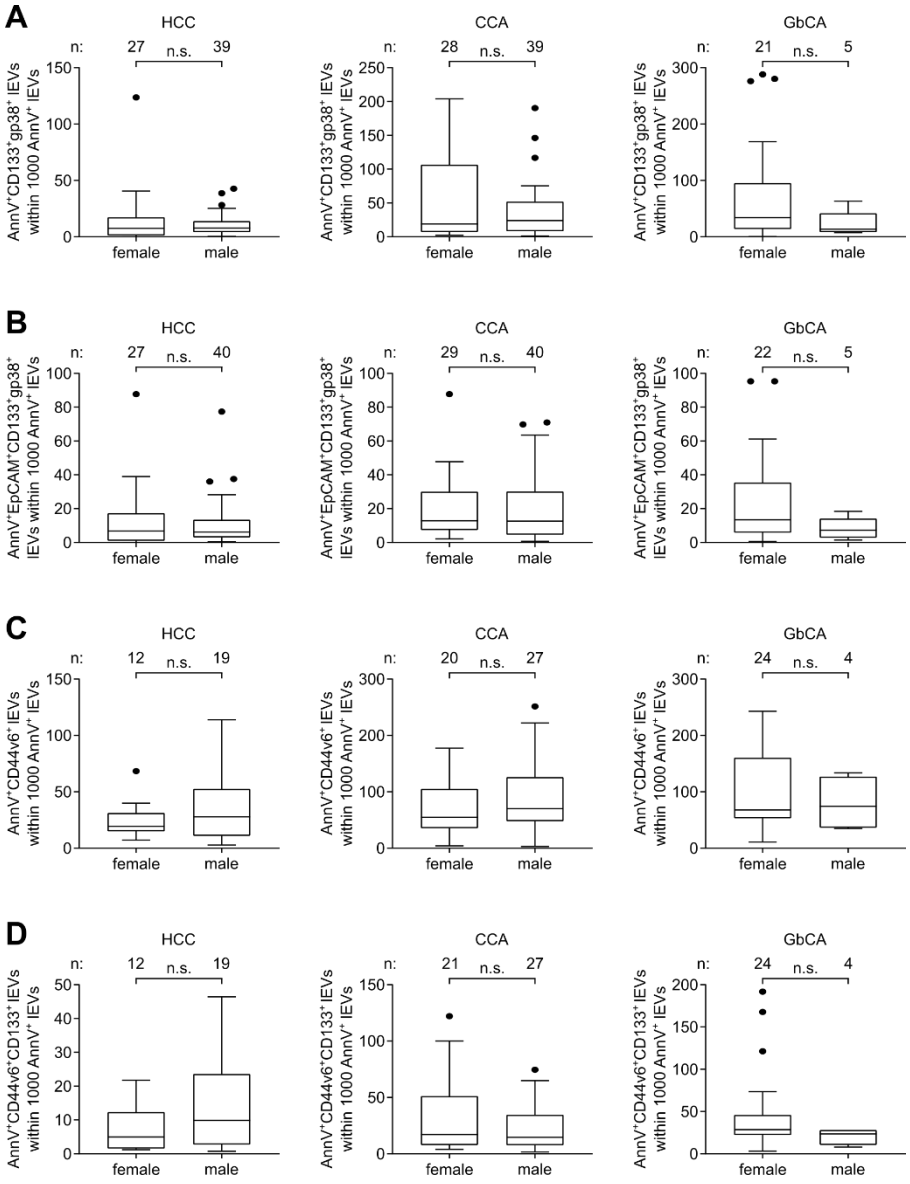

Supplementary Fig. 1: Large EV numbers are comparable in both genders among the hepatobiliary cancer entities. After isolation of serum lEVs and immunofluorescent labelling, they were analyzed by flow cytometry. General gating was applied as described in Fig. 15A, successive gating strategy can be found in Fig. 17A and Fig. 22A. In **A** the distribution of AnnV$^+$CD133$^+$gp38$^+$ lEV levels among the two genders for HCC (left panel), CCA (middle panel) and GbCA (right panel) patients is shown. The same setup is depicted for AnnV$^+$EpCAM$^+$CD133$^+$gp38$^+$ (**B**), AnnV$^+$CD44v6$^+$ (**C**) and AnnV$^+$CD44v6$^+$CD133$^+$ (**D**) lEVs. Data is shown as medians with interquartile range (IQR), whiskers represent 1.5 × IQR (Tukey) with potential outliers plotted as dots. n indicates number of patients. Statistical significance was assessed by two-tailed Mann-Whitney *U* tests with $p \leq 0.05$ considered statistically significant. n.s.: non-significant.

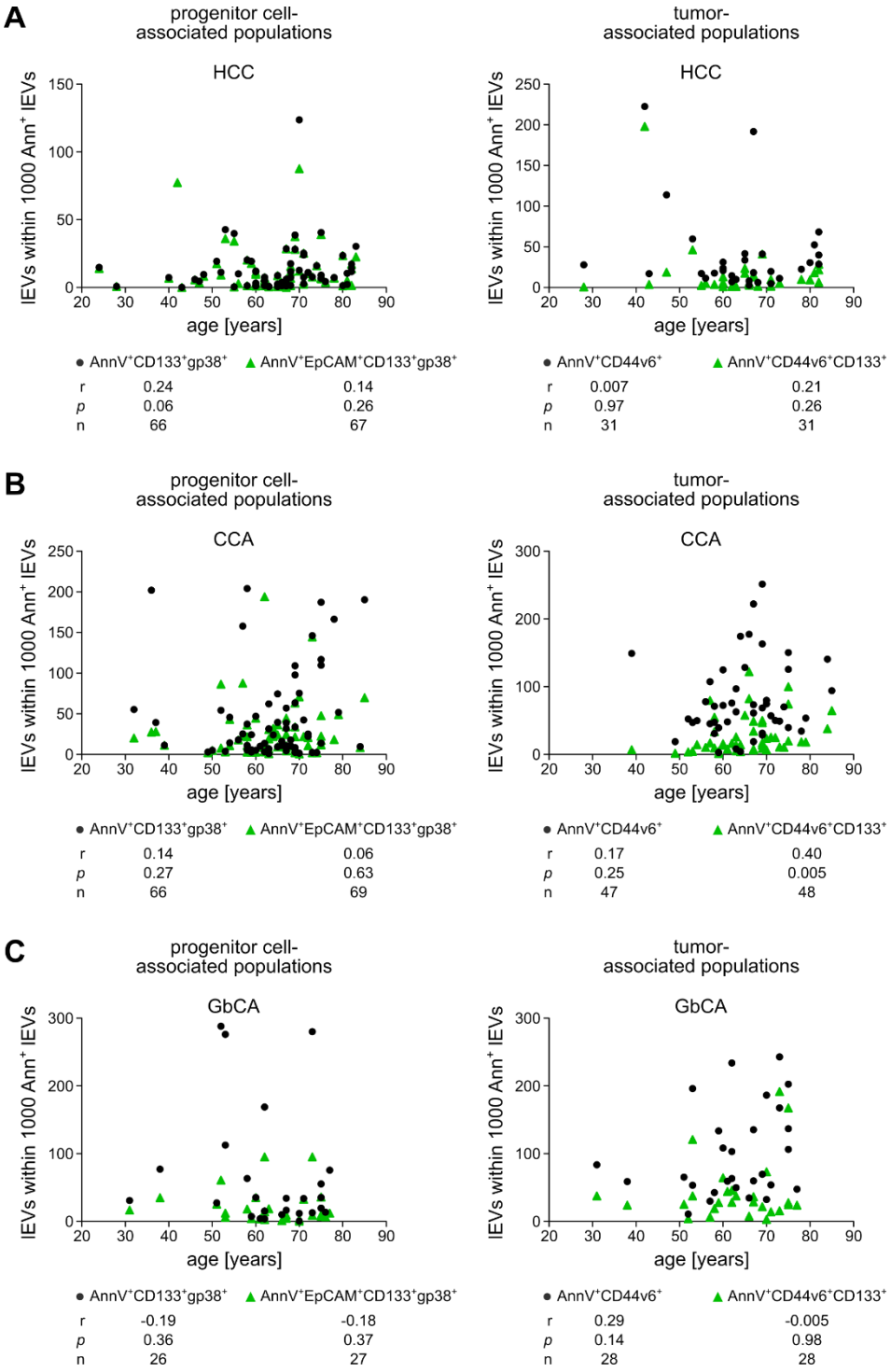

Supplementary Fig. 2: Large EV numbers do not correlate with age distribution among the hepatobiliary cancer entities. After isolation of serum lEVs and immunofluorescent labelling, they were analyzed by flow cytometry. General gating was applied as described in Fig. 15A, successive gating strategy can be found in Fig. 17A and Fig. 22A. In **A** correlations between progenitor cell-associated (left panel) or tumor-associated (right panel) lEV levels and patients' age for HCC patients is shown. The same setup is depicted for CCA (**B**) and GbCA (**C**) patients. Spearman's correlation (r), *p*-values and cohort sizes (n) are indicated for each individual population and patient cohort.

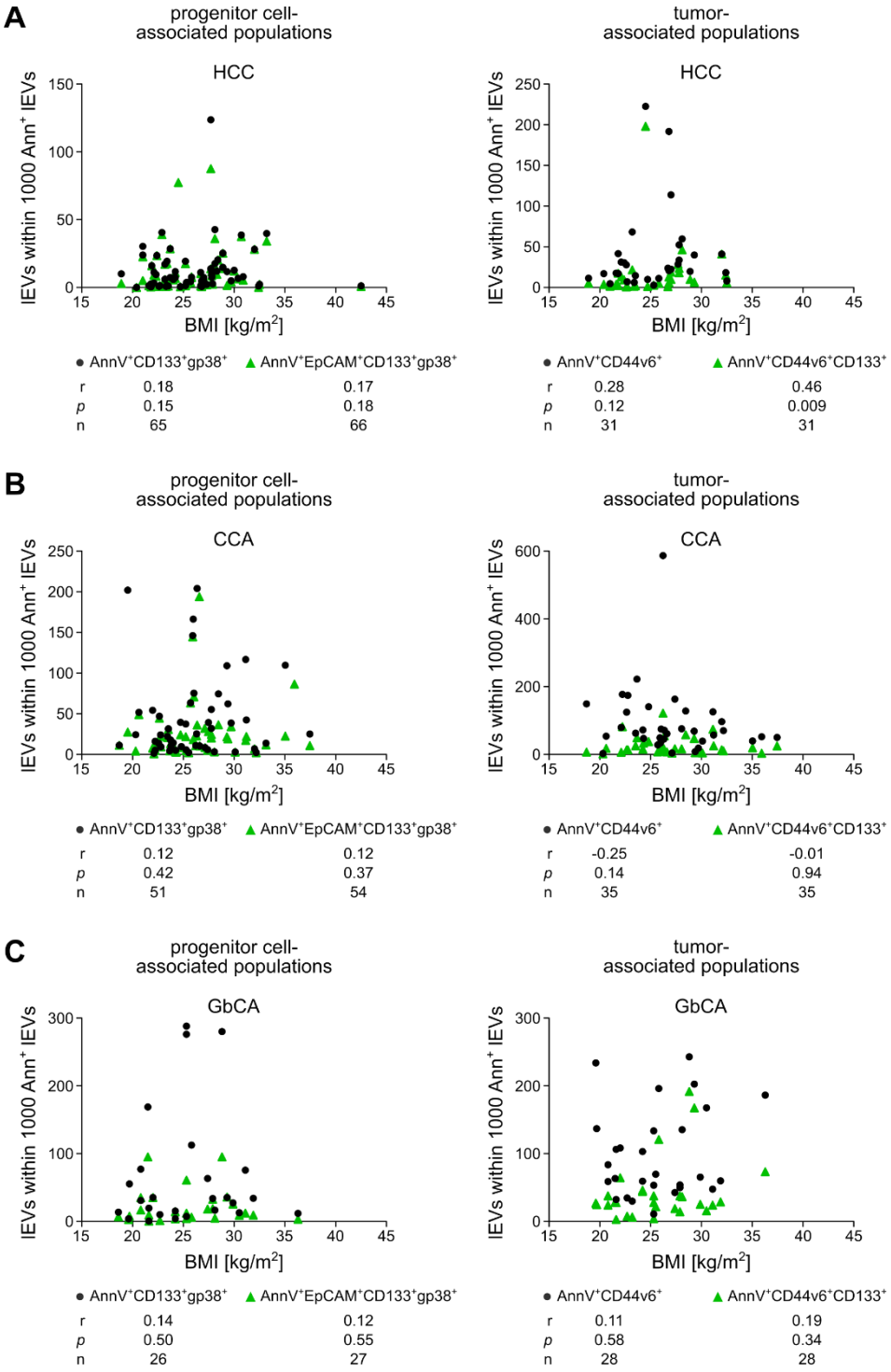

Supplementary Fig. 3: Large EV numbers do not correlate with BMI distribution among the hepatobiliary cancer entities. After isolation of serum lEVs and immunofluorescent labelling, they were analyzed by flow cytometry. General gating was applied as described in Fig. 15A, successive gating strategy can be found in Fig. 17A and Fig. 22A. In **A** correlations between progenitor cell-associated (left panel) or tumor-associated (right panel) lEV levels and patients' BMI for HCC patients is shown. The same setup is depicted for CCA (**B**) and GbCA (**C**) patients. Spearman's correlation (r), *p*-values and cohort sizes (n) are indicated for each individual population and patient cohort.

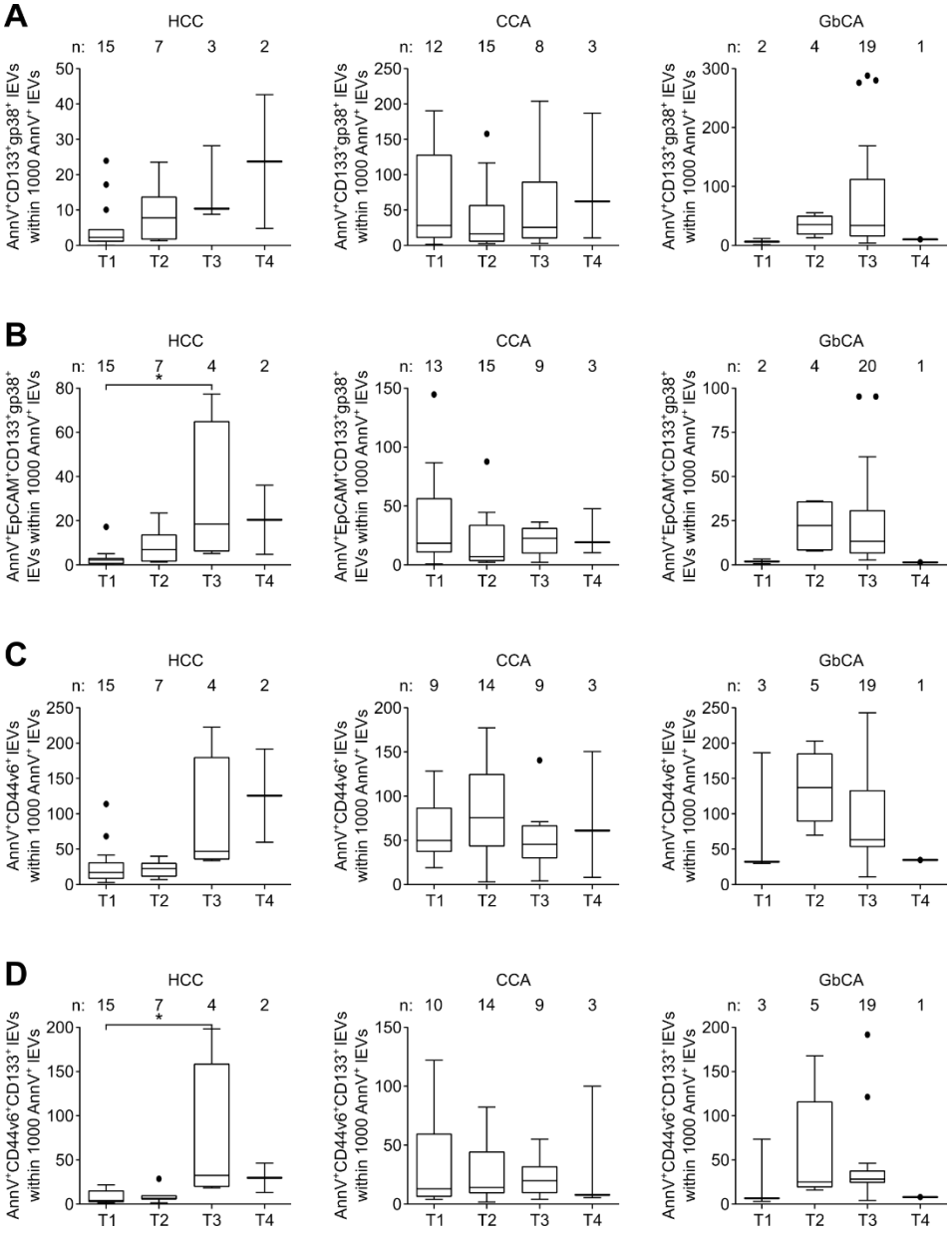

Supplementary Fig. 4: Large EV numbers tend to correlate with tumor stage in HCC, but not in CCA or GbCA. After isolation of serum lEVs and immunofluorescent labelling, they were analyzed by flow cytometry. General gating was applied as described in Fig. 15A, successive gating strategy can be found in Fig. 17A and Fig. 22A. In **A** the distribution of AnnV$^+$CD133$^+$gp38$^+$ lEV levels among the tumor severity stages T1 to T4 for HCC (left panel), CCA (middle panel) and GbCA (right panel) patients is shown. The same setup is depicted for AnnV$^+$EpCAM$^+$CD133$^+$gp38$^+$ (**B**), AnnV$^+$CD44v6$^+$ (**C**) and AnnV$^+$CD44v6$^+$CD133$^+$ (**D**) lEVs. Data is shown as medians with interquartile range (IQR), whiskers represent 1.5 × IQR (Tukey) with potential outliers plotted as dots. n indicates number of patients. Statistical significance was assessed by Kruskal-Wallis non-parametric test followed by Dunn's multiple comparison post hoc test with $p \leq 0.05$ considered statistically significant. (* = $p \leq 0.05$, ** = $p \leq 0.01$, *** = $p \leq 0.001$, **** = $p \leq 0.0001$).

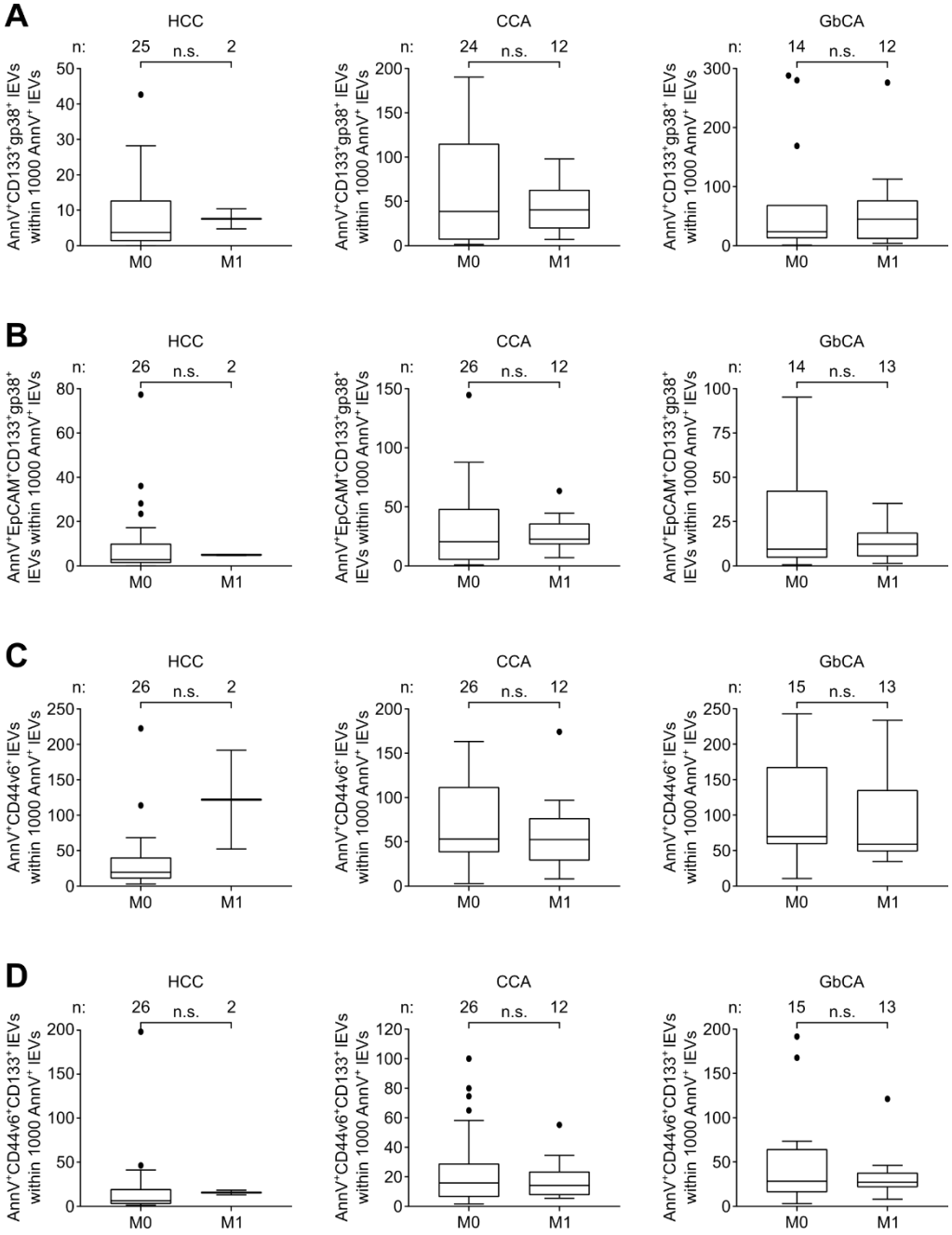

Supplementary Fig. 5: Large EV numbers are comparable in hepatobiliary cancer patients with and without occurrence of distant metastases. After isolation of serum lEVs and immunofluorescent labelling, they were zby flow cytometry. General gating was applied as described in Fig. 15A, successive gating strategy can be found in Fig. 17A and Fig. 22A. In **A** the distribution of AnnV$^+$CD133$^+$gp38$^+$ lEV levels among patients suffering from distal metastases (M1) or without metastases (M0) for HCC (left panel), CCA (middle panel) and GbCA (right panel) patients is shown. The same setup is depicted for AnnV$^+$EpCAM$^+$CD133$^+$gp38$^+$ (**B**), AnnV$^+$CD44v6$^+$ (**C**) and AnnV$^+$CD44v6$^+$CD133$^+$ (**D**) lEVs. Data is shown as medians with interquartile range (IQR), whiskers represent 1.5 × IQR (Tukey) with potential outliers plotted as dots. n indicates number of patients. Statistical significance was assessed by two-tailed Mann-Whitney *U* tests with $p \leq 0.05$ considered statistically significant. n.s.: non-significant.

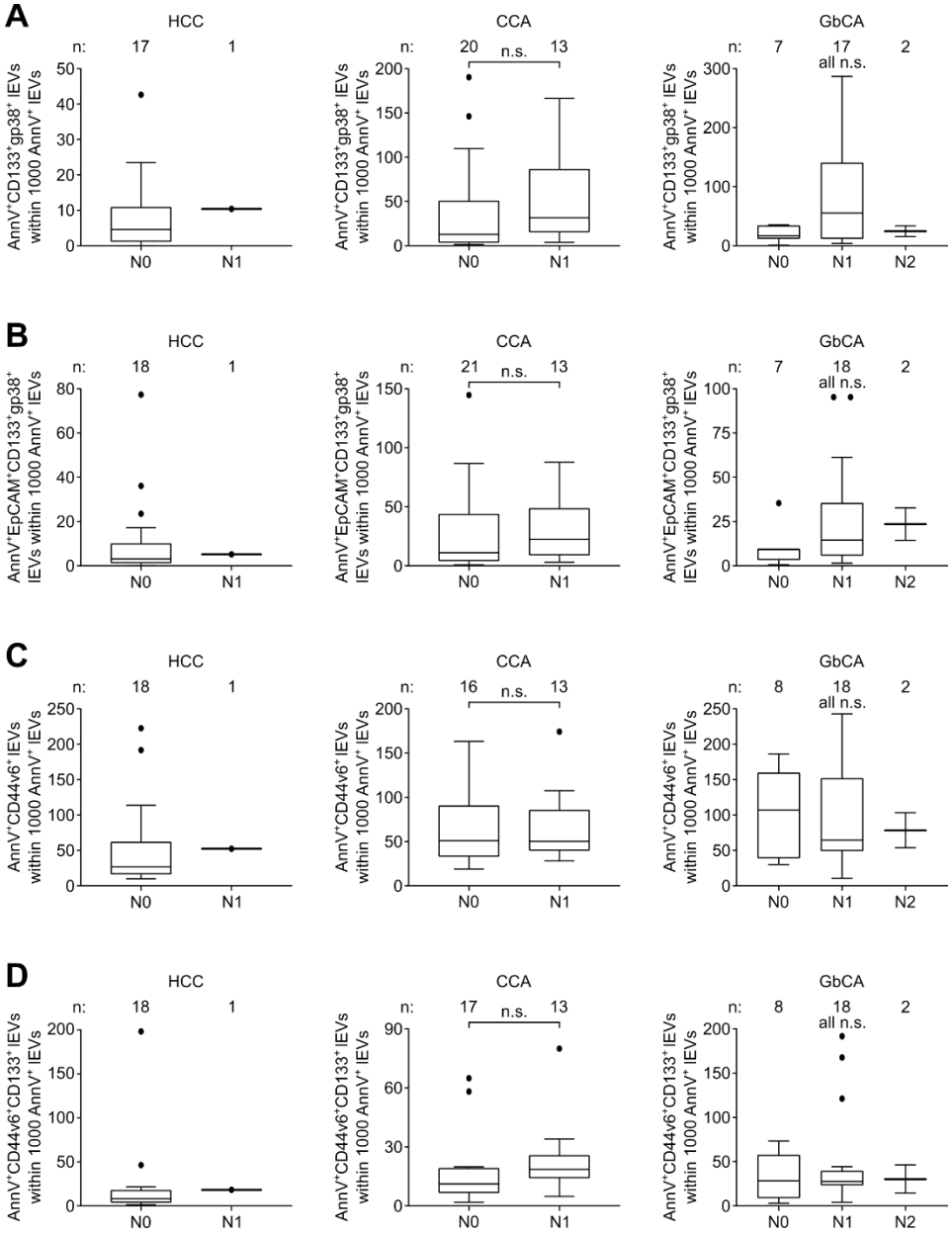

Supplementary Fig. 6: Large EV numbers are comparable in hepatobiliary cancer patients with and without occurrence of lymph node nodules. After isolation of serum lEVs and immunofluorescent labelling, they were analyzed by flow cytometry. General gating was applied as described in Fig. 15A, successive gating strategy can be found in Fig. 17A and Fig. 22A. In **A** the distribution of AnnV$^+$CD133$^+$gp38$^+$ lEV levels among patients without proximal lymph node nodules (N0) or with increasing amounts of nodules (N1-2) for HCC (left panel), CCA (middle panel) and GbCA (right panel) patients is shown. The same setup is depicted for AnnV$^+$EpCAM$^+$CD133$^+$gp38$^+$ (**B**), AnnV$^+$CD44v6$^+$ (**C**) and AnnV$^+$CD44v6$^+$CD133$^+$ (**D**) lEVs. Data is shown as medians with interquartile range (IQR), whiskers represent 1.5 × IQR (Tukey) with potential outliers plotted as dots. n indicates number of patients. Statistical significance for HCC and CCA was assessed by two-tailed Mann-Whitney *U* tests and for GbCA by Kruskal-Wallis non-parametric test followed by Dunn's multiple comparison post hoc test. In both cases $p \leq 0.05$ was considered statistically significant. n.s.: non-significant.

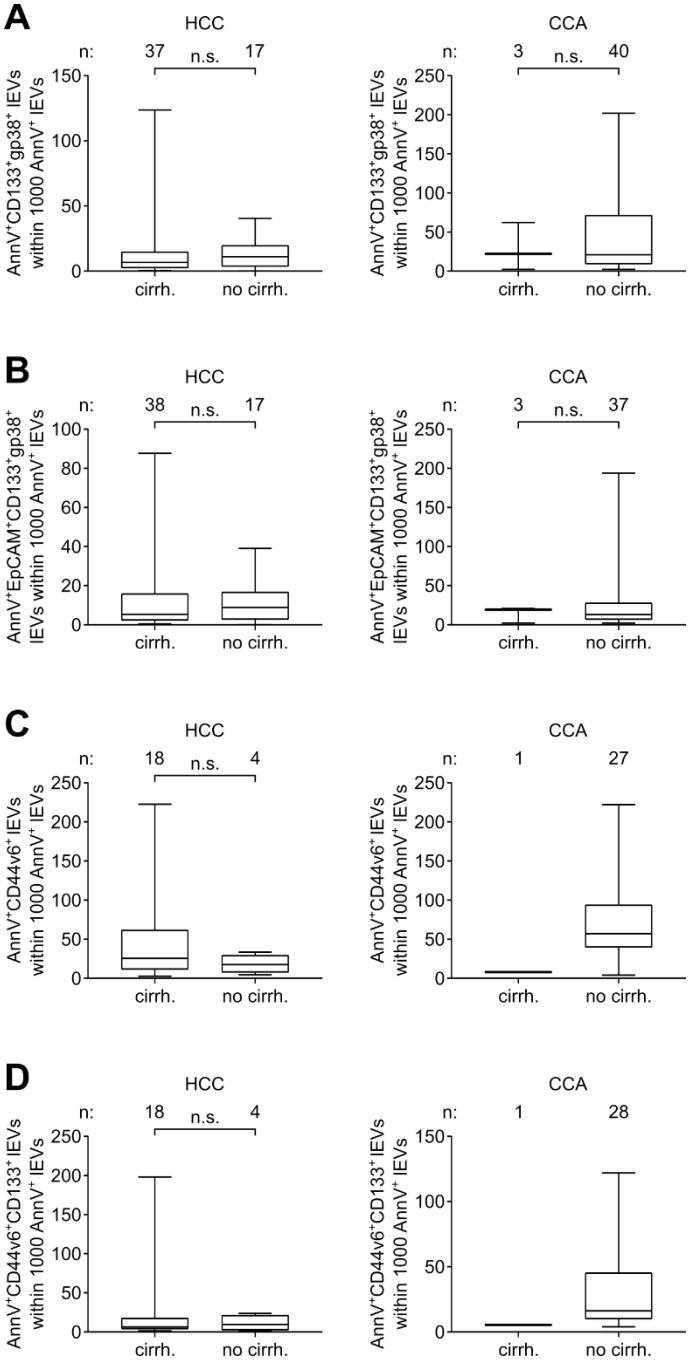

Supplementary Fig. 7: Large EV numbers are comparable in hepatic cancer patients with and without prior underlying cirrhosis. After isolation of serum lEVs and immunofluorescent labelling, they were analyzed by flow cytometry. General gating was applied as described in Fig. 15A, successive gating strategy can be found in Fig. 17A and Fig. 22A. In **A** the distribution of AnnV$^+$CD133$^+$gp38$^+$ lEV levels of patients with and without underlying liver cirrhosis for HCC (left panel) and CCA (right panel) patients is shown. The same setup is depicted for AnnV$^+$EpCAM$^+$CD133$^+$gp38$^+$ (**B**), AnnV$^+$CD44v6$^+$ (**C**) and AnnV$^+$CD44v6$^+$CD133$^+$ (**D**) lEVs. Data is shown as medians with interquartile range (IQR), whiskers represent 1.5 × IQR (Tukey) with potential outliers plotted as dots. n indicates number of patients. Statistical significance was assessed by two-tailed Mann-Whitney *U* tests with $p \leq 0.05$ considered statistically significant. n.s.: non-significant.

11.2. Supplementary Tables

Supplementary Tab. 1: Biochemical parameters of the different patient cohorts within the progenitor cell-associated and tumor-associated study cohorts. AFP, CA19-9, CEA, ALT and bilirubin are given as mean. #: absolute number of patients in each cohort, n.a.: not available, s.d.: standard deviation.

progenitor cell-associated study cohort							
	healthy	**cirrhosis**	**GbCA**	**CCA**	**HCC**	**NSCLC**	**CRC**
AFP [ng/mL]		11.8			181.2	3.4	6.6
s.d.	n.a.	42.7	n.a.	n.a.	216.9	2.4	12.0
range		0.8-293.4			1.8-820.4	0.9-16.3	1.8-60.3
CA19-9 [U/mL]		23.9	24.3	20.5	30.4	2,808	5,475
s.d.	n.a.	27.3	29.4	11.8	54.5	12,545	9,943
range		2.0-133.9	1.1-120.0	12.1-28.8	0.0-308.0	0.6-100,000	5.4-43,147
CEA [ng/mL]		3.3	4.9	3.6	3.0	7.5	15.4
s.d.	n.a.	2.3	4.0	4.0	3.1	11.4	36.4
range		0.8-8.1	0.4-13.5	0.4-13.6	0.5-18.3	0.3-50.4	0.9-177.0
ALT [U/L]		65.0	35.9	47.5	68.5	102.5	73.6
s.d.	n.a.	54.5	36.6	116.7	63.0	127.2	84.2
range		8.0-320.0	6.0-159.0	9.0-661.0	9.0-349.0	11.0-701.0	8.0-391.0
bilirubin [mg/dL]		4.5	1.1	0.5	3.8	17.9	7.4
s.d.	n.a.	6.9	2.2	0.3	5.5	80.5	9.9
range		0.6-33.7	0.1-10.0	0.2-1.4	0.0-23.9	0.2-644.0	0.2-31.2
T stage [%], 1/2/3/4	n.a.	n.a.	n.a.	n.a.	54/25/14/7	33/38/22/7	7/15/74/4
N stage [%], 0/1/2	n.a.	n.a.	n.a.	n.a.	95/5/0	68/32/0	26/67/7
M stage [%], 0/1	n.a.	n.a.	n.a.	n.a.	93/7	62/38	52/48
underlying cirrhosis [%]	n.a.	n.a.	n.a.	n.a.	69	7	n.a.
tumor-associated study cohort							
	healthy	**cirrhosis**	**GbCA**	**CCA**	**HCC**	**NSCLC**	**CRC**
AFP [ng/mL]		77.5			285.4	3.2	6.3
s.d.	n.a.	143.9	n.a.	n.a.	215.1	1.8	11.6
range		2.2-293.4			1.8-820.4	0.9-10.3	1.6-60.3
CA19-9 [U/mL]		10.8	24.3		29.6	1,538	5,322
s.d.	n.a.	7.7	29.4	n.a.	39.4	3,567	9,775
range		2.8-18.1	1.1-120.0		0.6-137.4	6.5-19387	5.4-43,147
CEA [ng/mL]		1.7	4.9	3.0	2.9	7.7	14.5
s.d.	n.a.	0.3	4.0	3.5	1.8	11.1	35.0
range		1.1-1.6	0.4-13.5	0.4-13.6	1.1-6.3	0.3-47.1	0.8-177.0
ALT [U/L]		53.3	36.8	65.7	51.3	92.3	70.6
s.d.	n.a.	24.0	37.4	165.0	35.8	109.1	83.2
range		26.0-78.0	6.0-159.0	9.0-661.0	9.0-184.0	11.0-651.0	8.0-391.0

bilirubin [mg/dL] s.d. range	n.a.	1.7 1.0 0.6-2.9	1.1 2.2 0.1-10.0	0.5 0.3 0.3-1.4	6.9 6.8 0.3-23.9	23.5 95.5 0.2-644.0	7.0 9.8 0.2-31.4
T stage [%], 1/2/3/4	n.a.	n.a.	n.a.	n.a.	54/25/14/7	28/39/25/8	10/18/68/4
N stage [%], 0/1/2	n.a.	n.a.	n.a.	n.a.	95/5/0	57/43/0	29/64/7
M stage [%], 0/1	n.a.	n.a.	n.a.	n.a.	93/7	68/32	54/46
underlying cirrhosis [%]	n.a.	n.a.	n.a.	n.a.	69	3	n.a.

Supplementary Tab. 2: Biochemical parameters of the different patient cohorts for small EV analysis. AFP, CA19-9, CEA, ALT and bilirubin are given as mean. #: absolute number of patients in each cohort, n.a.: not available, s.d.: standard deviation.

	HCC	**iCCA**
AFP [ng/mL] s.d. range	5.0 1.4 3.6-7.8	29.7 36.6 1.0-100.0
CA19-9 [U/mL] s.d. range	51.4 64.4 3.4-146.2	170.9 193.2 1.1-400.0
CEA [ng/mL] s.d. range	32.7 21.2 15.0-80.0	47.8 41.2 10.0-137.0
ALT [U/L] s.d. range	37.2 35.6 8.7-112.0	58.4 138.5 1.7-400.0
bilirubin [mg/dL] s.d. range	1.1 0.7 0.5-2.6	3.3 4.6 0.3-13.5
T stage [%], 1/2/3/4	50/38/12/0	25/38/12/25
N stage [%], 0/1/2	100/0	25/75
M stage [%], 0/1	100/0	37/63
underlying cirrhosis [%]	100	100

Received: 1 February 2020 | Revised: 12 June 2020 | Accepted: 24 June 2020

DOI: 10.1111/liv.14585

ORIGINAL ARTICLE

Liver INTERNATIONAL WILEY

Synergistic effects of extracellular vesicle phenotyping and AFP in hepatobiliary cancer differentiation

Sabine K. Urban[1,2] | Hanna Sänger[2,3] | Marcin Krawczyk[2,4] | Henrike Julich-Haertel[2] | Arnulf Willms[5] | Joanna Ligocka[6] | Mikel Azkargorta[7] | Tudor Mocan[8] | Christoph Kahlert[9] | Beata Kruk[4] | Krzysztof Jankowski[10] | Waldemar Patkowski[6] | Marek Krawczyk[6] | Krzysztof Zieniewicz[6] | Wacław Hołówko[6] | Łukasz Krupa[11] | Mateusz Rzucidło[11] | Krzysztof Gutkowski[11] | Wojciech Wystrychowski[12] | Robert Król[12] | Joanna Raszeja-Wyszomirska[13] | Artur Słomka[14] | Robert Schwab[5] | Aliona Wöhler[5] | Maria A. Gonzalez-Carmona[1] | Sebastian Gehlert[15] | Zeno Sparchez[8] | Jesus M. Banales[16] | Christian P. Strassburg[1] | Frank Lammert[2] | Piotr Milkiewicz[13,17] | Miroslaw Kornek[1,2]

[1]Department of Internal Medicine I, University Medical Center Bonn, Bonn, Germany

[2]Department of Medicine II, Saarland University Medical Center, Saarland University, Homburg, Germany

[3]Institute of Experimental Immunology, Rheinische Friedrich-Wilhelms-Universität, Bonn, Germany

[4]Laboratory of Metabolic Liver Diseases, Centre for Preclinical Research, Department of General, Transplant and Liver Surgery, Medical University of Warsaw, Warsaw, Poland

[5]Department of General, Visceral and Thoracic Surgery, German Armed Forces Central Hospital, Koblenz, Germany

[6]Department of General, Transplant and Liver Surgery, Medical University of Warsaw, Warsaw, Poland

[7]Proteomics Platform, Bizkaia Science and Technology Park, Derio, Spain

[8]Octavian Fodor Institute for Gastroenterology and Hepatology, Iuliu Haţieganu University of Medicine and Pharmacy, Cluj-Napoca, Romania

[9]Department of Visceral, Thoracic and Vascular Surgery, University Hospital Carl Gustav Carus, Technische Universität Dresden, Germany

[10]Department of Internal Medicine and Cardiology, Medical University of Warsaw, Warsaw, Poland

[11]Department of Gastroenterology and Hepatology with Internal Disease Unit, Specialist District Hospital in Rzeszow, Rzeszow, Poland

[12]Department of General, Vascular and Transplant Surgery, School of Medicine in Katowice, Medical University of Silesia, Katowice, Poland

[13]Liver and Internal Medicine Unit, Department of General, Transplant and Liver Surgery, Medical University of Warsaw, Warsaw, Poland

[14]Department of Pathophysiology, Nicolaus Copernicus University in Toruń, Ludwik Rydygier Collegium Medicum in Bydgoszcz, Poland

[15]Department for Biosciences of Sports, Institute of Sports Science, University of Hildesheim, Hildesheim, Germany

[16]Department of Liver and Gastrointestinal Diseases, Biodonostia Health Research Institute – Donostia University Hospital, University of the Basque Country (UPV/EHU), San Sebastian, Spain

[17]Translational Medicine Group, Pomeranian Medical University, Szczecin, Poland

Abbreviations: AnnV, Annexin V; AUC, area under the curve; CA 19-9, carbohydrate antigen 19-9; CCA, cholangiocarcinoma; CRC, colorectal carcinoma; ENS-CCA, European Network for the Study of Cholangiocarcinoma; EpCAM, epithelial cell adhesion molecule; ESMO, European Society for Medical Oncology; EVs, extracellular vesicles; FACS, fluorescence-activated cell scanning; FBS, fetal bovine serum; GbCA, gallbladder carcinoma; HCC, hepatocellular carcinoma; ISEV, International Society for Extracellular Vesicles; MISEV, minimal information for studies of extracellular vesicles; nm, nanometer; NPV, negative predictive value; NSCLC, non-small cell lung carcinoma; PPV, positive predictive value; QM, quality management; ROC, receiver operating characteristic; TICs, tumour-initializing cells.

Sabine K. Urban, Hanna Sänger, Marcin Krawczyk, Henrike Julich-Haertel and Arnulf Willms contributed equally (shared first-author).

Correspondence
Miroslaw Kornek, Department of Internal Medicine I, University Medical Center Bonn, Venusberg-Campus 1, 53127 Bonn, Germany.
Email: miroslawkornek@web.de

Funding information
This work was funded by the Deutsche Forschungsgemeinschaft (DFG, German Research Foundation) to MK (project number 410853455). JMB was funded by the Spanish Carlos III Health Institute (ISCIII) [FIS PI15/01132, PI18/01075 and Miguel Servet Program CON14/00129 and CPII19/00008)] cofinanced by 'Fondo Europeo de Desarrollo Regional' (FEDER), 'Fundación Científica de la Asociación Española Contra el Cáncer' (AECC Scientific Foundation: 'Rare cancers grant 2017') and European Commission Horizon 2020 program (SEP-210503876; ESCALON project #825510).

Handling Editor: Isabelle Leclercq

Abstract

Background: Biliary cancer, comprising cholangio- and gallbladder carcinomas, is associated with high mortality due to asymptomatic disease onset and resulting late diagnosis. Currently, no robust diagnostic biomarker is clinically available. Therefore, we explored the feasibility of extracellular vesicles (EVs) as a liquid biopsy tool for biliary cancer screening and hepatobiliary cancer differentiation.

Methods: Serum EVs of biliary cancer, hepatocellular carcinoma, colorectal cancer and non-small cell lung cancer patients, as well as from healthy individuals, were isolated by sequential two-step centrifugation and presence of indicated EVs was evaluated by fluorescence activated cell sorting (FACS) analysis.

Results: Two directly tumour-related antigen combinations ($AnnV^+CD44v6^+$ and $AnnV^+CD44v6^+CD133^+$) and two combinations related to progenitor cells from the tumour microenvironment ($AnnV^+CD133^+gp38^+$ and $AnnV^+EpCAM^+$ $CD133^+gp38^+$) were associated with good diagnostic performances that could potentially be used for clinical assessment of biliary cancer and differentiation from other cancer entities. With 91% sensitivity and 69% specificity $AnnV^+CD44v6^+$ EVs showed the most promising results for differentiating biliary cancers from HCC. Moreover using a combined approach of EV levels of the four populations with serum AFP values, we obtained a perfect separation of biliary cancer and HCC with sensitivity, specificity, positive and negative predictive value all reaching 100% respectively.

Conclusions: EV phenotyping, especially if combined with serum AFP, represents a minimally invasive, accurate liquid biopsy tool that could improve cancer screening and differential diagnosis of hepatobiliary malignancies.

KEYWORDS
biomarker, cholangiocarcinoma, diagnosis, extracellular vesicles, gallbladder cancer, hepatocellular carcinoma

1 | INTRODUCTION

Biliary tract cancers are considered rare diseases on a worldwide scale, yet incidence rates are rising. Gallbladder cancer (GbCA) and cholangiocellular carcinoma (CCA) are characterized by high mortality rates owing to the tumour's aggressiveness and lack of early diagnosing possibilities.[1,2] Currently, no GbCA or CCA-specific serum, bile, urine or other non-invasive marker is available for reliable early detection, monitoring or screening.[3] If diagnosed in time, surgical resection of the gallbladder and bile duct represents the only curative option.[3] In most cases, GbCA and CCA progress asymptomatically until a metastatic and inoperable stage is reached,[4] resulting in 5-year survival rates of around 5% for GbCA and 20% for CCA.[5,6] Despite multiple imaging techniques for staging of biliary tract malignancies, less than 10% of GbCA and only about 50% of CCA are resectable at the time of diagnosis.[7]

Recently, circulating extracellular vesicles (EVs) have been considered as a minimally invasive screening tool for early cancer diagnosis.[8-11] According to the MISEV2018 guidelines, circulating EVs can be classified into small EVs (sEVs), typically with a diameter below 100 nm, and large EVs (lEVs) with typical diameters ranging between 100 and 1000 nm.[12] If not specified otherwise the term 'EVs' is subsequently used to describe large EVs throughout the manuscript. Essentially, the two types differ in size and mode of cellular release. Whereas small EVs are generated within the endomembranous system of the cell and reside within so-called multi-vesicular bodies before their release, large EVs are shed

Keypoints

- No reliable diagnostic serum biomarkers for biliary cancer, that are fatal diseases with high mortality rates, are available.
- Extracellular vesicles could be a new clinically relevant serum biomarker for biliary cancer screening/diagnosis.
- Combination of extracellular vesicle levels and AFP values enhances the screening/diagnostic capacity for biliary cancer detection.

directly from the plasma membrane of their parental cell.[13] By isolating circulating EVs from peripheral blood and analysing them by fluorescence-activated cell scanning (FACS), it is possible to create disease-specific EV profiles. Tumour-associated EVs have been investigated in many forms of cancer, that is, glioblastoma and hepatocellular carcinoma (HCC).[8,14] Therefore, EVs may be considered a novel type of minimally invasive liquid biopsy as highlighted recently by others and our group.[8,11,15,16]

Considering the fatality of GbCA and CCA that is due to insufficient diagnostic measures, the need for novel early and accurate cancer diagnosis tools is omnipresent.[16,17] By making use of circulating EV profiling, we aim to find surface antigen combinations for biliary cancer-derived EVs and for EVs associated with the tumour microenvironment that might aid in early diagnosis of GbCA and CCA.

2 | MATERIALS AND METHODS

2.1 | Mice

Animals were obtained from Charles River (Sulzfeld) and housed in pathogen-free conditions in an assigned mouse cabinet (Bioscape) at the Department of Medicine II at Saarland University. All experimental procedures were performed on male 7-9-week-old wildtype C57Bl/6 mice, fed with standard diet, with the approval of the ethics and animal care committee Homburg.

2.2 | Preparation of organ single cell suspensions and FACS measurement

Murine single cells were digested and stained for flow cytometry as described earlier.[18] Briefly, mouse organs were removed, cut into pieces and enzymatically digested for 60-90 minutes at 37°C. After digestion, cells were collected and red blood cells were lysed in liver and lung using ACK lysis buffer (Life Technologies). Single cell suspensions were counted on a MACSQuant® Analyzer 10 (Miltenyi Biotec). For each staining, 3×10^5 (liver), 1×10^4 (gallbladder), 1×10^5 (colon) or 4×10^5 (lung) single living cells were incubated with antibodies against CD45 (103116, BioLegend), CD31 (102406, BioLegend), ASGPR1 (AF2755, R&D Systems), EpCAM (118225, BioLegend), CD133 (130-102-210, Miltenyi Biotec), gp38 (127410, BioLegend) and CD44 (130-102-904, Miltenyi Biotec). ASGPR1 was only included for liver, not for other organs. Liver cells were stained with a secondary antibody against goat IgG (A11055, Invitrogen). Detailed information about all applied antibodies can be found in Table S1. All cells were measured on a MACSQuant® Analyzer 10 (Miltenyi Biotec).

2.3 | Human study cohort

The Ethics commissions of (a) the State Chambers of Medicine in Rhineland-Palatinate, Ger-many approval number: 837.151.13 (8836-F)); (b) Saarland, Germany (167/11); (c) San Sebastian, Spain (PI2014187); (d) Warsaw, Poland (KB/41/A/2016 and AKB/145/2014) and (e) Cluj-Napoca, Romania (3042/07.03.2018) approved this study. All patients gave their informed consent.

Patients that received chemotherapy or were subjected to any other anti-tumour therapy during the time blood samples were taken were excluded. The characteristics of the patients are summarized in Table 1. GbCA patients who had undergone previous cholecystectomy were excluded from the current study.

2.4 | Isolation of extracellular vesicles and subsequent FACS analysis

Human blood samples were collected in Clotting Activator S-Monocuvettes (7.5 mL, Sarstedt) and were allowed to coagulate at RT for 30-60 minutes. Subsequently, samples were centrifuged for 20 minutes at 1500 *g*. Isolated serum was collected and stored at −80°C.

All large EV isolation and staining procedures were performed according to previously established and published protocols.[8,19] Briefly, 1 mL patient serum was successively centrifuged at 2000 *g* and 20 000 *g*. Small EVs were isolated using the Total Exosome Isolation Reagent (Invitrogen by Thermo Fisher Scientific) following the manufacturer's specifications. Isolated EVs were incubated with Annexin V (AnnV)-FITC (130-093-060, Miltenyi Biotec) and were subsequently stained with antibodies against EpCAM (130-097-324), CD133 (130-107-453), gp38 (130-106-954) and CD44v6 (130-111-425, all Miltenyi Biotec). Detailed information about all applied antibodies can be found in Table S2. All samples were analysed using the MACSQuant Analyzer (Miltenyi Biotec). Cohort sizes within the progenitor cell- and tumour-associated cohorts were eventually not coherent due to flow cytometric measurement errors.

2.5 | LC-MS analysis

Details can be obtained from Supporting information.

2.6 | Human cancer cell lines

Information about the used cancer cell lines and details on staining protocols for FACS analysis can be obtained from Supporting information.

2.7 | Nanoparticle tracking analysis

Details can be obtained from Supporting information.

TABLE 1 Patient characteristics. Summary of demographic and biochemical parameters of patients with indicated diseases and healthy controls. Age, BMI, CEA, CA 19-9, ALT, AFP and bilirubin are given as mean; #: absolute number of patients in each cohort, S.D.: standard deviation, n.a.: not available

	Healthy CTRL	Cirrhosis	GbCA	CCA	HCC	NSCLC	CrC
Patients [#]	48	54	29	77	67	32	20
Female [#]	33	15	24	34	27	9	5
Male [#]	15	39	5	43	40	23	15
Age [y]	30.7	52.5	63.0	63.6	64.1	64.4	69.9
S.D.	12.3	9.5	11.1	9.9	12.3	9.6	13.8
Range	17-75	21-72	31-77	32-85	24-83	49-81	33-89
BMI [kg/m^2]	24.8	26.2	25.4	26.2	26.1	26.7	27.6
S.D.	5.0	4.8	4.3	3.9	3.9	4.4	5.7
range	18.8-38.3	20.0-38.6	18.6-36.3	18.7 –37.5	18.9-42.5	20.2-44.5	20.2-44.5
CEA [ng/mL]	n.a.	3.3	14.5	7.3	3.0	3.6	4.9
S.D.		2.3	35.0	11.2	3.1	4.0	4.0
Range		0.8-8.1	0.8-177.0	0.3-50.4	0.5-18.8	0.4-13.6	0.4-13.5
CA 19-9 [U/mL]	n.a.	23.9	5,137	2,564	30.4	20.5	24.3
S.D.		27.3	9,633	11,945	54.5	11.8	29.4
Range		2.0-133.9	5.4-43,152	0.6-100,000	0.0-308.0	12.1-28.8	1.1-120.0
ALT [U/L]	n.a.	65.0	70.8	94.7	68.5	47.5	35.9
S.D.		54.4	81.8	122.0	63.0	116.7	36.6
Range		8.0-320.0	8.0-391.0	11.0-701.0	9.0-349.0	9.0-661.0	6.0-159.0
AFP [ng/mL]	n.a.	11.8	6.3	3.4	181.2	n.a.	n.a.
S.D.		42.7	11.6	2.3	216.9		
Range		0.8-293.4	1.6-60.3	0.9-16.3	1.8-820.4		
Bilirubin [mg/dL]	n.a.	4.5	6.9	16.3	3.8	0.5	1.1
S.D.		6.9	9.7	76.7	5.5	0.3	2.2
Range		0.6-33.7	0.2-31.4	0.2-644.0	0.0-23.9	0.2-1.4	0.1-10.0
T stage [%], 1/2/3/4	n.a.	n.a	10/17/69/4	31/36/19/14	54/25/14/7	n.a.	n.a.
N stage [%], 0/1/2	n.a.	n.a	28/65/7	63/37/0	95/5/0	n.a.	n.a.
M stage [%], 0/1	n.a.	n.a	55/45	67/33	57/43	n.a.	n.a.
Underlying cirrhosis [%]	n.a.	n.a	n.a	6	69	n.a	n.a

2.8 | Data processing and analysis

FACS data were analysed using FlowJo 10 for MAC OSX (Tree Star Inc). Statistical analysis was performed using GraphPad Prism 5 (GraphPad Software Inc). Figures were created using GraphPad Prism 5 and Adobe Illustrator (Adobe Systems Inc).

2.9 | Statistical analysis

All EV profiles depict the population median with interquartile range (IQR) and whiskers representing 1.5 × IQR according to Tukey. Multiple cohorts (>2) were assessed by Kruskal-Wallis non-parametric tests followed by Dunn's multiple comparison post hoc tests. Each degree of freedom (*df*) is indicated in the corresponding figure legend. To assess the diagnostic benchmarks of EV populations, we calculated sensitivity, specificity, positive predictive values (PPV) and negative predictive values (NPV), and area under ROC curve (AUC) values. Overall, $P < .05$ was considered significant. The total experimental strength was calculated with the G*Power program (Heinrich-Heine-Universität Düsseldorf, version 3.1.9.2) for different effects (effect size f: 0.25, 0.45 and 0.65). An α error of 0.05 was assumed. In detail, our validation study (Figure 3A,C) were associated with a test strength of >0.98 (1-β err prob) (f = 0.25, 3 *df*) each and (Figure 3E,G) with 0.85 (1-β err prob) (f = 0.25, 3 *df*) each respectively.

3 | RESULTS

3.1 | Selecting potential biomarkers for biliary cancer diagnosis

As published by us 2017 in the *Journal of Hepatology*, where we provide several useful large EV surface antigen combinations allowing us to differentiate liver tumour entities from other non-hepatic

malignancies,[8] now we had aimed to distinguish hepatobiliary cancer entities from each other, in particular biliary cancers (CCA and GbCA) from HCC. As a starting point we used our published hepatobiliary EV antigen combination consisting of AnnV, CD133 (Prominin-1), CD326 (EpCAM) but minus ASGPR1. Furthermore, we added CD44v6 to the combination, acknowledging several reports that had indicated that CCA might be associated with CD44v6 expression.[20] Besides quantifying EVs derived directly form biliary cancer cells, we addressed the question if EVs shed from podoplanin$^+$ (gp38) liver progenitor cells, as published by us, could indirectly indicate biliary cancer presence.[21]

Podoplanin (gp38) and Prominin-1 (CD133) are both transmembrane glycoproteins that are typically expressed on progenitor cells in the liver tumour microenvironment, whereas CD44 variant 6 (CD44v6) and epithelial cell adhesion molecule (EpCAM, CD326) are both transmembrane cell adhesion proteins that can be found on the surface of various carcinomas.

First, we compared in vitro expression levels of the selected markers EpCAM, CD44v6, CD133 and gp38 by FACS on CCA tumour cell lines (TFK-1, EGI-1 and CCC-5) and HCC tumour cell lines (HuH7, HepG2 and Hep3B), addressing the question if our selection of surface EV antigens could separate CCA from HCC at the cellular level (Figure 1A,B). Unfortunally, to our knowledge no GbCA cell line is commercially available. Gating strategy, performance of antibodies and their corresponding isotype controls are depicted in Figure S2. The expression profiles of the three tumour cell lines within each cohort (HCC or CCA) were similar, with EpCAM being universally present on all investigated tumour cell lines in relatively high levels (Figure 1A). Gp38 could not be detected on any tumour cell line, which is in agreement with available data since it is rather expressed on cancer stem cells and several types of squamous cell carcinomas, malignant mesothelioma and brain tumours.[22,23] So far no expression of gp38 was reported on HCC cell lines.[24] With exception of the CCA tumour cell line EGI-1, high CD133 expression was almost exclusively limited to HCC cell lines. CD133 was significantly ($P \leq .001$) higher expressed by 6.6-fold in HCC than CCA cell lines (HCC: mean of 92% ± 3.625 SEM and CCA: mean of 14% ± 6.665 SEM). On the contrary, all three CCA cell lines expressed CD44v6 in high levels, CD44v6 expression was significantly ($P \leq .001$) elevated in CCA cell lines by 58.5-fold (HCC: mean of 1.3% ± 0.223 SEM and CCA: mean of 76% ± 5.117 SEM, respectively), whereas no expression on HCC cell lines could be detected arguing strongly for being a suitable biliary cancer antigen that could be very likely utilized in our EV biliary cancer related surface antigen combination. Even though EpCAM was highly expressed on all cell lines, the cohort comparison revealed a significantly ($P \leq .001$) lower EpCAM expression on CCA cell lines, with a mean of 99% ± 0.389 SEM and a mean of 96% ± 0.542 SEM on HCC and CCA cells respectively (Figure 1B).

Our in vitro tumor cell line data was supported by already published data that was upon our request analysed for EpCAM, CD133 and CD44 in EVs extracted from CCA tumour cell lines (TFK-1 and EGI-1, each n = 3), additionally complemented by EVs derived from human primary cholangiocytes (NHC; n = 3) and analysed by liquid chromatography–mass spectrometry.[10] Corresponding statistics are provided in Table S3. In detail, EpCAM was detected in EVs derived from tumour cell lines and primary cholangiocytes, but was shown to be significantly ($P \leq .01$) more abundant in CCA-derived EVs than in non-malignant primary cell EVs. CD133 was particularly enriched in EVs derived from EGI-1 cells, whereas CD44 was predominantly restricted to TFK-1-derived EVs. Importantly, CD133 and CD44 were less abundant in EVs derived from non-malignant primary cholangiocytes. Unfortunately, it was not possible to analyse any CD44 variants retrospectively.

3.2 | Identifying possible parental cell populations expressing the candidate markers

After verifying the presence and differential expression of our candidate markers on malignant cells in vitro, we aimed to identify possible physiological donor cell populations in vivo that express one or more of the markers simultaneously on their surface and could thus be a source for circulating EVs presenting the respective markers. For FACS analysis, wild type C57Bl/6J mouse organs were enzymatically digested to single cell suspensions and subsequently stained with a panel of antibodies (CD45, CD31, ASGPR1 (liver only), CD133, gp38, EpCAM and CD44). Corresponding isotype performances are depicted in Figure S3. The general gating strategy applied to all organs is exemplarily summarized in Figure 1C. In short, after excluding cellular debris, cell clusters, dead cells (PI), nucleated hematopoietic cells (CD45$^+$), endothelial cells (CD31$^+$) and hepatocytes (ASGPR1$^+$, liver only), mesothelial cells were additionally excluded based on their high gp38 expression profile. Double positive CD133$^+$gp38$^+$ progenitor cells were detected in every organ except for the colon (Figure 1D, upper panel). Additionally, triple positive CD133$^+$gp38$^+$EpCAM$^+$ cells could be found to various degrees in all organs except for the colon (Figure 1D, lower panel). CD44 could clearly be detected in colon but was weakly expressed in liver, gallbladder and lung (Figure 1E, upper panel). Accordingly, double positive CD44$^+$CD133$^+$ cells were rare in all mouse organs with a slightly increased abundance in murine gallbladder cells (Figure 1E, lower panel). In sum, our marker selection comprising the combinations CD133$^+$gp38$^+$, CD133$^+$gp38$^+$EpCAM$^+$, CD44$^+$ and CD44$^+$CD133$^+$ were found to be expressed under steady state conditions in wild type mice.

3.3 | Quality management (QM) for FACS analysis of EVs

We thoroughly tested the quality of every reagent used for EV analysis and could not detect any accountable contamination (Figure S4A). In agreement with the guidelines provided by the International Society for Extracellular Vesicles (ISEV),[25] typically, fractions of large EVs isolated by centrifugation result in cross-contaminations

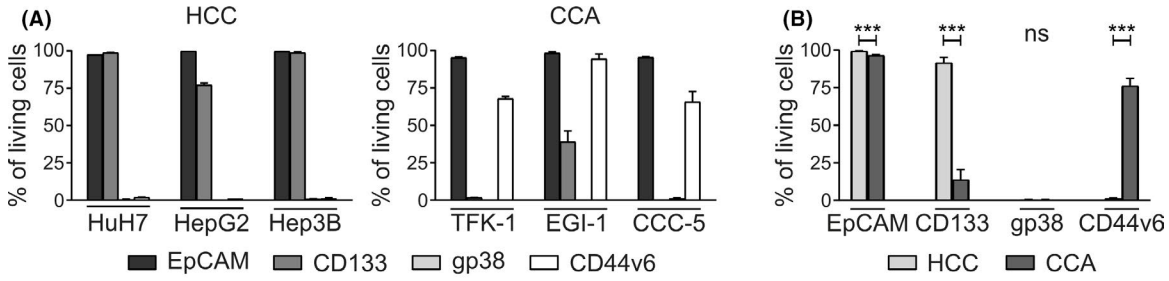
(A)
HCC
CCA
% of living cells
100
75
50
25
0
HuH7
HepG2
Hep3B
TFK-1
EGI-1
CCC-5
EpCAM
CD133
gp38
CD44v6
(B)
***
***
ns
***
EpCAM
CD133
gp38
CD44v6
HCC
CCA

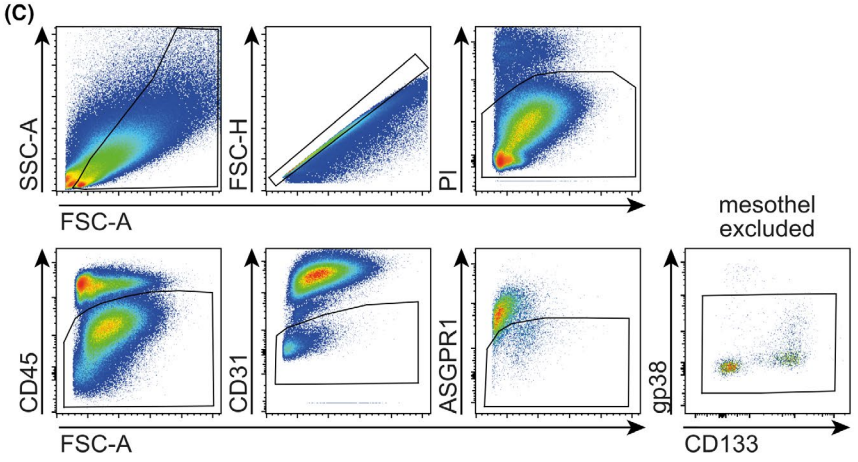
(C)
SSC-A
FSC-A
FSC-H
PI
mesothel excluded
CD45
CD31
ASGPR1
gp38
CD133

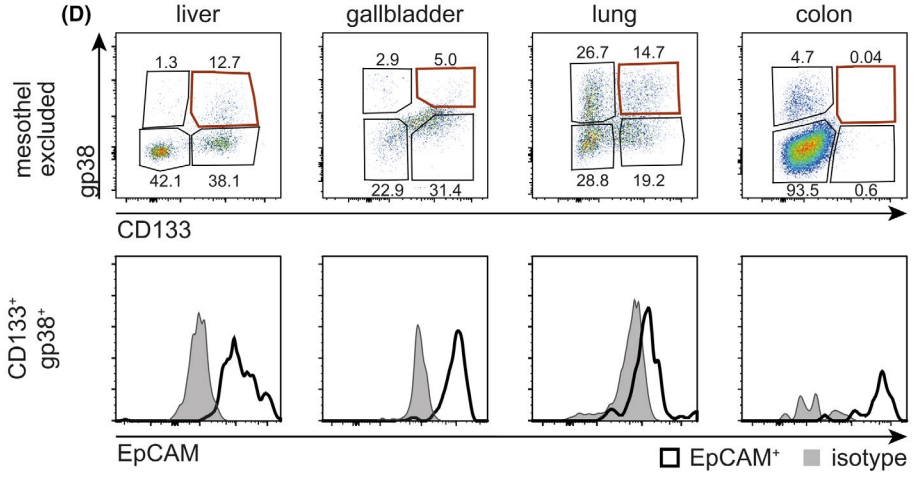
(D)
liver
gallbladder
lung
colon
mesothel excluded
gp38
CD133
1.3
12.7
42.1
38.1
2.9
5.0
22.9
31.4
26.7
14.7
28.8
19.2
4.7
0.04
93.5
0.6
CD133+ gp38+
EpCAM
EpCAM+
isotype

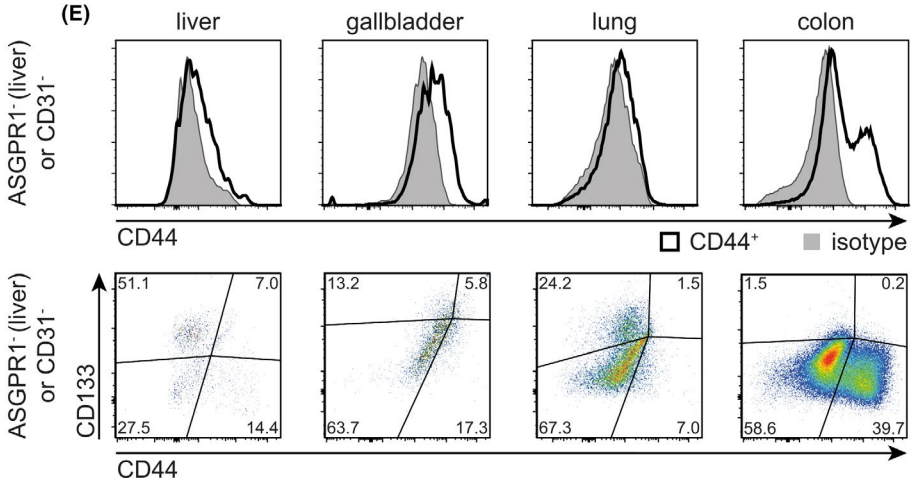
(E)
liver
gallbladder
lung
colon
ASGPR1- (liver) or CD31-
CD44
CD44+
isotype
ASGPR1- (liver) or CD31-
CD133
CD44
51.1
7.0
27.5
14.4
13.2
5.8
63.7
17.3
24.2
1.5
67.3
7.0
1.5
0.2
58.6
39.7

FIGURE 1 EpCAM, CD133, gp38 and CD44v6 are potential biomarkers for biliary cancer detection. Surface expression of the marker selection among living cells on CCA (TFK-1, EGI-1 and CCC-5, each n = 3) and HCC (HuH7, HepG2 and Hep3B, each n = 3) cell lines was analyzed by FACS. Graphs show means (percentage of living cells) with SEM of all HCC and CCA cell lines individually (A) and of CCA and HCC cell lines combined (B, each n = 9). For statistics a two-tailed Mann-Whitney *U* test was performed with $P \leq .05$ considered statistically significant (* = $P \leq .05$, ** = $P \leq .01$). Corresponding gating strategy and isotype controls are provided in Figure S2. C-E, Single cell suspensions were prepared from wild type C57Bl/6J liver, gallbladder, lung and colon. Cells were stained with a panel of surface markers: CD45, CD31, ASGPR1 (liver only), gp38, CD133, EpCAM and CD44. Propidium iodide was used for dead cell exclusion. Corresponding gating strategy and isotype controls are provided in Figure S3. All depicted dot plots and histograms are representative of three independent experiments. C, Representative dot plots of the general gating strategy for all organs are exemplarily depicted for murine liver. ASGPR1 was only included for liver, not for other organs. D, $CD133^+gp38^+$ populations are depicted in the upper panel. Numbers indicate percent of parent population (mesothel excluded). Double positive cells were additionally tested for EpCAM positivity (white) as compared to corresponding isotype controls (grey) in the lower panel. E, Histograms of $CD44^+$ cells (white) as compared to isotype (grey) are depicted in the upper panel. The lower panel represents dot plots of double positive $CD44^+CD133^+$ cells. Numbers indicate percent of parent population ($ASGPR1^-$ for liver or $CD31^-$ for other organs). A, area; FSC, forward scatter; H, height; SSC, sideward scatter

with small EVs and vice versa.[26] Complying with our QM, we tested the sensitivity of our FACS analysis assessing the numeric effect of a given small EV cross-contamination on our FACS-based large EV phenotypic analysis. In short, staining and FACS measurement parameters including gating strategy as utilized for large EV analysis (see Figure S5A) were applied to serum small EVs (Figure S4B). They were counted and confirmed in size by nanoparticle tracking analysis (NTA) prior to FACS, revealing a median diameter of 87.4 nm (D50), ranging from 35.7 (D10) to 139.8 nm (D90) (Figure S4C). The FACS sensitivity was set and confirmed by an initial number of employed small EVs for FACS measurement of 1.175×10^9, from which only a total of 130 events were positive for AnnV, an established EV marker, ruling out any substantial influence of small EV cross-contaminations on large EV quantification in this explicit experimental setting (Figure S4B). Large EVs that were employed to conduct the following diagnostic experiments were confirmed in size by NTA and revealed a median diameter of 209.0 nm (D50), ranging from 153.8 (D10) to 323.9 nm (D90) (Figure S4D). Note: small EVs were only used for QM. The whole study is based on large EVs. Thus, if not specified otherwise the term 'EVs' is subsequently used to describe large EVs throughout the manuscript.

3.4 | Explorative study – EVs discriminate biliary cancer from healthy controls

With our selection of surface antigens proven present in vivo, we aimed to confirm their pertinence in a pathophysiologically relevant setting. Serum EVs were isolated from 10 patients with biliary cancer (5 CCA and 5 GbCA) and from 10 healthy controls by differential centrifugation and stained using antibodies against CD133, gp38, EpCAM and CD44v6. All stainings included AnnV, a common EV marker. Stained samples were subsequently analysed by flow cytometry (FACS) using the gating strategy described in Figure S5A. For every combination of surface markers, the gates for each antibody were applied successively (Figure S5B,C). Importantly, all antibodies were titrated against their matching isotype prior use (Figure S5D). Statistical analysis by two-tailed Mann-Whitney *U* tests revealed that EVs from patients with biliary cancer were significantly elevated as compared to healthy controls in all four investigated EV populations (Figure 2A-D). In detail, $AnnV^+CD133^+gp38^+$ EV levels of biliary cancer patients showed a 7.1-fold increase as compared to healthy donors ($P \leq .01$; biliary CA: median 20.9, healthy CTRL: median 3.0) (Figure 2A). $AnnV^+EpCAM^+CD133^+gp38^+$ EV levels of biliary cancer patients were 5.7-fold increased compared to healthy controls ($P \leq .001$; biliary CA: median 13.6, healthy CTRL: median 2.4) (Figure 2B). $AnnV^+CD44v6^+$ EV levels of biliary cancer patients showed a 2.5-fold elevation as compared to healthy donors ($P \leq .05$; biliary CA: median 93.4, healthy CTRL: median 37.7) (Figure 2C) and $AnnV^+CD44v6^+CD133^+$ EV levels of biliary cancer patients were 2.3-fold elevated compared to healthy controls ($P \leq .01$; biliary CA: median 28.4, healthy CTRL: median 12.3) (Figure 2D).

3.5 | Validation study – progenitor cell-associated and tumour-associated EVs for biliary cancer diagnosis

Based on the results of our explorative study we next evaluated EV levels of the four surface antigen combinations on EVs in a large validation study, additionally including several cancer cohorts as negative control, that is, hepatocellular carcinoma (HCC), colorectal carcinoma (CRC) and non-small cell lung carcinoma (NSCLC) and patients with cirrhosis. Patient characteristics can be obtained from Table 1. Sample preparation of patient serum and analysis of EV surface antigens were performed as described in the explorative study. EV levels of the individual cohorts can be obtained from Figure S6. The group analysis between healthy donors, patients with cirrhosis, biliary cancer (GbCA and CCA), HCC and non-biliary cancer (HCC, CRC and NSCLC) entities revealed that EV levels were significantly elevated in biliary cancers as compared to every control group in all four EV populations (Figure 3A,C,E,G). In detail, $AnnV^+CD133^+gp38^+$ EV levels of biliary cancer patients were 3.0-fold increased compared to healthy controls ($P \leq .01$; biliary CA: median 24.3, healthy CTRL: median 8.2), 3.2-fold increased compared to HCC subjects ($P \leq .001$; HCC: median 7.7) and 3.6-fold increased compared to non-biliary cancer patients ($P \leq .001$; non-biliary CA: median 6.7) (Figure 3A). $AnnV^+EpCAM^+CD133^+gp38^+$ EV levels of biliary cancer

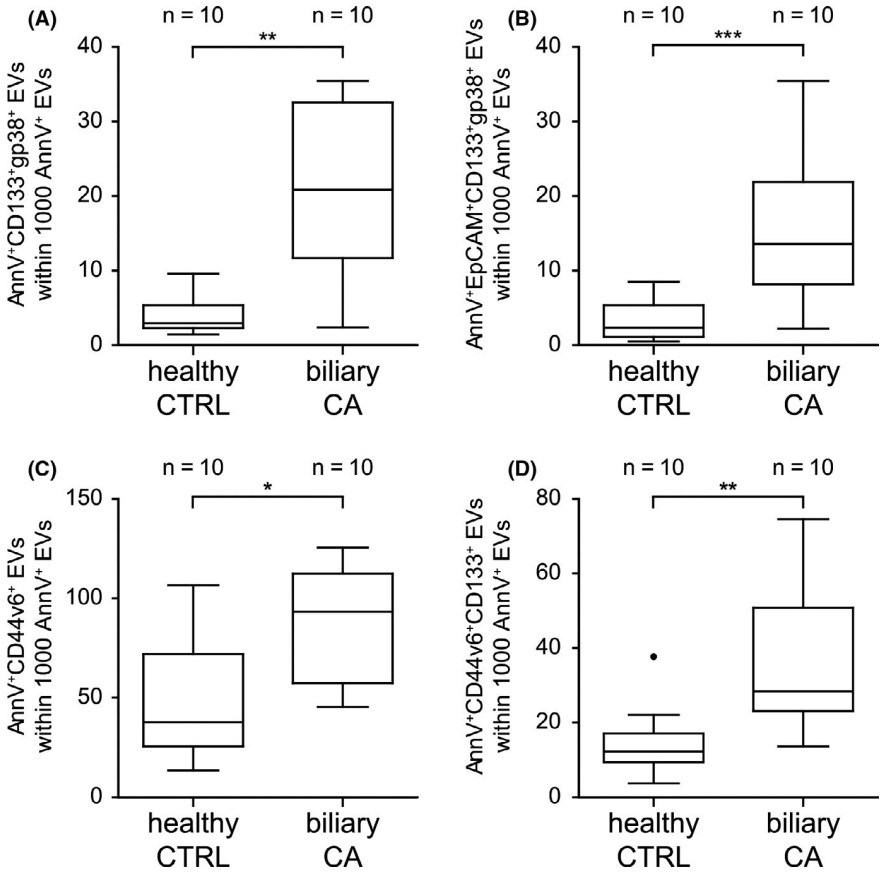

FIGURE 2 Explorative study – CD133, gp38, EpCAM and CD44v6 positive extracellular vesicles discriminate biliary cancer from healthy controls. EVs were isolated and characterized by FACS from serum of indicated biliary cancer patients (biliary CA, comprising GbCA and CCA patients) and healthy donors (healthy CTRL). Corresponding gating strategy and isotype controls are provided in Figure S5. Data shown represent medians with interquartile range (IQR), whiskers represent 1.5 × IQR (Tukey) with outliers plotted as dots. (A-D) EV profiles for the populations $Ann^+CD133^+gp38^+$ (A), $AnnV^+EpCAM^+CD133^+gp38^+$ (B), $AnnV^+CD44v6^+$ (C) and $AnnV^+CD44v6^+CD133^+$ (D) are depicted. Statistical significance was assessed by two-tailed Mann-Whitney *U* tests with $P \leq .05$ considered statistically significant (* = $P \leq .05$, ** = $P \leq .01$, *** = $P \leq .001$)

patients showed a 2.2-fold elevation as compared to healthy controls ($P \leq .01$) and non-biliary cancer patients ($P \leq .001$), respectively (biliary CA: median 12.3, healthy CTRL and non-biliary CA: median 5.5, respectively), and a 1.9-fold elevation as compared to HCC patients ($P \leq .001$; HCC: median 6.4) (Figure 3C). $AnnV^+CD44v6^+$ EV levels of biliary cancer patients were 2.2-fold elevated compared to healthy controls ($P \leq .001$; biliary CA: median 65.4, healthy CTRL: median 29.5), 2.9-fold elevated compared to HCC subjects ($P \leq .001$; HCC: median 22.4) and 2.3-fold elevated compared to non-biliary cancer patients ($P \leq .001$; non-biliary CA: median 28.5) (Figure 3E). $AnnV^+CD44v6^+CD133^+$ EV levels of biliary cancer patients showed a 2.4-fold increase as compared to healthy controls ($P \leq .01$; biliary CA: median 23.8, healthy CTRL: median 9.9), a 3.7-fold increase as compared to HCC subjects ($P \leq .001$; HCC: median 6.5) and a 4.2-fold increase as compared to non-biliary cancer patients ($P \leq .001$; non-biliary CA: median 5.7) (Figure 3G). Considering the clinical importance of differential HCC/CCA diagnosis, ROC curves for all four EV populations were computed showing diagnostic AUC values ranging from 0.68 to 0.81 for biliary CA vs HCC (Figure 3A,C,E,G). We additionally evaluated the potential of EV profiling to differentially diagnose the biliary cancers GbCA and CCA (data not shown) but obtained no discriminatory findings. Furthermore, EV profiling did not yield a significant discrimination between CCAs of intra- or extrahepatic origin (Figure 3B,D,F,H).

FIGURE 3 Validation study – CD133, gp38, EpCAM and CD44v6 positive extracellular vesicles are comprehensive biomarkers for biliary cancer. EVs were isolated and characterized by FACS from serum of indicated cancer patients and healthy donors. Corresponding gating strategy and isotype controls are provided in Figure S5 and summarized patient characteristics can be found in Table 1. A, $AnnV^+CD133^+gp38^+$ EV profile for biliary (biliary CA) and non-biliary cancer patients (non-biliary CA) as well as for negative controls (HCC, cirrhosis and healthy CTRL).'Biliary CA' combines GbCA and CCA patients. 'Non-biliary CA' comprises the cancer cohorts HCC, CRC and NSCLC. EV values for the individuals cohorts can be found in Figure S6. Data shown represent medians with interquartile range (IQR), whiskers represent 1.5 × IQR (Tukey) with outliers plotted as dots. (a) depicts the corresponding ROC curve for $AnnV^+CD133^+gp38^+$ EVs including AUC and *P* values as well as the diagnostic cut-off for biliary CA vs HCC. EV profile for the populations $AnnV^+EpCAM^+CD133^+gp38^+$ (C), $AnnV^+CD44v6^+$ (E) and $AnnV^+CD44v6^+CD133^+$ (G) and their corresponding ROC curves (c, e, g, respectively) are depicted. Dotted lines indicate diagnostic cut-offs for discrimination between biliary CA and HCC for the respective EV population (see Table 2). Statistical significance was assessed by Kruskal-Wallis nonparametric test with 3 *df* followed by Dunn's Multiple Comparison post hoc test ($P \leq .05$). $AnnV^+CD133^+gp38^+$ (B), $AnnV^+EpCAM^+CD133^+gp38^+$ (D), $AnnV^+CD44v6^+$ (F) and $AnnV^+CD44v6^+CD133^+$ (H) EV profiles of intra- and extrahepatic CCA within the total CCA cohort are shown. Statistical significance was assessed by two-tailed Mann-Whitney *U* tests with $P \leq .05$ considered statistically significant (* = $P \leq .05$, ** = $P \leq .01$, *** = $P \leq .001$)

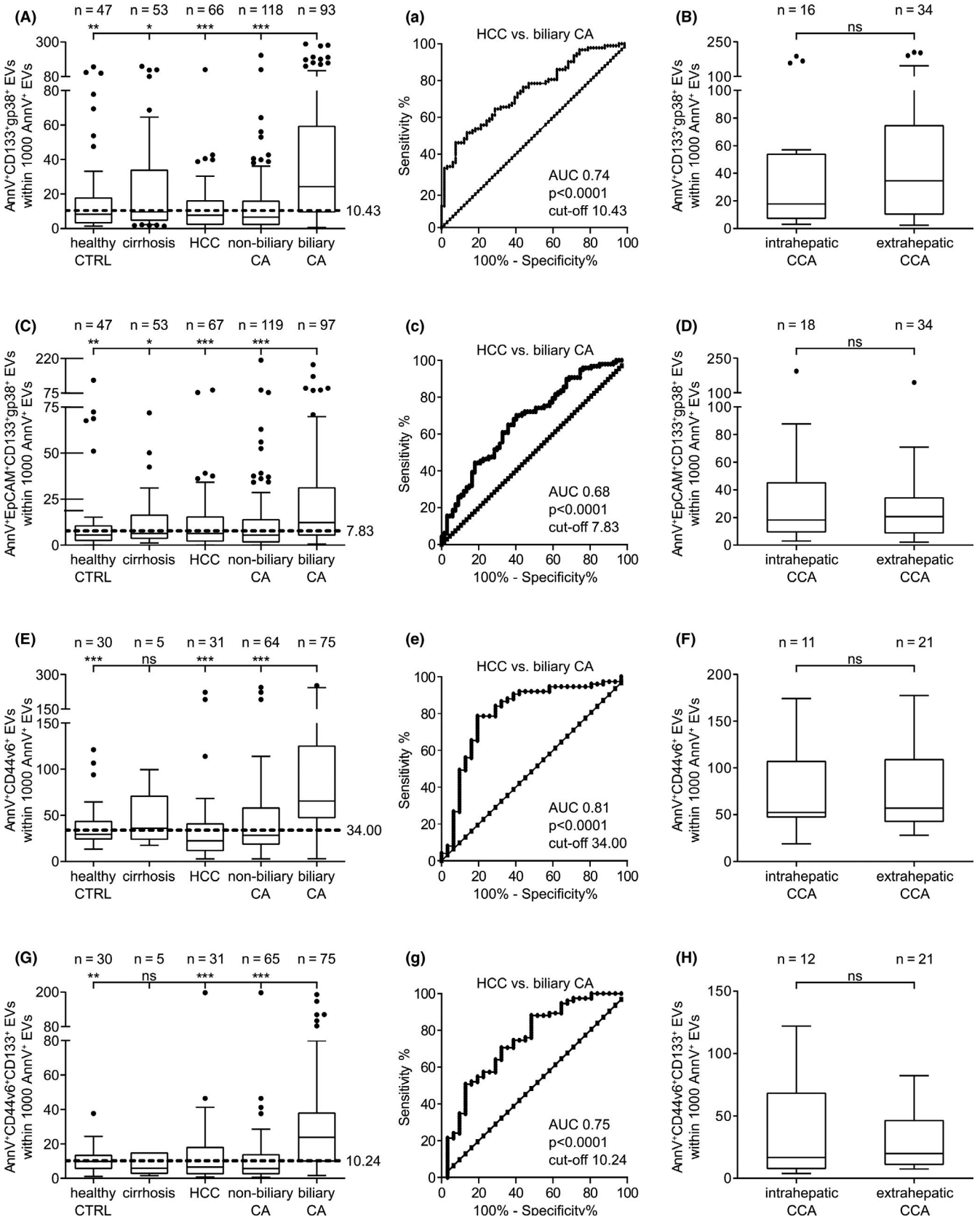
(A)
n = 47 n = 53 n = 66 n = 118 n = 93
** * *** ***
AnnV+CD133+gp38+ EVs within 1000 AnnV+ EVs
10.43
healthy CTRL
cirrhosis
HCC
non-biliary CA
biliary CA
(a)
HCC vs. biliary CA
Sensitivity %
100% - Specificity%
AUC 0.74
p<0.0001
cut-off 10.43
(B)
n = 16 n = 34
ns
AnnV+CD133+gp38+ EVs within 1000 AnnV+ EVs
intrahepatic CCA
extrahepatic CCA
(C)
n = 47 n = 53 n = 67 n = 119 n = 97
** * *** ***
AnnV+EpCAM+CD133+gp38+ EVs within 1000 AnnV+ EVs
7.83
(c)
HCC vs. biliary CA
AUC 0.68
p<0.0001
cut-off 7.83
(D)
n = 18 n = 34
ns
(E)
n = 30 n = 5 n = 31 n = 64 n = 75
*** ns *** ***
AnnV+CD44v6+ EVs within 1000 AnnV+ EVs
34.00
(e)
HCC vs. biliary CA
AUC 0.81
p<0.0001
cut-off 34.00
(F)
n = 11 n = 21
ns
(G)
n = 30 n = 5 n = 31 n = 65 n = 75
** ns *** ***
AnnV+CD44v6+CD133+ EVs within 1000 AnnV+ EVs
10.24
(g)
HCC vs. biliary CA
AUC 0.75
p<0.0001
cut-off 10.24
(H)
n = 12 n = 21
ns

3.6 | Combining AFP and EV surface screening yields a diagnostically powerful biomarker for biliary cancer diagnosis as compared to HCC

Next, we addressed the question if our antigen combinations could be of diagnostic benefit when combined with other serum tumour markers that are already under investigation, especially in the context of differential HCC and CCA diagnosis. Therefore, we correlated serum AFP values, a serum tumour marker widely investigated in HCC diagnosis and surveillance, with serum EV levels of all four combinations for HCC and biliary cancer patients. Computed r-values (Spearman) ranging from −0.17 to 0.24 for HCC subjects and from −0.13 to 0.08 for biliary cancer patients revealed no significant correlation ($P > .05$) between the two parameters (Figure 4A). Consequently, AFP and EV levels can be considered as two independent biomarkers. In a following step we evaluated the diagnostic performance of the two markers separately and in a combined approach by calculating sensitivity, specificity and positive and negative predictive values (Table 2). To assess the diagnostic potential of progenitor cell-derived EV populations (AnnV$^+$CD133$^+$gp38$^+$ and AnnV$^+$EpCAM$^+$CD133$^+$gp38$^+$ EVs) and tumour-associated EV populations (AnnV$^+$CD44v6$^+$ and AnnV$^+$CD44v6$^+$CD133$^+$ EVs) for detecting biliary cancers individually, we combined the respective EV populations into two separate cohorts and compared the results to serum AFP levels for each cohort. For combined analysis of AFP and EV populations biliary cancer patients were considered positive if they fulfilled the requirements for at least one of the parameters, for example, AFP below 20 ng/mL or EV levels above the respective cut-off or both, and vice versa for patients with HCC. Twenty ng/mL represents the screening cut-off for HCC surveillance as

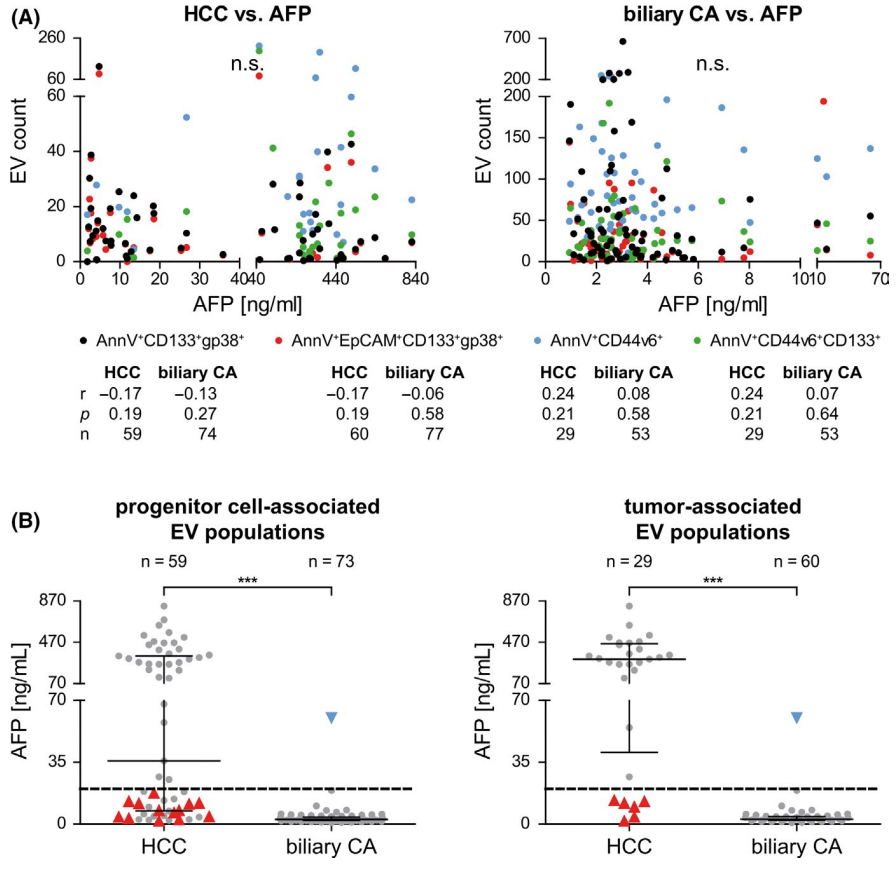

FIGURE 4 Combined analysis of AFP levels and EV profiling reliably discriminates HCC from biliary cancer. A, Correlation between AFP levels and EV counts from different populations for HCC (left panel) or biliary CA patients (right panel) are depicted. Two-tailed Spearman's correlation (r), *P* values and cohort sizes (n) are indicated for each population. B, Displayed are AFP values for HCC and biliary CA patients. In the left panel all patients with EV profiles for progenitor cell-associated EV populations (AnnV$^+$CD133$^+$gp38$^+$ and AnnV$^+$EpCAM$^+$CD133$^+$gp38$^+$) are included, whereas in the right panel all patients with EV profiles for tumour-associated EV populations (AnnV$^+$CD44v6$^+$ and AnnV$^+$CD44v6$^+$CD133$^+$) are included. Indicated in red are patients that based on AFP levels are not classified as HCC patients (AFP < 20 ng/mL) but can positively be identified as HCC by AnnV$^+$CD133$^+$gp38$^+$ EVs (left panel, EVs < 10.43) or AnnV$^+$CD44v6$^+$ EVs (right panel, EVs < 34). Indicated in blue are biliary CA patients that are not classified as such according to AFP levels (AFP > 20 ng/mL) but can be identified as biliary CA by AnnV$^+$CD133$^+$gp38$^+$ EVs (left panel, EVs > 10.43) or AnnV$^+$CD44v6$^+$ EVs (right panel, EVs > 34). Corresponding diagnostic values can be found in Table 2. Dotted line indicates diagnostic cut-off of 20 ng/mL for AFP. Statistical significance was assessed by two-tailed Mann-Whitney *U* tests with $P \leq .05$ considered statistically significant (* = $P \leq .05$, ** = $P \leq .01$, *** = $P \leq .001$, n.s. = non significant)

TABLE 2 Diagnostic performance of the indicated EV populations individually and combined with AFP in biliary cancers (GbCA and CCA) as compared to HCC. Depicted are diagnostically relevant cut-offs (AFP: ng/mL, EVs: number per 10^3 $AnnV^+$ EVs) as well as sensitivities, specificities, positive (PPV) and negative predictive values (NPV). n indicates cohort size, (*combined AUROC were not calculated)

Progenitor cell-associated EVs (biliary CA: n = 73, HCC: n = 59)	**AUROC**	***P-value***	**Cut-off**	**Sensitivity [%]**	**Specificity [%]**	**PPV [%]**	**NPV [%]**
$AnnV^+CD133^+gp38^+$	0.74	<.0001	10.43	72.6	59.3	68.8	63.6
$AnnV^+EpCAM^+CD133^+gp38^+$	0.68	<.0001	7.83	71.2	59.3	68.4	62.5
AFP	0.89	<.0001	20.00	98.6	54.2	72.7	97.0
AFP and $AnnV^+CD133^+gp38^+$	*	*	20.00 and 10.43	100.0	76.3	83.9	100.0
AFP and $AnnV^+EpCAM^+CD133^+gp38^+$	*	*	20.00 and 7.83	100.0	76.3	83.9	100.0
Tumor-associated EVs (biliary CA: n = 60, HCC: n = 29)	**AUROC**	***P-value***	**Cut-off**	**Sensitivity [%]**	**Specificity [%]**	**PPV [%]**	**NPV [%]**
$AnnV^+CD44v6^+$	0.81	<.0001	34.00	91.7	69.0	85.9	80.0
$AnnV^+CD44v6^+CD133^+$	0.75	<.0001	10.24	81.7	58.6	80.3	60.7
AFP	0.95	<.0001	20.00	98.3	79.3	90.8	95.8
AFP and $AnnV^+CD44v6^+$	*	*	**20.00 and 34.00**	**100.0**	**100.0**	**100.0**	**100.0**
AFP and $AnnV^+CD44v6^+CD133^+$	*	*	20.00 and 10.24	100.0	96.6	98.4	100.0

recommended by the AASLD and EASL Clinical Practice Guidelines for the Management of Hepatocellular Carcinoma.[27,28] For biliary cancer diagnosis, progenitor cell-associated EV populations showed sensitivities ranging from 71%-73% and positive predictive values (PPVs) of 68%, respectively, while specificities (59%, respectively) and negative predictive values (NPVs; 63%-64%) were less diagnostically relevant. AFP as a tumour marker by itself achieved very good diagnostic values with 98.6% sensitivity and a NPV of 97%, although lacking in specificity (54.2) and PPV (72.7%). Interestingly, by combining AFP and progenitor cell-associated EV levels, sensitivity and NPV were increased to 100%, respectively, while simultaneously increasing specificity to 76.3% and PPV to 83.9%. In respect to tumour-associated EV populations in biliary cancer diagnosis, they showed a better diagnostic performance than progenitor cell-associated EVs (sensitivities: 81.7%-91.7%, specificities: 58.6%-69.0%, PPVs: 80.3%-85.9%, NPVs: 60.7%-80.0%) and were only slightly surpassed by the diagnostic values for AFP in this cohort (sensitivity: 98.3%, specificity: 79.3%, PPV: 90.8%, NPV: 95.8%). Interestingly, sensitivity and NPV could be increased to 100%, when combining AFP levels with $AnnV^+CD44v6^+CD133^+$ EVs, while simultaneously specificity and PPV reached very good diagnostic values of 96.9% and 98.4% respectively. Most importantly, sensitivity, specificity, PPV and NPV all achieved 100%, when combining AFP levels with $AnnV^+CD44v6^+$ EVs.

In Figure 4B AFP values of HCC and biliary cancer patients are displayed, separated into the two EV population cohorts (progenitor cell- or tumour-associated). It represents an illustration of the diagnostic values obtained in Table 2 and indicates patients that, based on AFP values, could additionally be identified as patients with HCC (red) or as biliary cancer patients (blue) by $AnnV^+CD133^+gp38^+$ EVs (left panel) and $AnnV^+CD44v6^+$ EVs (right panel), thus highlighting the benefit of a combined analysis. Furthermore, we investigated, if combining CA19-9, a proposed tumour marker for bilio-pancreatic cancer diagnosis,[29] and our EV populations in the same manner as with AFP could be of diagnostic benefit but did not obtain better results (data not shown). Additionally, we evaluated if EV levels correlated with TNM stage or extent of metastatic spread of HCC and biliary tumours but did not observe any significant correlations (data not shown).

4 | DISCUSSION

Recently, we showed that a minimally invasive, liquid biopsy-based approach involving large EVs is advantageous for detecting hepatobiliary malignancies, however, without being able to discriminate between them.[8] Here, in this subsequent study the potential of large EVs as a diagnostic biomarker for biliary cancer was investigated, in order to detect and differentiate between those malignancies. Except for ultrasonography (US) in patients suffering from gallstones as a possible indication for a given GbCA risk, early detection presents difficult.[29-32] Furthermore, GbCA diagnosis often only occurs incidentally during pathological assessment of routine cholecystectomy specimens due to benign diseases such as gallstones.[33] Hence, biliary cancers are highly fatal diseases, characterized by high mortality and poor 5-year survival rates.[5,6] Therefore, several specialist societies such as ENS-CCA and ESMO are strongly in favour of developing new tools for (early and specific) biliary cancer diagnosis.[3,29]

Podoplanin, alias gp38, is a novel yet not completely understood player in tumour immunology, tumour progression and recurrence besides being a liver progenitor cell marker.[21,22,34,35] Since hepatic progenitor cells are activated in most chronic liver diseases and apparently are associated with hepatic carcinogenesis,[36] increasingly appearing liver progenitor cells during chronic hepatic inflammation

could potentially reveal the presence of hepatobiliary cancers. These liver progenitor cells were typically identified as double positive for CD133 and podoplanin.[21] Furthermore, podoplanin is regarded as a potential marker for tumour-initializing cells (TICs) with stem cell-like properties, defined by their self-renewal, differentiation and tumour initiation capacities.[37] EpCAM is highly overexpressed and associated with various cancer entities in regard to cancer prognosis and cancer targeting.[38] We reported its feasibility as part of a diagnostic biomarker combination on large EVs.[8,9,39] Moreover simultaneous expression of EpCAM and CD133 has been found to be strongly increased in biliary cancer and to be related to progression, invasive and metastatic behaviour and prognosis.[40]

Since both CD44v6 as well as CD133 are well-established tumour stem cell and cancer markers for gallbladder carcinoma, CCA and other cancers, their single as well as combined expression on EVs was additionally of interest.[41-44] Antigen expression analyses on CCA cell line-derived EVs and CCA and HCC cell lines supported our hypothesis of gp38, CD133, EpCAM and CD44v6 being suitable markers (Figure 1A,B; Figure S1), hence we tested the indicated EV antigen combination being simultaneously positive for these. The human cancer cell line expression profiles indicated that CD44v6 might be of interest for CCA and HCC differentiation, since CD44v6 was highly differentially expressed on the investigated CCA and HCC cell lines (Figure 1B). The murine data suggested that $CD133^+gp38^+$ and $EpCAM^+CD133^+gp38^+$ progenitor cell subsets as well as $CD44^+$ and $CD44^+CD133^+$ tumour-associated subsets in fact were detectable under steady state conditions in varying amounts in murine liver, gallbladder, lung and colon (Figure 1D,E). Interestingly, murine gallbladder showed the highest expression of double positive $CD44^+CD133^+$ cells, which is consistent with the finding that these double positive primary human gallbladder carcinoma cells displayed cancer stem cell-like characteristics, highlighting their important role in gallbladder carcinogenesis.[45] Although not every marker combination was detectable in every organ, one has to keep in mind that a lack of expression in a healthy mouse model does not necessarily correlate with expression levels in a tumour environment. Our hypothesis of the benefit of the proposed progenitor cell-associated and tumour-associated EV populations for hepatobiliary cancer diagnosis was further supported by our explorative study, revealing significantly elevated EV levels in 10 patients with biliary cancer as compared to 10 healthy controls for all four combinations (Figure 2A-D). In a next step, we verified our preliminary results in a large validation study associated with the needed power to be conclusive and additionally including several cancer cohorts as negative controls, namely HCC, CRC and NSCLC. The group analysis between healthy donors, HCC, non-biliary cancer and biliary cancer entities showed that $AnnV^+CD133^+gp38^+$, $AnnV^+EpCAM^+CD133^+gp38^+$, $AnnV^+CD44v6^+$ and $AnnV^+CD44v6^+CD133^+$ EVs all were significantly elevated in biliary cancers and remained low in the indicated negative controls (Figure 3A,C,E,G). Except for CD44v6 singular expression profile analysis of CD133, EpCAM and gp38 on EVs were not beneficial (data not shown). With an AUC value of 0.81 $AnnV^+CD44v6^+$ EVs were the most powerful biomarker for biliary cancer detection in this study. Our observation that patients with biliary cancer display elevated levels of $AnnV^+CD44v6^+$ EVs is consistent with previous findings that demonstrated by immunohistochemistry and real time PCR, that CD44v6 is not detected in healthy gallbladder mucosa, but strongly expressed in GbCA.[46] High $CD44v6^+$ EV levels in both GbCA and CCA concur with observations that linked increased CD44v6 expression in biliary epithelium of both gallbladder and bile ducts to cancer progression.[47] We have to note that our selected EV antigens were not capable of distinguishing between intra- and extrahepatic CCA and between GbCA and CCA. This might be due to the fact that there exists a more optimal EV antigen combination for these discriminations, but we doubt that any EV surface antigen or antigen combinations will have the needed sensitivity to differentiate between intra- and extrahepatic CCA. From the surface antigenic view we do not expect any differences caused by a different location of the primary CCA tumour. We suppose that intra-vesicular differences on protein, mRNA or miRNA levels might be noticeable due to an environment-depending interaction of the EV donor CCA cells.

Next the question arose, if our EV-based phenotyping could be improved and if synergistic effects could be observed by taking advantage of other serological screening markers such as AFP (Figure 4). AFP is a widely investigated serum tumour marker for HCC, whose use for diagnostic purposes is not recommended by the AASLD and EASL Clinical Practice Guidelines for the Management of Hepatocellular Carcinoma, whereas it has proven beneficial for HCC surveillance at a cut-off of 20 ng/mL.[27,28] In contrast to the recommendations of the AASLD/EASL guidelines, serum AFP levels by itself, at a cut-off of 20 ng/mL, showed a diagnostic capacity for differentially diagnosing HCC and biliary cancers in this study, surpassing the performance of our investigated EV populations (Table 2). However, importantly, the diagnostic performance of AFP could be enhanced, when combined with EV levels, especially when combining it with the tumour-associated EV populations $AnnV^+CD44v6^+$ and $AnnV^+CD44v6^+CD133^+$. Remarkably, the combination of $AnnV^+CD44v6^+$ EVs and AFP values led to a perfect separation of biliary cancer and HCC patients, with sensitivity, specificity, PPV and NPV all achieving 100%. Biliary cancers are commonly associated with low AFP levels. Except for one patient, this observation was confirmed in our study. The patient in question might display a mixed hepatocellular cholangiocarcinoma, which would explain the slightly elevated AFP levels. According to the AASLD and EASL Clinical Practice Guidelines HCCs cannot reliably be detected by AFP values alone,[27,28] which was confirmed in our study. However, depending on the EV population added to the analysis, all or almost all previously undetected HCCs with low AFP values could be correctly diagnosed. Thus, our synergistic approach illustrates the benefit of adding EV levels to AFP-based diagnosis. It might have particular clinical relevance for differential hepatobiliary cancer detection and should be followed up by a large multi-centre study. A current alternative serum biomarker for biliary cancer diagnosis as proposed by the ESMO Clinical Practice Guidelines is CA 19-9[29] but it is associated with low sensitivity and specificity of 62% and 63%,

respectively,[32,48] and is not suitable to discriminate between cancer entities. Several serum biomarkers and metabolites have been identified as potential candidates for minimal invasive discrimination of HCC and intrahepatic CCA[10,49] but until now no liquid biopsy marker achieving a better clinically useful performance exists underlining the relevance of our study in terms of hepatobiliary cancer management. Moreover screening EVs offers a cheap, minimally invasive technique to detect cancer, while causing minimum distress to the patient. To perform an EV liquid biopsy screen only a small blood sample is required. For most patients, drawing blood is an uncritical and acceptable procedure. It requires minimum equipment and is performed quickly without special need for long medical observation afterwards. Therefore, EV profiling represents a potent tool for early cancer screening as discussed by others and us.[9,16,49]

5 | CONCLUSION

In summary, our study provides valuable data arguing that EV phenotyping together with AFP assessment is a powerful diagnostic biomarker in detection and differentiation of hepatobiliary cancers. We presented four EV surface antigen combinations that confidently differentiated between patients with biliary cancer and HCC and whose performance could even be enhanced by combined AFP measurements. Considering the results of this and other studies, liquid biopsy-based differential diagnosis of hepatobiliary cancers might be in reach.

ETHICS APPROVAL AND CONSENT OF PARTICIPATION

The Ethics commissions of (i) the State Chambers of Medicine in Rhineland-Palatinate, Ger-many approval number: 837.151.13 (8836-F)); (ii) Saarland, Germany (167/11); (iii) San Sebastian, Spain (PI2014187); (iv) Warsaw, Poland (KB/41/A/2016 and AKB/145/2014) and (v) Cluj-Napoca, Romania (3042/07.03.2018) approved this study. All patients gave their informed consent.

ACKNOWLEDGEMENTS

The authors thank the organizers of the EASL HCC Summit 2018 in Geneva, the EASL ILC 2018 in Paris and the ENS-CCA II Biennal Congress 2018 in Rome for the possibility to present parts of this work in invited talks. Additionally, the authors thank Björn Zapke from Dr Lukacs-Kornek's lab, University of Bonn, for his valuable inputs and assistance during the Nano Tracking Analysis (NTA) of EVs.

CONFLICT OF INTEREST

The authors declare that they have no conflict of interests.

AUTHORS' CONTRIBUTIONS

M.Ko contributed to conceptionalization and supervision. SKU, HJ-H., HS and M.Ko contributed to methodology. M.Kr, A.Wi., JL, MA, TM, CK, BK, KJ, WP, Marek K., KZ, WH, Ł.K., MR, KG, WW, RK, JR-W., AS, RS, A.Wö., MG-C., SG, ZS, JMB, CPS, FL, PM and M.Ko contributed to resources. SKU, HS, HJ-H. and M.A contributed to investigation. SKU, HS, M.Kr, MA HJ-H. and M.Ko contributed to formal analysis. M.Ko contributed to project administration. M.Ko contributed to funding acquisition. SKU, HS and M.Ko contributed to writing – original draft.

ORCID

Jesus M. Banales https://orcid.org/0000-0002-5224-2373
Christian P. Strassburg https://orcid.org/0000-0001-7870-5359
Frank Lammert https://orcid.org/0000-0003-4450-7201
Piotr Milkiewicz https://orcid.org/0000-0002-1817-0724
Miroslaw Kornek https://orcid.org/0000-0002-1682-1765

REFERENCES

1. Cancer.Net ASoCOA. Gallbladder cancer – medical illustrations. *Cancernet Articles*. 2012.
2. Lewis DR, Chen H-S, Cockburn MG , et al. Early estimates of SEER cancer incidence, 2014. *Cancer*. 2017;123(13):2524–2534.
3. Banales JM, Cardinale V, Carpino G, et al. Expert consensus document: cholangiocarcinoma: current knowledge and future perspectives consensus statement from the European Network for the Study of Cholangiocarcinoma (ENS-CCA). *Nat Rev Gastroenterol Hepatol*. 2016;13(5):261-280.
4. Lazcano-Ponce EC, Miquel JF, Munoz N, et al. Epidemiology and molecular pathology of gallbladder cancer. *CA Cancer J Clin*. 2001;51(6):349-364.
5. Guglielmi A, Ruzzenente A, Campagnaro T, et al. Intrahepatic cholangiocarcinoma: prognostic factors after surgical resection. *World J Surg*. 2009;33(6):1247-1254.
6. Levy AD, Murakata LA, Rohrmann Jr CA. Gallbladder carcinoma: radiologic-pathologic correlation. *Radiographics*. 2001;21(2):295-314; questionnaire, 549–255.
7. Lang H, Sotiropoulos GC, Frühauf NR, et al. Extended hepatectomy for intrahepatic cholangiocellular carcinoma (ICC): when is it worthwhile? Single center experience with 27 resections in 50 patients over a 5-year period. *Ann Surg*. 2005;241(1):134-143.
8. Julich-Haertel H, Urban SK, Krawczyk M, et al. Cancer-associated circulating large extracellular vesicles in cholangiocarcinoma and hepatocellular carcinoma. *J Hepatol*. 2017;67:282-292.
9. Julich H, Willms A, Lukacs-Kornek V, Kornek M. Extracellular vesicle profiling and their use as potential disease specific biomarker. *Front Immunol*. 2014;5:1-6.
10. Arbelaiz A, Azkargorta M, Krawczyk M, et al. Serum extracellular vesicles contain protein biomarkers for primary sclerosing cholangitis and cholangiocarcinoma. *Hepatology*. 2017;66(4):1125-1143.
11. Melo SA, Luecke LB, Kahlert C, et al. Glypican-1 identifies cancer exosomes and detects early pancreatic cancer. *Nature*. 2015;523:177-182.
12. Théry C, Witwer KW, Aikawa E, et al. Minimal information for studies of extracellular vesicles 2018 (MISEV2018): a position statement of the International Society for Extracellular Vesicles and update of the MISEV2014 guidelines. *J Extracell Vesicles*. 2018;7(1):1535750.
13. Kornek M, Schuppan D. Microparticles: Modulators and biomarkers of liver disease. *J Hepatol*. 2012;57:1144-1146.
14. Shao H, Chung J, Balaj L, et al. Protein typing of circulating microvesicles allows real-time monitoring of glioblastoma therapy. *Nat Med*. 2012;18:1835-1840.
15. Mocan T, Simão AL, Castro RE, et al. Liquid biopsies in hepatocellular carcinoma: are we winning? *J Clin Med*. 2020;9(5).
16. Urban SK, Mocan T, Sanger H, Lukacs-Kornek V, Kornek M. Extracellular vesicles in liver diseases: diagnostic, prognostic, and therapeutic application. *Semin Liver Dis*. 2019;39(1):70-77.
17. Macias RIR, Kornek M, Rodrigues PM, et al. Diagnostic and prognostic biomarkers in cholangiocarcinoma. *Liver Int*. 2019;39(Suppl 1):108-122.

18. Julich-Haertel H, Tiwari M, Mehrfeld C, Krause E, Kornek M, Lukacs-Kornek V. Isolation and enrichment of liver progenitor subsets identified by a novel surface marker combination. *J Vis Exp*. 2017(120).
19. Lukacs-Kornek V, Julich-Haertel H, Urban SK, Kornek M. Multi-surface antigen staining of larger extracellular vesicles. *Methods Mol Biol*. 2017;1660:201-208.
20. Gu MJ, Jang BI. Clinicopathologic significance of Sox2, CD44 and CD44v6 expression in intrahepatic cholangiocarcinoma. *Pathol Oncol Res*. 2014;20(3):655-660.
21. Eckert C, Kim YO, Julich H, et al. Podoplanin discriminates distinct stromal cell populations and a novel progenitor subset in the liver. *American J Physiol-Gastrointestinal Liver Physiol*. 2016;310:G1-G12.
22. Astarita JL, Acton SE, Turley SJ. Podoplanin: emerging functions in development, the immune system, and cancer. *Front Immunol*. 2012;3:283.
23. Quintanilla M, Montero-Montero L, Renart J, Martín-Villar E. Podoplanin in inflammation and cancer. *Int J Mol Sci*. 2019;20(3).
24. Cioca A, Ceausu AR, Marin I, Raica M, Cimpean AM. The multifaceted role of podoplanin expression in hepatocellular carcinoma. *Eur J Histochem*. 2017;61(1):2707.
25. Lötvall J, Hill AF, Hochberg F, et al. Minimal experimental requirements for definition of extracellular vesicles and their functions: a position statement from the International Society for Extracellular Vesicles. *J Extracell Vesicles*. 2014;3:26913.
26. Ettelaie C, Collier ME, Maraveyas A, Ettelaie R. Characterization of physical properties of tissue factor-containing microvesicles and a comparison of ultracentrifuge-based recovery procedures. *J Extracell Vesicles*. 2014;3.
27. Marrero JA, Kulik LM, Sirlin CB, et al. Diagnosis, staging, and management of hepatocellular carcinoma: 2018 practice guidance by the American Association for the Study of Liver Diseases. *Hepatology*. 2018;68(2):723-750.
28. European Association for the Study of the Liver. Electronic address eee, European Association for the Study of the L. EASL clinical practice guidelines: management of hepatocellular carcinoma. *J Hepatol*. 2018;69(1):182-236.
29. Valle JW, Borbath I, Khan SA, et al. Biliary cancer: ESMO Clinical Practice Guidelines for diagnosis, treatment and follow-up. *Ann Oncol*. 2016;27(suppl 5):v28-v37.
30. Tian Y, Liu L, Yeolkar NV, Shen F, Li J, He Z. Diagnostic role of staging laparoscopy in a subset of biliary cancers: a meta-analysis. *ANZ J Surg*. 2017;87(1–2):22-27.
31. Wang W, Fei Y, Wang F. Meta-analysis of contrast-enhanced ultrasonography for the detection of gallbladder carcinoma. *Med Ultrason*. 2016;18(3):281-7.
32. Bridgewater J, Galle PR, Khan SA, et al. Guidelines for the diagnosis and management of intrahepatic cholangiocarcinoma. *J Hepatol*. 2014;60:1268-1289.
33. Dorobisz T, Dorobisz K, Chabowski M, et al. Incidental gallbladder cancer after cholecystectomy: 1990 to 2014. *OncoTargets and Therapy*. 2016;9:4913-4916.
34. Lukacs-Kornek V, Lammert F. The progenitor cell dilemma: Cellular and functional heterogeneity in assistance or escalation of liver injury. *J Hepatol*. 2017;66(3):619-630.
35. Wicki A, Lehembre F, Wick N, Hantusch B, Kerjaschki D, Christofori G. Tumor invasion in the absence of epithelial-mesenchymal transition: podoplanin-mediated remodeling of the actin cytoskeleton. *Cancer Cell*. 2006;9(4):261-272.
36. Roskams T. Liver stem cells and their implication in hepatocellular and cholangiocarcinoma. *Oncogene*. 2006;25:3818-3822.
37. Atsumi N, Ishii G, Kojima M, Sanada M, Fujii S, Ochiai A. Podoplanin, a novel marker of tumor-initiating cells in human squamous cell carcinoma A431. *Biochem Biophys Res Commun*. 2008;373(1):36-41.
38. Baeuerle PA, Gires O. EpCAM (CD326) finding its role in cancer. *Br J Cancer*. 2007;96(3):417-423.
39. Willms A, Muller C, Julich H, et al. Tumour-associated circulating microparticles: a novel liquid biopsy tool for screening and therapy monitoring of colorectal carcinoma and other epithelial neoplasia. *Oncotarget*. 2016;7(21):30867-30875.
40. Jiang S, Pei L, Yang Z-L, Liu G. Prognostic value of the stem cell markers Epcam and CD133 expression of gallbladder adenocarcinoma. *Hepatogastroenterology*. 2014;61:574-579.
41. Wang J, Wu Y, Gao W, et al. Identification and characterization of CD133(+)CD44(+) cancer stem cells from human laryngeal squamous cell carcinoma cell lines. *J Cancer*. 2017;8(3):497-506.
42. Yu J, Tang Z, Gong W, Zhang M, Quan Z. Isolation and identification of tumor-initiating cell properties in human gallbladder cancer cell lines using the marker cluster of differentiation 133. *Oncol Lett*. 2017;14(6):7111-7120.
43. Suzuki A, Sekiya S, Onishi M, et al. Flow cytometric isolation and clonal identification of self-renewing bipotent hepatic progenitor cells in adult mouse liver. *Hepatology*. 2008;48(6):1964-1978.
44. Ashida K, Terada T, Kitamura Y, Kaibara N. Expression of E-cadherin, alpha-catenin, beta-catenin, and CD44 (standard and variant isoforms) in human cholangiocarcinoma: an immunohistochemical study. *Hepatology*. 1998;27:974-982.
45. Shi C, Tian R, Wang M, et al. CD44+ CD133+ population exhibits cancer stem cell-like characteristics in human gallbladder carcinoma. *Cancer Biol Ther*. 2010;10(11):1182-1190.
46. Yanagisawa N, Mikami T, Mitomi H, Saegusa M, Koike M, Okayasu I. CD44 variant overexpression in gallbladder carcinoma associated with tumor dedifferentiation. *Cancer*. 2001;91:408-416.
47. Tsuchida A, Nagakawa Y, Kasuya K, et al. Significance of CD44s and CD44v6 expression in pancreaticobiliary maljunction. *Hepatogastroenterology*. 2011;58:1877-1881.
48. Rupesh P, Manoj P, Vijay KS. Biomarkers in carcinoma of the gallbladder. *Expert Opin Med Diagn*. 2008;2(5):511-526.
49. Banales JM, Iñarrairaegui M, Arbelaiz A, et al. Serum metabolites as diagnostic biomarkers for cholangiocarcinoma, hepatocellular carcinoma, and primary sclerosing cholangitis. *Hepatology*. 2019;70(2):547-562.

SUPPORTING INFORMATION

Additional supporting information may be found online in the Supporting Information section.

How to cite this article: Urban SK, Sänger H, Krawczyk M, et al. Synergistic effects of extracellular vesicle phenotyping and AFP in hepatobiliary cancer differentiation. *Liver Int*. 2020;00:1–14. https://doi.org/10.1111/liv.14585